

THE NAVY'S CORPORATE LABORATORY

2007

NRRL REVIEW



FIGHTING THE
GLOBAL WAR
ON TERRORISM

NAVAL RESEARCH LABORATORY
Washington, DC 20375

General information on the research described in this *NRL Review* can be obtained from the Public Affairs Office, Code 1030, (202) 767-2541. Information concerning Technology Transfer is available from the Technology Transfer Office, Code 1004, (202) 767-7230. Sources of information on the various educational programs at NRL are listed in the chapter entitled "Programs for Professional Development."

For additional information about NRL, the *Fact Book* lists the organizations and key personnel for each division. It contains information about Laboratory funding, programs, and field sites. The *Fact Book* can be obtained from the Technical Information Services Branch, Code 3430, (202) 404-4963. The web-based *NRL Major Facilities* publication, which describes each NRL facility in detail, can be accessed at <http://www.nrl.navy.mil>.

NRL REVIEW STAFF

SENIOR SCIENCE EDITOR

John D. Bultman

COORDINATOR

Jonna Atkinson

CONSULTANT

Kathy Parrish

DESIGN, LAYOUT, AND GRAPHIC SUPPORT

Jonna Atkinson, Donna Gloystein, and Peggy Newman

EDITORIAL ASSISTANCE

Saul Oresky, Kathy Parrish, and Claire Peachey

HISTORICAL UPDATE

John D. Bultman

PHOTOGRAPHIC PRODUCTION

Jamie Baker, Gayle Fullerton, and Michael Savell

Cover pictures:



◀ U.S. Marine wearing NRL-developed QuadGard extremity protection in Iraq.



◀ A blended composite of satellite datasets for terrain (NASA Blue Marble), city lights (NGDC 2003 OLS city lights database), and cloud cover (Meteosat-5 visible imagery).
NGDC = National Geophysical Data Center
OLS = the Defense Meteorological Satellite Program's Operational Linescan System



◀ The Tactical Aircraft Directable Infrared Countermeasures (TADIRCM) system has now performed two test flights on an F-18E. A stimulator located on the ground at the Naval Air Station Patuxent River triggered the missile warning system, initiating the full system response and culminating in laser irradiance of several threat missile seeker heads co-located with the stimulator and tracking the aircraft. Preliminary results show that the system successfully defeated the missile seekers on all ten aircraft passes.

REVIEWED AND APPROVED

NRL/PU/3430--07-501

RN: 07-1226-3806

April 2008

Daniel R. Gahagan, Captain, USN
Commanding Officer



NRL's MISSION

To conduct a broadly based multidisciplinary program of scientific and advanced technological development directed toward maritime applications of new and improved materials, techniques, equipment, systems, and ocean, atmospheric, and space sciences and related technologies.

The Naval Research Laboratory provides primary in-house research for the physical, engineering, space, and environmental sciences; broadly based applied research and advanced technology development programs in response to identified and anticipated Navy and Marine Corps needs; broad multidisciplinary support to the Naval Warfare Centers; and space and space systems technology, development, and support.

View from the Top

from the Commanding Officer and Director of Research



CAPT Daniel R. Gahagan
Commanding Officer



Dr. John A. Montgomery
Director of Research

Before losing his long battle with cancer in 2005, VADM Arthur K. Cebrowski was one of the U.S. military's most respected advocates for technological innovation. As director of DoD's Office of Force Transformation, he championed the development of revolutionary new capabilities, such as Operationally Responsive Space. NRL's micro-satellite, TacSat, is the first experiment in that initiative. VADM Cebrowski believed that,

“... our security and the prospects for peace and stability for much of the rest of the world depend on the success of our transformation.” [Military Transformation, 2003]

In this year's View From the Top, we want to focus on one area, among the many, in which the Naval Research Laboratory (NRL) is working to achieve force transformation – the Electric Ship. This platform will revolutionize the Navy's war-fighting capabilities. To help achieve that goal, NRL is focusing its scientific and engineering efforts on four technologies: Superconducting Motors, Power Electronics, Laser Weapons, and the Electromagnetic Railgun.

Superconducting Motors

Electric motors for ship propulsion require power densities two to three times that of today's motors and will need the properties offered by superconducting materials. Superconducting wire can be used to generate large magnetic fields, with no electrical loss, in order to excite the motor's rotor coils. This unique ability (zero electrical resistance) of superconductive materials can allow the development of motors that are one-half the size and one-third the weight of conventional motors, thus meeting the high power density requirement and increasing the overall efficiency of the motor.

To achieve this goal, the rotor magnet must withstand both the mechanical torque generated by the motor and the rotational and cyclic forces from motor operation — over the full 30 years or so the typical Navy ship stays in use. NRL, in close collaboration with the Office of Naval Research and industry partners, has played an important role in developing the stress-strain-fatigue tolerances of the superconducting wire prior to design of the Navy's first full-scale superconducting propulsion motor. NRL's work led to a high-strength design of the superconducting wire and set key mechanical tolerance specifications for the rotor magnet itself. Future work will explore new superconducting materials and wire configurations to expand the use of superconducting technology to future Naval applications.



Power Electronics

High-performance, high-voltage silicon carbide (SiC) switches offer the potential for a significant reduction in weight, volume, and thermal dissipation for power converters used in electric-drive propulsion, ship-service machinery, weapons, directed energy, defense systems, radar, and acoustic sensors. Their high switching frequency can provide further reductions to the weight and volume of capacitors and inductors, and their low switching loss will yield increases in conversion efficiency, significantly reducing heat-exchanger volume. Finally, the high-temperature properties of SiC will enable the use of forced air cooling for the motors used to drive the Advanced Gun System.

NRL is focused on improving the reliability, yield, and performance of high-voltage silicon and silicon carbide power switches. Scientific and technological issues being investigated include characterizing defects in SiC material; identifying the mechanism by which defects affect the reliability, yield, and performance of SiC devices; developing SiC epitaxial growth technology to minimize defects; and developing novel SiC devices with improved performance and improved reliability.

Laser Weapons

Electrically driven, ultra-high-power solid-state lasers are one of the more promising technologies for rapid response shipboard defense against potential missile attacks. A new approach to scaling laser system power that is based on combining noncoherently the outputs of high-power fiber lasers is being explored at NRL.

Another approach to achieving high laser power is the Radiation Balanced Laser. It offers a revolutionary change in the way that lasers can be scaled and provides a means of combining the power of many conventional lasers into a single ultra-high-power beam. It incorporates fluorescent cooling directly into the laser medium, which dramatically reduces the detrimental heating that limits the power output of solid-state lasers. The approach holds the potential

for a 100-fold increase in state-of-the-art laser power. The characteristics of this system also make it ideal for operation aboard the Electric Ship. Among these are compactness, low cooling requirements, low maintenance, long lifetime, and low operating cost.

The Electromagnetic Railgun

The railgun would use electric power to launch precision-guided munitions from a 12-m long barrel, at 2.5 km/s (Mach 7), with a range of 200 nautical miles, from a sea-based platform. Flight times of 5 to 7 minutes make it a rapid response weapon for long-range fire support of littoral combat operations. Low-cost projectiles would allow deep magazines for high volume of fire and significantly ease design constraints on the launch platform.

NRL is focusing its research on railgun bore science and engineering. A railgun operates by the flow of large currents through an armature sliding between two conducting rails that form the gun's bore. The interaction of the sliding armature and the rail can result in severe damage to the conducting rails. Heating at the interface leads to local softening or melting of the materials, which can deform or erode surfaces and limit the life of the bore. To understand these scientific issues better, NRL has performed post-shot analyses of bore materials and built a moderate energy railgun that is coupled to a modeling and simulation capability.

NRL's science and technology contributions are crucial to bringing the Electric Ship to fruition. This ship is a large step toward achieving the force transformation envisioned by VADM Cebrowski.

contents

NRL's Involved!

- 3** Our People Are Making a Difference
- 7** VXS-1 – Scientific Development Squadron One
- 11** NRL's Contributions to Fighting the Global War on Terrorism
- 16** NRL's GelMan Technology
- 18** ONR and NRL Receive Meritorious Unit Commendation

The Naval Research Laboratory

- 21** NRL – Our Heritage
- 22** 2006 in Review
- 26** NRL Today
- 51** The Corporate Facilities Investment Plan

Featured Research

- 55** Optical Guidance for Shoreline-Following UAVS
B. Kamgar-Parsi, P. Baker, A. Kahn, and J. Kellogg
- 63** Reducing Corrosion Control Costs with Rapid-Cure Coatings
A.A. Webb, J. Verborgt, J.R. Martin, W. Groeninger, P.F. Slebodnick, K.E. Lucas, and E. Hogan
- 73** NRL Launches SiC Epitaxial Growth Effort for Future Power Systems
C.R. Eddy, Jr., D.K. Gaskill, K.-K. Lew, B.L. VanMil, R.L. Myers-Ward, and F.J. Kub
- 83** Vega is a Rapidly Rotating Star
T.A. Pauls and D.M. Peterson
- 89** Advanced Surge and Inundation Modeling: A Case Study from Hurricane Katrina
C.A. Blain, T.C. Massey, J.D. Dykes, and P.G. Posey
- 99** By the Light of the Sea
S.D. Miller, S.H.D. Haddock, T.F. Lee, and C.D. Elvidge
- 107** A Multi-Sensor Aerogeophysical Study of Afghanistan
J. Brozena, V. Childers, J. Gardner, R. Liang, J. Jarvis, and J. Bowles

Acoustics

- 121** Modeling Reverberation Time Series for Shallow Water Clutter Environments
K.D. LePage
- 125** Remote Intense Laser Acoustic Source
T.G. Jones, A. Ting, J. Peñano, P. Sprangle, and L.D. Bibee
- 127** Fiber Optic Towed Arrays
C. Kirkendall, T. Barock, A. Tveten, and A. Dandridge

Atmospheric Science and Technology

- 133** The Terrain-Induced Rotor Experiment (T-REX)
J.D. Doyle and V. Grubišić
- 136** Polar Clouds from Space Shuttle Exhaust
M.H. Stevens and C.R. Englert
- 137** An Advanced Framework for Battlespace Environment Data Assimilation
L. Xu, T. Rosmond, N. Baker, and J. Goerss
- 139** Understanding and Forecasting the Sun's Impact on the Battlespace Environment
J.L. Lean, J.M. Picone, J.T. Emmert, and J.P. Dahlburg
- 142** Understanding the Effect of Atmospheric Turbulence on Optical and Infrared Propagation using Hilbert Phase Analysis
C. Font, G.C. Gilbreath, M.P.J.L. Chang, and E.S. Oh

Chemical/Biochemical Research

- 147** Polymeric Protection of Navy Fighter Jet Towlines
M.K. Kolel-Veetil and T.M. Keller
- 148** Single-Domain Antibodies: Rugged Recognition Elements
E.R. Goldman, J.L. Liu, J.B. Delehanty, G.P. Anderson, and A. Hayhurst

Electronics and Electromagnetics

- 153** Numerical Analysis of Electromagnetic Bandgap Structures
S.-T. Chun and R.S. Schechter
- 155** Broadband Over Power Lines (BPL) and Its Impact on Spectrum Allocation
L.S. Cohen and A. Light
- 156** Near-Earth Radio Frequency Propagation
R.A. Wert and A.K. Goroch
- 159** Unmanned Sea Surface Vehicle Electronic Warfare
D. Tremper and J. Heyer

Information Technology and Communications

- 165** High Altitude Relay and Router
M. Rupar, J. Doffoh, and R. Mereish
- 167** Comprehensive Maritime Awareness (CMA) Joint Capabilities Technology Demonstration (JCTD)
C.T. Dwyer
- 169** Efficient Linearization of Microwave Power Amplifiers
J.X. Qiu, D.K. Abe, T.M. Antonsen, Jr., B.G. Danly, B. Levush, and R.E. Myers

Materials Science and Technology

- 175 Initial Microstructural Evolution during Friction Stir Welding**
R.W. Fonda, J.A. Wert, A.P. Reynolds, and W. Tang
- 177 3D Unsteady Computations of Flapping Flight in Insects and Fish**
R. Ramamurti and W.C. Sandberg
- 180 Highly Efficient Surface Enhanced Raman Scattering (SERS) Nanowire/Ag Composites**
S.M. Prokes, O.J. Glembocki, and R.W. Rendell

Ocean Science and Technology

- 185 Measuring Undersea Noise from Breaking Waves**
S.L. Means and M.A. Sletten
- 187 Real-Time Coastal Monitoring and Prediction for Operations and Research**
J.W. Book, P. Martin, M. Rixen, J. Dykes, D. Wang, S. Ladner, M. Tudor, and J. Chiggiato
- 191 A Roughness Estimation Algorithm for Sidescan**
M.L. Gendron, M.C. Lohrenz, G. Layne, and J. Sample

Optical Sciences

- 195 Distributed Fiber Optic Sensing for Homeland Security**
C.K. Kirkendall, R. Bartolo, J. Salzano, and K. Daley
- 196 Transduction of the Spin State Variable Between the Electron and Optical Polarization at Zero Magnetic Field**
A.T. Hanbicki, O.M.J. van 't Erve, G. Kioseoglou, C.H. Li, and B.T. Jonker
- 199 Optical Manipulation of Ultracold Atoms**
F.K. Fatemi and M. Bashkansky
- 201 Real-Time Fleet Protection**
L.N. Smith and J.R. Waterman

Remote Sensing

- 207 Pyroconvection and Climate Change**
M. Fromm, S. Miller, J. Turk, and T. Lee
- 208 Joint Demodulation of Low-Entropy Narrowband Cochannel Signals**
T. Meehan, F. Kragh, and K. Clark
- 211 Remotely Measuring Turbulent Coastal Atmospheres**
W.P. Hooper, G.M. Frick, B.P. Michael, and R.J. Lind

Simulation, Computing, and Modeling

- 217 Impact of Uncertainty on Terror Forecasting**
G.S. Schmidt, J. Goffeney, and R. Willis

- 219 IR Photonic Bandgap Fibers for Missile Defense**

I.D. Aggarwal, J.S. Sanghera, D. Gibson, F. Kung, L.E. Busse, L.B. Shaw, V.Q. Nguyen, and P.C. Pureza

- 221 Computational Materials Theory: Optimizing the Use of the Electromagnetic Spectrum**
M.R. Pederson, M.J. Mehl, and L.L. Boyer

Space Research and Satellite Technology

- 227 On-Orbit Microwave Curing of Space Shuttle Repair Materials**
A.W. Fliflet, M.T. Lombardi, S.H. Gold, D. Lewis III, R.W. Bruce, and A.K. Kinkead
- 229 The STEREO Mission: A Three-Dimensional View of the Sun and Heliosphere**
J.W. Cook, J.S. Newmark, and R.A. Howard
- 232 The NRL Precision Orbital Transfer Vehicle**
M.S. Johnson, S.R. Morgan, W.S. Vincent, K.H. Gallelli, B.P. Whalen, A. Hope, S.S. Chappie, and R.G. Skalitzky

Special Awards and Recognition

- 239 Special Awards and Recognition**
- 256 Alan Berman Research Publication and Edison (Patent) Awards**

Programs for Professional Development

- 263 Programs for NRL Employees — Graduate Programs, Continuing Education, Professional Development, Equal Employment Opportunity (EEO) Programs, and Other Activities**
- 265 Programs for Non-NRL Employees — Recent Ph.D., Faculty Member, and College Graduate Programs, Professional Appointments, and College and High School Student Programs**

General Information

- 269 Technical Output**
- 270 Key Personnel**
- 271 Contributions by Divisions, Laboratories, and Departments**
- 274 Subject Index**
- 278 Author Index**
- 279 Employment Opportunities**

NRL'S INVOLVED!





- 3 Our People Are Making a Difference**
- 7 VXS-1 – Scientific Development Squadron One**
- 11 NRL’s Contributions to Fighting the Global War on Terrorism**
- 16 NRL’s GelMan Technology**
- 18 ONR and NRL Receive Meritorious Unit Commendation**

VXS-1

SCIENTIFIC DEVELOPMENT
SQUADRON ONE





VXS-1 – dedicated to scientific and technology research

On February 18, 2005, the former Flight Support Detachment (NRL FSD) was established as a Navy squadron and renamed Scientific Development Squadron One (VXS-1). Today VXS-1 is the Navy's only squadron dedicated to scientific and technology research. VXS-1 is stationed at Naval Air Station Patuxent River, Maryland, and is manned by approximately 12 officers, 84 enlisted, and 8 civilians, comprising aircrew, maintenance, and administrative personnel. CDR Heidi Fleming and Executive Officer CDR Darrell Vance command the squadron and its five aircraft: two research-configured NP-3D's, one AEW-configured NP-3D, one RC-12C, and one RC-12M. All aircraft have been modified to easily accommodate the installation of equipment for scientific research projects.

VXS-1 provides airborne research platforms to conduct and support scientific research projects around the world. VXS-1 has flown research missions for many activities of the Department of the Navy, the Joint Armed Task Forces South (JATFS), the Nation-

al Science Foundation, the National Aeronautics and Space Administration (NASA), and the Department of Homeland Security. These agencies utilize the airborne research platforms to develop technologies that will support their missions well into the 21st century.

Projects flown on VXS-1 aircraft have taken the squadron throughout the world, to North and South America, Europe, the Middle East, Africa, Asia, and Russia. Investigation is currently under way into operating the NP-3D aircraft in Antarctica. The research conducted on these missions has included radio frequency and infrared anti-ship missile testing of Navy surface vessels, development of the synthetic/inverse synthetic aperture radars, geological surveys, oceanographic mapping, satellite communications, electro-optical science, and mapping of hazardous weather events including hurricanes and tornadoes. These and many other missions by VXS-1 help NRL provide cutting-edge science and technology research to the U.S. Navy.

VXS-1 has flown research missions for the Department of the Navy, the Joint Armed Task Forces South (JATFS), the Office of Naval Research, the National Science Foundation, the National Aeronautics and Space Administration, and the Department of Homeland Security.



VXS-1 DEPLOYMENT LOCATIONS

Christmas Island, Australian Territory
 Diego Garcia, British Indian Ocean Territory
 Grand Caymans, British Overseas Territory
 Afghanistan
 Argentina
 Brunei
 Goose Bay, Canada
 Puerto Montt, Chile
 Denmark
 Bali, Indonesia
 Iwakuni, Japan
 Misawa, Japan
 Kazakhstan
 Kuala Lumpur, Malaysia

Kadena, Okinawa
 Pakistan
 Manila, Philippines
 Puerto Rico
 Singapore
 Utopao, South Korea
 Phuket, Thailand
 Pattaya Beach, Thailand
 Anchorage, Alaska
 Elmendorf AFB, Alaska
 Tucson, Arizona
 North Island, California
 Point Mugu, California
 Boulder, Colorado

Eglin AFB, Florida
 Pensacola, Florida
 Tampa, Florida
 West Palm Beach, Florida
 Fort Benning, Georgia
 Kaneohe Bay, Hawaii
 Des Moines, Iowa
 Boston, Massachusetts
 St. Louis, Missouri
 Great Falls, Montana
 Kirtland AFB, New Mexico
 Corpus Christi, Texas
 Norfolk, Virginia
 Whidbey Island, Washington



NP-3D AEW with dome – This P-3 at VX-1 is modified with the APS-145, or Hawkeye 2000, airborne early warning (AEW) system commonly found on the Navy E-2 Hawkeye aircraft. This system makes the aircraft ideal for airborne surveillance and cooperative engagements. The aircraft is currently used on a regular basis by the Missile Defense Agency in operations out of Hawaii.

The Squadron's five aircraft have been modified to accommodate custom equipment for scientific research projects...



NP-3D AEW – VX-1 owns two research-modified NP-3D aircraft that can deploy around the world. These are identical to the Navy's submarine-hunting aircraft on the outside, but all internal non-flight systems have been removed. The inside of the plane has been modified to accommodate a wide range of scientific equipment. This makes the aircraft an ideal airborne laboratory for scientists at the Naval Research Laboratory and at other government agencies. The P-3 is normally operated by a crew of three pilots, two flight engineers, and a navigator.

C-12 – VX-1 has one RC-12M and one RC-12C that have also been modified to fly with scientific equipment. The C-12's are smaller project aircraft with approximately 4-hour flight durations and a flight crew of two pilots. They can carry less equipment and are far less expensive to operate.



NRL'S CONTRIBUTIONS TO FIGHTING THE **Global War on Terrorism**

NRL is on the front lines in the Global War on Terrorism. From forward-looking research to applied technologies in use by our military forces and civilians right now, NRL is supporting the fight. The following are just a few examples of NRL contributions.



SYSTEMS

NAVIS

Digital reconnaissance cameras require an image screening station capable of displaying a real-time montage or waterfall of the camera output together with a simultaneous display of selected frames or regions of interest. The NAVy Input



Station (NAVIS) accepts image data in standard formats with two displays, providing the capability to

roam, zoom, crop, generate latitude and longitude, and take measurements. A portable version has been developed for use by ground forces.

AAR-47

The AAR-47 missile warning system operates in the ultraviolet region, detecting the emissions from the missile rocket plume. A signal



is automatically sent to a counter-measure system when a threat is declared. Nearly 2,000 of these systems have been deployed, primarily in Marine Corps helicopters.

HSV-X1

The *Joint Venture* (HSV-X1) project explores the concepts and capabilities of advanced hull and propulsion technologies with advanced communications technology. NRL's Transmission Technology Branch designed, installed, and supported a Ku-band satellite communications capability and an entire shipboard network infrastructure and its integration into the DoD/NIPR/SIPR networks. The group was also responsible for developing the land-based hub terminal and network. Recently, *Joint Venture* participated in the congressionally mandated Millennium Challenge 2002 and was deployed in support of Operation Iraqi Freedom as an Afloat Forward Staging Base for Naval Special Forces.



SHARP

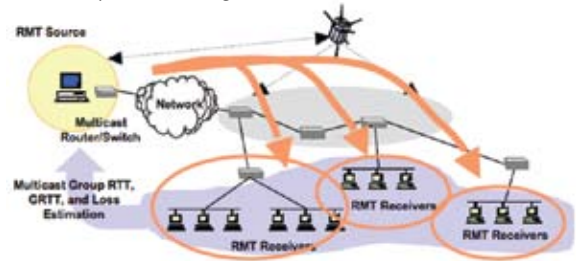
The SHARED Reconnaissance Pod (SHARP) is a digital reconnaissance system that replaces the film-based Tactical Airborne Reconnaissance Pod system. SHARP provides visible and infrared digital imagery from cameras with a medium-altitude and high-altitude capability. A data link and onboard digital recording provide the means for delivering the imagery.



Reliable Multicast Technology

The NRL Multicast Dissemination Protocol (MDP) provides reliability at a higher (transport) protocol layer, making novel use of Forward Error Correction (FEC). Parity packets are sent in response to receiver requests for repair, proactively to support EMCOM, or in a hybrid fashion. MDP parity packets can repair lost

user data more efficiently than resending original data.



NRL IS SUPPORTING THE FIGHT...

MATERIALS SCIENCE AND COMPONENT TECHNOLOGY

Nimbus

Nimbus is an engineering testbed for the hardware and software integration of several



key technologies for the support of low-power unattended ground-based intelligence, surveillance, and reconnaissance (ISR) in remote locations. The heart of the system is the low-power embedded computer vision system that can track and identify targets while selecting imagery for near real-time up-link to any computer that has access to the Internet.

CASPAR

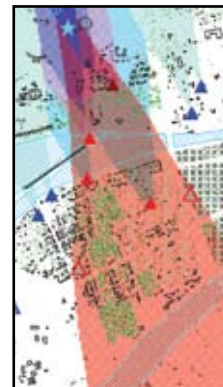
CASPAR (Cascade Avalanche Sorbent Plate Array) is a micromachined preconcentrator that has been successfully demonstrated to enhance trace detection for chemical agents



and explosives on more than 10 commercial and prototype detectors. CASPAR has the ability to selectively collect and concentrate the vapors of illicit substances due to its coating of NRL-developed sorbent polymer.

CT-Analyst™

CT-Analyst™ provides accurate, instantaneous, 3D predictions of chemical/biological/radiological (CBR) agent transport in urban settings. It performs instant sensor fusion for complex operations such as back-tracking to an unknown source location or computing personnel evacuation routes. CT-Analyst™ has “zero latency”—100 to 10,000 times faster than real time for instant visual interpretation and comprehension.



QuadGard

The QuadGard arm and leg protective armor are designed to counter injury and amputations from improvised explosive devices (IEDs). The QuadGard design protects 85% of the surface area of the arms and legs and is lightweight, flexible, compatible with weapons and other equipment, integrates with the soft outer tactical vest (OTV), cool enough to be worn in desert climate, and comfortable to increase acceptance by the individual Marines, sailors, soldiers, and airmen.



DE-ATR™

The Dragon Eye Advanced Tactical RECCE (DE-ATR™) performs real-time chemical agent detection and data transmission to ground stations. It collects biological agents



and performs ground-based bio-agent analysis in 30 to 45 minutes. Split sampling is performed for verification, forensics, or archival. Dragon Eye ATR™ successfully flew more than 30 recon missions during the conflict period in Operation Iraqi Freedom.

NQR

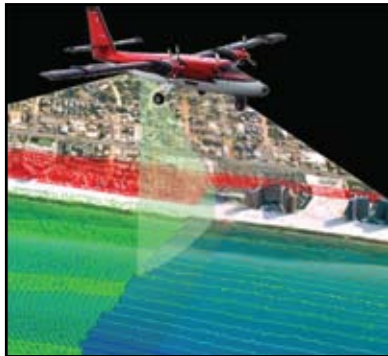
Nuclear Quadrupole Resonance (NQR) is used for detection of certain bulk explosives in baggage, packages, mail, and on personnel. Two QScan 160s were deployed and are in use in the National Capital Region.



OCEAN & ATMOSPHERIC SCIENCE AND TECHNOLOGY

Hyperspectral Remote Sensor

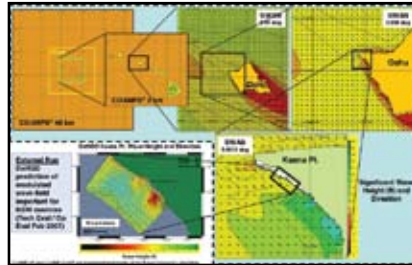
NRL is developing methods to use lidar and hyperspectral imagery together to address issues of



concern in the littoral areas of the world. Bathymetric lidar can return information on bathymetry and in-water and sea bottom characteristics. That information can then be used with the hyperspectral imagery to make more accurate determination of sea bottom type and water properties. This may also include identification of underwater hazards.

Battlespace Environmental Assessment

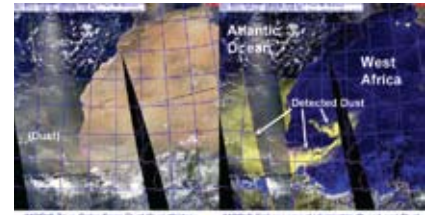
A coupled air-ocean-wave modeling system is being used to study and optimize air-sea coupled forecast and rapid environmental assessment (REA) methods in support of multiple warfare and mission areas. By leveraging expertise



in both oceanographic and atmospheric modeling, data analysis, data fusion, and data assimilation, we expect to determine the best method for applying disparate atmospheric and oceanographic measurements together to properly represent the state of the environment while minimizing initialization errors in the coupled data assimilation system.

MODIS

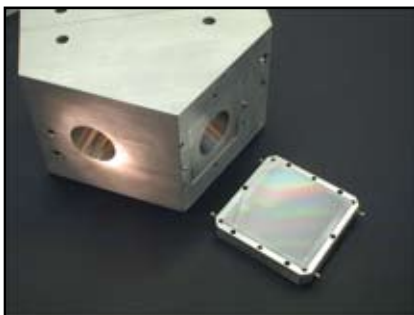
MODIS multispectral techniques enable the detection of dust plumes



over land that are otherwise invisible to the human eye. The MODIS dust enhancements are based on multi-channel techniques developed by the Marine Meteorology Division. The principles of detection include color discrimination between dust and clouds (blue light absorption), thermal contrasts (cooler airborne dust atop hot background surfaces), and infrared channel transparency differences (wavelength-dependent absorption characteristics). Dust concentrations can directly impact visibility that affects weapons and sensors onboard satellites, ships, fixed and rotary wing aircraft, and unmanned aerial vehicles (UAVs).

SHIMCAD

NRL is developing an intrinsically rugged, new type of long-wave infrared hyperspectral sensor for the measurement of anthropogenic atmospheric constituents. The long-wave infrared is a key spectral region (the so-called fingerprint region) for the detection of tropospheric trace gases. For this effort, NRL will use the innovative optical technique known as spatial heterodyne spectroscopy (SHS). Shown is the first Spatial Heterodyne Imager for Chemicals and Atmospheric

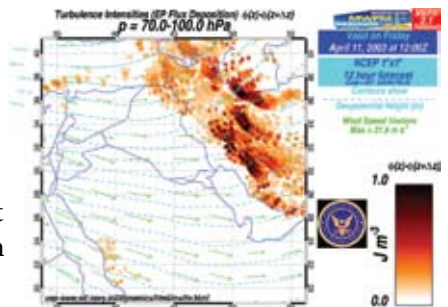


Detection (SHIMCAD) breadboard interferometer with its input port on the left and the end of one interferometer arm on the right, where the grating will be attached. The structure is fabricated with sufficient precision to avoid post-integration alignment.

MWFM

Forecasts of mountain-wave-induced turbulence over Iraq at U-2 and Global Hawk cruise

altitudes were generated daily at NRL in support of Operations Enduring Freedom and Iraqi Freedom. These requests come from Beale Air Force Base, home of the high-altitude U-2 and Global Hawk fleets. The Mountain Wave Forecast Model (MWFM) has recently been transitioned to the Air Force Weather Agency, where it now runs operationally.



NAVAL CENTER FOR SPACE TECHNOLOGY

InfraLynx

InfraLynx delivers a complete, interoperable communication infrastructure to support local, state, Federal, and DoD response to natural or man-made disasters. Using satellite communications and advanced networking, InfraLynx can augment or replace communications with 96 voice circuits (telephone lines), micro-cell cellular base station, wired and wireless network access, broadcast quality video, and land mobile radios all integrated together on a converged network for transport to any commercial/DoD teleport.

**4-Way Voice Access Unit**

Prior to deployment of the 4-Way Voice Access Unit, the Marine commander had one handset for each radio network monitored. This approach did not allow the commander to monitor multiple radios simultaneously. The 4-Way Access Unit now allows the commander to simultaneously interact on four networks with a single handset. The unit is compatible with all standard military radios and handsets and is supplied with an under-the-helmet headset microphone. Weighing less than 2 lb and requiring no power, this rugged unit has full military temperature range and sealed components.

**Comprehensive Maritime Awareness Scenario**

Effective maritime security and homeland defense relies on ensuring maritime shipping is not used to transport WMD, other terrorist mechanisms, or terrorists themselves. Since economic requirements mandate the rapid flow of goods, the U.S. can interdict and inspect only a fraction of all inbound maritime traffic due to resource limitations and the sheer volume of maritime shipping into its ports. This is a global challenge. NRL is engaged in developing a framework, automated tools, and information sharing liaisons that will deliver a dramatic increase in the U.S. ability to provide timely and accurate maritime situational awareness.



NRL's

GelMan

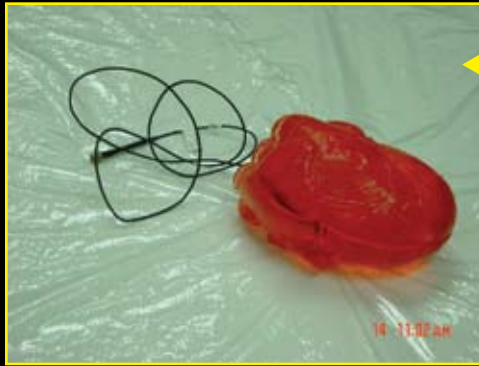
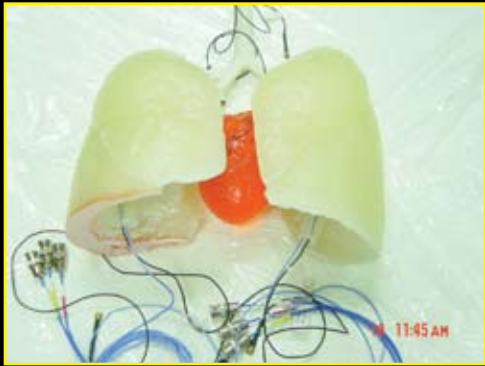
TECHNOLOGY

Combat casualties

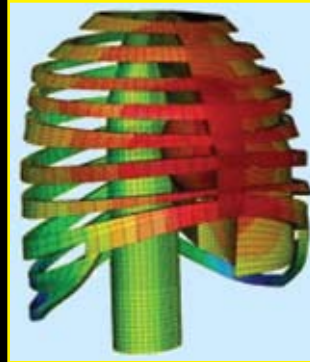
are often the result of blast pressure, high-velocity ballistic impact from small arms fire or blast fragments, or low-velocity impact with an object such as a building wall or vehicle interior. The specific weapons producing these threats to Marines and soldiers may change over time, but what remains the same is the need to understand the dynamic responses in the body that lead to injuries, and to prevent these injuries with personal protective equipment and operational tactics.

NRL's Materials Science and Technology Division plays a role in both of these areas by developing instrumented measurement devices that act as human surrogates in blast and ballistic test environments. The NRL "GelMan" technology reproduces the properties of human tissues with unique simulant materials, fabricates simulated organs, places sensors at critical locations in the surrogate devices, and integrates the entire system to record and analyze the dynamic responses to blast pressure and impacts.

Initial development of torso surrogates for blast pressure has been followed by development of additional specialized torso devices to measure behind-armor effects and underwater environments, head surrogates to address traumatic brain injury, and arm and leg surrogates to address extremity wounds. These devices are designed to complement the growing body of military medical knowledge, and translate this information into new and more effective design solutions for body armor vests and helmets.

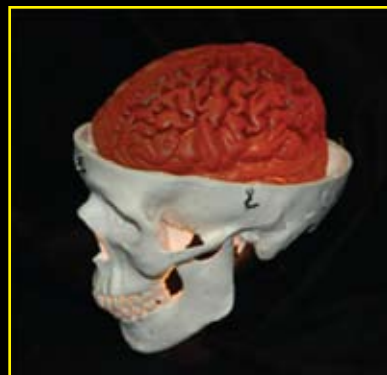


Simulated organs, such as the lungs and heart, are embedded with motion and pressure sensors to record dynamic responses.



Computational simulations are used to simulate dynamic response and integrate the GelMan components.

GelMan torso measurement systems assess pressure transmission directly into the body, and through body armor into the body.



Surrogate materials and sensors are incorporated into the GelMan-Brain measurement systems to quantify headborne protective equipment performance with the aim of reducing traumatic brain injury.

ONR and NRL receive MERITORIOUS UNIT COMMENDATION



THE SECRETARY OF THE NAVY

WASHINGTON, D.C. 20350-1000

The Secretary of the Navy takes pleasure in presenting the
MERITORIOUS UNIT COMMENDATION to

OFFICE OF NAVAL RESEARCH AND NAVAL RESEARCH LABORATORY

for service as set forth in the following

CITATION:

For meritorious service from 11 September 2001 to 30 September 2005. The personnel of the Office of Naval Research (ONR) and Naval Research Laboratory (NRL) distinguished themselves by their outstanding record of accomplishments and delivery of key technology to the Department of Defense Warfighters and First Responders. Immediately following the terrorist attacks of 11 September 2001, ONR and NRL established an Emergency Response Cell that worked closely with the Combating Terrorism Technology Task Force to rapidly provide today's advanced technology to our Sailors and Marines fighting the Global War on Terrorism. During this period, more than 50 technology solutions were delivered in support of Operations ENDURING FREEDOM and IRAQI FREEDOM. ONR and NRL's ability to swiftly respond to emerging requirements, while maintaining a long-term basic research and focus provided research solutions to today's problems while ensuring our Armed Forces of the future remain the most technologically superior in the world. By their outstanding level of scientific leadership, unwavering commitment to excellence, and exemplary performance of duty, the officers, enlisted personnel, and civilian employees of the Office of Naval Research and Naval Research Laboratory reflected credit upon themselves and upheld the highest traditions of the United States Naval Service.


Secretary of the Navy



Awarded in 2006 for meritorious service from September 11, 2001 to September 30, 2005.

THE NAVAL RESEARCH LABORATORY





- 21** **NRL – Our Heritage**
- 22** **2006 in Review**
- 26** **NRL Today**
- 51** **The Corporate Facilities Investment Plan**

NRL — OUR HERITAGE

The Naval Research Laboratory (NRL), the first modern research institution created within the United States Navy, began operations in 1923.

Thomas Edison’s Vision: The first step came in May 1915, a time when Americans were deeply worried about the great European war. Thomas Edison, when asked by a *New York Times* correspondent to comment on the conflict, argued that the Nation should look to science. “The Government,” he proposed in a published interview, “should maintain a great research laboratory....In this could be developed...all the technique of military and naval progression without any vast expense.” Secretary of the Navy Josephus Daniels seized the opportunity created by Edison’s public comments to enlist Edison’s support. He agreed to serve as the head of a new body of civilian experts—the Naval Consulting Board—to advise the Navy on science and technology. The Board’s most ambitious plan was the creation of a modern research facility for the Navy. Congress allocated \$1.5 million for the institution in 1916, but wartime delays and disagreements within the Naval Consulting Board postponed construction until 1920.

The Laboratory’s two original divisions—Radio and Sound—pioneered in the fields of high-frequency radio and underwater sound propagation. They produced communications equipment, direction-finding devices, sonar sets, and perhaps most significant of all, the first practical radar equipment built in this country. They also performed basic research, participating, for example, in the discovery and early exploration of the ionosphere. Moreover, the Laboratory was able to work gradually toward its goal of becoming a broadly based research facility. By the beginning of World War II, five new divisions had been added: Physical Optics, Chemistry, Metallurgy, Mechanics and Electricity, and Internal Communications.

World War II Years and Growth: Total employment at the Laboratory jumped from 396 in 1941 to 4400 in 1946, expenditures from \$1.7 million to \$13.7 million, the number of buildings from 23 to 67, and the number of projects from 200 to about 900. During WW II, scientific activities necessarily were concentrated almost entirely on applied research. New electronics equipment—radio, radar, sonar—was developed. Countermeasures were devised. New lubricants were produced, as were antifouling paints, luminous identification tapes, and a sea marker to help

save survivors of disasters at sea. A thermal diffusion process was conceived and used to supply some of the ^{235}U isotope needed for one of the first atomic bombs. Also, many new devices that developed from booming wartime industry were type tested and then certified as reliable for the Fleet.

NRL Reorganizes for Peace: Because of the major scientific accomplishments of the war years, the United States emerged into the postwar era determined to consolidate its wartime gains in science and technology and to preserve the working relationship between its armed forces and the scientific community. While the Navy was establishing its Office of Naval Research (ONR) as a liaison with and supporter of basic and applied scientific research, it was also encouraging NRL to broaden its scope and become, in effect, its corporate research laboratory. There was a transfer of NRL to the administrative oversight of ONR and a parallel shift of the Laboratory’s research emphasis to one of long-range basic and applied investigation in a broad range of the physical sciences.

However, rapid expansion during the war had left NRL improperly structured to address long-term Navy requirements. One major task—neither easily nor rapidly accomplished—was that of reshaping and coordinating research. This was achieved by transforming a group of largely autonomous scientific divisions into a unified institution with a clear mission and a fully coordinated research program. The first attempt at reorganization vested power in an executive committee composed of all the division superintendents. This committee was impracticably large, so in 1949, a civilian director of research was named and given full authority over the program. Positions for associate directors were added in 1954.

The Breadth of NRL: During the years since WW II, the areas of study at the Laboratory have included basic research concerning the Navy’s environments of Earth, sea, sky, and space. Investigations have ranged widely—from monitoring the Sun’s behavior, to analyzing marine atmospheric conditions, to measuring parameters of the deep oceans. Detection and communication capabilities have benefitted by research that has exploited new portions of the electromagnetic spectrum, extended ranges to outer space, and provided a means of transferring information reliably and securely, even through massive jamming. Subma-

rine habitability, lubricants, shipbuilding materials, firefighting, and the study of sound in the sea have remained steadfast concerns, to which have been added recent explorations within the fields of virtual reality, superconductivity, biomolecular science and engineering, and nanotechnology.

The Laboratory has pioneered naval research into space—from atmospheric probes with captured V-2 rockets, through direction of the Vanguard project (America’s first satellite program), to inventing and developing the first satellite prototypes of the Global Positioning System (GPS). Today, NRL is the Navy’s lead laboratory in space systems research, fire research, tactical electronic warfare, microelectronic devices, and artificial intelligence.

The consolidation in 1992 of NRL and the Naval Oceanographic and Atmospheric Research Laboratory, with centers at Bay St. Louis, Mississippi, and Monterey, California, added critical new strengths to the Laboratory. NRL now is additionally the lead Navy center for research in ocean and atmospheric sciences, with special strengths in physical oceanography, marine geosciences, ocean acoustics, marine meteorology, and remote oceanic and atmospheric sensing. Although not abandoning its interests in blue-water operations and research, the Navy is also focusing on defending American interests in the world’s littoral regions. NRL scientists and engineers are working to give the Navy the special knowledge and capabilities it needs to operate in these waters.

2006 IN REVIEW

The scientific community at NRL conducts innovative research across a wide spectrum of technical areas, much of it detailed in the *NRL Review* chapters ahead. The following brief vignettes present a selection of the many projects pursued in 2006.

Cryptographic Modernization Initiative: The Department of Defense Cryptographic Modernization Initiative (CMI) is an effort to transform and modernize Information Assurance (IA) capabilities for the 21st century. The CMI focus is on the replacement of obsolete algorithms. NRL has developed a new family of cryptographic engines: the Programmable Embeddable Information Security (INFOSEC) Product (PEIP). The PEIP Phase II (PEIP-II) is a programmable cryptographic engine that is key-, algorithm-, and mission-agile, and has the ability to perform software-based cryptographic applications. Its secure hardware and software architecture permits up to ten cryptographic applications to be performed independently and securely. It is an enabling technology for DoD’s Cryptographic Modernization Initiative.

Counterinsurgency Pattern Assessment: The NRL modeling program ORION™ provides a capability for spatial forecasting of insurgent and terrorist events using statistical pattern recognition approaches. The key innovation is its robust spatial data analytics that process hundreds of spatial variables to build a mathematical representation of the location of previously observed events, then project that model onto future ground conditions to find the greatest probability match for a particular problem. A signature can be generated for any set of spatial data across any local, state, or national landscape. ORION™ forecasting abilities

can be used to improve force protection by providing a basis for hardening physical facilities and security using reliable vulnerability assessment. This can significantly reduce terrorist threats and potential damage to personnel and facilities.

Cat’s Eye Modulating Retro-Reflectors for Optical Communications: On small platforms with weight and power limitations, such as UAVs, a modulating retro-reflector (MRR) optical link can be used for free-space optical communication. MRR systems couple passive optical retro-reflectors with electro-optic modulators to allow long-range, free-space optical communications with a laser and pointing/acquisition/tracking system required on only one end of the link. NRL has developed the concept of a cat’s eye MRR, which uses mirrors and lenses rather than prisms. By placing an array of small modulators in the focal plane of a cat’s eye, a large optical aperture can be obtained while still using low-capacitance modulators. A custom diffraction-limited cat’s eye optic was designed, fabricated, and integrated with a coupled quantum well modulator array. The 45-Mbps 7-km link and the 5-Mbps 16-km link obtained during testing are the longest-range high-speed retro-reflecting links ever demonstrated. The cat’s eye is about the size of a camera lens and draws about 1 watt of power.

MATADOR Mars Aerial Vehicle: For planetary exploration, aircraft-based sensors can cover a much greater surface area than rovers, at a much greater resolution than orbiting platforms, and with a flight path control not possible using balloon systems. Ground aircraft operations require prepared launch sites, not normally available for extraterrestrial mis-

sions, but atmospheric deployment techniques eliminate the need for surface launch sites. The MATADOR (Mars Advanced Technology Airplane for Deployment, Operations, and Recovery) aircraft configuration was developed specifically for the constraints of an extra-terrestrial exploration aircraft using an atmospheric entry deployment. It has completed simulation and wind tunnel testing to validate the unique high-angle-of-attack airborne deployment approach. The highly swept folded delta wing configuration coupled with a pitch-up thruster allows a non-parachute-assisted deployment and “pull-out” maneuver. A high-durability airframe allows for survival of the sensor and communications systems after landing.

Pentacene and Silole Derivatives as New Electro-active Materials: NRL materials scientists have been working to discover and establish new materials with electronic, optical, and carrier transport properties and to relate their properties to the arrangement of molecules in the solid state. Two classes of organic molecules have emerged as new electro-active materials with intense solid-state fluorescence and good electron transport properties. Crystal structure analyses by X-ray diffraction techniques have established an unusual and unexpected aggregation motif for the molecules in the solid state. The molecular structure on an atomic scale and the precise arrangement of the molecules in the crystals have been established for tetramethoxy-spiro-silabifluorene and bis(dimethyl phenyl) pentacene in crystals grown at highly elevated temperatures. The crystal structure information shows directly how the individual molecules are attracted to each other and indicates the probable path for electron transfer/mobility.

Channel-forming Peptides in Sensors: The β helix is unusual among peptide structures in that the adjacent amino acids that make up the peptide strands look like mirror images of one another. In molecules longer than about six amino acids, this causes a twisting action, which causes the peptide to form a helix with a hollow space running the length of the helical axis. These channel-forming peptides are being developed as alternatives to ion channel proteins for application in nanopore-based chemical and biological sensors. Channel-forming peptides offer thermodynamic stability and ease of synthesis, but have limitations caused by fluctuations in conformation and/or degree of oligomerization. An unprecedented nanoscale molecular architecture—a cyclic, double-stranded peptide helix having a well-defined conformation and oligomerization state—has been devised. The structure is formed by intertwining two linear peptide strands into a cyclic structure, thus constraining the peptides into a double-

stranded structure and preventing dissociation into single-stranded forms.

QuadGard Limb Protection against IEDs: The use of a soft outer tactical vest with hard ceramic plate inserts is standard equipment to protect the torso in combat operations. However, recent combat casualties include high incidences of limb amputations and serious injuries from improvised explosive devices (IEDs). Limb protection options were not available in the equipment inventory, except in ordnance disposal units. Thus, NRL led a team that designed and developed QuadGard arm and leg protective armor, incorporating extensive warfighter feedback. The QuadGard Phase V modular design protects 85% of the surface area of the arms and legs. It is lightweight (10 lb), flexible, compatible with weapons and other equipment, integrated with the soft tactical vest, cool enough to be worn in a desert climate, and comfortable so as to increase acceptance. The QuadGard Phase V system provides protection against small blast fragments at V50 velocities of almost 1800 ft/s and 9-mm small arms projectiles at over 1100 ft/s. The predicted benefits to the warfighter are a 13% reduction in fatalities and a 39% reduction in serious extremity injuries.

Electromagnetic Railgun Deformation: The electromagnetic railgun has the promise of providing high-velocity launch of kinetic-energy projectiles without the use of high explosives. To achieve this goal, however, a rail-armature system must be developed that provides thousands of launches on a single set of rails. To evaluate rail material deformation, armature material deposition, and rail surface erosion, profiles of both front and rear surfaces of rails were measured by optical profilometry at several locations along the length of a launcher. The rear surface profiles showed a double-hump deformation due to the magnetic pressure produced by the armatures. The results indicate that deposition of armature material on the rail initiated near the outer edges and progressed toward the rail center. In addition, grooves were seen near the outer edges of the rail and could be detected to nearly two-thirds the rail length. The maximum groove depth reached nearly 1 mm on the 20-shot rail. These results indicate that additional material and/or design developments are required to achieve the goal of an operational railgun that is capable of thousands of shots on a single set of rails.

Flapping Foil Propulsion: Flapping foil propulsion has received considerable attention in the past few years as an alternative to the propeller. It is possible to use flapping foil principles in ways that are inspired by biological flight mechanisms but do not copy them

directly. Unsteady computations of the hovering and maneuvering fruit fly *Drosophila* were performed to investigate the force production in the hovering insect and how subtle changes in wing kinematics lead to the yaw moment required for a turning maneuver. During the maneuver, the largest change between the right and left wings occurs in the stroke angle. These computations will enable development of controllers for unconventional vehicles with flapping wings.

Microwave Curing for Space Shuttle Repairs:

The loss on re-entry of the space shuttle *Columbia* because of damage to the reinforced carbon composite (RCC) wing leading edge showed a need for on-shuttle inspection and repair capabilities. An experimental microwave curing system for repairing damage to the space shuttle was designed and tested by NRL scientists with participation by astronaut James F. Reilly. This system incorporates a commercial off-the-shelf magnetron and power supply, standard S-band wave guide components, and a specialized applicator designed for sealing the applicator tip to a highly curved surface for repair curing. The tests showed that NOAX-repaired cracks in the RCC material could be heated to 800 °F in 5 minutes. Samples (cracks) cured in this way survived arcjet testing at temperatures up to 3000 °F. Both power and energy requirements for microwave curing are far lower than for other types of heat sources.

Optical Sensing and a New Dielectric/Silver Nanowire SERS Substrate: There is a current DoD emphasis on standoff chemical/biological/explosive agent sensing and covert tagging technologies. Optically based sensing can uniquely fingerprint a chemical compound, eliminating false alarms and simplifying the detection process. One promising technique is surface enhanced Raman scattering (SERS). Raman scattering is weak, but can be enhanced by the use of a metal nanoparticle surface, which can produce a vibrational fingerprint for trace amounts of material. All molecules that land on a SERS substrate experience the electronic component of the enhancement, and the intensity of the observed Raman spectra varies dramatically. A new SERS substrate material has been developed consisting of dielectric/metal composite nanowires arranged in a dense geometry. These nanowire composites have shown sensitivities (in the range of 0.2 picogram) one hundred times greater than commercial substrates.

Sequence-based Pathogen Identification: The purpose of this work was to develop methods for DNA microarray-based detection of environmental pathogens. NRL researchers have developed multi-pathogen identification systems using re-sequencing microarrays and computer algorithms for pathogen identification from partial sequence reads. An integrated system has

been demonstrated for performing genetic sequence-based identification of 25 different viral and bacterial pathogens and hundreds of near-neighbors from complex matrices at high sensitivity within 8.5 hours. This required the uniform isolation of both RNA and DNA pathogen gene targets, amplification of each target using a highly multiplexed reverse transcriptase-polymerase chain reaction (RT-PCR) process, and novel bioinformatics algorithms for unambiguous identification of pathogens based on database similarity metrics.

Measuring Ocean Surface Velocities: Ocean surface velocities are derived from sequential satellite images of the ocean surface. Present techniques employ information at the sea surface only: the velocity field is inferred from the apparent motion of features in IR imagery from one image to the next. A new technique has been developed that uses the equations of motion to constrain the surface velocities with the physics of the underlying water column, resulting in a substantial improvement in the accuracy of the remotely derived velocity field. When correlated with estimates of in situ velocity fields derived using coastal radar (CODAR) measurements, the present techniques give correlation coefficients for the velocity magnitudes on the order of 0.65 and average angular discrepancy of about 30 degrees, while the new technique gives average magnitudes with a correlation coefficient greater than 0.80 and an average velocity discrepancy of about 13 degrees.

Ocean Dynamics under Hurricane Ivan: A much improved understanding of currents, waves, and scour generated by Category 4 hurricanes has been accomplished from direct measurements taken by acoustic Doppler current profilers and wave/tide gauges located directly in the path of Hurricane Ivan, which hit the southeastern U.S. in 2004. Currents were observed to be frictionally dominated, with the strongest currents, transports, and temperature fluctuations generated to the left of the hurricane eye. Topographic Rossby waves with periods of two to five days were observed for the first time on the continental slope. A record surface wave height of 91 ft was measured and waves in excess of 130 ft were hypothesized. These waves and currents caused significant bottom scour at water depths of 90 m. These measurements under Hurricane Ivan form the best data set of current and wave measurements ever collected directly under a Category 4 storm on the outer continental shelf and slope, and will form the basis for future hurricane studies and modeling efforts.

COAMPS-OS® and the Centralized Atmospheric Analysis and Prediction System: The new Centralized Atmospheric Analysis and Prediction System (CAAPS)

hosted at Fleet Numerical Meteorology and Oceanography Center (FNMOC) implements the COAMPS-OS[®] software suite developed by NRL-Monterey. COAMPS-OS[®] is the Navy's on-scene weather prediction system, used daily in operations; it significantly enhances the capabilities of FNMOC to provide timely, high-resolution, mission-tailored atmospheric analyses and forecasts in reach-back mode. COAMPS-OS[®] includes eight web-based graphical user interfaces to configure the COAMPS[®] model and access the input and output data streams with a high degree of automation. It includes the database hooks and automated processing to visualize user-defined graphical products on the web, provide verification statistics on the web, perform file housekeeping and maintenance, and provide a web-based meta-monitoring system for remote administration and troubleshooting.

Low-Light Sensor Satellites and Milky Seas

Bioluminescence: Over the centuries, mariners have reported witnessing "milky seas"—incredible nocturnal displays in which the ocean gives off a glow of such intensity that it casts shadows on the ship's deck. For the first time, a milky sea phenomenon has been detected via low-light space sensors, a discovery bearing high interdisciplinary relevance to satellite remote sensing, atmospheric science, oceanography, and microbiology. Under the assumption that luminous bacteria were responsible for milky seas, laboratory cultures of bioluminescent bacteria were grown to record their spectrum and per-cell photon emission, to estimate the minimum population that would be detectable by the Operation Linescan System (OLS) sensor. Given the OLS minimum detectable power per unit area, the total equivalent bacteria per unit area was computed, and then the total population of the milky sea was extrapolated based on the satellite-observed glowing surface area. The figure of 4×10^{22} cells participating in this event is immense—roughly the same as the estimated total background free-living bacteria present in the upper 200 m of all the oceans worldwide.

Solar-B Extreme-ultraviolet Imaging Spectrometer: NRL is participating in the Japanese Solar-B (Hinode) Extreme-ultraviolet Imaging Spectrometer (EIS) solar physics space mission to investigate the interaction between the Sun's magnetic field and its corona. The Solar-B satellite was launched on September 23, 2006, from the Uchinoura Space Center

in Japan on the Japanese M-V rocket. Final orbit was obtained, and the EIS instrument front door was opened at the end of October 2006. NRL participated in launch operations, is participating in the post-launch instrument checkout, science planning, and observing, and will participate in the scientific analysis of the data. The understanding of solar activity will allow better prediction of adverse solar influences in the near-Earth environment.

Vessel Tracking Project: Ship tracking is vital to the U.S. Navy and the U.S. Coast Guard (USCG) since both services need the ability to know who is coming into their area of interest (AOI) long before they actually arrive. The objectives of the NRL/USCG Vessel Tracking Project (VTP) are to define and create an architecture that accesses all available current data applicable to ship tracking; to develop AOI sensors that will improve the ship knowledge base and extend the area of coverage; and to integrate all available data from existing sources/databases with data from these AOI sensors in a common distributed virtual database for use by the analysts. The initial project concept has defined the AOI to be a 200-mile radius around a port or harbor anywhere in the world. The prototype developed under VTP will be deployed at a selected site on the East Coast for integrated system demonstration and integrated system assessment.

Microsatellite Technology Experiment: The Microsatellite Technology Experiment (MiTeX) was a joint technology concept demonstration between government and industry to develop innovative satellites and launch technologies supporting DoD rapid and responsive access to space. The Upper Stage spacecraft, designed and built by NRL's Naval Center for Space Technology, was launched from Cape Canaveral on June 21, 2006. The Upper Stage spacecraft successfully completed its mission by transferring its payload of two small satellites from the launch vehicle insertion orbit to geosynchronous orbit. Then the spacecraft began a period of on-board subsystem and component characterization and continues to operate normally. The Upper Stage program has resulted in the design, manufacture, and flight demonstration of an innovative, prototype propulsion system. The Upper Stage provides the change in velocity (ΔV) and autonomous maneuvering capabilities needed to support a wide variety of emerging applications.

NRL TODAY

ORGANIZATION AND ADMINISTRATION

The Naval Research Laboratory is a field command under the Chief of Naval Research, who reports to the Secretary of the Navy via the Assistant Secretary of the Navy for Research, Development and Acquisition.

Heading the Laboratory with joint responsibilities are CAPT Daniel R. Gahagan, USN, Commanding Officer, and Dr. John A. Montgomery, Director of Research. Line authority passes from the Commanding Officer and the Director of Research to three Associate Directors of Research, the Director of the Naval Center for Space Technology, and the Associate Director for Business Operations. Research divisions are organized under the following functional directorates:

- Systems
- Materials Science and Component Technology
- Ocean and Atmospheric Science and Technology
- Naval Center for Space Technology.

The *NRL Fact Book*, published every two years, contains information on the structure and functions of the directorates and divisions.

NRL operates as a Navy Working Capital Fund (NWCF) Activity. All costs, including overhead, are charged to various research projects. Funding in FY06 came from the Chief of Naval Research, the Naval Systems Commands, and other Navy sources; government agencies, such as the U.S. Air Force, the Defense Advanced Research Projects Agency, the Department of Energy, and the National Aeronautics and Space Administration; and several nongovernment activities.

PERSONNEL DEVELOPMENT

At the end of FY06, NRL employed 2643 persons—35 officers, 76 enlisted, and 2532 civilians. In the research staff, there are 806 employees with doctorate degrees, 320 with master's degrees, and 442 with bachelor's degrees. The support staff assists the research staff by providing administrative support, computer-aided design, machining, fabrication, electronic construction, publication and imaging, personnel development, information retrieval, large mainframe computer support, and contracting and supply management services.

Opportunities for higher education and other professional training for NRL employees are available through several programs offered by the Employee Relations Branch. These programs provide for graduate work leading to advanced degrees, advanced train-

ing, college course work, short courses, continuing education, and career counseling. Graduate students, in certain cases, may use their NRL research for thesis material.

For non-NRL employees, several postdoctoral research programs exist. There are also agreements with several universities for student opportunities under the Student Career Experience Program (formerly known as Cooperative Education), as well as summer and part-time employment programs. Summer and interchange programs for college faculty members, professional consultants, and employees of other government agencies are also available. These programs are described in the *NRL Review* chapter "Programs for Professional Development."

NRL has active chapters of Women in Science and Engineering (WISE), Sigma Xi, Toastmasters International, and the Federal Executive and Professional Association. An amateur radio club, a drama group, and several sports clubs are also active. NRL has a Recreation Club that provides sports leagues and swim, whirlpool bath, gymnasium, and weight-room facilities. NRL also has an award-winning Community Outreach Program. See "Programs for Professional Development" for details on all these programs and activities.

NRL has an active, growing credit union. Since its creation in 1946, NRL Federal Credit Union (NRLFCU) has grown to about \$360 million in assets and serves about 22,000 NRL employees, contractors, select employee groups, and their families. Focusing its mission of *Trusted Partners for Life*, NRLFCU provides a wide array of no-fee services including free checking with free bill pay, as well as financial education and assistance such as the MyChoice program geared toward 16- to 24-year-old members, and webinars (seminars on the web) on timely financial topics. NRLFCU is a full-service financial institution offering various savings programs, creative lending services, and mortgage programs. NRLFCU also offers full-service investment and brokerage services. For information about membership or any financial services, call 301-839-8400 or click www.nrlfcu.org.

Public transportation to NRL is provided by Metrobus. Metrorail service is three miles away.

SITES AND FACILITIES

NRL's main campus in Washington, DC, consists of 85 main buildings on about 130 acres. NRL also maintains 11 other research sites, including a vessel for fire research and a Flight Support Detachment. The many diverse scientific and technological research and support facilities are described here.

RESEARCH FACILITIES

Institute for Nanoscience

The revolutionary opportunities available in nanoscience/nanotechnology have led to a National Nanotechnology Initiative. NRL has been a major contributor to the science of nanostructures and is making a commitment to expand that effort. The NRL Institute for Nanoscience was established in 2001 with a \$10 million annual budget in core research funds. The mission of the Institute for Nanoscience is to conduct highly innovative, interdisciplinary research at the intersections of the fields of materials, electronics, and biology in the nanometer-size domain. The Institute exploits the broad multidisciplinary character of the Naval Research Laboratory to bring together scientists with disparate training and backgrounds to pursue common goals at the intersection of their respective fields at this length scale. The objectives of the Institute's programs are to provide the Navy and DoD with scientific leadership in this complex, emerging area and to identify opportunities for advances in future defense technology. Its current research program emphasizes multidisciplinary, cross-division efforts in nanomaterials, nanoelectronics, and nanosensors/devices.

The Institute for Nanoscience building opened in January 2004. It has 5000 ft² of Class 100 clean room for device fabrication, 4000 ft² of "quiet" space with temperature controlled to 0.5 °C, acoustic isolation at the NC35 standard (35 dB at 1 kHz), floor vibration isolation to <150 μm/s rms at 10 to 100 Hz and <0.3 mOe magnetic noise at 60 Hz. There are also 1000 ft² of "ultra-quiet" space with temperature controlled to 0.1 °C and acoustic isolation at the NC25 standard (25 dB at 1 kHz).

Radar

NRL has gained worldwide renown as the "birth-place of radar," and for more than half a century has maintained its reputation as a leading center for radar-related research and development. A number of facilities managed by NRL's Radar Division continue to contribute to this reputation.

A widely used major facility is the Compact Antenna Range (operated jointly with the Space Systems Development Department) for antenna design and development and radar cross-section measurements. The range is capable of simulating far-field conditions from 1 to 110 GHz, with a quiet zone approximately 7 ft in diameter and 8 ft in length. Instrumentation covers from 1 to 95 GHz. Another strong division capability is in the Computational Electromagnetics (CEM) Facility, which has capabilities for complex electromagnetic modeling, including

radar target and antenna structures. The Radar Signature Calculation Facility within this group produces detailed computations of radar cross sections of various targets, primarily ships. The CEM facility includes multiple-CPU supercomputers that are also used to design phased array radar antennas. The tremendous synergism between the CEM group and the Compact Antenna Range Facility provides the ability to design in the CEM environment, to test in the compact range, and to have immediate feedback between the theoretical and experimental aspects to shorten the development cycle for new designs.

In connection with airborne radar, the division operates a supercomputer-based Radar Imaging Facility and an inverse synthetic aperture radar (ISAR) deployed either in the air, on the ground, or aboard ship for radar-imaging data collection. A P-3 aircraft equipped with the AN/APS-145 radar and cooperative engagement capability is also available for mounting experiments.

In connection with ship-based radar, the division operates the Radar Testbed Facility at the Chesapeake Bay Detachment (CBD), Randle Cliffs, Maryland. The site has radars for long-range air search and surface search functions and features the newly developed W-band Advanced Radar for Low Observable Control (WARLOC), a fully operational high-power coherent millimeter-wave radar operating at 94 GHz. The WARLOC transmitter is capable of producing 10 kW average power with a variety of waveforms suitable for precision tracking and imaging of targets at long range. Waveforms with a bandwidth of 600 MHz can be transmitted at full power. A 6-ft Cassegrain antenna is mounted on a precision pedestal and achieves 62 dB of gain.

The Advanced Multifunction Radio Frequency Concept (AMRFC) testbed is a new installation at CBD, operated by the Radar Division, with joint participation of several other NRL divisions as well. The goal of the AMRFC program is to demonstrate the integration of many sorts of shipboard RF functions, including radar, electronic warfare (EW), and communications, by utilizing a common set of broadband array antennas, signal and data processing, and signal generation and display hardware. The testbed consists of separate active transmit and receive arrays that operate over the 6 to 18 GHz band (nominally). Current functionality of the testbed includes a multimode navigation/surface surveillance Doppler radar, multiple communication links (line-of-sight and satellite), and passive and active EW capabilities. Testbed electronics are housed in seven converted 20-ft shipping containers and trailers. The arrays are mounted on a 15° tilt-back in the ends of two of the trailers overlooking the Chesapeake Bay, simulating a possible shipboard installation.



The AMRFC testbed, located at NRL's CBD, was developed as a proof-of-principle demonstration system that is capable of simultaneously transmitting and receiving multiple beams from common transmit and receive array antennas for radar, electronic warfare, and communications. These RF functions are controlled by common resource allocation manager (RAM) software over a real-time control network. New RF functionality may be readily added to the testbed as required for further demonstrations.

The division also has access to other radar systems: the Microwave Microscope (MWM); the Navy's relocatable over-the-horizon radar (AN/TPS-71); and an experimental Cooperative Aircraft Identification system. The internally developed MWM has a high-resolution (2 cm) ultrawideband capability that is used to investigate backscatter from surface and volumetric clutter, has through-wall detection capability, and characterizes the impulse responses of scattering objects. With respect to the AN/TPS-71, the division provides direct technical support and has direct access to data. The Cooperative Aircraft Identification system is used to explore system concepts and engineering developments in connection with target identification.

Information Technology

NRL's Information Technology Division (ITD) conducts basic research, exploratory development, and advanced technology demonstrations in the collection, transmission, and processing of information to provide a basis for improving the conduct of military operations. Funded by a variety of customers and sponsors within DoD, the U.S. government, and industry, ITD's research program spans the areas of artificial intelligence, high assurance systems, modeling and simulation, virtual reality, human/computer interaction, computer and communication networks, communication systems, transmission technology, and high performance computing.

ITD research networks connect internal NRL networks via high-speed links to OC48c on the Defense Research and Engineering Network (DREN) to a range of DoD sites; and to OC192c and all-optical wavelengths across ATDnet and BoSSNET to form the DoD's Global Information Grid Evaluation Facility (GIG-EF). GIG-EF provides a coalition of early adopters the key test validation infrastructure for transforming the DoD to network-centric IPv6/MPLS

convergence for future use by the services, NASA, the intelligence community, and coalition partners. ATDnet and BoSSNET also provide the core of an extended all-optical network that supports advanced signaling and transparent wavelength routing and switching. Optical research includes introduction of emergent technology to facilitate tunable 40G and 100G all-optical operation across single wavelengths and testing of new network protocols that emphasize low latency transport across the wide area, greatly increased network capacity for both aggregate and single flows, and the evolution of all-optical networks with direct switching and tuning at the optical layer.

ITD maintains several test labs containing a wide variety of networking equipment and test gear such as network traffic generators and analyzers, signal generators, and spectrum analyzers, which allow real-time injection and monitoring of wired and wireless traffic flows from simulated and "real world" data sources. The Integrated Communications Technology (ICT) Test Lab provides testing and evaluation of advanced networking technologies in support of multiple DoD programs such as Joint Tactical Radio System, Fleet Battle Experiments, Joint Forces Command Modeling & Simulation, Joint Experimentation, JTF WARNET, and Dragon Warrior. ICT Lab computers running NRL-developed software test programs can assess the performance of military and commercial off-the-shelf (COTS) equipment such as network radios, routers, and communications security devices.

The Mobile and Dynamic Network Laboratory supports development and evaluation of next-generation communication technologies for mobile and dynamic data networks. This laboratory provides for large-scale network simulation, real-time network emulation, and live field tests of wireless, mobile networks. The General Electronics Environmental Test Facility includes automated electronic test equipment and instrumentation, a phase noise measurement system, a noise figure mea-

surement system, precision spectrum analyzers, wide-band signal generators, a 40 ft³ environmental chamber, and an EMI test chamber located off-site. This facility provides resources for testing the performance of electronic and fiber-optic equipment under conditions that represent deployment to and installation in a Naval ship or Marine Corps tactical environment.

ITD also hosts a number of secure labs that support research in the areas of high assurance computing and networks. The Naval Cryptographic Technology Laboratory conducts research and prototype development of programmable cryptographic technologies for Navy and DoD applications. This laboratory also allows for development of certifiable Communications Security (COMSEC)/Information Security (INFOSEC) products, including programmable cryptographic devices, cryptographic applications, and high assurance cross-domain solutions. The Naval Key Management Laboratory investigates electronic key management and networked key distribution technologies for the Navy and DoD and serves as a testbed for developing new key management components and key delivery protocols developed for the Electronic Key Management System (EKMS) and the modernized Key Management Infrastructure (KMI).

The Cyber Defense Development Lab provides unique facilities for NRL research into Navy and DoD information and network security. This lab provides direct support in the areas of computer network defense and visualization, cross-domain solutions, and reverse code analysis and support. From architectural design, review, and prototyping, to component evaluation and integration, the Cyber Defense Development Lab ensures secure capability and availability of DoD and Navy network-centric information operations. It also serves as the research and development facility for the Navy Cyber Defense Operations Command (NCDOC). It not only supports and maintains NCDOC's Prometheus CND suite, but also serves as the mission critical facility for Naval reverse code and malware analysis in support of both NCDOC and NCIS operations.

ITD's Center for Computational Science (CCS) provides early access to next-generation computing and imaging technologies to NRL researchers. Assets at the CCS include a Silicon Graphics Altix 3700 Supercomputer with 256 Intel Itanium-2 Madison processors with 9 megabytes local cache, a dual-plane NUMA-link-4 low latency fat tree routing infrastructure, 2.048 terabytes of shared memory, and a SHMEM architecture operating under a SUSE/SLES10 Linux kernel. A similar Silicon Graphics Prism Supercomputer with 128 Itanium-2 Madison processors and 8 graphics pipes supports real-time visualization-intensive supercomputer applications. A Silicon Graphics 4700 blade-based

system provides researchers with access to dual-core Itanium-2 Montecito technology with 18 megabytes local cache, augmented with 16 reconfigurable field programmable gate array (FPGA) accelerator blades, dual-plane NUMALink-4 fat tree router, and 0.5 terabytes of FB-DDR shared memory. Emergent Infiniband SDR (10G) and DDR (20G) RDMA technology provides a "single-wire" interconnect for common access between the Center's various computational architectures, and to 300+ terabytes of direct attach shared disk array under the CXFS common file system. ITD's CCS also operates a unique Cray XD1 supercluster that integrates 864 AMD Opteron processor cores with 150 closely coupled FPGAs capable of providing one to two orders of magnitude processing gain. This Opteron system likewise operates under open-source Linux and employs a Lustre file system.

ITD has a variety of facilities dedicated to simulation and visualization of complex datasets. The Motion Imagery Laboratory (MIL) provides a flexible, immersive visualization baseline for experiments in the convergence of progressive motion imagery; peer-to-peer agent driven high performance distributed computing; distributed, federated access to petabyte datasets; and a dynamic SIP control plane for direct wavelength switching.

The Robotics Laboratory provides the ability to develop and evaluate intelligent software and interfaces for autonomous vehicles. Software can be evaluated in simulation, or in the real world using individual or teams of mobile robots. An 82-node computational cluster is also available for simulation, allowing faster than real-time evaluation of the performance of software agents, and is particularly suited to fast convergence of solutions using evolutionary computation methods.

The Immersive Simulation Laboratory (ISL) utilizes a collection of COTS and specially developed components to support R&D in interfaces to virtual simulators, ranging from fully immersive to desktop simulations. This includes three optical motion capture systems for full-body tracking of multiple users and specially designed centering harnesses for dismounted infantry simulation. The lab also includes a variety of head-mounted displays, large screen displays, input control devices, graphics and audio rendering computers, and simulation software to support a wide range of research in the field of human-computer interaction.

The Audio Laboratory has facilities for rendering and analyzing complex sound for military applications. The rendering systems include a 28-speaker array arranged in five rings within a space that is deadened by 16 RPG Diffuser VariScreens, which produce realistic audio environments using pre-recorded or synthesized sound.



The Navy Center for Applied Research in Artificial Intelligence is investigating learning and adaptation within teams of autonomous robots. Recent work has focused on a team of robots performing force protection.

The 3D Virtual and Mixed Environments Laboratory (3DVMEEL) explores methods by which 3D computer graphics assists in the collection, interpretation, and dissemination of information for both operational and training purposes. Augmented reality equipment includes wearable computers, optical and video see-through head-worn displays, vision-based and non-vision-based tracking components, global positioning system antennas including differential and real-time kinematic correction, and inertial tracking systems.

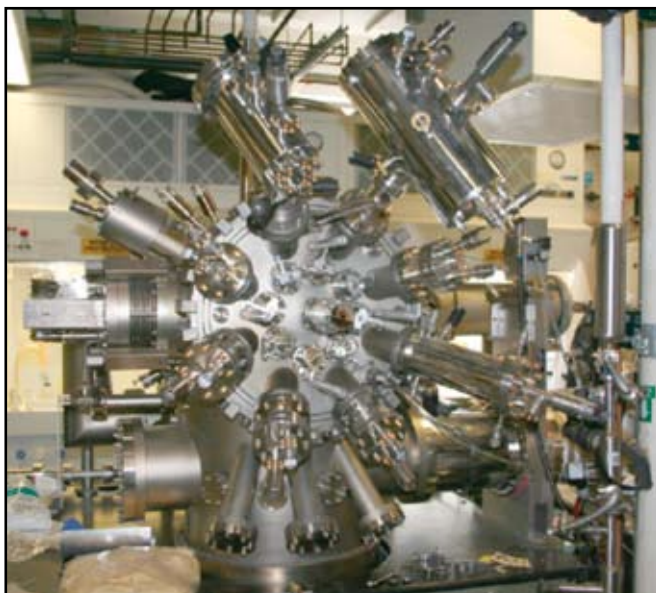
The Intent/Deception (ID) Laboratory tests various sensor suites, algorithms, and processes associated with behavioral indicators of deception. Sensors include computer vision cameras, pupil trackers, thermographic IR cameras, and high-end audio collection equipment. The ID Lab serves as an integration facility for the various sensors and an evaluation center for the

algorithms needed to automate the process of determining deception.

ITD's Transmission Technology Branch is developing transportable high-frequency digital receivers and antenna arrays to be used at various field sites of interest. These utilize COTS high-speed digitizing PCI boards with desktop/and or laptop computers. The data collected is expected to provide new insights into ionospheric wave interactions caused by high-power radio transmitters such as the High Frequency Active Auroral Research Program (HAARP).

Optical Sciences

The Optical Sciences Division has a broad program of basic and applied research in optics and electro-optics. Areas of concentration include fiber optics,



Optical Sciences molecular beam epitaxy system that is dedicated to quantum confined GaSb/InAs/AlSb structures for midwave infrared laser development.

integrated optical devices, signal processing, fiber-optic and infrared sensors, optical information processing, panchromatic and hyperspectral imaging for surveillance and reconnaissance, and laser development.

The division occupies some of the most modern optical facilities in the country. The newest facility in Optical Sciences is a molecular beam epitaxial growth system dedicated to quantum confined GaSb/InAs/AlSb structures for midwave infrared laser development. Other facilities include several fiber-optic facilities including preform fabrication, draw towers, optical fiber coaters, fiber splicers, and fiber-optic sensor testing stations such as an acoustic test cell and a three-axis magnetic sensor test cell. There is also an Ultralow-loss Infrared (IR) Fiber-Optic Waveguide Facility using high-temperature IR glass technology. The Focal Plane Array Evaluation Facility allows measurement of the optical and electrical characteristics of infrared focal plane arrays being developed for advanced Navy sensors. The IR Missile-Seeker Evaluation Facility performs open-loop measurements of the susceptibilities of IR tracking sensors to optical countermeasures. The Large-Optic, High-Precision Tracker system is used for atmospheric transmission and target signature measurements. The Infrared Test Chamber is an ultradry test chamber used to measure the IR signatures of new surface treatments, scale models, and components used for signature control on ships, aircraft, and missiles. A UHV multi-chamber deposition apparatus for fabrication of electro-optical devices is interfaced to a surface analysis chamber equipped with ultraviolet photoelectron spectroscopy (UPS), X-ray photoelectron spectroscopy (XPS), atomic force microscopy (AFM), and scanning tunneling microscopy (STM). Other scanning probe facilities are equipped with atomic force and magnetic force microscopes. Other laboratories in the division develop and test new laser and nonlinear frequency conversion concepts and evaluate nondestructive test and evaluation techniques.

Electronic Warfare

The scope of the Tactical Electronic Warfare (TEW) Division's program for electronic warfare (EW) research and development covers the entire electromagnetic spectrum. The program includes basic technology research and advanced developments and their applicability to producing EW products. The range of ongoing activities includes components, techniques, and subsystems development as well as system conceptualization, design, and effectiveness evaluation. The focus of the research activities extends across the entire breadth of the battlespace. These activities emphasize providing the methods and means to counter enemy hostile actions—from the beginning, when enemy forces are being mobilized for an attack, through to the final



AN/ALQ-228(V)1 communications jamming pod.

stages of the engagement. In conducting this program, the TEW Division has an extensive array of special research and development laboratories, anechoic chambers, and modern computer systems for modeling and simulation work. Dedicated field sites and an NP-3D EW flying laboratory allow for the conduct of field experiments and operational trials. This assemblage of scientists, engineers, and specialized facilities also supports the innovative use of all Fleet defensive and offensive EW resources now available to operational forces through the Naval Fleet/Force Technology Innovation Office.

Laboratory for Structure of Matter

This laboratory investigates the atomic arrangements in materials to improve them or facilitate the development of new substances. Various diffraction methodologies are used to make these investigations. Subjects of interest include the structural and functional aspects of energy conversion, ion transport, device materials, and physiologically active substances such as drugs, antibiotics, and antiviral agents. Theoretical chemistry calculations are used to complement the structural research. A real-time graphics system aids in modeling and molecular dynamics studies. The facilities include two state-of-the-art X-ray diffraction units.

Chemistry

NRL has been a major center for chemical research in support of naval operational requirements since the late 1920s. The Chemistry Division continues this tradition. It is pursuing a broad spectrum of basic and applied research programs focusing on controlled energy release (fuels, fire, combustion, countermeasure decoys, explosives), surface chemistry (corrosion, adhesion, tribology, adsorbents, film growth/etch), advanced materials (high-strength/low-weight struc-



Moored in Mobile Bay, Alabama, the ex-USS *Shadwell* is regularly set ablaze in a controlled environment to further the safety of operational Navy and civilian firefighting measures.

tures, drag reduction, damping, polymers, thin films, nanostructures), and advanced detection techniques (environment, chemical/biological, surveillance). The division has several research facilities.

Chemical Analysis Facilities include a wide range of modern photonic/electronic, magnetic- and ionic-based spectroscopic/microscope techniques for bulk and surface analysis.

The Synchrotron Radiation Facility has intense, monochromatic X-ray photon beams tunable from 10 eV to 12 KeV available from four beam lines developed by NRL at the National Synchrotron Light Source at the Brookhaven National Laboratory. Environmental target chambers span a pressure range from 10^{-12} to 10^5 atm and temperatures from 10 to 1500 K.

The Nanometer Measurement/Manipulation Facility includes fabrication and characterization capability based on scanning tunneling microscopy/spectroscopy, atomic force microscopy, and related techniques.

A Materials Synthesis/Property Measurement Facility has special emphasis on polymers, surface-film processing, and directed self-assembly.

Fire Research Facilities include a 10,000 ft³ fire-research chamber (Fire I) and the 475-ft ex-USS *Shadwell* (LSD-15) advanced fire research ship. Commensurate support has been devoted to survivability of the new classes of ships, DDX, LUN21, LPD17, and LHA(R).

The Marine Corrosion Test Facility located on Fleming Key at Key West, Florida, offers an ocean-air environment and clean, unpolluted, flowing seawater for studies of environmental effects on materials. Equipment is available for experiments involving weathering, general corrosion, fouling, and electrochemical phenomena, as well as coatings, cathodic protection devices, and other means to combat environmental degradation.

The Chemistry Division has focused on force protection/homeland defense (FP/HD) since September 11, 2001, especially on the development of improved detection techniques for chemical, biological, and explosive threats. As part of a multidivisional program to develop new technology systems, the Chemistry Division is a major contributor to the NRL Nanoscience Research Institute. Nanoscience complements FP/HD in that nanoscience is expected to provide dramatic improvements to chemical/biological detection, protection, and neutralization. Chemistry will approach the nanoscale from the bottom-up—building smaller atoms and molecules into nanostructures with new properties and developing the directed assembly of nanostructures into hierarchical systems. The NRL Nanoscience building is linked directly into the Chemistry building to provide both controlled access and auxiliary space for work not requiring a “low noise” environment.

Materials Science and Technology

The Materials Science and Technology Division at NRL conducts materials research using seven major division facilities.

The Magnetolectronics Fabrication Facility consists of a Class 1000 clean room equipped with tools for lithographic construction of magnetolectronic and spintronic devices. It provides pattern definition, metallization, dielectric layer deposition, and both reactive and Ar⁺ ion etching of wafers and small pieces.

The Electrical, Magnetic, and Optical Measurement Facility is comprised of several complementary instruments that allow for the magnetic, electrical, optical, and heat capacity characterization of materials and devices. SQUID (superconducting quantum interference device) magnetometry and vibrating sample



The Magnetolectronics Fabrication Facility consists of a Class 1000 clean room equipped with tools for lithographic construction of magnetolectronic and spintronic devices.

magnetometry are used to determine important properties of superconducting, paramagnetic, diamagnetic, and ferromagnetic materials. The transport properties of materials, namely the temperature- and magnetic-field-dependent resistivity combined with heat-capacity measurements, allow for a fundamental physical understanding of electronic properties.

The Materials Processing Facility includes apparatuses for powder production by fluid atomization, thermal evaporation, and arc erosion, and a physical vapor deposition system designed to produce and coat submicron powders in situ. Facilities to process powder into bulk specimens by hot and cold isostatic pressing permit a variety of consolidation possibilities. The isothermal heat treatment facility and quenching dilatometer permit alloy synthesis and single crystal growth. Bulk alloys can be prepared by induction melting, while rapid solidified metals of thin cross section can be made by splat quenching and melt spinning. Ceramic and ceramic-matrix composites processing facilities include a wide variety of conventional, controlled atmospheric furnaces, hot presses, a ball milling apparatus, particle size determination capability, and sol-gel and organometallic coating processing capabilities.

The Mechanical Characterization Facility consists of various testing systems, many with automated computer control and data acquisition, for determining the mechanical response of materials under controlled loading/deformation and environmental conditions. Basic capabilities include quasistatic tensile and fracture testing, dynamic storage and loss moduli as a function of frequency and temperature, cyclic fatigue crack growth and corrosion fatigue testing, and stress-corrosion cracking testing.

The Thin-Film Materials Synthesis and Processing Facility provides users a wide variety of techniques for

growth and processing of thin films (thickness 1 μm or less). Sputter deposition offers a versatile method of depositing metallic and dielectric films and is a primary tool of this facility. Thermal evaporation of metals is implemented in both high-vacuum and ultrahigh-vacuum systems. Pulsed laser deposition (PLD) with temperature-variable stage temperature and controlled atmosphere allows growth of oxides. Electrolytic deposition offers efficient growth of gold and silver films. Laser direct write—both ablation and deposition—provide unique methods for imposing CAD-defined features via ablation of a substrate film and ablative mass transfer to a substrate.

The 3-MV Tandem Pelletron Accelerator Facility uses two “pelletron” charging chains to produce a terminal voltage up to 3 MV in the accelerator. Negative ions are injected at 10 to 70 keV, accelerated up to the terminal where they undergo collisions with a stripper gas or a carbon stripper foil and lose electrons, then are accelerated as positive ions back to ground potential. Protons can be accelerated up to 6 MeV, He up to 9 MeV, and highly stripped Au (+12) up to 39 MeV. The lower limit of beam energy is about 400 keV. On the analysis beam line, the sample of interest is located at the end of the beam line, and a signal generated by scattering of incident high-energy ions indicates the composition of the sample. Incident high-energy ions can also be used to damage the surface of a sample of interest, or to introduce a dopant.

The Micro-Nano Structure Characterization Facility is capable of performing transmission electron microscopy (TEM), scanning transmission electron microscopy (STEM), atomic resolution transmission electron microscopy (ARTEM), electron energy loss spectroscopy (EELS), Z-contrast imaging, and spectral imaging through the use of a JEOL 2010F transmission



The Micro-Nano Structure Characterization Facility is capable of performing TEM, STEM, ARTEM, EELS, and Z-contrast imaging and spectral imaging.

electron microscope, a Phillips CM30 transmission electron microscope, and a Leo scanning electron microscope. Other standard microstructure characterization instruments are also available.

Laboratory for Computational Physics and Fluid Dynamics

The Laboratory for Computational Physics and Fluid Dynamics (LCP&FD) maintains a very powerful collection of computer systems applied to a broad collection of work. There are currently 120 parallel SGI processors, 512 clustered x86 processors, and several other support systems. In addition, there are more than 50 Macintoshes in the group, most of which are capable of large calculations both independently and in parallel ad hoc clusters.

The SGI computer systems comprise an SGI Altix with 64 Itanium-2 processors, an SGI Altix with 12 Itanium-2 processors, a 28-R12K-processor Origin 3800, an 8-R14K-processor Origin, and an 8-R12K-processor Origin 2000. There are two 256 x86 processor clusters well coupled with Myrinet high-speed switched interconnect.

Each system has on the order of 200 gigabytes of disk space for storage during a simulation, and at least 512 megabytes of memory per processor. All unclassified systems share a common disk space for home directories as well as almost 250 gigabytes of AFS space, which can be used from any AFS-capable system throughout the allowed Internet.

The AFS capability also allows access to other storage systems including NRL's multiresident AFS (MRAFS) system, which automatically handles archiving to a multi-terabyte tape archival system.

Plasma Physics

The Plasma Physics Division is the major center for in-house Navy and DoD plasma physics research. The division conducts a broad experimental and theoretic

cal program in basic and applied research in plasma physics, which includes laboratory and space plasmas, pulsed-power sources, plasma discharges, intense electron and ion beams and photon sources, atomic physics, laser physics, advanced spectral diagnostics, plasma processing, nonlinear dynamics and chaos, and numerical simulations.

The facilities include an extremely high-power laser, Pharos III, for the laboratory simulation of space plasmas and nuclear weapons effects studies, and two short-pulse high-intensity lasers—the Table-Top Terawatt (T^3) laser and the Ti:Sapphire Femtosecond Laser (TFL)—to study intense laser-plasma, laser-electron beam, and laser-matter interactions. The division also has an 11 m³ space chamber capable of reproducing the near-Earth space plasma environment and a Large Area Plasma Processing System (LAPPS) facility to study material modification such as surface polymerization or ion implantation. The division has developed a variety of pulsed-power sources to generate intense electron and ion beams, powerful discharges, and various types of radiation. The two largest of these pulsers, Gamble II and Mercury, are used to study the production of terawatt electron and ion beams and to produce very hot, high-density plasmas. Other generators are used to produce particle beams that are injected into magnetic fields and/or cavities to generate intense microwave pulses. A large array of high-frequency microwave sources (2.45, 35, and 83 GHz) are available to conduct research on microwave processing of advanced ceramic materials. In particular, the division added a 20-kW, continuous-wave, 83-GHz gyrotron to its facility for research on high-frequency microwave processing of materials. The Russian-made gyrotron produces a focused, high-intensity millimeter-wave beam (10^3 – 10^5 W/cm²) that has unique capabilities for rapid, selective heating of a wide range of nonmetallic materials.

The Nike 3-kJ KrF laser facility is made up of 56 laser beams and is single-pulsed (4-ns pulse). This facility provides intense radiation for studying inertial



The NRL Electra system is used to develop high-energy high-repetition-rate KrF laser technology. The Electra 30-cm aperture electron-beam-pumped amplifier is shown in the photograph. A portion of the recirculating system that cools the laser gas can be seen at the top. This amplifier is capable of a 5-Hz repetition rate and has produced up to 700 J of laser light per pulse.

confinement fusion (ICF) target heating at short wavelengths ($0.25\ \mu\text{m}$) and high-pressure physics. A second major inertial fusion system, Electra, is used to develop high-energy, high-repetition-rate KrF technology. The amplifier is capable of a 5-Hz repetition rate and has produced up to 700 J of laser light in extended operation.

The Plasma Physics Division has established a new Electromagnetic Gun Laboratory to study barrel materials science issues associated with an electric gun for a future all-electric warship. The laboratory will house a 6-m-long railgun, an 11 MJ capacitive energy storage bank, and solid-state switching hardware capable of driving up to 2 MA current in a barrel. The interface between the sliding projectile and the rails will be studied by a multidivision research team in an effort to design a high-performance and long-lived electric gun barrel.

The Plasma Physics Division also operates the new High Energy Laser Laboratory, which will study laser propagation in the atmosphere, laser-aerosol interactions, laser-target interactions, and beam combining techniques. The facility currently houses two high-power continuous-wave lasers, a 700-watt, 1.064-micron-wavelength Nd:YAG laser and a 1-kilowatt, 1.075-micron-wavelength Yb: fiber laser. Several more high-power fiber lasers will be installed in the near future. These lasers will be used to demonstrate a new incoherent beam combining technique that could be the key enabling technology for a new generation of compact laser directed energy weapons.

Electronics Science and Technology

The Electronics Science and Technology Division conducts a multidisciplinary basic and applied research program to exploit the creation/discovery/invention of new enabling materials, components, and techniques in electronics. In-house efforts include research and development in solid-state electronics; electronic materials

including growth, theory, and characterization of semiconductors, heterostructures, and superconductors; surface and interface science; microwave and millimeter-wave components and techniques; microelectronic device research and fabrication; nanoelectronics science and technologies; vacuum electronics; power electronics; device and process modeling and simulation; and cryoelectronics.

The division operates the Compound Semiconductor Processing Facility (CSPF), the Laboratory for Advanced Materials Synthesis (LAMS), the Epicenter, the Ultrafast Laser Facility (ULF), the Advanced Silicon Carbide Epitaxial Research Laboratory (ASCERL), the Silicon Carbide Processing Facility (SCPF), the Wafer Bonding Facility (WBF), the Power Device Characterization Facility, the Space Solar Cell Characterization Facility (SSCCF), the Vacuum Electronics Fabrication Facility (VEFF), and the Millimeter-Wave Structure Synthesis Facility (MWSSF).

The CSPF processes compound semiconductor devices and circuits, provides micro- and nanofabrication processing support, and selectively serves the hands-on fabrication needs of NRL scientists. The LAMS uses metallorganic chemical vapor deposition to synthesize a wide range of thin films, particularly wide bandgap semiconductors such as GaN and related alloys. The Epicenter (a joint activity of the Electronics Science and Technology, Materials Science and Technology, Optical Sciences, and Chemistry Divisions) is dedicated to the growth of multilayer nanostructures by molecular beam epitaxy (MBE). Current research involves the growth and etching of conventional III-V semiconductors, ferromagnetic semiconductor materials, $6.1\ \text{\AA}$ III-V semiconductors, magnetic materials, and II-VI semiconductors. The structures grown in this facility are analyzed via in situ scanning tunneling microscopy and angle-resolved electron spectroscopy. The ULF is optimized for the characterization of photophysical and photochemical processes in materials on a timescale of tens of femtoseconds. It includes



The Electronics Science and Technology Division's advanced silicon carbide epitaxial research laboratory.

a synchronously pumped dye laser system for simulating the effects of charge deposited in semiconductors characteristic of space radiation.

The ASCERL was dedicated in 2006 as the centerpiece of NRL efforts to develop the materials needed for the realization of high-voltage, high-power electronic components needed in future Naval systems. It employs an EPIGRESS reactor capable of growing thick, low-defect ultra-purity homo-epitaxial silicon carbide layers. The SCPF encompasses processing tools and equipment to support fabrication of silicon carbide (SiC) electronic power devices and emerging novel devices based on SiC and related heterojunctions. The WBF is a Class 100 clean room facility for conducting research on the fabrication of high-voltage wafer-bonded power devices and the development of novel high-performance wafer-bonded substrates for epitaxial growth of both narrow bandgap and wide bandgap material layers. The Power Device Characterization Facility characterizes the performance and reliability of silicon and SiC power devices. The SSCCF studies the effect of particle irradiation on new and emerging solar cell technologies for space applications. The VEFF provides electrical and mechanical design, fabrication, assembly, modification, repair, and processing services for vacuum electronic devices. The MWSSF contains a computer numerically controlled (CNC) milling machine and a CNC precision lathe capable of fabricating intricate millimeter-wave vacuum electronic components to 2.5 micron accuracy. Components include amplifiers, filters, circuits, multiple-beam amplifier cavities, gyro-TWT interaction structures and electron gun/waveguide structures.

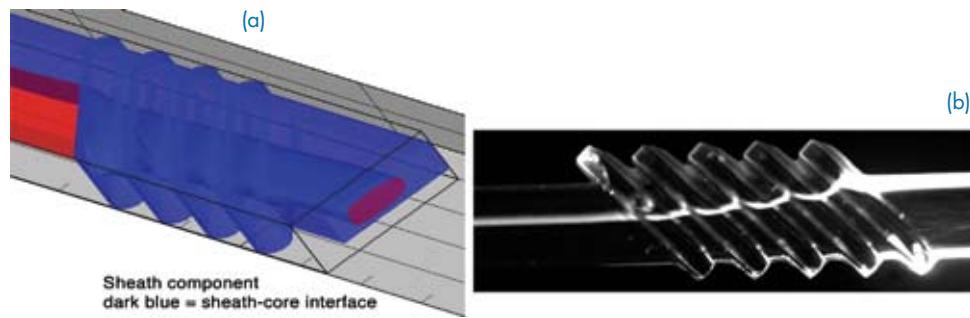
Bio/Molecular Science and Engineering

The Center for Bio/Molecular Science and Engineering conducts research and development using

biotechnological approaches to support the Navy, DoD, and the nation at large. Studies are currently under way to investigate biomaterial development for electronic and structural applications, environmental quality (including pollution cleanup and control), and chemical/biological warfare defense. Other program areas of interest include optical biosensors, nanoscale manipulations, genomics and proteomics, controlled sustained release, bio/molecular and cellular arrays, surface modification and patterning, energy harvesting, viral particles as scaffolds, advanced materials from self-assembly, and liquid-crystal-based electro-optic materials.

The staff of the Center is an interdisciplinary team with expertise in biochemistry and surface chemistry, biophysics, genetic engineering, cell biology, advanced organic synthesis, solid-state and theoretical physics, and electronics and materials engineering. In addition, the Center has collaborations throughout NRL, with other government laboratories, at universities, and in industry.

The Center's modern facilities include general laboratories for research in chemistry, biochemistry, molecular biology, and physics. Specialized areas include a 600 ft² Class 1000 clean room, an advanced electron microscope facility, and a scanning probe microscope laboratory. Instrument rooms provide access to a variety of spectrophotometers and other equipment used in biochemical or physical analyses of biomaterials. Additional laboratories accommodate an X-ray diffraction instrument, a liquid crystal fabrication facility, and equipment for advanced electronics, microarrays, and biosensor programs. The Center has added a plastic microfabrication facility, which enables fabrication of microfluidic and micro-optical systems in polymers, and a state-of-the-art liquid chromatograph-mass spectrometer (LC-MS) for molecular characterization.



Microfabrication of sensor components: NRL microfabrication facilities were used to design, build and demonstrate microfluidic devices for sensors. Shown above is a schematic (a) and demonstration (b) of how precisely milled grooves wrap sheath solution around a sample stream in a microchannel. The demonstration was performed in a 250 μm channel. Optical fibers were used to illuminate the stream and collect the scattered signal. In this image, the sample stream was labeled with a fluorescent dye for visibility.

The Center's facilities were recently used to demonstrate the capabilities of a microarray system developed at NRL for analyzing thousands of samples in a high-throughput production process. Two dozen infectious and bioterrorism agents could be detected. This successful demonstration used the Center's laboratory facilities with NRL staff, Air Force medical personnel, and contractors. At the completion of that program, a smaller-scale version of the microarray system remained at the Center to continue research in the area of multiplex genomics-based molecular diagnostic arrays.

Acoustics

The Acoustics Division has three integrated structural acoustic facilities—two pools (including one with a sandy bottom) and a large in-air, semi-anechoic

laboratory—that support research in submarine target characteristics for antisubmarine warfare, submarine acoustic design and quieting, sensors for hull-mounted sonars, mine detection and identification, torpedo quieting, and interior noise control in air platforms and submarines. Scaled submarine structures, real mines, sensors on hull simulators, underwater buried objects, torpedoes, aircraft fuselages, and space payload launch fairings and containers can all be examined with advanced nearfield holographic and scanning 3D laser vibrometer systems to measure nearfield, farfield, and interior sound fields as well as the physics of the sound-structure-fluid interactions.

The division operates state-of-the-art laboratories equipped to study the structural dynamics and performance of high-Q oscillators and other micro-mechanical systems. A number of laser Doppler vibrometers, including a super-resolution nearfield scanning optical



Laboratory for Structural Acoustics.

microscope (NSOM), permit spatial mapping of the complex vibratory motion down to resolutions of 100 nm. The laboratories include the ability to measure the mechanical and electrical properties of the micro-oscillators, and of thin films applied to them, down to 370 mK.

The division operates a portable, ocean-deployable synthetic aperture acoustic measurement system. The primary elements are sources and receivers attached to a robotic carriage that can be positioned precisely at any point along a 100-meter rail using an encoder feedback system. A separate source tower enables bistatic scattering data collection. Bidirectional control and data transfers are made over a dedicated RF link to a surface platform. This facility supports the collection of high-quality scattering cross sections of mines, and the associated clutter necessary for the implementation of new broadband MCM technologies on UUVs.

The Acoustics Division Salt Water Tank Facility is designed to provide a controlled environment for studying a variety of complex ocean processes under saline conditions, especially the study of the acoustics of bubbly media. Instrumentation includes acoustic sources, amplifiers, hydrophones, environmental sensors, a digital holographic imaging system, high-speed digital cameras, and a LabVIEW-based data acquisition system.

The division operates several sound sources for the generation and reception of sound in at-sea experiments. Sound sources include three XF-4 units, one ITC 2077 source that can be operated while being towed by a ship, two battery-operated organ-pipe sources that can project single tones from offboard moorings, and a towable, directional source array

for active sonar studies consisting of ten individually controllable elements, at frequencies of 2.5 to 5 kHz. In addition, the division has several battery-operated rubidium-clock-controlled, programmable sound source moorings that can transmit sounds having arbitrary waveforms.

The division has a 64-channel broadband source-receiver array with time-reversal mirror functionality. Projects involving scanning focused acoustic fields and phase conjugation for multistatic sonar utilize this array to test and study time reversal methods. The transducers for the array are 6-inch spheres that operate from 500 to 3500 Hz.

The Acoustics Division performs research to relate acoustic array gain variability to fluid dynamic variability and bottom heterogeneity in the littorals. The measurements are made with an autonomous acoustic data acquisition suite. Three independent autonomous 32-channel vertical arrays receive and store 24-bit data at a 4-kHz sample rate for 22 days. Two autonomous acoustic sources operate at 300 and 500 Hz center band with $\pm 10\%$ bandwidth and generate programmable waveforms at 50% duty cycle for 22 days. As presently configured, the systems will operate to water depths of 500 m. The division also has unique, self-recording digital acquisition buoy systems (DABS) that are used to obtain multichannel (up to 128) acoustic data in the 10 Hz to 5 kHz regime. These systems provide up to 250 gigabytes of data storage on a single 15-inch reel of 1-inch tape.

The Acoustics Division has a radio-controlled buoy system with underwater receive arrays to collect acoustic and oceanic data, unattended, for periods of up to one month. The system can currently handle 64



Source-receiver array for at-sea time-reversal experiments.

channels of acoustic data (distributed on one or two arrays), and can implement onboard signal processing prior to data transmission. The system contains a high-speed line-of-sight data link utilizing a GPS-linked directional antenna. A low-speed command and control link is available to remotely control buoy functions and array settings.

The division conducts research addressing the channel capacity of multinode underwater acoustic communications networks. The research is conducted in the 2 to 5 kHz, 6 to 14 kHz, and 10 to 24 kHz frequency bands using two 8-channel acoustic communications data acquisition systems or modems, which can be moored or towed. The 8-element vertical arrays are configured in a 2-m or 20-m aperture and remotely controlled using a wireless LAN.

Narrowbeam 200 and 350 kHz acoustic backscattering (flow visualization) systems are used to study fine structure, internal wave, and larger-scale fluid dynamic perturbation of the density and sound speed field in the ocean. A deck-mounted towing assembly consists of transducers, power amplifiers, and a real-time display and digital data acquisition system. A 25 kW radar system is used in conjunction with the flow visualization system to record the surface expression of internal waves.

The division operates high-frequency (up to 600 kHz) acoustic measurement systems to obtain scattering, target strength, and propagation data using bottom-moored instrumentation towers and a remotely operated vehicle. These data are used to simulate the performance of weapons and mine countermeasure sonars.

The Geoacoustic Model Fabrication Laboratory allows researchers to fabricate rough topographical surfaces in various materials (usually plastics) for acoustic scattering and propagation measurements in water-tank facilities. The facility consists of a three-axis computer-controlled milling machine equipped with vacuum holddown and capable of cutting with 100- μ m accuracy over a 1.37 \times 1.27 m region.



Fabrication of rough surfaces for acoustic analysis.

Remote Sensing

The Remote Sensing Division conducts a program of basic research, science, and applications to develop new concepts for sensors and imaging systems for objects and targets on Earth, in the near-Earth environment, and in deep space. The developmental effort includes active and passive sensor systems used to study and analyze the physical characteristics of phenomena that evolve from naturally occurring background radiation, such as that caused by the Earth's atmosphere and oceans, and man-made or induced phenomena, such as ship/submarine hydrodynamic effects. The research includes theory, laboratory, and field experiments leading to ground-based, airborne, or space systems for use in remote sensing, astrometry, astrophysics, surveillance, nonacoustic antisubmarine warfare (ASW), meteorological/oceanographic support systems, and environmental/global climate change initiatives. Special emphasis is given to developing space-based platforms and exploiting existing space systems.

Maritime Hyperspectral Imaging (HSI): The Remote Sensing Division conducts airborne hyperspectral data collections for characterization of the environment. Hyperspectral data are series of pictures, taken simultaneously, of a scene at many different wavelengths (colors). The sensors are built and calibrated in-house, although they rely heavily on COTS elements. Our current operational sensor is the airborne Portable Hyperspectral Imager for Low-Light Spectroscopy (PHILLS) system, specifically designed for use over maritime areas. It covers the 400 to 1000 nm wavelength range with 128 different wavelengths (channels). PHILLS consists of a standard video camera lens, a grating spectrograph, and a 1024 \times 1024-pixel charge-coupled device (CCD). The system is designed for maximum sensitivity in the blue end of the spectrum in order to optimize water-penetrating measurements. This allows retrieval of in-water geophysical parameters such as ocean bottom type (coral, sea grass, sand, rock, etc.) to water depths of 20 m (in clear water), and identification of material in the water column (phytoplankton, sediments, colored dissolved organic matter, etc.). PHILLS is very compact and can be flown at heights of 8000 to 10,000 ft. The division has also acquired a commercial Compact Airborne Spectrographic Imager (CASI-1500) hyperspectral imager with similar capabilities to the NRL-built PHILLS.

Proper interpretation of the hyperspectral data requires both radiometric and spectral calibration of the sensor. The Remote Sensing Division operates an Optical Calibration Facility to perform these calibrations, which includes a NIST-traceable integrating sphere and a set of gas emission standards for wavelength calibration. The complete process of data collection through data analysis can be handled in-house.

To validate the results of airborne hyperspectral sensing, and to support interpretation of the physical processes they reveal, the division has developed a Profiling Optics Package. This system measures the inherent optical properties of water (absorption, attenuation, and scattering) in the 400 to 700 nm range, and collects water samples for various laboratory measurements. The package has a maximum depth rating of 300 m, although it is usually operated in coastal waters of less than 50 m.

The Remote Sensing Division is beginning a two-phase, rapid-development program for maritime hyperspectral imaging from space. The first phase, now under way, is to develop a PHILLS airborne imager for use in space. The second phase will be to build and launch the fully space-qualified Coastal Ocean Imaging Spectrometer (COIS) with significantly improved performance and the capability to image 20 coastal regions per day.

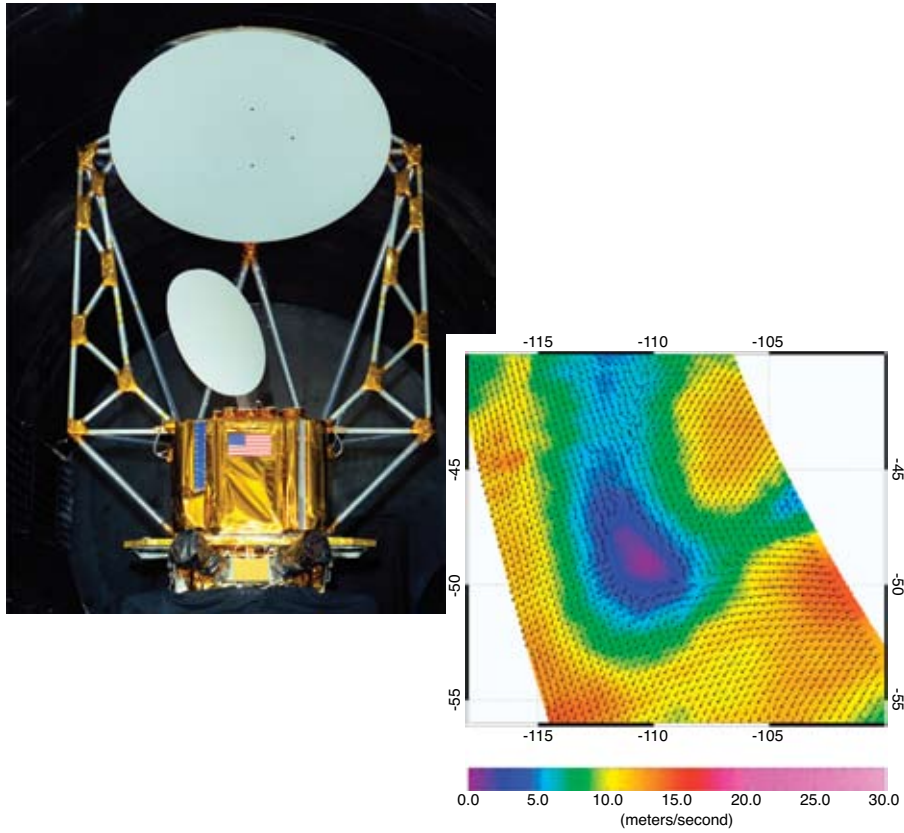
Hydrodynamics: The Remote Sensing Division conducts a wide range of numerical and analytical research dealing with the physics of the ocean's free surface. Direct numerical simulations (DNS) of turbulence are made in which the free surface is treated as either flat, or as a fully nonlinear, deformable surface with waves. To test and validate the numerical results and analytical theories, experiments are conducted in the Free-Surface Hydrodynamics Laboratory to study interactions of turbulence with the free surface; wave-generation phenomena; jet flows; vorticity dynamics; and free-surface/surfactant interactions. Emphasis is placed on those processes that determine the fluxes of heat, mass, and momentum across the air-sea interface. State-of-the-art diagnostic tools are available, such as a Langmuir film balance to measure the properties of surface films, hot-wire and laser-Doppler anemometry, and the new quantitative flow techniques of laser speckle, particle tracking, and particle image velocimetry. The laboratory is also equipped with an IR camera with a 0.02 K resolution. These experimental diagnostic techniques use high-powered lasers, high-tolerance optical lenses, and extensive ultra-high-resolution video-imaging hardware and PC-based computerized systems. Further computational assets consist of powerful graphical computer work stations, the NRL Connection Machine, and other off-site Cray supercomputer systems. The newest addition to the laboratory is a high-precision, computer-controlled wave generator. It spans the entire 2.4 m width of the basin, and is capable of generating breaking waves from 0.2 to 1.2 m in length.

Astronomy: The Navy Prototype Optical Interferometer (NPOI), a major facility of the Remote Sensing Division, is actually two collocated instruments for making high-angular-resolution optical measurements of stars. Light from widely separated individual siderostats is combined simultaneously to synthesize

the angular resolution of a telescope tens to hundreds of meters in diameter. Four siderostats are placed in an array with extremely accurate metrology to enable very-high-precision measurements of stellar positions (wide-angle astrometry). These measurements are used by the U.S. Naval Observatory to refine the celestial reference frame, determine Earth rotation parameters, and thus satisfy Navy requirements for precise time and navigation data. They also provide determinations of basic astrophysical parameters, such as stellar masses and diameters. Additional relocatable siderostats can be placed out to distances of up to (when complete) 250 m from the array center, and used to construct very-high-resolution images of stars. These images provide fundamental astrophysical information on stellar structure and activity. When complete, the NPOI will be the most advanced high-resolution imaging optical interferometer in the world.

The Remote Sensing Division also has a strong program in radio astronomy, with emphasis on low-frequency (< 100 MHz) observations. The division has developed and installed 74-MHz receivers on the National Radio Astronomy Observatory's (NRAO) Very Large Array (VLA), thereby producing the world's highest-angular-resolution and most sensitive astronomical interferometric array operating below 150 MHz. The VLA's maximum baseline is 35 km; all previous astronomical interferometers operating below 150 MHz had baselines of less than 5 km because ionospheric structure had been thought to impose phase variations that would corrupt the interferometric imaging. Work in the Remote Sensing Division has shown that radio astronomical techniques can now remove the ionospheric phase variations and extend interferometer baselines to arbitrary lengths. The success of the NRL/NRAO 74-MHz system indicates that it is possible to open a new, high-resolution, high-sensitivity astronomical window by going to an even larger, more sensitive system. Several such large interferometric systems are now in various stages of planning and development. This includes the Long Wavelength Array (LWA), a joint collaboration between the University of New Mexico, University of Texas, Los Alamos National Laboratory, and NRL Remote Sensing Division.

The LWA will provide high spatial and temporal sampling of the ionosphere for characterizing ionospheric phenomenology, and probing ionospheric microstructure and physics. It is also the ideal receiver for proposed solar radar systems which can be used to image Earthward-bound coronal mass ejections for geomagnetic storm prediction. Development of a prototype station for the LWA is under way. Contingent upon funding levels, the LWA will be constructed in phases with the last phase scheduled for completion in 2011.



NRL WindSat polarimetric radiometer prior to spacecraft integration, and a retrieved wind vector field obtained on September 12, 2003, in the South Pacific.



The Navy Prototype Optical Interferometer (NPOI) is used for operational astrometry and for development of distributed aperture imaging techniques.

Remote Sensing of the Atmosphere and Ocean Surface: The NRL Polar Ozone and Aerosol Measurement (POAM) instrument is a space-based 9-channel UV-Vis solar photometer for measuring ozone and other important constituents of the stratosphere using the solar occultation technique. The POAM program consists of two missions: POAM II was launched in October 1993 on the French SPOT 3 satellite, and operated until contact with the host satellite was lost in November 1996; POAM III was launched in March 1998 on the SPOT 4 satellite, and was operational until December 2005. POAM has been an important part of the national ozone monitoring effort because for most of its mission life it was the only instrument making high-vertical-resolution (1 km) measurements of ozone in the polar regions of both hemispheres on a continuous basis, including unprecedented space-based coverage of the Antarctic ozone hole. As such, POAM has contributed data on a major policy issue: global ozone depletion. POAM's orbit was ideal for monitoring the effect of chlorofluorocarbon (CFC) restrictions, and the effect of replacement chemicals, because ozone depletions are most severe in the polar regions during the late winter/early spring season in each hemisphere.

WindSat, developed and built by NRL and launched in January 2003, is the first spaceborne polarimetric microwave radiometer. Its primary mission is to demonstrate the capability to remotely sense the ocean surface wind speed and direction (wind vector) with a passive system. WindSat, the primary payload on the DoD Space Test Program Coriolis mission, provides major risk reduction for development of the National Polar-orbiting Operational Environmental Satellite System (NPOESS) Conical-scanning Microwave Imager/Sounder (CMIS). Although WindSat wind vector retrieval algorithm development is still an important R&D effort in the Remote Sensing Division, the current algorithm is run operationally at the Navy Fleet Numerical Meteorology and Oceanography Center (FNMOC). Wind vectors are available in real time, and are included in the NRL-Monterey satellite cyclone Web site. In addition, the Remote Sensing Division is exploiting WindSat's unique data set to develop retrievals for other environmental parameters such as sea surface temperature, soil moisture, and sea ice concentration.

The Airborne Polarimetric Microwave Imaging Radiometer (APMIR) is a state-of-the-art multichannel microwave radiometer system designed and built by the Remote Sensing Division. APMIR was built primarily to provide extensive airborne calibration and validation of spaceborne remote sensing assets: the NRL WindSat mission, the Defense Meteorology Space Program (DMSP) Special Sensor Microwave Imager/Sounder (SSMIS) mission, and the future CMIS to fly on the converged NPOESS. APMIR covers five

frequency bands from 5 to 37 GHz, and the 10.7, 18.7, and 37 GHz measurement bands are fully polarimetric. Frequency agility allows for frequency matching to each of the spaceborne systems of interest. In addition to validation, APMIR provides measurements of the ocean surface wind vector, sea surface temperature, atmospheric water vapor and cloud parameters below the airplane, soil moisture, and ice/snow properties. The APMIR system is deployed on the NRL P-3 aircraft (mounted in the bomb bay), and flown at altitudes ranging from 500 to 25,000 ft over the ocean.

The Remote Sensing Division has developed a unique eye-safe volume-imaging lidar system to remotely characterize aerosol backscatter variations in coastal boundary layers, and to map those variations over hundreds of meters. In the NRL lidar system, deuterium cells are used to produce a Raman wavelength shift that converts near-infrared laser pulses to 1.5 microns (an eye-safe wavelength). The deuterium cells were developed at NRL and do the conversion in a single pass—substantially simpler and more reliable than the multi-pass methane cells that are currently being used by other lidar systems. The lidar uses a dual mirror scanning system to map aerosol structures and detect their movement. Unlike Doppler lidar systems that can measure only radial wind speeds, the NRL lidar uses correlation methods and measures the wind vector (speed and direction) and turbulence.

Oceanography

The Oceanography Division is the major center for in-house Navy research and development in oceanography. It is known nationally and internationally for its unique combination of theoretical, numerical, experimental, and remotely sensed approaches to oceanographic problems. The division's modeling focus is on a truly integrated global-to-coastal modeling strategy, from deep water up to the coast including straits, harbors, bays, and inlets. This requires emphasis on both ocean circulation and wave/surf prediction, with additional emphasis on coupling the ocean models to biological, optical, and sediment models. This modeling is conducted on the Navy's and DoD's most powerful vector and parallel processing machines. The division has an in-house Ocean Dynamics and Prediction Computational Network Facility that provides computer services to scientists for program development, graphics, data processing, storage, and backup. To study the results of this intense modeling effort, the division operates a number of highly sophisticated graphic systems to visualize ocean and coastal dynamic processes.

The seagoing experimental programs of the division range worldwide. Unique measurement systems include a wave measurement system to acquire in situ



The NRL Oceanography Division's new capabilities for sensing the littoral environment include a Vertical Microstructure Profiler (VMP) (top left), a Scanfish (top right), and four Slocum Gliders (bottom). They will be used to measure the variability of temperature, salinity, currents, and optical properties both horizontally and vertically, on scales ranging from micro- to mesoscale.

spatial properties of water waves; a salinity mapper that acquires images of spatial and temporal sea surface salinity variabilities in littoral regions; an integrated absorption cavity, optical profiler system, and towed optical hyperspectral array for studying ocean optical characteristics; self-contained bottom-mounted upward-looking acoustic Doppler current profilers (ADCPs) for measuring ocean variability; and an in situ volume scattering function measurement system to support remote sensing and in-water optical programs. NRL is working jointly with the NATO Undersea Research Center (NURC) for development and deployment of the SEPTR instrument, a trawl-resistant, bottom-mounted ADCP system that includes a pop-up profiling float for real-time observation and reporting.

The Oceanography Division has acquired new capabilities for sensing the littoral environment. These include a Vertical Microstructure Profiler (VMP), a Scanfish, and four Slocum Gliders. The turbulent dissipation rate can be quickly obtained with very high accuracy from measurements collected by the VMP. The Scanfish allows efficient and rapid three-dimensional mapping of mesoscale oceanic features. The Gliders rely on a low-powered battery-induced change of buoyancy to glide autonomously through the coastal ocean collecting both physical and optical data that are uplinked to satellite and then relayed to the laboratory or ship in near-real time.

In the laboratory, the division operates an environmental scanning electron microscope for detailed

studies of biocorrosion in naval materials. The division's remote sensing capabilities include the ability to analyze and process multi/hyperspectral, IR, SAR, and other satellite data sources. The Ocean Optics section has added the capability to download MODIS data directly using the new X-band receiving system. The division is a national leader in the development and analysis of MODIS ocean color data for oceanographic processes and naval applications in littoral areas.

Marine Geosciences

The Marine Geosciences Division is the major Navy in-house center for research and development in marine geology, geophysics, geodesy, geoacoustics, geotechnology, and geospatial information and systems. The division has unique suites of instrumentation and facilities to support laboratory and field experimental programs.

The instrumentation used in the field is deployable from ships, submarines, remotely operated and unmanned vehicles, undersea platforms, airborne platforms, and by divers. Instrumentation includes an integrated airborne geophysical sensor suite with gravity, magnetic, and sea/ice/land topographic profiling sensors, all based on cm-level KGPS aircraft positioning. Seafloor and subseafloor measurements use the Deep-Towed Acoustics/Geophysics System, DTAGS (220 to 1000 Hz); a chirp sub-bottom profiler; high-resolution sidescan sonars (100 and 500 kHz); the

Acoustic Seafloor Characterization System, ASCS (15, 30, and 50 kHz); an optically pumped marine magnetometer; several gravimeters; the In Situ Sediment Acoustic Measurement System (ISSAMS); underwater stereo photography; and nearshore video imaging systems. ISSAMS has specialized probes that measure acoustic compressional and shearwave velocities and attenuation, sediment shear strength, and electrical conductivity in surficial marine sediments.

Five instrumented, 8-ft-long, 2220-lb, minelike cylinders are used to gather impact burial data (one system) and scour and sand wave burial data (four systems) for validation of mine burial prediction models.

Laboratory facilities include the Sediment Physical and Geotechnical Properties Laboratory and Sediment Core Laboratory. The Transmission Electron Microscopy Facility is the focal point for research in microscale biological, chemical, and geological processes. The key instrumentation includes a 300 kVa transmission electron microscope with environmental cell. The environmental cell allows hydrated and gaseous experiments. A high-resolution industrial CT scanner is a recent addition to the laboratory. It is used for investigating volumetric heterogeneity of sediments.

The Moving Map Composer Facility is used to design and write mission-specific map coverages for F/A-18 and AV-8B tactical aircraft onto militarized optical disks. The Geospatial Information Data Base (GIDB) capability provides Internet access to the Digital Nautical Chart data, mapping data, imagery, and other data types such as video and pictures. This development tool can be used for planning, training, and operations.

Marine Meteorology

The Marine Meteorology Division is located in Monterey, California. NRL-Monterey (NRL-MRY) serves the Navy's need for basic and applied research in atmospheric sciences and develops meteorological analysis and prediction systems and other products to support warfighting customers at the theater, operational, and tactical levels.

NRL-MRY is collocated with Fleet Numerical Meteorology and Oceanography Center (FNMOC), the Navy's operational production center for numerical weather prediction (NWP) and satellite data. NRL-MRY's Atmospheric Prediction System Development Laboratory has direct connectivity to FNMOC's classified and unclassified world-class computer resources and databases, which enables the division to efficiently develop and transition analysis and prediction systems to operational use. Links to the Defense Research and Engineering Network (DREN) provide access to supercomputing resources around the country with gigabit/

second speed. The in-house Supercomputer Resource Center currently includes an SGI Origin 2000 128-processor supercomputer and a 44-processor LINUX cluster along with a 28-terabyte Storage Area Network. This Center enables the division to support research in atmospheric processes such as air-sea interaction, terrain-induced flows, atmospheric predictability, and cloud/aerosol processes, and to develop and improve numerical prediction systems critical to Fleet operators around the globe. A considerably larger cluster and significant additional storage will be added to the center in early 2007.

A state-of-the-art Satellite Data Processing Laboratory allows direct downlink of real-time NOAA geostationary data (imagery and sounder data from GOES-E and GOES-W) and data relays from three other geostationary satellites. It also receives data from numerous polar orbiting platforms (three from NOAA, four from the Defense Meteorological Satellite Program, and five from NASA—Tera, Aqua, TRMM, SEAWifs, and Quikscat). NRL-MRY processes data from 23 orbiting satellites and uses the data to conduct research and develop multi-sensor, multi-platform applications to support a variety of DoD operations. These range from monitoring and analyzing tropical cyclone intensity in support of the Joint Typhoon Warning Center, to providing dust enhancement imagery in support of combat operations in Southwest Asia. These products are transitioned to FNMOC as they reach maturity. The Satellite Data Processing Laboratory is supported by the 24-terabyte Bergen Data Center, which has a hierarchical storage management capability to provide archival and easy retrieval of research data sets. The Bergen Data Center also provides support for the data that is archived as part of the Master Environmental Library (MEL).

NRL-MRY's Classified Satellite/Radar Data Processing Facility hosts classified computer systems to



NRL Marine Meteorology Division has a direct downlink capability for real-time geostationary data from NOAA's GOES-E and GOES-W satellites.

receive, process, and store classified and unclassified satellite, radar, and observational data, and to develop applications for their operational use. This facility has a 22-processor LINUX cluster for high performance computing along with SIPRNET connectivity in a shielded workspace. It provides a real-time testbed for the integration of classified high-resolution data and fusion with “through-the-sensor” information collected from shipboard radars and direct broadcast meteorological satellite sensors to generate on-scene NOWCAST products used to support operational and tactical decision makers.

To support the division’s expanding program in aerosol research and aerosol prediction system development, NRL-MRY designed and built the Mobile Atmospheric Aerosol and Radiation Characterization Observatory (MAARCO). MAARCO is a climate-controlled, modified, 20-ft standard container with an integrated suite of meteorological, aerosol, gas, and radiation instruments, with space available for additional sensors, that can be rapidly deployed to operate in austere locations. MAARCO can enable research of atmospheric aerosols, gases, and solar radiation in strategic areas, including remote regions, overseas locales, and onboard ships at sea. Data collected during the United Arab Emirates United Aerosol Experiment (UAE²) in 2004 is being used to investigate boundary layer meteorology, aerosol microphysics, and electro-optical propagation. A second MAARCO unit was delivered in September 2006.

Space Science

The Space Science Division conducts and supports a number of space experiments in the areas of upper atmospheric, solar, and astronomical research aboard NASA, DoD, and other government agency space platforms. Division scientists are involved in major research thrusts that include remote sensing of the upper and middle atmospheres, studies of the solar

atmosphere, and studies of astronomical radiation ranging from the ultraviolet through gamma rays and high-energy particles. In support of this work, the division maintains facilities to design, construct, assemble, and calibrate space experiments.

The division’s Vacuum Ultraviolet Space Instrument Test Facility is an ultraclean solar instrument test facility designed to satisfy the rigorous contamination requirements of state-of-the-art solar spaceflight instruments. The facility has a 400 ft² Class 10 clean room and a large Solar Coronagraph Optical Test Chamber (SCOTCH). This completely dry-pumped, 550 ft³ vacuum chamber is maintained at synchrotron levels of cleanliness. Solar instrumentation up to 1 m in diameter and 5 m in length can be accommodated in the chamber. The instrument’s optical performance is probed and calibrated with a variety of visible and XUV sources mounted on the chamber’s 11-m beamline. The facility has a small thermal bake/vacuum test chamber used for vacuum conditioning and thermal testing of spaceflight components and subassemblies. The facility was originally developed to support the optical testing and characterization of the Large Angle Spectrometric Coronagraph (LASCO) instrument for the European Space Agency’s Solar and Heliospheric Observatory (SOHO) spacecraft. More recently, components of the NRL Sun Earth Connection Coronal and Heliospheric Investigation (SECCHI) experiment, developed for the NASA Solar Terrestrial Relations Observatory (STEREO), were tested in the facility. The two SECCHI visible light coronagraphs were calibrated for instrumental efficiency, and their stray light level was characterized. The SECCHI extreme ultraviolet telescope was also characterized in visible wavelengths and in the EUV. The twin STEREO spacecraft were launched on October 26, 2006, from Kennedy Space Center. In the near future, the Helium Resonance Scatter in the Corona and Heliosphere (HERSCHEL) experiment will enter the NRL test facility for its calibration program.



The SECCHI POC at NRL showing the command and telemetry stations for the two spacecraft instrument suites, SECCHI-A (left) and SECCHI-B (right).

The division has many new space instruments under development or recently completed, including SECCHI; EIS, the Extreme Ultraviolet Imaging Spectrometer for Japan's HINODE mission launched September 22, 2006, from the Uchinoura launch facility in Japan; Gamma Ray Large Area Space Telescope (GLAST), a high-energy gamma-ray detector for NASA to be launched late 2007; Spatial Heterodyne Imager for Mesospheric Radicals (SHIMMER), a spatial heterodyne spectrometer for middle atmospheric research for a DoD mission; and Tether Physics and Survivability Experiment (TiPS), ultraviolet spectrometers for upper atmospheric research for Taiwan's COSMIC program.

A network of computers, workstations, image-processing hardware, and special processors is used to analyze and interpret space data. The division's space science data acquisition and analysis effort currently includes observations and analysis of the evolution and structure of the solar corona from the disk to 0.14 AU using data from LASCO and the Extreme Ultraviolet Imaging Telescope (EIT) on the SOHO spacecraft. More recently, data is being acquired from the newly launched EIS instrument on HINODE and the twin SECCHI instruments on the STEREO mission. NRL maintains a complete database of spacecraft observations and control over acquisition of data from new observations. These data are available to qualified investigators at DoD and civilian agencies. In addition, the division has a sounding rocket program that affords the possibility of obtaining specific data of high interest and of testing new instrument concepts. These include the general area of high-resolution solar and stellar spectroscopy, extreme ultraviolet imagery of the Sun, and high-resolution ultraviolet spectral imaging of the Sun.

The SECCHI Payload Operations Center (POC) supports ten telescopes aboard the two STEREO spacecraft orbiting the Sun. The SECCHI POC (see figure) provides observational planning and image scheduling tools, data reduction and analysis, and data archiving. Daily responsibilities include monitoring SECCHI experiment health and status, and uplink of commands, data, and observing schedules. When either STEREO spacecraft is in communication with the Deep Space Network, the SECCHI POC provides real-time commanding and obtains telemetry, including the latest solar images from all telescopes. The SECCHI POC was started before STEREO launch and supported the development, testing, and integration of the SECCHI instruments with the STEREO spacecraft.

Division scientists have developed and maintain physical models in support of their research, including Mass Spectrometer and Incoherent Scatter Radar (MSIS), the standard model for the density of the upper atmosphere; Navy Operational Global Atmo-

spheric Prediction System—Advanced Level Physics High Altitude (NOGAPS-ALPHA), a model to extend weather modeling into the upper atmosphere; Cosmic Ray Effects on Micro Electronics (CRÈME 96), the standard model of the effect of energetic solar particles and cosmic rays on satellite electronics, solar panels, and instruments; and Global Assimilation of Ionospheric Measurement (GAIM), a physics-based model of the ionosphere that is gaining acceptance as the standard ionospheric model.

Space Technology

In its role as a center of excellence for space systems research, the Naval Center for Space Technology (NCST) designs, builds, analyzes, tests, and operates spacecraft and identifies and conducts promising research to improve spacecraft and their support systems. NCST facilities that support this work include large and small anechoic radio frequency chambers, clean rooms, shock and vibration facilities, an acoustic reverberation chamber, large and small thermal/vacuum test chambers, a heat pipe integration and test facility, a spacecraft robotics engineering and control system interaction laboratory, satellite command and control ground stations, a fuels test facility, and modal analysis test facilities. Also, the Center maintains and operates a number of electrical and electronic development laboratories and fabrication facilities for space and airborne payloads, radio frequency equipment, spacecraft power systems, telemetry, and command and control systems, and includes an electromagnetic interference—electromagnetic compatibility test chamber. NCST has a facility for long-term testing of satellite clock time/frequency standards under thermal/vacuum conditions linked to the Naval Observatory; a 5-m optical bench laser laboratory; and an electro-optical communication research laboratory to conduct research in support of the development of space systems.

RESEARCH SUPPORT FACILITIES

Office of Technology Transfer

The Office of Technology Transfer is responsible for coordinating NRL's implementation of the Federal Technology Transfer Act. This office facilitates the transitioning of NRL's innovative technologies for use in products and services to benefit the public. Office of Technology Transfer personnel draft Cooperative Research and Development Agreements (CRADAs) under which NRL scientists and engineers work together with industry, academia, state or local governments, or other Federal agencies to develop NRL



Left photo: Upper Stage spacecraft attached to Star48 3rd stage of Delta II 7925 booster.
Right photo: MiTeX/Upper Stage launch, 21 June 2006, 2215Z. (Courtesy USAF)

technologies for government and/or commercial applications. This office is also responsible for negotiating patent licensing agreements (PLAs) whereby NRL grants licensees the right to use NRL technologies in products for commercial sale.

Part of the Office of Technology Transfer is the Exhibits Office, which works with the Technical Information Services Branch to design and develop full-sized and portable displays, posters, and videos for technical conferences and symposia, Capitol Hill and DoD briefings, sponsor presentations, Laboratory special events, recruitment events, and public events. The NRL booth at trade shows and technical conferences provides a platform for scientists and engineers to market research projects and also enhances NRL's technology transfer efforts.

The Exhibits Office also designs and develops static displays for buildings, such as wall arrangements, division research highlights, and award panels and cases. The static displays in Buildings 72, 43, 226, 28, 222, and Quarters A are maintained by the Exhibits Office. Other services available to the researcher and Laboratory management are assistance in presentation development including research, writing, layout, design, photo/video archival searches, and finalized presentation products; and working with researchers and artists to develop an art concept that visually explains the research concept.

Technical Information Services

The Technical Information Services (TIS) Branch combines publication, graphics, photographic, multimedia, and video services into an integrated organization. Publication services include writing, editing,

composition, publications consultation and production, and printing management. Quick turnaround digital black-and-white and color copying/printing services are provided. TIS uses digital publishing technology to produce scientific and technical reports that can be used for either print or Web. Graphics support includes technical and scientific illustrations, computer graphics, design services, photographic composites, display posters, and framing. The NovaJet Pro 600e and HP Designjet 5500ps printers offer exceptional color print quality up to 600 dpi. They produce large-format indoor posters and signs with 56 inches being the limitation on one side. Lamination and mounting are available. Photographic services include digital still camera coverage for data documentation, both at NRL and in the field. Photographic images are captured with state-of-the-art digital cameras and can be output to a variety of media. Photofinishing services provide custom printing from digital files on a digital minilab. Quick-service color prints are also available. Video services include producing video reports and presentations of scientific and technical programs. TIS digital video editing equipment allows in-studio and on-location editing. The video production, "A Tour of NRL," won four international awards: the Crystal, the Gold Aurora, and two Bronze Tellys.

Administrative Services

The Administrative Services Branch is responsible for collecting and preserving the documents that comprise NRL's corporate memory. Archival documents include personal papers and correspondence, laboratory notebooks, and work project files—documents that are appraised for their historical or informational



Sorting mail for distribution in the Mail Processing Center.

value and considered to be permanently valuable. The Branch provides records management services, training, and support for the maintenance of active records, including electronic records, as an important information resource. The Branch is responsible for processing NRL's incoming and outgoing correspondence and provides training and support on correct correspondence formats and practices. The Branch is responsible for NRL's Forms and Reports Management Programs (including designing electronic forms and maintaining a website for Lab-wide use of electronic forms), compiles and publishes the NRL Code Directory and Organizational Index, and is responsible for providing NRL postal mail services for first class and accountable mail and for mail pickup and delivery throughout NRL. The Branch also provides NRL Locator Service.

Ruth H. Hooker Research Library

The NRL Ruth H. Hooker Research Library exists to enhance and support NRL and ONR scientists in accomplishing their research objectives through the comprehensive availability of all relevant scholarly information sources; a strategic effort to capture the NRL research portfolio; and the deployment, customization, and creation of cutting edge information resources and services as part of the NRL Digital Library.

Traditional library services include an extensive technical report, book, and journal collection dating back to the 1800s housed within a physical facility configured for study and research, staffed with subject specialists and information professionals. The collections include 46,000 books, 80,000 bound historical journal volumes, 3,000 current journal subscriptions, and nearly 2 million technical reports in paper, microfiche, or digital format (classified and unclassified). Services include advanced information consulting; professional literature searches against all major scholarly online databases including classified databases, to

produce on-demand subject bibliographies; circulation of materials from the collection including classified literature up to the SECRET level; retrieval of nearly any article, report, proceeding, or document from almost any source around the world; and training/orientation to help researchers improve productivity through effective use of the library's resources and services.

To enhance traditional services, the NRL Research Library has developed and is continuing to expand the NRL Digital Library. The Digital Library currently provides desktop access to thousands of journals, books, and reference sources at NRL-DC; NRL-Stennis, MS; NRL-Monterey, CA; and the Office of Naval Research.

To provide immediate access to scholarly information, all relevant current journals and conference proceedings in the NRL Research Library's collection are now fully searchable at the researcher's desktop (nearly 3,000 titles) and over 60% of the print journal volumes are also available online. The breadth and depth of content available through TORPEDO Ultra, NRL's locally-loaded digital archive (<http://torpedo.nrl.navy.mil>), continues to grow and is realizing its potential as a single point of access for scholarly information by providing full text search against journals, books, conference proceedings and technical reports from 15 publishers (7+ million items, 60+ million pages in 2006).

The NRL Research Library has also created the innovative NRL Online Bibliography service, which is ensuring that the entire research portfolio of written knowledge from all NRL scientists and engineers since the 1920s will be captured, retained, measured, and shared with current and future generations. It is serving as a model for other commands across the Navy and Federal Government.

As a "partner in research," the NRL Research Library continues to be the most advanced research library in the Department of Defense, serving as a productivity multiplier and a transformational force that



Associate librarian and reference librarian working in the NRL Research Library.

has changed the way science is done at NRL—making the NRL Research Library a sought-after resource around the world.

FIELD STATIONS

NRL has acquired or made arrangements over the years to use a number of major sites and facilities for research. The largest facility is located at the Stennis Space Center (NRL-SSC) in Bay St. Louis, Mississippi. Others include a facility at the Naval Postgraduate School in Monterey, California (NRL-MRY), and the Chesapeake Bay Detachment (CBD) and Scientific Development Squadron One (VXS-1) in Maryland. Additional sites are located in Virginia, Alabama, and Florida.

Stennis Space Center (NRL-SSC)

The NRL Detachment at Stennis Space Center, Mississippi (NRL-SSC), consists of NRL's Oceanography Division and portions of the Acoustics and Marine Geosciences Divisions. NRL-SSC, a tenant activity at NASA's John C. Stennis Space Center (SSC), is located in the southwest corner of Mississippi, about 50 miles northeast of New Orleans, Louisiana, and 20 miles from the Mississippi Gulf Coast. Other Navy tenants at SSC include the Naval Meteorology and Oceanography Command, the Naval Oceanographic Office, the Navy Small Craft Instruction and Training Center, the Special Boat Team-Twenty-two, and the Human Resources Service Center Southeast. Other Federal and State agencies at SSC involved in marine-related science and technology are the National Coastal Data Development Center, the National Data Buoy Center, the U.S. Geological Survey, the Environmental Protection Agency's Gulf of Mexico Program and Environmental Chemistry Laboratory, the Center for Higher Learning, University of Southern Mississippi, and Mississippi State University.

The Naval Meteorology and Oceanography Command and the Naval Oceanographic Office are major operational users of the oceanographic, acoustic, and geosciences technology developed by NRL researchers. The Naval Oceanographic Office operates the Major Shared Resource Center (MSRC), one of the nation's High Performance Computing Centers, which provides operational support to the warfighter and access to NRL for ocean and atmospheric science and technology.

The Acoustics, Marine Geosciences, and Oceanography Divisions occupy more than 175,000 ft² of research, computation, laboratory, administrative, and warehouse space. Facilities include the sediment core laboratory, transmission electron microscope, moving-

map composer facility, underwater navigation control laboratory, computed tomography scanning laboratory, visualization laboratory, ocean color data receipt and processing facility, environmental microscopy facility, maintenance and calibration systems, environmental modeling and simulation high-speed network, and numerous laboratories for acoustic, geosciences, and oceanographic computation, instrumentation, analysis, and testing. Special areas are available for constructing, staging, refurbishing, and storing seagoing equipment.

Monterey (NRL-MRY)

NRL's Marine Meteorology Division is located in Monterey, California (NRL-MRY), about 1 mile from the Naval Postgraduate School (NPS) campus on the grounds of the Navy Region Southwest Support Detachment (NSD) Annex. The NRL facility is collocated with the Navy's Fleet Numerical Meteorology and Oceanography Center (FNMOC) and a NOAA National Weather Service Forecast Office (NWSFO). The five-acre NSD Annex campus comprises four primary buildings—one occupied by NOAA, one shared by NRL and FNMOC supercomputer/operating facilities, and two large buildings dedicated to NRL-MRY and FNMOC office spaces, computer laboratories, and conference facilities. The site also provides two modular office buildings and warehouse space. NRL-MRY occupies 30,000 ft² of office and meeting space, a small library, the Supercomputing Resource Center, the Bergen Data Center, the Satellite/Radar Processing Facility, and spaces to support the Navy Integrated Tactical Environmental System (NITES), the Coupled Ocean/Atmosphere Mesoscale Prediction System—On Scene (COAMPS-OS®), and the Master Environmental Library.

NRL-MRY is dedicated to advancing fundamental scientific understanding of the atmosphere, including the air-sea interface, and to applying those scientific discoveries to develop innovative objective weather prediction systems. FNMOC and the Navy's operating forces are the primary customers for the numerical weather prediction and satellite product systems developed by NRL-MRY. FNMOC is the Navy's central facility for the production and distribution of numerical weather prediction and satellite products in support of Navy operations around the globe, as well as to other defense-related activities. The collocation of the scientific developer and the operational customer results in a "Team Monterey" effort offering unique advantages to successfully implement new systems and system upgrades, and to rapidly integrate new research results into operating systems. NRL-MRY has direct access to FNMOC's large classified supercomputers, allowing advanced development to take place using the real-time

on-site global atmospheric and oceanographic databases. Collocation benefits FNMOC and NRL-MRY scientists as they transition and implement mature systems. NRL-MRY scientists remain readily available to offer assistance should problems arise during system operation.

NRL-MRY benefits from the proximity of NPS, conducting collaborative research with its Meteorology and Oceanography departments. NPS in turn leverages the expertise of NRL scientists as guest lecturers and thesis committee members. NRL-MRY also maintains collaborative relationships with a number of the 25 local organizations that make up the Monterey Bay Crescent Ocean Research Consortium, which coordinates and promotes research, education, and outreach activities using the Monterey Bay as a natural laboratory.

Chesapeake Bay Detachment (CBD)

CBD occupies a 168-acre site at Randle Cliffs, Maryland, and provides facilities and support services for research in radar, electronic warfare, optical devices, materials, communications, and fire research. A ship-motion simulator (SMS) is used to test and evaluate radar, satellite communications, and line-of-sight RF communications systems under dynamic conditions (various sea states). The SMS can handle up to 12,000 lb of electronic systems. A roll motion of up to 30° (15° to port and 15° to starboard) can be applied to this axis. The pitch axis has a fixed motion of 10° (5° to stern and 5° to bow). Periods along both axes, pitch and roll, are variable—from a slow 32-s to a brisk 4-s rate. Variable azimuth motion can also be added to the pitch and roll action. Synchronized positioning information ($\times 1$ and $\times 36$) is available for each of the three axes of the SMS.

Because of its location high above the western shore of the Chesapeake Bay, unique experiments can be performed in conjunction with the Tilghman Island site, 16 km across the bay from CBD. Some of these experiments include low-clutter and generally low-background radar measurements. By using CBD's support vessels, experiments are performed that involve dispensing chaff over water and characterizing aircraft and ship radar targets. Basic research is also conducted in radar antenna properties, testing of radar remote-sensing concepts, use of radar to sense ocean waves, and laser propagation. CBD also hosts facilities of the Navy Technology Center for Safety and Survivability, which conducts fire research on simulated carrier, surface, and submarine platforms.

Scientific Development Squadron One (VXS-1)

Scientific Development Squadron One located at Naval Air Station, Patuxent River, Maryland, is manned

by approximately 11 officers, 75 enlisted, and 12 civilians. VXS-1 is currently responsible for the maintenance, operations, and security of three uniquely configured NP-3D Orion aircraft and two RC-12 Beech King Air research aircraft. The squadron conducts numerous worldwide detachments in support of a wide range of scientific research projects.

In FY06, VXS-1 provided flight support for diverse research programs including direct support capability testing in coordination with the Massachusetts Institute of Technology; aerial support for missile testing by the Missile Defense Agency operating from Honolulu, Hawaii; APY-6, testing a ship identification system using synthetic aperture radar; and Rampant Lion, a project combining the efforts of the Office of Naval Research, Department of State, National Geospatial-Intelligence Agency, and United States Geological Survey. Rampant Lion was a presidential priority mission conducted out of Kandahar, Afghanistan, designed to identify potential oil, natural gas, mineral, and water resources, as well as civil infrastructure throughout the country. VXS-1's flight safety record spans 44 years and includes more than 64,000 mishap-free flight hours.

Midway Research Center

The Midway Research Center (MRC) is located on a 162-acre site in Stafford County, Virginia. Located adjacent to the Quantico Marine Corps' Combat Development Command, the MRC has 16,000 ft² of operations and administration area. Instruments include three precision 18.5-m-diameter parabolic antennas housed in 100-ft radomes, a fast-tracking 1-m telescope currently used for satellite laser ranging, and a transportable 16-inch telescope capable of passive optical tracking and laser communications. The MRC, under the auspices of the Naval Center for Space Technology, provides NRL with state-of-the-art facilities dedicated solely to space-related applications in naval communications, navigation, and basic research.

Research Platforms

Mobile research platforms contribute greatly to NRL's research. These include six P-3 Orion turbo-prop aircraft and one ship, the ex-USS *Shadwell* (LSD-15), berthed in Mobile Bay, Alabama. The ex-USS *Shadwell* is used for research on aboard-ship fire-suppression techniques.

Marine Corrosion Test Facility

The Chemistry Division's Marine Corrosion Test Facility, described above in the Chemistry section, is located in Key West, Florida.

THE CORPORATE FACILITIES INVESTMENT PLAN (CFIP)

To conduct preeminent research for tomorrow's Navy, NRL must maintain and upgrade its scientific and technological equipment and provide modern research facilities. The physical plant to house this equipment must also be state of the art. NRL has embarked on a Corporate Facilities Investment Plan (CFIP) to accomplish these goals. This plan and future facility plans are described below.

The CFIP is a capital investment plan that uses both Congressionally approved military construction (MILCON) funds and Laboratory overhead funds to provide modern, up-to-date laboratory facilities for NRL. Planning for future MILCON projects includes an **Autonomous Systems Research Lab** in the FY09 time frame, a **Space Systems Technology Lab** (FY10), an **Electronics Research Lab** (FY11), and the **Marine Meteorology Center** (FY11).

To complement these efforts, overhead funds are being used to renovate and upgrade laboratory and support areas in several existing buildings.

A few recent and planned upgrades are described below.

Plasma Physics

The FY06 NRL Space Physics Simulation Chamber (SPSC) CPP upgrade is designed to facilitate the long duration experimental operation required for full 3D spatio-temporal volumetric data acquisition of large-volume plasmas. The vacuum and magnetic field sub-

systems are being upgraded to facilitate such operation. Five new water-cooled electromagnets are replacing the existing non-cooled magnets, allowing for higher magnetic field strengths and long-duration operational times. Two new cryogenic vacuum pumps have been added to the SPSC allowing for lower base pressures and faster chamber cycling time.

Electronics Science and Technology

The Millimeter-Wave Structure Synthesis Facility (MWSSF) is being augmented by the procurement and installation of a wire electric discharge machining (EDM) tool in 2007. This EDM tool will allow for the realization of millimeter-wave to submillimeter-wave vacuum electronic amplifier and filter components that cannot be fabricated by conventional rotary cutting tools. EDM offers a non-contact process for both hard and soft metals as well as silicon carbide and doped silicon.

Space Science

A recent FY07 CPP grant to the Space Science Division will fund purchase of new laboratory equipment used to perform the precise optical alignments required by space flight instrumentation developed within the Solar Physics Branch for a wide range of sponsors (NASA, NOAA, and DoD). The new equipment will replace aging equipment purchased three decades ago that now requires frequent costly repairs and calibrations.

FEATURED RESEARCH





- 55 Optical Guidance for Shoreline-Following UAVS**
B. Kamgar-Parsi, P. Baker, A. Kahn, and J. Kellogg
- 63 Reducing Corrosion Control Costs with Rapid-Cure Coatings**
A.A. Webb, J. Verborgt, J.R. Martin, W. Groeninger, P.F. Slebodnick, K.E. Lucas, and E. Hogan
- 73 NRL Launches SiC Epitaxial Growth Effort for Future Power Systems**
C.R. Eddy, Jr., D.K. Gaskill, K.-K. Lew, B.L. VanMil, R.L. Myers-Ward, and F.J. Kub
- 83 Vega is a Rapidly Rotating Star**
T.A. Pauls and D.M. Peterson
- 89 Advanced Surge and Inundation Modeling: A Case Study from Hurricane Katrina**
C.A. Blain, T.C. Massey, J.D. Dykes, and P.G. Posey
- 99 By the Light of the Sea**
S.D. Miller, S.H.D. Haddock, T.F. Lee, and C.D. Elvidge
- 107 A Multi-Sensor Aerogeophysical Study of Afghanistan**
J. Brozena, V. Childers, J. Gardner, R. Liang, J. Jarvis, and J. Bowles



Optical Guidance for Shoreline-Following UAVs

B. Kamgar-Parsi,¹ P. Baker,¹ A. Kahn,² and J. Kellogg²

¹Information Technology Division

²Tactical Electronic Warfare Division

Recent counterinsurgency combat operations in and around inland waters indicate the need for specialized technological capabilities to meet the unique challenges of warfighting in riverine theaters. The ability to conduct close surveillance of enemy activities in the riverine arena is of crucial importance to our warfighters. Over the past several years, the Information Technology Division, in collaboration with the Tactical Electronic Warfare Division, has been developing autonomous unmanned air vehicles (UAVs) capable of guiding their flight course along riverbanks and shorelines. Autonomous UAV guidance based on sensory input rather than GPS promises to increase the flexibility in tasking for single or multiple UAVs. This article describes a guidance and autopilot system that successfully navigated a curved shoreline. The project demonstrated that the near infrared spectrum is particularly good for navigating on shorelines since the land and water are easily distinguishable in these wavelengths, as are objects in the water. Also presented is a new control technique which is able to find control parameters in the image space. This overcomes the need for specialized edge extraction and path generation. Attitude control was maintained by the use of matched long wave infrared thermopiles.

UAVS WITHOUT GPS

Surveillance of terrain, bathymetry, and enemy activities in riverine combat theaters is of crucial importance to our warfighters. To meet the special challenges of operating in riverine and littoral environments, the Information Technology Division, in collaboration with the Tactical Electronic Warfare Division and as a part of the CoastWatcher program, has developed autonomous unmanned air vehicles (UAVs) capable of guiding their flight course along riverbanks and shorelines. Field tests demonstrate that these UAVs can navigate autonomously along waterways and can detect the presence of objects in the water.

Current UAV systems operate by using global positioning system (GPS) waypoints, or are controlled by a direct video downlink (teleoperated), or both. However, GPS may be denied or may be ineffective if maps are not available or are outdated due to the dynamic nature of the riverine environment. Dedicating precious manpower to pilot UAVs is expensive, and the benefits of UAV reconnaissance will not be fully realized until they are autonomous. It is highly desirable to control a UAV without having to specify coordinates and without a remote pilot having to fly it. Furthermore, to conduct surveillance in a riverine theater, it is essential for the UAV to be able to recognize water from non-water. Our UAV guidance system integrates navigation and water detection, simplifying the design and increasing the flexibility and robustness of the UAVs.

We have developed an optical UAV guidance system that directs a UAV along a shoreline via images

captured from a silicon CMOS camera mounted underneath the vehicle. This type of autonomous guidance system can reduce the cognitive load on the warfighter, as well as confer immunity to GPS outages. Autonomous guidance will free up warfighters to give supervisory commands to the UAV, which will report back when a surveillance update is available.

GUIDANCE APPROACH

In order for the UAV to follow a shoreline, it must be able to distinguish water and land, and control itself to remain on or near that boundary. This section describes the general approach to the system, and later sections provide the details.

The system first must identify pixels in the images from the camera as water or land, and put the result into a coordinate system from which the air vehicle can calculate guidance. Because of weight and power constraints, it is important to solve the water detection problem with as little sensing and computation effort as possible. Land and water, while difficult to distinguish in the visible spectrum, are easily distinguished in the near-infrared (NIR) spectrum.¹ Fortunately, the silicon used for conventional image sensors is strongly sensitive to this NIR radiation (700–1000 nm), which is why most consumer cameras come with an infrared-cut filter blocking this “nuisance” radiation. Off-the-shelf cameras with appropriate filters can be used to detect water via a NIR image of the ground.

Since the camera is mounted rigidly on the fuselage of the air vehicle, the image of water versus land is pro-

jected onto the ground plane using altitude and attitude information received from the autopilot. Appropriate geometric transforms are applied to accomplish this. There has been prior work on path-following with UAVs, in which a path is first extracted and then a control algorithm directs the aircraft to follow that path.^{2,3} The work described here differs from previous work in that the curve corresponding to the shoreline is not extracted into parametric form. Instead, the algorithm transforms the image into a coordinate system with one axis being a hypothesized bank angle and the other axis being the arc length flown. From here the bank angle resulting in a path tangent to the shoreline can be extracted. This allows the image processing to forgo complicated computations of path, and directly compute the roll angle that will result in the aircraft flying tangent to the path. The simplicity of this algorithm makes it more robust to image processing problems where more complicated edge detectors might fail.

Interestingly, the sensors the UAV uses for attitude control use infrared light, but in a different band, the thermal band. The fact that the sky is colder than the ground allows the attitude to be measured by assuming that the plane is inside a sphere where the top hemisphere is cold and the bottom hemisphere is hot. These sensors are inexpensive and reliable and allow the vehicle to be controlled effectively.

NEAR-IR INFRARED IMAGING FOR WATER DETECTION

While water has a distinct color and texture, these attributes are highly variable. Detecting water using these cues with a standard red-green-blue (RGB) camera can be difficult, since water can take on many colors, depending on turbidity, depth, waves, and time of day. Simulations using such cues were not sufficiently stable or general. However, NIR imaging worked much better in our simulations, producing images that were much more easily interpreted. The satellite mapping community has used these wavelengths for years for water delineation. Both clear and turbid waters strongly absorb NIR wavelengths from 750 nm to 1000 nm, while most other natural substances (vegetation, soil, rocks) reflect them. Because silicon imagers are quite sensitive to these NIR wavelengths (in fact, more sensitive than to visible wavelengths), the systems can use a standard silicon CCD or CMOS camera with a filter that blocks out wavelengths shorter than 800 nm, although the particular wavelength cutoff is not crucial.

The images, when filtered to capture only NIR wavelengths, are straightforward to process into a map of land versus water. The camera exposure is set so that

the land pixels are bright but not saturated. Given this, the pixel values follow a roughly trimodal distribution. The darkest pixels are water, because they do not reflect much NIR light, and the bright pixels are land. The saturated pixels are reflected sunlight from water. Some of the pixels around the reflected Sun on water will be bright but not saturated, so that some additional image morphology operators need to be applied to remove an annulus around the saturated Sun to improve detection performance. Figure 1 is an example of imagery taken on a sunny day. The water detection algorithm detects water as large areas of uniformly dark pixels, or saturated pixels, and land is everything else. This procedure has proved reliable in live tests, and is a fast operation even on the relatively slow CPU currently installed on the vehicle. The most time-consuming task for the computer is warping the image onto the ground's coordinate system.

AIR VEHICLE ROLL CONTROL

The challenge for the guidance system is to follow an irregular shoreline in real-world conditions. Shorelines are usually highly variable, with multiple inlets and peninsulas, resulting in flight paths that will double back, breaking assumptions of many path-following algorithms. In addition, most autopilots work by maintaining the heading of the airplane, and this is the approach that the system used in the initial simulations. However, this approach was highly ineffective at controlling the airplane in simulation because the vehicle's path is controlled indirectly through heading updates that are in turn controlled by bank angles. It is simpler and more effective to use the guidance to control the airplane's path directly by issuing roll commands.

The guidance system sends the roll angle to the autopilot, which operates in coordinated flight, meaning the rudder operates to keep the airplane at a fixed altitude. For robustness it is desirable for the algorithm to minimize the state information carried from one iteration to the next. This lack of state information means that it is important to keep the coastline in view as much as possible, which means that the airplane should turn around sooner if there is a peninsula that will cause a turn of more than ninety degrees. The algorithm in the work of Frezza⁴ satisfies these constraints, but relies on previously extracted path data, which can be expensive to extract and parameterize. Our algorithm avoids this. The algorithm warps the image into the control coordinate space. This "turn map" has as its x-axis the arc length that the airplane travels, and has as its y-axis possible roll angles. Each pixel thus corresponds to the terrain expected to be underneath the airplane given a fixed roll for a certain distance. Horizontal lines in the turn map correspond to circular

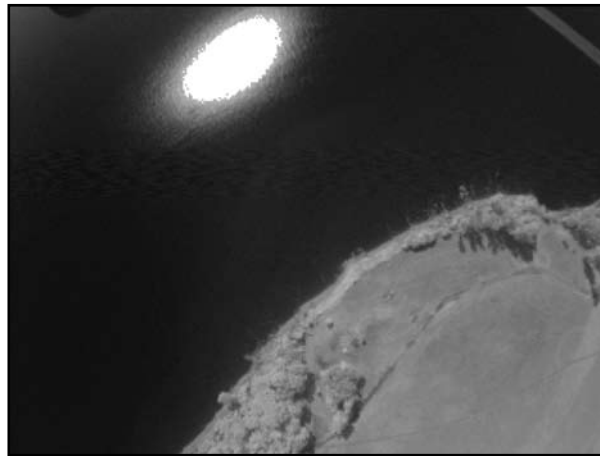


FIGURE 1
In-flight imagery on a sunny day.

paths in the map of the ground plane. Figure 2 shows an actual calculated world map from an experiment, and Fig. 3 shows the turn map generated from that world map. The intuition behind the turn map is that it maps out the predicted terrain under the aircraft for all constant roll parameters, which in the absence of wind, are circles. In most cases, only one of these circles will be tangent to the coastline, and this will occur when there is a sharp transition of terrain between two rows (i.e. possible roll commands).

In this space, the calculation of a suitable path is transformed into a simple image-processing problem of finding a large change from horizontal line to line. The line at which the largest change occurs is the roll angle chosen, thus obviating the need for any fragile edge extraction/parameterization. Many possible trajectories will cause the airplane to follow a trajectory close to the shoreline. The algorithm must find only one of these reasonable trajectories, in the absence of further constraints on the flight path.

FIGURE 2
World example showing separation of water and land.

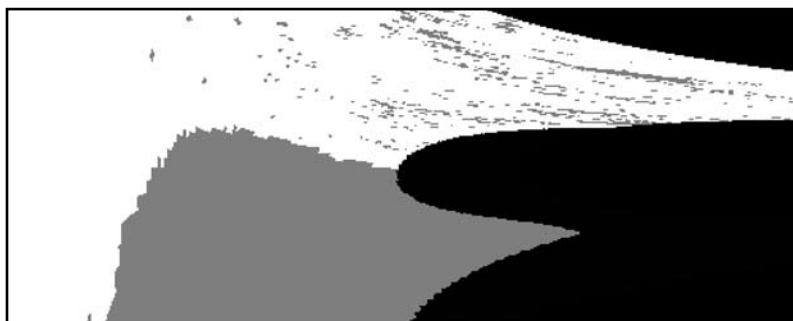
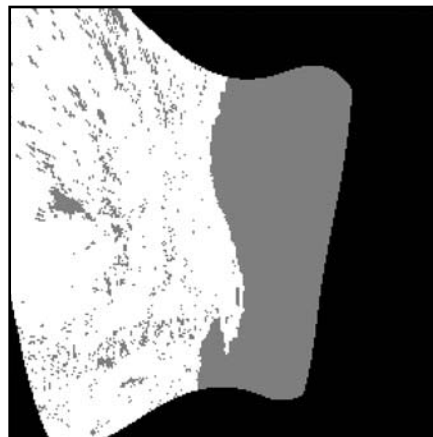


FIGURE 3
Turn map generated from world map of Fig. 2.

The guidance system sends roll commands to the autopilot in order to guide the airplane along the coast. The following algorithm generates the roll commands:

- Analyze the image to find land and water pixels.
- Project image pixels onto the ground plane.
- Compute the turn map.
- Choose the roll angle that corresponds to the largest line-to-line change in the turn map.

Convergence properties of this algorithm are not known at this point, but limited testing has shown it to be a stable method.

GUIDANCE HARDWARE DESIGN

The camera system chosen is a Unibrain Fire-I camera with a resolution of 640×480 pixels. This camera is small and has a Firewire interface, which is easy to program in the Linux operating system. The CCD quality is not of prime concern because the algorithm looks at spectral data, and coarse resolution is adequate for UAV guidance. Using a 1.9 mm focal length lens on the type 1/4 CCD results in a horizontal field of view of 87 degrees and a vertical field of view of 71 degrees. Since the camera is attached to the fuselage of the UAV, a roll of 30 degrees will still result in a minimum 30 degree field of view to each side, sufficient to maintain view of the shoreline in expected flight circumstances.

An Ampro CoreModule 600 PC-104 board runs the operating system and guidance code, while an Ampro MiniModule 1394 connects to the Firewire camera interface. The processor is an Intel ULV Celeron, running at 400 MHz. This system is capable of handling the computational load of the guidance system. Storage consists of a SanDisk 4GB CompactFlash card, ample storage for image logging.

VEHICLE CONTROL

A prime requirement in the design of the autopilot for our work under the CoastWatcher program is to provide true attitude information, preferably without having to rely on the data from a GPS receiver. A simple, yet effective way of providing this attitude information is with the use of infrared thermopiles.⁵ In addition to the thermopiles, a GPS receiver was added to provide a ground-truth reference as to the actual flight path that the aircraft took, for later data analysis. The GPS altitude data was also used in the autopilot for altitude hold functionality, but this same feature could have been implemented as a barometric pressure system. A hobby model aircraft radio control receiver was integrated into the system for testing, launch, and recovery of the vehicle. The autopilot system commu-

nicates with the guidance computer via RS-232 serial. A system-level diagram of the autopilot is shown in Fig. 4.

The vehicle keeps no state and computes new roll angles at 5 Hz. The algorithm has proved to be stable and smooth in simulation and operation.

IR SENSOR OPERATION

The attitude measurement system of the autopilot is based on the use of MEMS thermopiles. These devices convert incident long-wave infrared radiation into a proportional voltage. When measuring attitude, these sensors sense the average background temperature of the sky and ground visible within each sensor's field of view. In most cases, there is a significant difference in temperature between sky and ground. During testing, a total temperature differential of up to 60 °F has been measured. An illustration of the roll sensing is shown in Fig. 5. As can be seen, the sensors are arranged such that a differential temperature between the port and starboard side of the aircraft can be measured.

This differential temperature, or voltage measurement, can then be used to compute the vehicle attitude relative to the thermal horizon. If the vehicle is flying at a high altitude, such that the ground can be assumed flat over the field of view of the sensor, then the assumption is valid in that the thermal horizon is equal to the inertial horizon.

In implementation, three pairs of sensors are used. The sensors are built into the structure of the vehicle, arranged to minimize the amount of aircraft structure in each sensor's field of view; this maximizes the accuracy of the attitude measurement. The sensors are arranged such that one pair is port and starboard to measure the roll attitude. Another pair of sensors is arranged fore and aft to measure pitch attitude. A final pair of sensors is arranged top and bottom to measure the maximum thermal differential possible. This last vertical pair is needed so that an accurate calculation of attitude can be made.

CONTROLLER

The controller design for the autopilot is based around three single-input single-output (SISO) linear controllers to regulate roll attitude, pitch attitude, and altitude. It is assumed that the base air vehicle is statically stable, and is highly damped in both roll and pitch, thus not requiring additional rate damping. The control design is also made around a single operating point. As the autopilot design does not include an airspeed sensor, no gain scheduling is possible to handle the change in sensitivity of the control surfaces with airspeed.

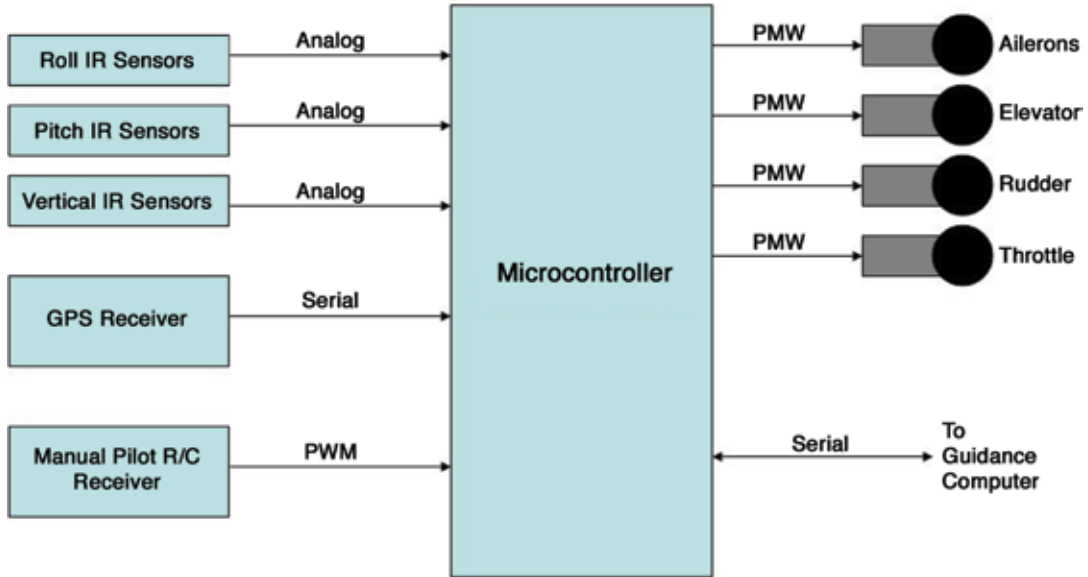


FIGURE 4
Autopilot architecture.

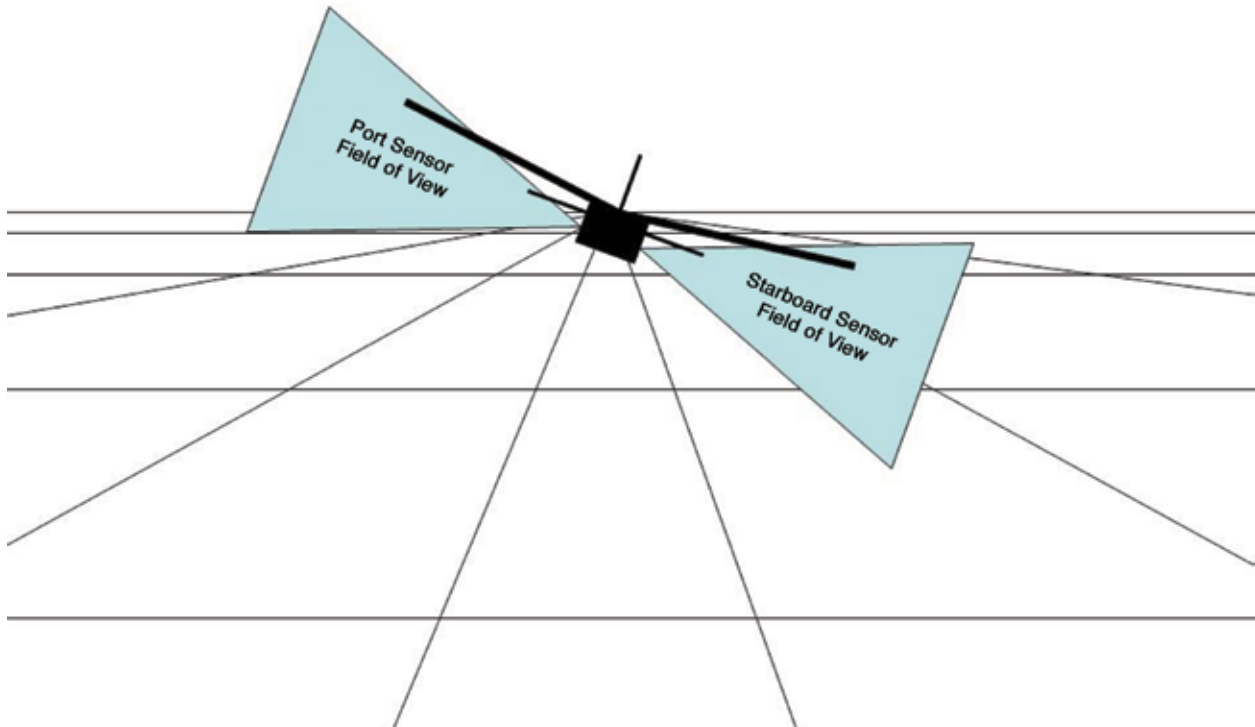


FIGURE 5
Roll sensor fields of view.

The roll and pitch control loops are both implemented as proportional-integral controllers featuring integrator anti-windup protection. The altitude control loop is a proportional-integral controller with flight path angle command as a feed-forward into the pitch control loop. Altitude measurement and commanded altitude are used with the gain based on the desired convergence time and designed flight speed to compute a bounded flight path angle. The resulting flight path angle is then used as the command for the pitch attitude controller.

VEHICLE DESCRIPTION

The airplane is roughly five and a half feet long and has a seven-foot wingspan. For propulsion it has an electric motor connected to two lithium polymer cells, which provide greater than thirty minutes of flight time when fully charged. The airplane has a GPS antenna, the output of which is used for altitude control, and to provide a ground track with which to judge the success of the coast following. The vehicle also has a FreeWave modem for downloading telemetry during the flight, although all data is logged as well.

TESTING AT BLOSSOM POINT PROVING GROUNDS

Our team took the UAV to Blossom Point Proving Grounds, MD, and flew the airplane on numerous tests to gauge its water-following abilities at different locations, including at the sharp peninsula depicted in Fig. 6. The aircraft took off under radio control, shown in Fig. 7. When the vehicle achieved an altitude of 200 m and was headed toward the coast, control was handed over to the guidance and autopilot system. The airplane consistently acquired the shoreline and rounded the peninsular point in both directions, maintaining altitude. This demonstrates the capacity to detect water and land, convert this information to roll commands, and guide the vehicle so that it stays close to the shoreline.

In Fig. 6, the track of the airplane as obtained by the GPS antenna is superimposed on a map of Blossom Point. The guidance system was engaged at the green end of the track, flying directly toward the shoreline. The track colors indicate

- red: hard right turn
- yellow: gentle right turn
- green: approximately straight
- cyan: gentle left turn
- blue: hard left turn

From the track you can see that the guidance system started while the aircraft was over land. The aircraft then acquired the shoreline, rounded the point,



FIGURE 6
Aircraft track at Blossom Point Proving Grounds. The track has not been corrected for wind effects, which can be accomplished with a simple wind module.



FIGURE 7
Aircraft used in testing.

and continued somewhat off the shoreline until control was retaken by the pilot.

The testing day was sunny, with a south wind of approximately 12 m/s, a significant fraction of the vehicle’s airspeed. The wind estimates were obtained by using the aircraft’s constant airspeed and the GPS coordinates, and finding the center of a circle fitted to the ground velocity estimates. The airplane tracked the shoreline in both instances without oscillations.

The northward bias in the track is due to the wind. The airspeed of the plane was approximately 30 m/s, and when the vehicle is traveling east to west, the bias is between 100 and 200 meters. The vehicle looks ahead a maximum of 500 meters. The wind speed of 12 m/s caused the aircraft to crab at about 20 degrees. Since the algorithm, when following a straight line, causes the airplane to aim for the farthest land point, this crab angle corresponds to approximately the bias seen. The bias was seen in both directions on both the north and

south coasts of the point, so it was not due to image processing.

CONCLUSION

This project has shown that an optical guidance system can control a small UAV. The test lasted for approximately three minutes, but the guidance system could have kept guiding the airplane for a longer time, had the radio control had a long enough range. The UAV acquired the shoreline, turned appropriately, and continued without oscillations around a peninsula.

The use of infrared thermopiles provides a reliable, simple, and inexpensive method for the autopilot to measure the attitude of the airplane. Alternative attitude control systems using gyroscopes are heavier and can have problems with integration error over long time periods. The success of this aircraft's flight shows that this technology can form an important attitude sensor in the future.

The use of infrared spectral information (both near and far) allows the guidance algorithm to be robust and simple, and constitutes an example for the design of autonomous guidance systems for UAVs. There has been much research into the spectral properties of water and land, and this knowledge can be used to navigate autonomously, not only to generate maps.

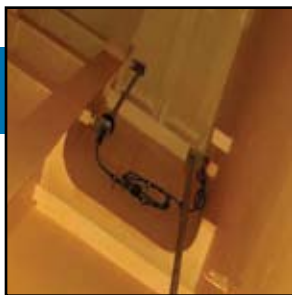
A UAV in a riverine environment can give crucial advance notice of possible courses, and locations of

threats, by flying ahead of a patrol boat or reporting to warfighters stationed in or near water. Future versions with sensors operating in different wavelengths could conduct bathymetry. This capability, combined with autonomous navigation, could enable a UAV to accomplish tasks such as finding the closest break in the reef so that the boat can land on the shore, or finding the best path for a boat down a river. This research supports the Navy's need for tactical intelligence information in riverine and littoral environments, bringing the surveillance capabilities to the warfighters who need them the most.

[Sponsored by ONR]

References

- ¹ W.R. Phillipson and W.R. Hafker, "Manual versus Digital Land-sat Analysis for Delineating River Flooding," *Photogrammetric Engineering and Remote Sensing* **47**, 1351-1356 (1981).
- ² E. Frew, T. McGee, Z. Kim, X. Xiao, S. Jackson, M. Morimoto, S. Rathinam, J. Padiyal, and R. Sengupta, "Vision-Based Road-Following Using a Small Autonomous Aircraft," *Proc. 2004 IEEE Aerospace Conference* **5**, 3006-3015 (2004).
- ³ S. Rathinam, Z. Kim, and R. Sengupta, "Vision-Based Following of Structures Using an Unmanned Aerial Vehicle," Tech. Rep. UCB-ITS-RR-2006-1, Institute of Transportation Studies, University of California at Berkeley, March 2006.
- ⁴ R. Frezza, "Path Following for Air Vehicles in Coordinated Flight," *Proc. 1999 IEEE/ASME International Conference on Advanced Intelligent Mechatronics*, 884-889 (1999).
- ⁵ B. Taylor, C. Bil, S. Watkins, and G. Egan, "Horizon Sensing Attitude Stabilization: A VMC Autopilot," *18th International UAV Systems Conference, Bristol, 2003*, Paper 22 (2003). ★



Reducing Corrosion Control Costs with Rapid-Cure Coatings

A.A. Webb,¹ J. Verborgt,¹ J.R. Martin,¹ W. Groeninger,¹ P.F. Slebodnick,¹ K.E. Lucas,¹ and E. Hogan²

¹Chemistry Division

²Materials Science and Technology Division

NRL's Center for Corrosion Science and Engineering began work on the ONR Future Naval Capabilities (FNC) "Single Coat Program" in 2000. The goal was to reduce maintenance time and provide cost savings by introducing rapid-cure coatings technology to the fleet. Since program inception, NRL in conjunction with NAVSEA05M has successfully demonstrated the new rapid-cure coatings and advanced application process in more than 60 ship ballast tanks, comprising nearly 200,000 ft². There have been no reported in-service failures, the program has demonstrated costs savings of 25–30%, and the Navy will benefit greatly from a new class of qualified coatings. In addition to working with commercial partners, the Marine Coatings Section patented a new resin system and has formulated a new series of solvent-free, rapid-cure coatings designed specifically for shipboard use. These coatings, currently known as "novel resins," are cost-competitive with existing products and are of great interest commercially. They are scheduled for upcoming ship demonstration and final qualification.

INTRODUCTION

In 2000 the U.S. Navy instituted a seven-year program aimed at reducing corrosion control painting costs by incorporating rapid-cure coatings. The Single Coat Program, or rapid-cure coatings program, is sponsored by the Office of Naval Research (ONR) Undersea Weapons and Naval Materials Research Division. It represents the final step in a process of employing solvent-free coatings, instituted by NAVSEA's Materials Engineering Directorate (05M) as a means of reducing preservation costs while providing lifecycle extension to the Navy's ships. At the inception of this program, the use of rapid-cure coatings in the maritime industry was relatively unknown. The program has resulted in a nearly 30% reduction in cost and time with respect to corrosion control and maintenance painting. The Navy's rapid-cure program has also led to a worldwide interest in the use of rapid-cure coatings in commercial shipbuilding and repair for cost savings and lifecycle extension under the new International Maritime Organization (IMO) ballast tank painting protocol. Furthermore, the program has resulted in the development of a new class of coatings at the Naval Research Laboratory that are currently gaining widespread interest within the U.S. Navy and especially in the global commercial shipbuilding community.

Products

Products investigated and employed in the Single Coat Program include a broad spectrum of materials

— epoxies, polyurethanes, polyureas, polyesters, and significant variations within these groups. The program focused mainly on two products: solvent-free, rapid-cure, epoxy-based coatings, and solvent-free, rapid-cure, polyurethane-based coatings.

Although no true definition of "rapid-cure" existed when the program began, any coating that exhibited a cure-to-handle time of three hours or less at an ambient temperature of 25 °C fit within the goals of the program.

Equipment

Successful and economical application of rapid-cure coatings depends on the use of specialized equipment called plural component equipment to supply and mix the base and hardener/catalyst components. The concept of plural component equipment is not new, but improvements for its use in the application of corrosion control coatings have been achieved through the efforts of this and other programs. Figure 1 shows typical plural component equipment configurations with the pump (or proportioner), supply lines, and mixing system for both static and impingement systems. The main difference between the two systems lies in where the coating components are mixed together — the faster the reaction time of the components, the closer to the spray gun the mixing is performed.

For materials with slow reaction speeds and/or minimal component solubility, a static mixer is employed. This configuration is typical for epoxy

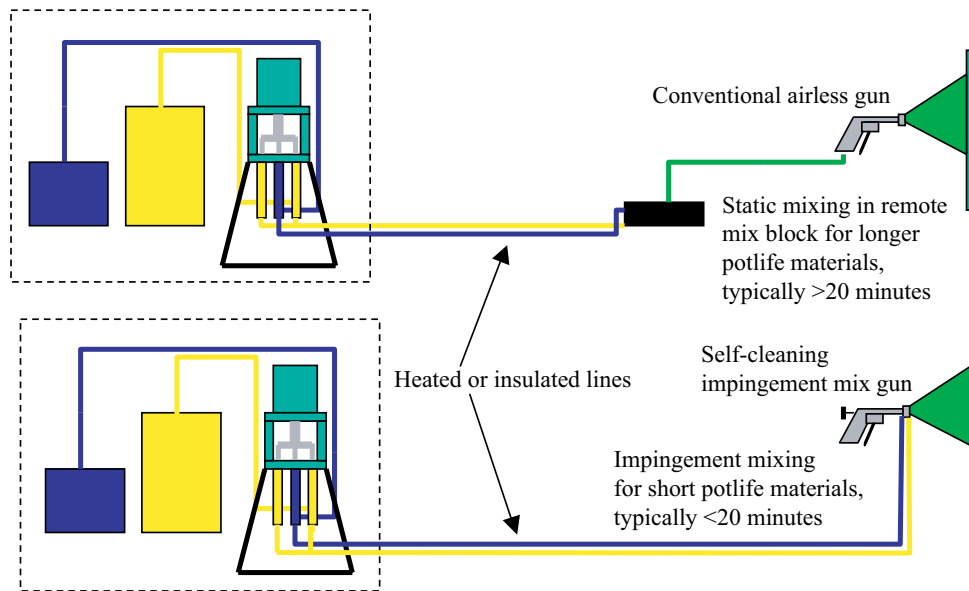


FIGURE 1
Basic attributes of static and impingement plural component systems.

coatings. The fast-cure epoxy coating components are fed via the proportioning pump in individual lines to a static mixer located on the pump itself or in a remote mix block typically located near the work area. From the mix block to the spray gun, the mixed coating is fed via a single line to a conventional airless spray gun.

For products with reaction times of less than one minute, the reaction speed is too fast to employ single-feed application of premixed material. For these products, an impingement mixing gun is employed, in which the components are kept separate until they reach the gun, where they mix and react. Each component must be 100% compatible and capable of thorough mixing at near instantaneous speeds. This is typical for polyurethane and polyurea products, which have extremely fast reaction speeds and very high component solubility. Because nearly all solvent-free polyurethanes have a working time of only a few seconds, that is, no “pot life,” the components must be mixed and applied within a fraction of a second before film setting occurs — although the applied film may not cure hard for more than an hour.

Processes

It was immediately realized that the Single Coat Program would require a complete change in maintenance philosophy and process planning. Indeed, one of the goals of the program was to revamp the entire corrosion control painting process for ship’s tanks and voids, and then to eventually transition this process to other areas within the ship maintenance painting community (i.e., exterior camouflage, internal quarters, and

other coatings application process areas). The ultimate goal was to reduce the preservation time and associated costs. Figure 2 compares the conventional and rapid-cure processes and shows the estimated savings to be achieved from implementation of the latter.

DISCUSSION

Rapid-cure coatings represent a class of products whose chemistry is not unique or unknown. Rapid-cure epoxy adhesives, for example, have been employed for nearly 40 years in the highway industry to adhere roadway reflectors. A plural component dispenser supplies heated epoxy resin and hardener to the applicator holding the reflector. Once the mixed material is dispensed, the worker immediately places the reflector on the pavement, where the adhesive sets to become a near-permanent fixture on the roadway. Polyurethanes have also been used for many years, employed as spray-applied foams and insulation. Again, a plural component dispenser supplies the base and hardener through an impingement mixing gun to the work area.

What separates rapid-cure coatings from rapid-cure adhesives and foams is the basics of formulation. Whereas adhesives and foams are applied in large masses or thick films for adhesion and insulation, coatings are employed for corrosion control and aesthetics. Therefore, the coating formulations require specific properties of flow, leveling, color, and appearance, and for corrosion control coatings, a barrier and/or anti-corrosive performance. Many of the coatings initially evaluated in this program were simple adaptations of quick-setting adhesive formulations modified to

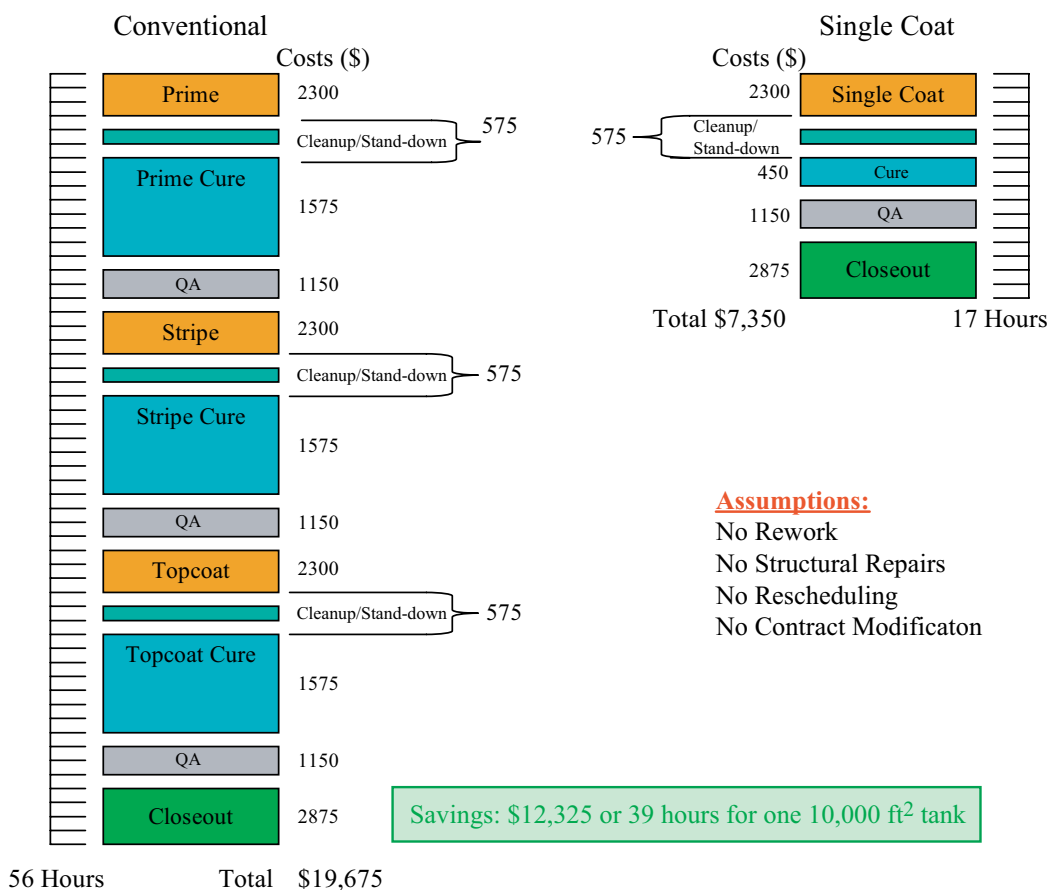


FIGURE 2
Original estimated cost savings using rapid-cure coatings on a 10,000 ft² tank.

perform as a coating. However, it became apparent that most, if not all, of these formulations lacked the attributes required for a corrosion control coating.

The Search for Rapid-Cure Coatings

Prior to and at the beginning of the Single Coat Program, the Marine Coatings Section at the Naval Research Laboratory identified commercial manufacturers of rapid-cure epoxy and polyurethane coatings to provide materials for testing. Emphasis was placed on securing a suitable commercial product to provide an early “proof of concept” to gain fleet support for the rapid-cure program. The rapid-cure epoxy systems available at the time were not suitable for shipboard tank applications — most were variations of existing solvent-based formulations filled with excessive catalyst, or were offensive-smelling polymercaptan-cured systems. Therefore, NRL chose commercial polyurethanes for initial testing and application. At the same time, because none of the available commercial products had all the attributes the Navy was looking for, NRL initiated development of its own materials and

sought the use of alternative technologies, resulting in NRL’s “novel resins,” described below.

By mid-2000, the results of performance evaluation on two commercial polyurethane products were deemed favorable and NRL issued a public statement that these products would be demonstrated on a U.S. Navy ship within a short time. Epoxy manufacturers then responded with efforts to develop an improved, solvent-free, rapid-cure epoxy coating, and submitted samples for evaluation. Early performance was marginal, but epoxy manufacturers agreed they could make additional improvements.

Rapid-Cure Polyurethane Coatings

The formulation of polyurethanes, like all coatings, is part art and part science. The science portion relies on the chemistry of the polyol-isocyanate reaction to fulfill the basic properties of forming a solid material from two liquid components. The art is in understanding the behavior of the polyol and isocyanate components. Because of the reactivity of isocyanates with water, polyurethane coatings must be formulated from

what the industry calls “urethane grade” raw materials. All components, including pigments, fillers, and additives, must be free of water and any residual moisture. As little as 0.01% water can cause foaming, blistering, and improper curing of polyurethane coatings. Therefore the manufacture of polyurethane coatings takes place under dry or anhydrous conditions and typically in an inert gas environment. This makes the cost of polyurethane coatings slightly higher than that of other coatings whose resin components are more tolerant of water and moisture.

A basic polyurethane coating formulation consists of the pigmented polyol component that also contains the fillers and additives, and the unpigmented or “neat” isocyanate hardener. Although the isocyanate component can be pigmented, it is typically left unpigmented to ensure long storage stability. The coatings are formulated in an NCO/OH ratio, which refers to the ratio of isocyanate to polyol. Because one isocyanate reacts with one hydroxyl of the polyol, polyurethane coatings are formulated in an NCO/OH volumetric ratio as close to 1:1 as possible. Once the formulation has been established, the formulator makes a final adjustment to bring the NCO/OH ratio to between 1.01:1 and 1.05:1, resulting in a slight excess of 1 to 5% isocyanate. During application, a small percentage of NCO can react with airborne moisture and thus be rendered inactive, so a slight excess of isocyanate ensures availability for every OH group in the resin, and thus complete reaction of all the polyol.

Polyurethane coatings are not formulated to require a dwell or “induction” time. At the time of application, the isocyanate-polyol reaction proceeds to near completion almost immediately, its rate governed by several factors including ambient temperature, catalyst level, and isocyanate/polyol compatibility. It is important that solvent-free, rapid-curing polyurethane coatings are formulated with polyols that are mutually soluble with the isocyanate, as there is no solvent to assist in assuring component solubility. Indeed, the rapid-cure characteristics of the system prohibit the use of solvents, to avoid solvent entrapment in the cured film.

In the bulk film, the isocyanate-polyol reaction results in nearly 100% polyurethane; however, at the surface, the reaction forms a mix of polyurethane and polyurea. The polyurea reaction is a result of unreacted isocyanate at the surface reacting with airborne moisture rather than with the polyol. As the isocyanate reacts with moisture, it is converted to an amine which in turn reacts extremely rapidly with any available isocyanate. The polyurea reaction at the surface is controlled by the amount of moisture in the air: the higher the relative humidity, the more pronounced the reaction. This phenomenon is less pronounced with solvent-borne polyurethanes, as the escaping solvent

shields the coating surface from moisture, thus preserving a more uniform urethane structure. The polyurea reaction in a solvent-free polyurethane coating formulation is important for industrial coatings application because it has a dramatic effect on the overcoat window of the applied system. Because the polyurea “skin” is highly solvent-resistant (not to be confused with commercial polyurea coatings, which do not have high chemical resistance), it presents a problem with adhesion of the next coat. Therefore each coat of a solvent-free polyurethane should be performed in rapid succession to minimize contamination of the base coat and maximize adhesion. Because a solvent-free polyurethane can be catalyzed to react quickly, the rapid application of successive coats is possible; this is one of the primary benefits of these systems.

RESULTS

Demonstrations of Commercial Products

Polyurethanes: In May 2002, the first rapid-cure demonstration took place when a simply configured 3,000 ft² seawater ballast tank was painted using a solvent-free, rapid-cure polyurethane; see Fig. 3. Figure 4 shows the same tank after six months of service. Despite the anticipation of massive failure and unforeseen difficulties, the application was a complete success. The operator had never applied a rapid-cure polyurethane, but the application was simple and straightforward; some initial difficulties were quickly resolved. This first-ever application of a solvent-free, rapid-cure polyurethane to a U.S. Navy ship represented the first step in perhaps the most significant change to affect shipbuilding in nearly 50 years. For the first time, a tank was painted from start to finish with the complete coating system in *one day*.

The first application came with a hefty price tag of nearly \$46/ft² (\$28/ft² for painting cost only). The high cost was due to the lack of familiarity with the new system; it included a “safety net” consisting of provisions to reblast the tank and apply a conventional coating should the experimental system fail or suffer from improper application. This risk aversion concept was put into practice several more times before it became apparent that application failures were not going to occur and that the use of rapid-cure coatings was meeting the program goals of saving time and money.

In early 2003, the second application of the same solvent-free, rapid-cure polyurethane took place in a seawater ballast tank of higher complexity and comprising approximately 2,500 ft². Using the lessons learned from the first application, the cost was reduced to \$32/ft² (\$18/ft² for painting only). The process took one day for application and a second day for touchup



FIGURE 3
Results of the first solvent-free, rapid-cure polyurethane application in a seawater ballast tank.



FIGURE 4
Results of the first polyurethane system application after six months in service.

in areas not accessible by spray application. In late 2003, a void space of similar area and increased complexity was coated with the same system at a cost of \$28/ft² (\$14/ft² for painting only). The application again took one day for full application and one day for touchup.

In early 2004, a second polyurethane product was demonstrated in a highly confined drinking (potable)

water tank and simultaneously in a complex seawater ballast tank for a combined cost of \$20/ft² (\$6/ft² for painting only). Both tanks were completed in a two day period. Figure 5 shows the polyurethane coating performance in the drinking water tank after two years of service. The original solvent-based epoxy system had barely lasted one year before failing.

Epoxies: In June 2003, after performance evaluation at NRL's Key West Marine Coatings Test Facility, the first rapid-cure epoxy coating made its debut in a U.S. Navy ship. Figure 6 shows the final application of a rapid-cure epoxy coating as applied to a 19,000 ft² seawater ballast tank over a period of two days. The cost for application was less than \$21/ft² (\$7/ft² for painting only). The primary contributor to this significant cost savings was the fast-curing performance of the coating, combined with the large surface area of the tank. The tank was large enough that as one painting crew was finishing application of the first coat, a second crew entered and began applying the stripe coat. A stripe coat is an additional application of product to corners, welds, edges, and other locations, performed as a safety precaution to ensure complete substrate coverage. On the second day, the topcoat was applied and the job was completed. This demonstration represented a significant achievement in the use of epoxy coatings for corrosion control in that it was the first time that two coats of an epoxy system (prime and stripe) were applied to a tank in one day. This would not have been possible with a conventional epoxy coating.

NRL's "Novel Resins"

At the same time that commercial products were being advanced, NRL initiated in-house development of new materials to support the rapid-cure program. Early in the Single Coat Program, it became apparent that there were notable deficiencies with the commercially available polyurethane and epoxy coatings. Although the coatings demonstrated a majority of

FIGURE 5
Performance results of solvent-free, rapid-cure polyurethane in a drinking water tank after two years of service. The tank is not equipped with sacrificial or induced cathodic protection; corrosion control is afforded only by the coating. The rust staining is from TLI mounting brackets only.

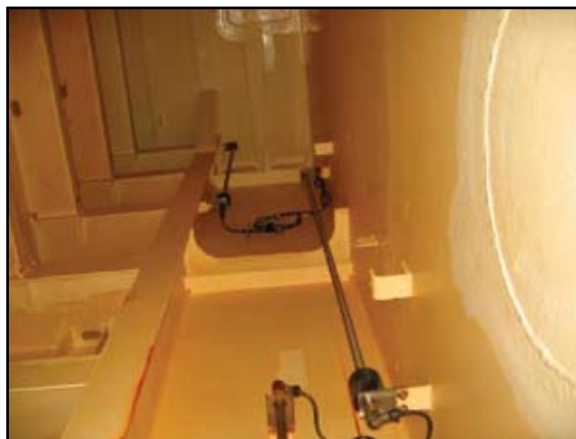


**FIGURE 6**

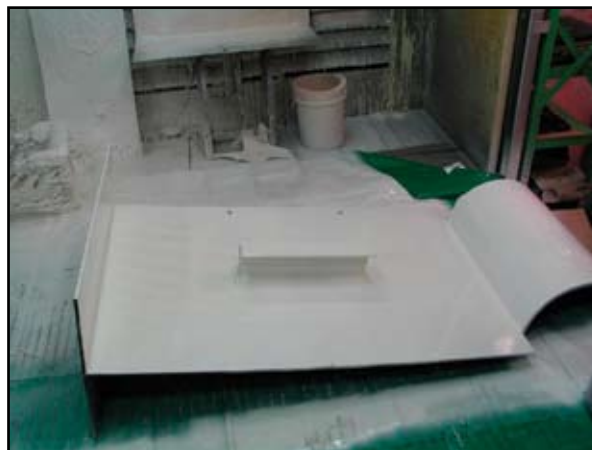
Completed application of fast-cure epoxy in a 19,000 ft² tank.

the required performance and handling attributes, their overall suitability and long-term performance were not clearly established. Therefore, researchers at NRL devised a series of radically new solvent-free polyol materials for rapid-cure polyurethanes. These “novel resins” are based on raw materials commercially available to any coatings manufacturer; furthermore, the synthesis reactions can be performed in any well equipped coatings manufacturing facility. For example, any facility equipped to manufacture its own alkyd or polyester resins has sufficient capital resources to manufacture the NRL resin systems.

The novel resins are a series of amino polyols that when fully synthesized possess the chemical resistance and corrosion control attributes of an epoxy coating along with the rapid-cure characteristics of a polyurethane. The term “amino polyol” is used because the resins are synthesized from two processes: the reaction of alkanol amines with polyfunctional epoxy materials, or the reaction of polyamines with mono-functional epoxide-containing materials — the perfect marriage of two distinct material classes into one universal product offering the most positive attributes of each.

Three main working formulations and about a dozen intermediates have been developed, each with specific performance attributes. The three main products are a low viscosity, low molecular weight material for use alone or as a reactive diluent, a medium viscosity material for light to medium duty coatings, and a higher viscosity version for heavy duty harsh chemical applications. To date, the most sought-after version is the light to medium duty medium viscosity version, as it offers the most epoxy-like handling characteristics with the most attractive rapid-cure polyurethane traits. At present, the product is being licensed and manufactured for commercial use. The system has also been the subject of a detailed and highly publicized productivity study in a commercial shipyard in the Far East; it has been deemed a viable candidate for changing the commercial shipbuilding industry to allow a nearly 40% increase in painting productivity resulting in 20% overall savings to the yard while also meeting the new IMO requirements for a 15-year coating system for seawater ballast tanks on commercial ships.

Figure 7 shows the results of a test application at the commercial shipyard in the Far East using the NRL system as a high-build two-coat product. The entire

**FIGURE 7**

Results of NRL novel resin application to a productivity study test piece.

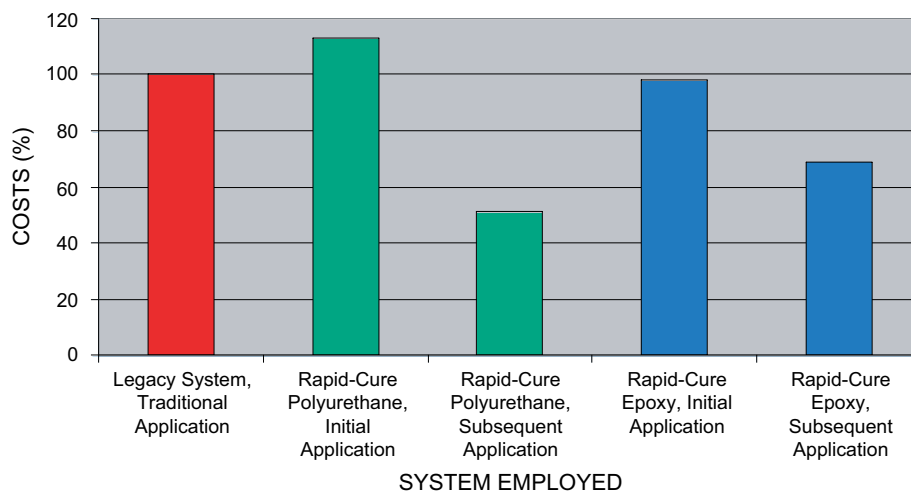


FIGURE 8
Application costs of rapid-cure polyurethane and epoxy systems relative to legacy system.

part was coated in less than 15 minutes, with the full system applied in two coats. The part was cured to handle 20 minutes after application of the second coat. A comparative application using a traditional solvent-based, three-coat epoxy took three days, as each coat had to cure eight hours before the next coat could be applied.

CONCLUSIONS

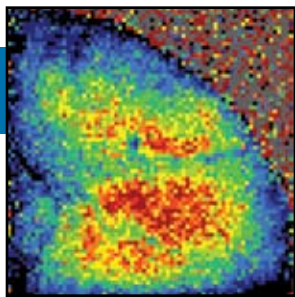
The rapid-cure program has been overwhelmingly successful and has gained significant interest within the fleet. Rapid-cure coatings are now on the Navy's Qualified Products List (QPL) and have also been adopted for corrosion control on submarines.

Figure 8 compares the costs of the polyurethane and epoxy technologies based on first-time (demonstration) application and follow-on (standard production) applications. In each case, reduction in job cost was directly related to the fast cure times. Faster curing lowers the risks of production delays and premature damage.

This program has clearly demonstrated that the application of rapid-cure coatings results in significant cost reduction under the maintenance and repair processes that are prevalent in the U.S. Navy. The cost savings realized under repair processes can be further realized under new building in the military and commercial ship construction sectors.

[Sponsored by ONR]





NRL Launches SiC Epitaxial Growth Effort for Future Power Systems

C.R. Eddy, Jr., D.K. Gaskill, K.-K. Lew, B.L. VanMil, R.L. Myers-Ward, and F.J. Kub
Electronics Science and Technology Division

The Navy's desire for an all-electric ship will require the creation of new devices with power performance far exceeding existing technologies. Silicon carbide has been identified as the primary candidate semiconductor to build such advanced devices. In January 2006, NRL dedicated a new state-of-the-art SiC epitaxial growth laboratory permitting fundamental research to address current limitations of the material, namely, basal plane dislocations (BPDs) and minority carrier lifetime. Equipped with customized in-situ process diagnostics and an accelerated research plan, the laboratory has already succeeded in growing material with minority carrier lifetimes near world record and is focusing on multiple BPD reduction approaches. This initial success was achieved in part by monitoring the gas phase carbon-to-silicon ratio, the primary variable linked to intrinsic defect levels. Further, a demonstration of mass spectrometer sensitivity of $<10^{14}$ dopant atoms/cm³ enables the low, controlled doping required by the device technologies.

NAVY NEEDS IN FUTURE POWER SYSTEMS

The future Navy has a clear need for advanced power systems that will employ integrated electric power architectures on all its ships, boats, and combat vehicles. Such systems significantly improve efficiency, effectiveness, and survivability while simultaneously increasing design flexibility and reducing costs by making the most efficient and effective use of their power plants. Currently, the vast majority of power plant output is dedicated to the propulsion system whether or not the situation requires maximum mobility. Integrated electric power systems utilize a common electrical bus permitting maximum operational flexibility in how the power plant output is distributed to suit the range of payloads, sensors, and propulsion needs for a given tactical situation. Integrated electric power systems will benefit a variety of platforms throughout the Navy including destroyers (DD-21), aircraft carriers (CVN-21), and Virginia-class submarines. Similar benefits are expected in applications to more electric aircraft and all electric combat vehicles throughout the Marine Corps, Army, and Air Force. Because a single common bus will be used for propulsion of future carriers and destroyers, the bus will be operated at high voltages, generally in excess of 10 kV. Such operational requirements place severe demands on the performance of existing power semiconductor device technologies that are based on silicon. Although silicon power device technologies continue to be improved and extended, the realization of a robust, reliable, and high-performance integrated electric power system will require device technologies based on new materials. Significant research over the last decade

has identified the wide band gap semiconductor silicon carbide as the new material of choice to satisfy such requirements.

THE PROMISE AND CHALLENGES OF SILICON CARBIDE

Silicon carbide (SiC) is a compound semiconductor made from silicon and carbon atoms bonded in a single crystalline structure. Of the many crystalline atomic arrangements (polytypes) that exist for SiC, the 4H polytype possesses the best combination of electronic, thermal, and chemical properties for robust high-voltage, high-power electronic device applications. The key attributes of SiC are compared to those of silicon in Table 1. The two key attributes that establish SiC as superior to silicon are its high break-

TABLE 1
 Comparison of Critical Power Electronic Materials Properties for Silicon and the Wide Bandgap Semiconductor Silicon Carbide.

	Si	4H SiC
Bandgap (eV)	1.1	3.26
Electron Mobility (cm ² /Vs)	1350	1000
2DEG Sheet Density ($\times 10^{12}$ cm ⁻²)	10	N/A
Peak Electron Velocity ($\times 10^7$ cm/s)	1	2.0
Critical E Field (MV/cm)	0.3	2.0
Thermal Conductivity (W/mK)	110	330
Power Figure of Merit	1	134

down field, which permits large blocking voltages to be attained with minimal semiconductor thicknesses, and wider band gap, which permits efficient operation of the power device at elevated temperatures, thereby relaxing cooling requirements for future integrated electric power systems. Additional benefits of SiC-based power devices include 400 times lower on-resistance, resulting in increased system efficiency; and a 10 times higher switching frequency which permits smaller passive components, resulting in smaller, lighter power systems. Altogether, SiC presents a more than hundred-fold improvement compared to silicon in potential power performance.

These and other properties of SiC have positioned the material to be of considerable commercial importance in a variety of other markets including substrates for visible and white light emitting diodes, short wavelength lasers, and microwave power transistors, as well as an active material for medium-voltage (1200 V or less) power electronics and ultra-high-frequency power transistors. These significant commercial markets have led to considerable research and development efforts over the last 10 years that have matured the materials technology and brought it to the brink of feasibility for employment in the high-voltage, high-power applications of Navy need. However, significant hurdles remain in the areas of extended defect reduction and low, controlled electron concentrations with very long free carrier lifetimes.

Unfortunately, most commercial applications of SiC materials will not motivate the required materials refinement needed for the high-voltage Navy applications. Recognizing this, researchers in the Electronics Science and Technology Division (ESTD) at NRL began to make a case for the creation of a SiC epitaxial materials research facility that would be charged with further developing the material to enable the realization of high-performance, high-reliability power electronic devices for unique high-voltage Navy applications.

NRL'S ADVANCED SILICON CARBIDE EPITAXIAL RESEARCH LABORATORY (ASCERL)

ESTD's case was presented to NRL management in the fall of 2003 where it received approval to move forward on the establishment of a state-of-the-art facility for SiC epitaxial materials research. Over the course of the next 26 months a customized commercial SiC epitaxial growth reactor was specified, bid, acquired, and qualified. At the same time, a comprehensive facility was specified, bid, and constructed to ensure that a safe, efficient, and effective infrastructure would be in place to support the reactor. Highlights of the facility construction and reactor installation are presented in Fig. 1. On December 21, 2005, NRL took ownership of

the facility and reactor. On January 23, 2006, NRL dedicated its new Advanced SiC Epitaxial Research Laboratory (ASCERL); see Fig. 2. NRL's ASCERL is comprised of two adjacent facilities — the Growth Facility and the Immediate Characterization Facility.

The Growth Facility is centered around an Epigress/Aixtron VP508 high-temperature chemical vapor deposition (CVD) reactor that is widely used in the SiC community to deposit homoepitaxial SiC epilayers on SiC substrates. The reactor is configured to enable a wide range of growth activities as it has n- and p-type doping and two process cells for 2-, 3-, and 4-inch substrates. The two growth cells share gas distribution and radio frequency power systems, yet permit independent processes to be run in each cell. A common configuration is to employ one cell for high-purity and nitrogen doping (to create free electrons in the material) and use the other cell for aluminum doping (to create free holes in the material). Another possibility is to employ novel growth chemistries in one cell while maintaining a conventional, high-purity chemistry in the other. NRL's VP508 was further customized to permit research activities that can advance the state of the art in SiC epitaxial materials quality for high-voltage power electronic applications. These customizations include (1) porting of the system for in-situ mass spectrometry characterization of reaction products; (2) a high-temperature option to elevate the growth temperature to 1800 °C (conventional growth temperature is ca. 1600 °C) for increased growth rates to realize thick films needed for high blocking voltage devices; (3) a modification to the gas handling system to permit the use of halogenated precursors and/or the addition of hydrogen chloride gas to the conventional growth process; and (4) optical access ports to permit in-situ, laser-based diagnostics of the epitaxial surface and near-surface regions. These customizations are a significant part of the research plan to advance SiC epitaxial materials through better understanding and control of conventional and advanced growth processes in a technologically relevant commercial tool.

Adjacent to the Growth Facility is the Immediate Characterization Facility which hosts tools that permit researchers to quickly (same day as grown) characterize epitaxial wafers. The available characterization tools include the following: Nomarski microscopy for surface morphological evaluation; wafer-scale cross polarization scanning for full-wafer defect characterization; Hg probe capacitance-voltage (CV) profiling for lateral and depth profiling of free carrier concentrations; and a Thermo-Nicolet FTIR spectrometer for full-wafer, high-precision thickness maps of epitaxial layers. The characterization tools are housed in a softwall clean room (< class 1000) to minimize particulate-based contamination and permit re-growth on characterized films.



(a)



(b)



(c)



(d)

FIGURE 1

Pictures of the ASCERL facility development: (a) workers install overhead spaceframe for utilities and instrumentation mounting; (b) facility construction completed; (c) installation of SiC epitaxial growth reactor; (d) installation complete.



FIGURE 2

Dedication of ASCERL on 23 January 2006. Participants from left to right: Keith Hull (Public Works Division), Dr. Gerry Borsuk (Superintendent of ESTD), Dr. Charles Eddy (Head, Power Electronic Materials Section), Dr. Bhatka Rath (Associate Director of Research), Dr. Fritz Kub (Head, Power Electronics Branch) and Dr. D. Kurt Gaskill (Power Electronic Materials Section).

A MULTIDISCIPLINARY TEAM, A MULTIFACETED APPROACH

ASCERL researchers routinely collaborate with a large number of physicists, chemists, materials scientists, and electrical engineers in NRL's ESTD who have extensive semiconductor characterization laboratories and who have well-established, world-recognized SiC characterization expertise. These diverse efforts are capable of identifying and analyzing a wide range of materials properties, from the structure, properties, and behaviors of point and extended defects to the physics of reliability of prototype devices. Such close collaborations facilitate rapid progress in research agendas and have helped ASCERL in production of world-class materials during its first year of existence, as described below.

In this first year, ASCERL was visited by representatives from nearly every academic and commercial SiC materials facility in the United States, a tribute to its design, unique capabilities, and people.

PUSHING THE STATE OF THE ART FOR NAVY NEEDS

In striving to further refine SiC epitaxial materials and make them suitable for ultimate application in future Navy power systems, several key thrusts were launched in the first year of ASCERL's function. Highlights of advancements in those thrusts are presented here.

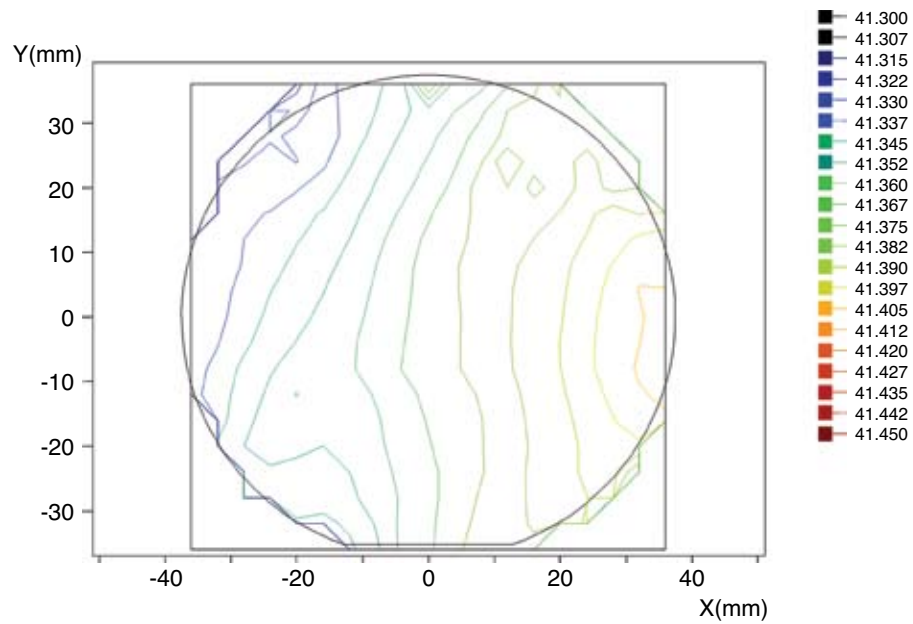
Substrates Matter

As with any epitaxial materials growth effort, the quality of the substrate is of critical importance to the quality of epilayers grown and intended for device applications. To ensure a thorough understanding of the SiC substrate technology, which demonstrates varying degrees of perfection at this time, a number of full-wafer characterization techniques are employed including X-ray diffraction (XRD) mapping. An example of a full-wafer map of the diffraction peak position (a measure of the direction of crystalline lattice planes) and diffraction peak width (a measure of crystalline quality) are shown in Fig. 3. As shown in Fig. 3(a), the lattice peak position varies across the wafer, indicating a curvature of the lattice plane. This curvature is independent of the mechanical shape of the wafer, which can be quite flat, and is observed in all SiC wafers to varying degrees. Such lattice curvature can have significant impacts on the quality of epitaxial layers grown on top of SiC wafers as it results in varying atomic step heights and terrace widths across the wafer surface. These variations can affect the purity

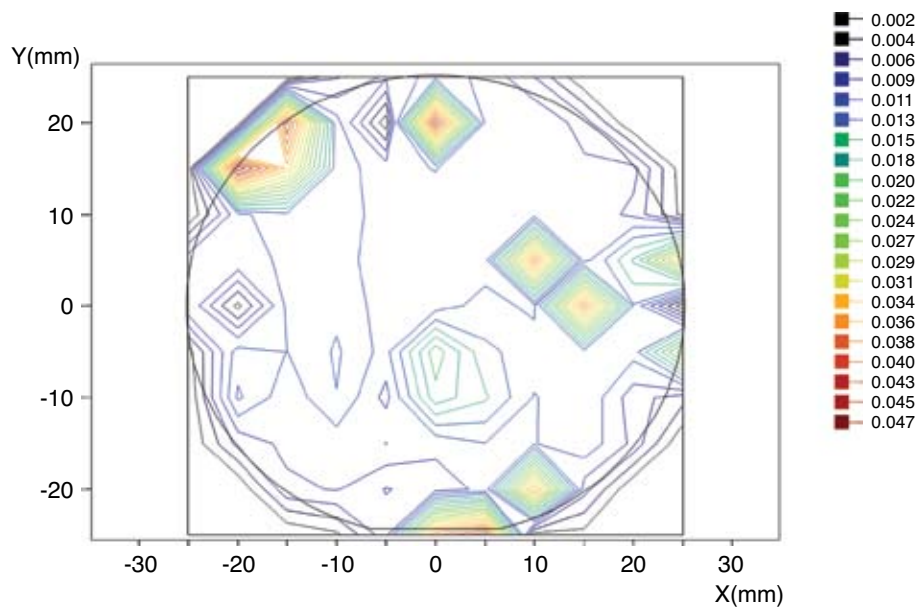
of growth modes of the epitaxial film and impact the defect structure, morphology, and overall quality of the epilayer. The data of Fig. 3(b) presents variations in the overall crystalline quality of the material through measurement of the full width of the diffraction peak at half maximum (FWHM). Wider peak widths are indicative of a more defective nature in the material, which generally leads to more defective epitaxially grown layers. Clearly, a thorough understanding of substrate quality is important not only to refining epitaxial growth processes and material quality, but also to advancing the quality and maturity of SiC substrates. These efforts have shown that X-ray diffraction mapping is a powerful tool in developing this understanding.

What's Going On In There?

The SiC epitaxial growth environment is an extreme environment, to say the least, and a very challenging one to investigate. Typically it is comprised of hydrogen gas under a high flow rate (80 liters per minute) carrying a small mass fraction (<1%) of silane and propane through a reaction zone held at 1600 °C. For this reason, there have been very few efforts to characterize the growth process in situ. However, gaining a better understanding of this environment may be critical to the development of epilayers suitable for high-voltage power electronic devices since the required thick layers of such device structures imply long growths (8–16 hours) and are very sensitive to impurities (at the parts per billion level) and to variations in the gas phase carbon-to-silicon ratio. Through the custom porting of the NRL reactor, we have been able to employ in-situ mass spectrometry to characterize reaction products downstream of the growth zone with surprising sensitivity. An example of such efforts is presented in Fig. 4(a), where the mass spectral signal of the nitrogen partial pressure is tracked during the growth of a "staircase" doping sample. Also shown on the plot is the nitrogen concentration as measured by secondary ion mass spectrometry and the equivalent free carrier density associated with these dopant atoms. This data demonstrates a strong correlation between the mass spectral signals and the ultimate dopant incorporation in the growing layer. As can be seen in Fig. 4(b), at the lowest doping levels, variations in the mass spectral signals for the 28 amu partial pressure correspond to a doping level of $\sim 1 \times 10^{14} \text{ cm}^{-3}$ (or one nitrogen atom in 10 billion carbon and silicon atoms). Such sensitivity is extremely important to the controlled growth of very thick (100 μm), very lightly doped ($5 \times 10^{14} \text{ cm}^{-3}$) drift regions of SiC power devices. Using this first-of-its-kind, in-situ mass spectrometry diagnostic, we will be able to monitor such



(a)



(b)

FIGURE 3
X-ray diffraction maps of a SiC substrate: (a) (0004) peak position and (b) its full width at half maximum.

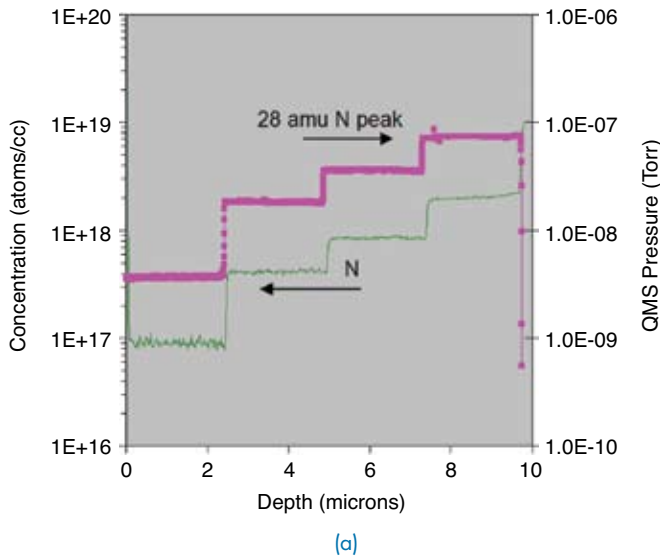
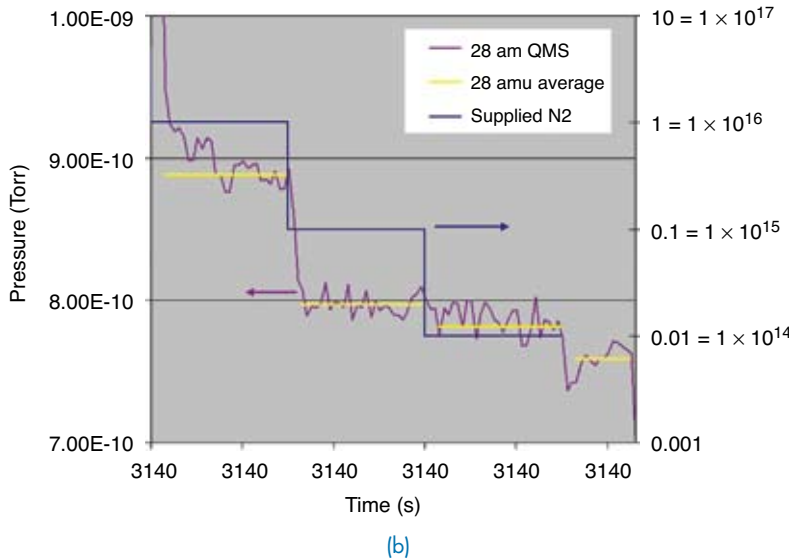


FIGURE 4
 (a) Quadrupole mass spectrometry (QMS) results of nitrogen doping staircase demonstrating the correlation between measured nitrogen during the growth and nitrogen incorporation in the film. (b) QMS data demonstrating the high level of sensitivity of the in-situ mass spectrometric diagnostic technique.



low doping levels in real time and adjust the growth to ensure the desired doping structure in the device epilayers. Such control will enhance the performance of power devices fabricated from such layers.

The Proof is in the Pudding

Although tools such as XRD mapping and in-situ mass spectrometry hold great promise in enabling materials advancements, the true test of ASCERL is the synthesis of state-of-the-art materials. Currently, SiC epilayer quality is often judged by two parameters, background concentration of impurities and lifetime of free carriers in unintentionally- or low-doped (n-type) epilayers. Figure 5 presents CV data on the net background carrier concentration in unintentionally doped SiC epilayers grown in ASCERL during its first year. As can be seen, background carrier concentra-

tions of ca. $mid-10^{13} \text{ cm}^{-3}$ can be routinely achieved. These very low concentrations are attributed to tight control of process conditions and reactor operation, and represent state-of-the-art equivalents. Further, the free carrier lifetime in lightly-doped layers is in the 2–3 microsecond range as measured by photoluminescence transients and the 4–6 microsecond range as measured by microwave photoconductance decay (Fig. 6). Again, these long lifetimes are equivalent to those measured in state-of-the-art materials. Both metrics, background carrier concentration and free carrier lifetime, are critical metrics of materials suitable for high-voltage, high-power electronic devices.

These highlighted advances in the first year of ASCERL's operation demonstrate the immediate relevance of the NRL effort and its potential to be a strong influence in SiC materials refinement for future Navy power needs. Near-term efforts in ASCERL will explore

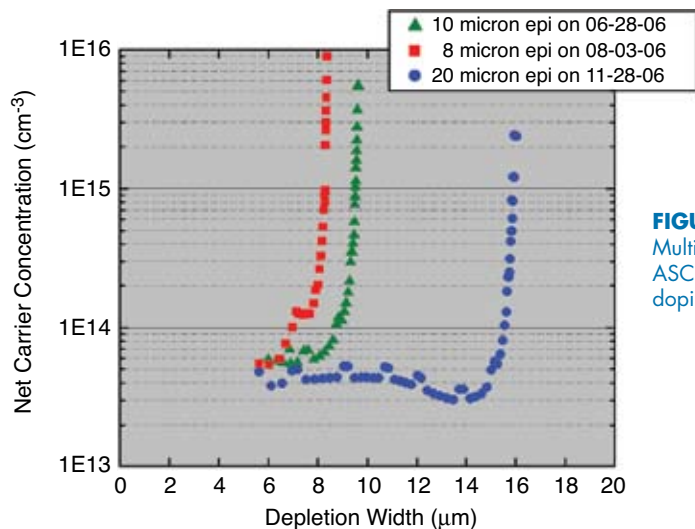
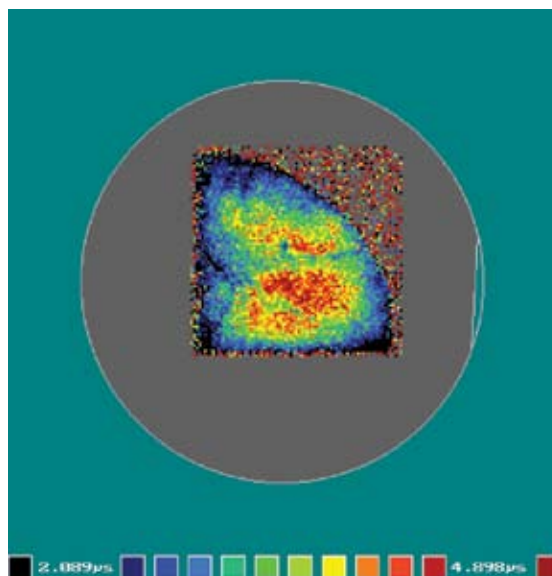


FIGURE 5
Multiple CV traces for unintentionally doped SiC films grown in ASCERL demonstrating ability to routinely achieve background doping levels below $1 \times 10^{14} \text{ cm}^{-3}$.

FIGURE 6
Free carrier lifetime map by microwave photoconductance decay method of SiC epilayer grown in ASCERL. Majority of the epilayer has free carrier lifetimes greater than 4 microseconds.



extended defect reduction and enhanced growth rate processes to push the material toward maturity for high-voltage, high-power bipolar device technologies such as PiN diodes, power metal-oxide-semiconductor field effect transistors (MOSFETs), and insulated gate bipolar transistors (IGBTs).

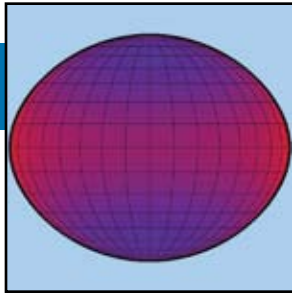
ACKNOWLEDGMENTS

Office of Naval Research (Dr. Colin Wood) for research and postdoctoral fellow support, Drs. Michael

Mastro and Mohammad Fatemi of NRL 6882 for X-ray diffraction assistance, Dr. Ronald Holm of NRL 6882 for assistance and useful discussion, Dr. Joshua Caldwell (ASEE Postdoctoral Fellow) and Dr. Orest Glembocki of NRL 6880.1 for microwave photoconductance decay lifetime measurements, Mr. Marko Tadjer and Dr. Karl Hobart of NRL 6881 for assistance in capacitance-voltage measurements, and Dr. Paul Klein of NRL 6876 for photoluminescence decay lifetime measurements.

[Sponsored by ONR]





Vega is a Rapidly Rotating Star

T.A. Pauls¹ and D.M. Peterson²

¹Remote Sensing Division

²Stony Brook University

A star's most important attributes are its mass, temperature, radius, composition, and rate of rotation. The Sun, for example, rotates once every 28 days, which implies a surface speed of about 2 kilometers per second at the equator. However, there are stars that rotate over 100 times faster. NRL scientists have recently shown that Vega, the brightest star in the constellation Lyra, is a member of this class of rapidly rotating stars. Due to its brightness, Vega has often been used as a standard for calibration purposes assuming it is a slowly rotating star, although there have been problems. The scientists have resolved these problems using the Navy Prototype Optical Interferometer to make observations showing that Vega is a rapid rotator with its axis of rotation pointing nearly directly at the earth. The techniques developed in the course of this work may someday be used to image objects in geosynchronous orbit.

INTRODUCTION

Vega, the second brightest star in the northern sky, is located in Lyra, a prominent northern hemisphere constellation. Because of its brightness and easy accessibility to northern observers, Vega serves as standard calibrator for many branches of astrophysics. In the classification scheme that arranges stars according to their apparent temperature, Vega is the prototype main sequence A star with a temperature of about 10,000 K and a light blue sapphire color. Vega also serves as an absolute photometric standard from the ultraviolet through to the infrared region of the electromagnetic spectrum. Simple analysis of Vega's spectral lines suggests it is rotating slowly, so it has been used to test computer models of stellar atmospheres and stellar evolution.

However, over the years the feeling has developed that our understanding of Vega may not be complete. Models that predict the intrinsic luminosity of a star based on the strength of its hydrogen spectral lines find that Vega is twice as luminous as the models predict. This has led to the suggestion that Vega is rotating rapidly. Rapid rotation, however, causes the observed spectral lines from a star to be broadened due to the Doppler effect, but Vega shows narrow lines. To resolve this seeming contradiction, it was suggested more than ten years ago, based on analysis of subtle peculiarities in the shapes of its spectral lines, that Vega must be a rapid rotator seen nearly pole-on; i.e., its axis of rotation is pointing almost directly at the observer.

Rapid rotation changes the shape of a star: it becomes an oblate spheroid, flattened at the poles and extended at the equator. According to theory,

the extended regions at the equator will have a lower temperature than at the poles, leading to an asymmetric brightness distribution, with the poles brighter than the equator. Thus, observations of Vega that show an asymmetric brightness distribution would confirm that it is a rapid rotator. Such observations require very high angular resolution to see details on the surface of the star. The Navy Prototype Optical Interferometer (NPOI), developed by NRL in partnership with the U.S. Naval Observatory and the Lowell Observatory, has recently made high-resolution observations confirming that Vega is a pole-on rapid rotator.

RESOLVING THE SURFACE OF A SINGLE STAR

What angular resolution do we need to resolve structure on the surface of a star? We can get an approximate answer to this question by calculating the angular diameter of the Sun if it were placed at the distance of the nearest star. The Sun's physical diameter is about 14×10^5 km, and the distance to the nearest star, Alpha Centauri, is about 40×10^{12} km. The ratio of these two numbers is about 35 nanoradians, or converting to angular measure, we find that the Sun would have an apparent angular diameter of 0.007 arc seconds, or 7 milliarcseconds (mas), at the distance of Alpha Centauri. Thus, in order to resolve surface structure on a star, we need a telescope that has a resolution of a few milliarcseconds.

The angular resolution of a telescope is inversely proportional to its diameter and directly proportional to the wavelength of light being observed. Thus, in order to increase the angular resolution of an observation we must either increase the diameter of the tele-

scope or observe at shorter wavelengths. If we choose to observe at visible wavelengths, around 500 nm, then we find that the telescope must have a diameter of over 100 m in order to have a resolution of a few milliarcseconds. Clearly, we can't build a telescope of this size out of a single piece of glass; another approach is needed.

SPARSE APERTURE IMAGING

The technique developed by astronomers to get angular resolution beyond that possible with a single telescope is called *sparse aperture imaging*. Since constructing a single large telescope is not feasible, this technique uses several small telescopes separated by a few tens or hundreds of meters. The light from all the telescopes is combined at a central location. The resulting image has an angular resolution that is related to the largest separation between the individual small telescopes. The origins of this technique can be traced back to the work of the French physicist H. Fizeau more than 140 years ago; it was further developed toward the end of the 19th century by A. A. Michelson who taught at the U.S. Naval Academy and was the first American Nobel prize winner in physics.¹

The underlying physical principle of sparse aperture imaging is the interference of light waves. If the light from two separate telescopes is combined, a pattern of light and dark bands appears. The spacing of the bands and the way they change as the separation of the telescopes is varied tells us something about the structure of the star being observed. This method of mapping the spatial structure of an object is called spatial interferometry, and the resulting instrument is called an *optical interferometer*.²

THE NAVY PROTOTYPE OPTICAL INTERFEROMETER

The Navy Prototype Optical Interferometer (NPOI), shown in Fig. 1, is located on Anderson Mesa near Flagstaff, Arizona, at an altitude of 2200 m.³ The NPOI can combine the light from up to six small telescopes simultaneously, with the telescopes currently separated by up to 79 m. For visible light, the highest angular resolution is a bit more than 1 milliarcsecond, and routine observations can be made at a resolution of 1–2 milliarcseconds. This is just the resolution we need to start to resolve the surfaces of hot stars.

The individual telescopes of the NPOI are arranged in the shape of a Y, as seen in Fig. 1. The telescopes can be moved to different positions along the arms of the Y to change the angular resolution of the instrument. Each arm is 250 m long, so the largest spacing will eventually be 428 m between the tips of two of the arms. Figure 2 shows a ground level view of the center of the array with one of the individual telescope sta-

tions in the foreground. These stations use flat mirrors, called *siderostats*, which reflect the starlight into horizontal vacuum pipes (also visible in Fig. 2), from where the light continues on to the central optics laboratory to be combined with the light from other telescopes. The beam combination takes place on the large optical table shown in Fig. 3.

One of the most difficult challenges for ground-based optical astronomy is the distorting effect of turbulence in the earth's atmosphere, which blurs images made with single telescopes and degrades the resolution to about one arc second. Some of these effects can be mitigated by taking data rapidly; NPOI takes data at a rate of 500 samples per second. Additionally, it turns out that optical interferometers can eliminate the effects of atmospheric turbulence under certain conditions. If we combine the light from three telescopes that form a closed triangle, we can construct a quantity called the *closure phase*, which contains information about the symmetry or asymmetry of the surface of the star, while the atmospheric distortion is cancelled out. The closure phase plays a central role in our discovery of the rotation of Vega.

RESOLVING A ROTATING VEGA

Hugo von Zeipel at the Uppsala Observatory in Sweden developed the theory describing the shape of a rotating star more than 80 years ago. This theory shows that a rapidly rotating star takes on the shape of an oblate spheroid, flattened at the poles and bulging out at the equator. The rotational velocity at the equator can reach several hundred kilometers per second and the resulting centrifugal force (the force causing objects to fly off the surface) reduces the local force of gravity. If the equatorial velocity is high enough, the effective gravity will be very small and the star will break up. For the case of small effective gravity at the equator, von Zeipel's theory predicts a large drop in the local surface temperature that leads to a reduction in the surface brightness, an effect called "gravity darkening." Because of gravity darkening, the temperature, and therefore the brightness of the stellar surface, varies with latitude, being brightest (hottest) at the pole (where the tangential velocity is smallest) and lowest (coolest) at the equator (where the tangential velocity is a maximum). Figure 4 shows such a rapidly rotating star viewed in the equatorial plane. A rapidly rotating star with its rotation axis oriented at some arbitrary angle to the observer's line of sight will show an asymmetric intensity distribution with the bright polar cap appearing off center.

We have developed a computer model of a rotating star incorporating von Zeipel's theory.⁴ The model generates parameters that describe the observations made with the NPOI on May 25, 2001 using three telescopes arranged in a triangle to give a single closure phase. We



FIGURE 1

Aerial view of the NPOI showing three arms arranged in a Y-shaped array; each arm is 250 meters long. There are two modes of operation. The astrometry mode is used to measure stellar positions and uses four fixed siderostats located in permanent huts near the center of the array. The imaging mode uses up to six movable siderostats that can be arranged along the arms of the array.



FIGURE 2

Ground-level view of the NPOI showing the center of the array. At left, one of the movable imaging siderostats is partially visible above its movable enclosure. Three of the permanent huts housing the astrometry siderostats are also visible, along with some of the horizontal vacuum pipes that carry the star light to the beam combination laboratory.

FIGURE 3
View of the optics laboratory showing the table where the light from up to six siderostats can be combined.

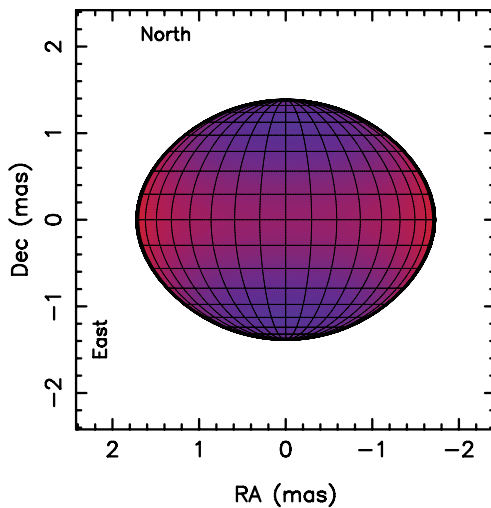
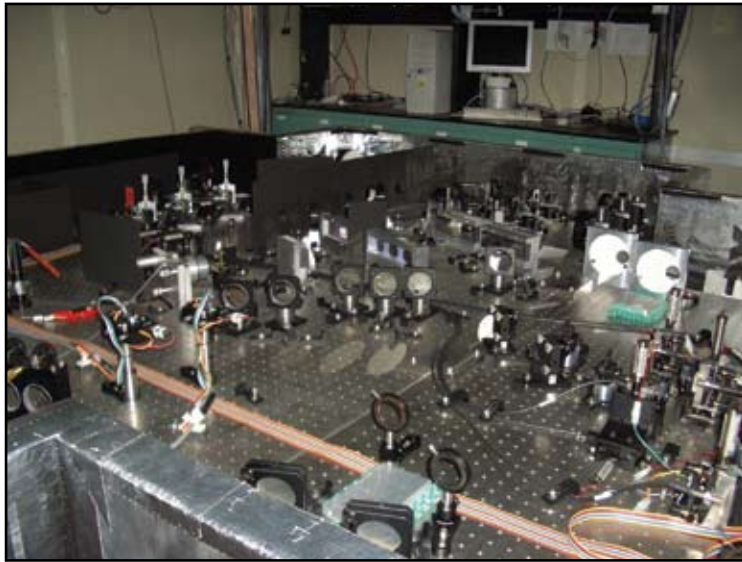


FIGURE 4
A model of a rapidly rotating star viewed in the equatorial plane, showing the extension at the equator and flattening at the poles. The surface temperature is shown in color, red representing cool regions and blue representing hot regions. Dec = declination; RA = right ascension.

then adjust the model parameters until we get the best fit to the data.

The result is shown in Fig. 5 where the open circles are data points from the NPOI and the solid line is the fit from the model. We find that Vega is rotating at nearly 93% of breakup velocity and its rotation axis is inclined 4.5° to the line of sight. In addition, the temperature at the equator is nearly 2,400 K lower than at the pole. A false-color image of the Vega model is shown in Fig. 6, where blue represents the bright parts and red the faint parts of the stellar surface.

As discussed in the introduction, Vega's rapid rotation will have an enormous impact on its use as a primary calibrator in astronomy. Since the emitted intensity varies over the surface, Vega cannot be used to infer intensities across the electromagnetic spectrum based on model atmospheres calculated assuming a single surface temperature. In addition, rapid rotation guarantees efficient mixing in the envelope, and the

results of previous analyses of the composition of the surface could be substantially altered and will need to be revisited. The element composition directly affects the age of Vega derived from evolutionary models, and if the surface abundances previously derived (assuming slow rotation) apply throughout the star, then Vega may be nearly twice as old as previously thought.

FUTURE APPLICATIONS

The Navy has a critical need to image objects in Earth's orbit. Standard ground-based imaging techniques often lack the resolution and sensitivity for this task. However, long baseline optical interferometry may be able to deliver the required detail. In fact, stars and satellites in geosynchronous orbit both present the same basic imaging challenges. Both are too distant to be resolved by existing single telescopes on the ground, and both classes of objects become resolved

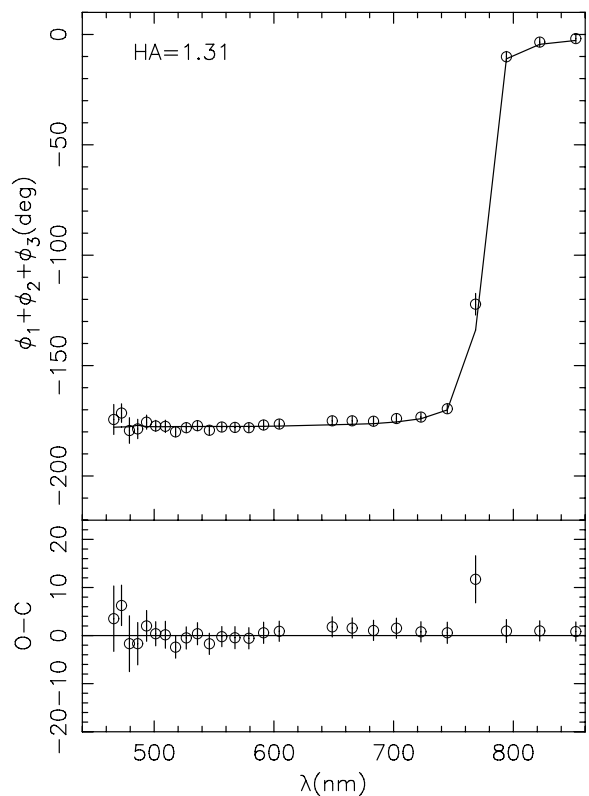


FIGURE 5
 Fitting a model to the Vega data. In the upper panel, the open circles are the NPOI closure phase measurements and the solid line is the best-fit model. The lower panel shows the residuals, the difference between the measurements and the model.

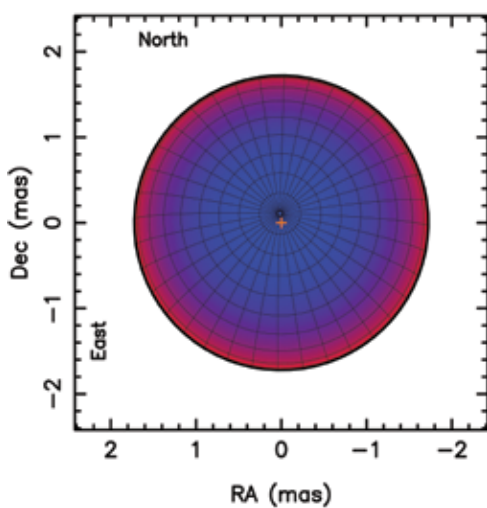


FIGURE 6
 An image of Vega as seen from Earth based on the model of the NPOI data. The blue represents hot bright regions, while red represents cool faint regions. The orange cross is the subsolar point, the geometrical center of Vega as seen from Earth. Dec = declination; RA = right ascension.

with baselines (i.e., the distance between telescopes in an interferometric array) of several tens of meters. The main difference in this context is brightness. Stars are significantly brighter than spacecraft for a given angular size, and provide high signal-to-noise ratio objects for developing and testing analysis algorithms. Thus, the current work at the NPOI on imaging stellar surfaces will act as a pathfinder to imaging satellites in geosynchronous orbit.

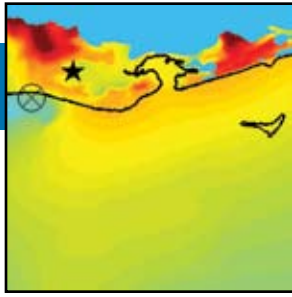
ACKNOWLEDGMENTS

Financial support for this work at NRL is provided by the Office of Naval Research through the NRL 6.1 Core program. We wish to thank our colleagues and

collaborators, including C.A. Hummel, J.T. Armstrong, J.A. Benson, G.C. Gilbreath, R.B. Hindsley, D.J. Hutter, K.J. Johnston, D.M. Mozurkewich, and H.R. Schmitt.
[Sponsored by ONR]

References

- ¹T.A. Pauls, "Origins of Sparse Aperture Imaging," *2001 IEEE Aerospace Conference Proceedings* **3**, 1421-1427 (2001), DOI 10.1109/AERO.2001.931372.
- ²A.R. Hajian and J.T. Armstrong, "A Sharper View of the Stars," *Scientific American* **284**, 56-63 (2001).
- ³J.T. Armstrong et al., "The Navy Prototype Optical Interferometer," *The Astrophysical Journal* **496**, 550-571 (1998).
- ⁴D.M. Peterson et al., "Vega is a Rapidly Rotating Star," *Nature* **440**, 896-899 (2006). ★



Advanced Surge and Inundation Modeling: A Case Study from Hurricane Katrina

C.A. Blain, T.C. Massey, J.D. Dykes, and P.G. Posey
Oceanography Division

The storm surge and inundation from Hurricane Katrina that devastated Gulf Coast communities on August 29, 2005, presented an opportunity to evaluate and advance coastal ocean modeling capabilities at NRL and within the Navy. A highly realistic simulation of Katrina's storm surge and inland inundation was developed using the ADvanced CIRCulation (ADCIRC) model. The finite-element basis of ADCIRC is advantageous in its utilization of unstructured triangular grids. The "Katrina" grid contains 375,479 computational points and 730,431 triangular elements with 225 m spatial resolution in coastal and inland areas, resulting in the largest Navy application of unstructured grid models to date. Comparison between the model-computed high water values at measured high water mark locations along the Gulf coast indicate very good agreement between observed and predicted water levels with average errors of just over one foot. NRL recently transitioned the ADCIRC model to fleet operations for coastal predictions and remains an active ADCIRC development partner.

INTRODUCTION

Throughout modern history, amphibious assaults and landings have been a mainstay of U.S. Navy operations. The vulnerability of landing craft to capsizing, swamping, stranding, and filling with sand and water was clearly realized following a post-World War II review of amphibious operations. Many amphibious landing problems and casualties during World War II were attributed to the waves, currents, and water levels of the local environment. Similar problems occurred during the Korean War. Following the major invasion of Incheon Harbor, a U.S. Navy Tank Landing Ship was stranded during low tide near the tidal basin on Incheon's waterfront on September 20, 1950.

More than fifty years later, the Navy still finds inundated environments challenging for operations. Since the declaration of the Global War on Terrorism following the events of September 11, 2001, military operations are increasingly focused on special operations that take place in coastal environments such as estuaries, shallow waterways, and inland rivers. Inundation in these operational theatres is typically caused by extreme tidal ranges, rainfall-induced flooding events, and/or wind-generated setup. These occurrences directly affect the insertion and movement of Naval Special Warfare (NSW) forces, who routinely operate in environments for which the only know information may be an outdated, perhaps 30-year-old topographic map. Areas subject to inundation processes are often located at the cusp of the land-sea interface where algorithms for processing satellite imagery break down or are sub-optimal.

Inundation from storm surge is a particular concern for stateside Navy installations. The two major homeports for the U.S. Navy's east coast fleet are at Norfolk, Virginia, and Mayport, Florida, both vulnerable to landfalling Atlantic hurricanes. A decision to relocate the Norfolk harbor fleet, for example, could cost \$5 million and would need to take place three days in advance of a predicted landfall in order to recall personnel and to ready ships in maintenance or overhaul for evacuation. Most recently, the Navy base at Pascagoula, Mississippi, on the Gulf of Mexico was directly impacted by the landfall of Hurricane Katrina on August 29, 2005.

As we now know, Naval Station Pascagoula was not alone in registering effects from Hurricane Katrina. The devastation to Gulf Coast communities on August 29, 2005, far exceeded all previously recorded storm events. The extent of storm damage to the coastal states of Louisiana, Mississippi, and Alabama categorizes Katrina as the most destructive and costliest natural disaster in the history of the United States. According to the National Oceanic and Atmospheric Administration (NOAA), the storm surge along the Mississippi coast was the highest ever recorded in the United States. Naturally, the location of NRL-Stennis Space Center (Bay St. Louis, Mississippi) directly in the path of the storm motivated NRL's interest in developing a hindcast representation of Katrina's surge and inland inundation. The events precipitated by Hurricane Katrina provide an invaluable opportunity to evaluate the Navy's capability to predict coastal surge and inundation and to direct future developments that enhance such a capability.

THE SURGE MODEL

Tropical storm and hurricane events can cause a significant rise in coastal sea level when strong winds combine with low barometric pressure. Storm surge forms as winds push elevated sea levels into shallow coastal waters. Winds directed onshore form a “wall of water” that moves towards the shoreline and eventually washes inland, leaving previously dry land covered with water (inundated). For a surge model, then, forcing is derived principally from wind, though tidal effects are also important as they can magnify the height of the surge. The amount of wind energy that translates to the ocean surface is determined by the drag force at the air-sea interface. Surface waves are also generated at this interface but their effects, while significant, are not considered here. Movement of the water is further modulated by frictional effects at the seabed and over land. All of these processes can be represented mathematically to form a numerical model for surge and inundation.

A numerical model predicting surge and inundation computes water height and movement (currents) in the coastal ocean and over inland regions. One such model used widely within the Army and Navy communities is the ADvanced CIRCulation model, ADCIRC (<http://adcirc.org>).¹ ADCIRC has its basis in the well-known, two-dimensional, vertically integrated shallow water equations. The discrete forms of these equations within ADCIRC use a finite element approach, which is particularly well suited to application in complex coastal regions. When using finite elements, the computational mesh is composed of variably sized triangles whose density can vary throughout the modeled region. The range of element density can span several orders of magnitude, lending tremendous flexibility to the construction of a computational mesh. Within a single mesh it is possible to resolve fine-scale features or gradients in the underlying seabed elevations (bathymetry) and/or overland elevations (topography), to represent the complexities of the shoreline and to allow for open ocean boundaries that are remote relative to the coastal area of interest. The inundation of dry land areas is handled by activating and de-activating grid elements using criteria based on a simplified momentum balance between the pressure gradient and bottom friction. The frictional resistance in very shallow water is designed to increase as the depth decreases.

The ADCIRC model is also designed to be portable across various computational platforms and is highly efficient, harnessing the latest parallel processing paradigms to speed the time to solution. The ADCIRC model has a successful history of predicting tides and storm surge spanning nearly fifteen years and is, in fact, the surge model that the Interagency Performance Evaluation Taskforce (IPET) applied to the recent

performance evaluation of the New Orleans and southeast Louisiana hurricane protection system following Hurricane Katrina.

A HINDCAST RECONSTRUCTION OF HURRICANE KATRINA

NRL began a reconstruction of Katrina’s storm surge three weeks after the storm, with a focus on events along the Mississippi Gulf Coast. The initial step was the creation of a computational mesh. The importance of a quality mesh cannot be understated. To accurately represent the surge and inundation it is necessary to resolve fine-scale changes in bottom slope, details of the coastline, and other geographic features such as islands, inlets, and channels, while simultaneously preserving properties of the triangular elements that promote model stability and retaining a computationally viable problem (i.e., a timely solution). Software developed at NRL for semi-automated mesh generation constructs an unstructured finite element mesh using refinement criteria based on specified bathymetric/topographic values and constrained by the coastal boundary points. Several iterations and manual interventions were necessary to obtain the final unstructured finite element mesh designed to capture Katrina’s storm surge and inland inundation; this mesh consists of 375,479 nodes and 730,431 triangular elements, the largest Navy unstructured grid model application to date (Fig. 1). The mesh centers on the northern Gulf Coast region encompassing inland areas, but also includes the entire Gulf of Mexico and extends out into the western North Atlantic Ocean. Such an expansive domain allows the surge to naturally build up within the modeled region as the hurricane moves from the deep ocean into coastal waters. Furthermore, ocean boundaries in deep water are subject to minimal surge and inverted barometer effects and can appropriately accept tidal forcing from a global tide model. These boundaries also are far removed from the coastal area of interest. The targeted spatial resolution of the mesh near the coast and inland is 225 m. The final mesh used for the hindcast of Katrina represents a balance between the desire for fine-scale resolution and the need for stability of the inundation algorithm, and accounts for computational constraints imposed by the necessarily small time-step integration.

To drive the surge model, the best available wind forcing was produced at NOAA’s Hurricane Research Division (HRD) at the Atlantic Oceanographic and Meteorological Laboratory (AOML) through the HRD Real-time Hurricane Wind Analysis System (H*Wind) project. The H*Wind product is an integrated tropical cyclone observing system that uses wind measurements from a variety of observation platforms to develop an objective analysis of the distribution of wind speeds in

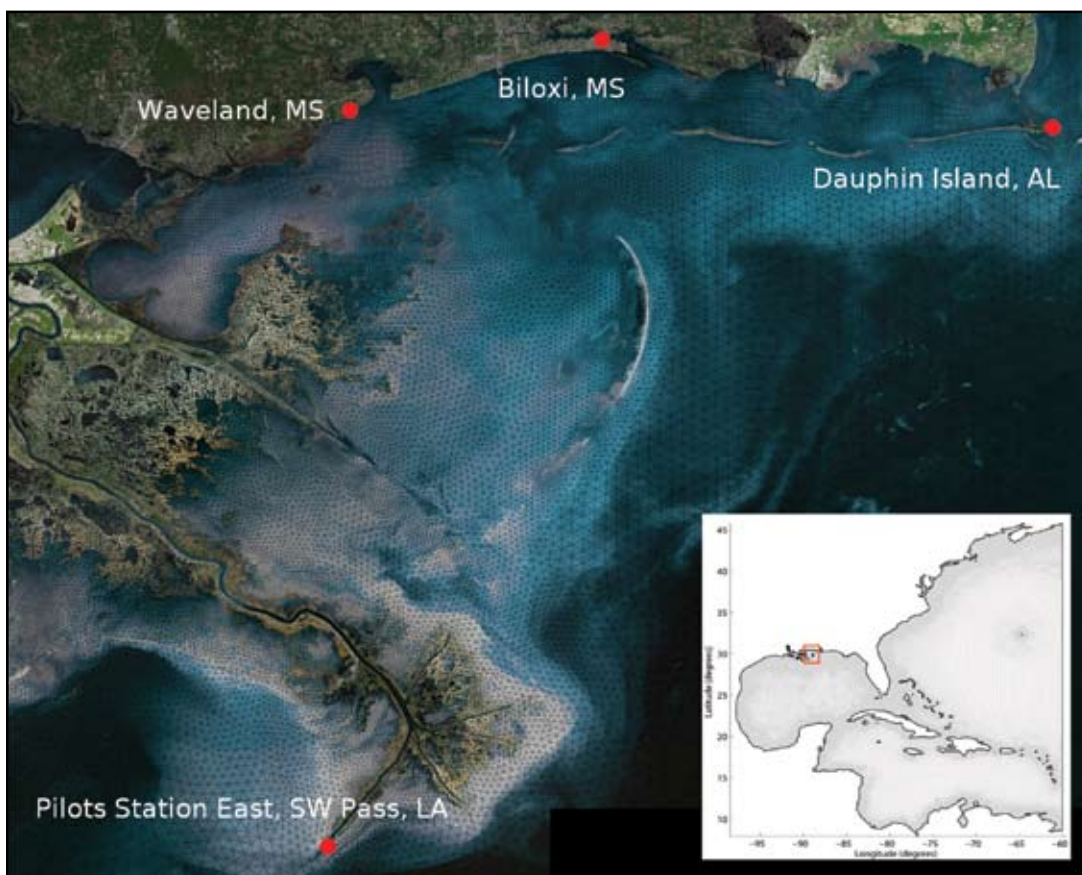


FIGURE 1

The density of the triangular elements in the northeast Gulf of Mexico contained in the computational mesh for the entire model domain (inset) overlays a true color satellite image that distinguishes land from water.

a hurricane.² The wind fields are typically constructed from a real-time analysis of flight-level reconnaissance data, satellite observations, pressure-wind relationships, and available surface data. We interpolate the three-hourly H*Winds using an approach that follows the storm center to preserve the integrity of the storm as it moves in time, and we further downscale the wind fields to fifteen-minute intervals. The time-interpolated wind fields are spatially interpolated to the computational mesh and then converted to wind stress. The wind drag at the sea surface is simply specified as a constant and with no distinction between winds over land or water or the directional history of the wind.

In addition to surface winds, tidal forces are applied, including those that act on the modeled body of water (tidal potential) and those caused by tides entering the domain at the open ocean boundary. At the deep ocean boundary, tidal forcing is applied at frequencies of the daily (K_1 , O_1) and twice-daily (M_2 , S_2 , and N_2) tides obtained from the Grenoble global tidal model. The tidal potential is applied on the interior of the domain for the same constituents.

The hindcast simulation of Hurricane Katrina storm surge began August 27, 2005, following a ramp-

up period of 15 days during which all forcings were gradually applied until full strength was reached at the end of the ramp-up phase. By this time in the simulation, Hurricane Katrina had crossed the state of Florida and had entered the warm waters of the Gulf of Mexico (Fig. 2). Katrina was past its peak intensity by the first landfall near Buras, Louisiana, at 6:10 a.m. CDT (1110 UTC) on August 29; a second landfall near the Louisiana/Mississippi border occurred about 9:45 a.m. CDT (1445 UTC) on August 29. The model hindcast of surge and inundation ended at 5:00 a.m. CDT (1000 UTC) on August 30, which coincided with the last available H*Wind product contained within the mesh. At every 1-second time integration of the model, the water levels and depth-integrated currents are computed by the ADCIRC model at all points in the model domain.

EVALUATION

The surface winds from Hurricane Katrina at 10:00 a.m. CDT (1500 UTC) on August 29, 2005 (Fig. 3) and the resulting storm surge computed by the ADCIRC model for the same time and date (Fig. 4) are presented. Surge heights well over 20 feet at the coastline

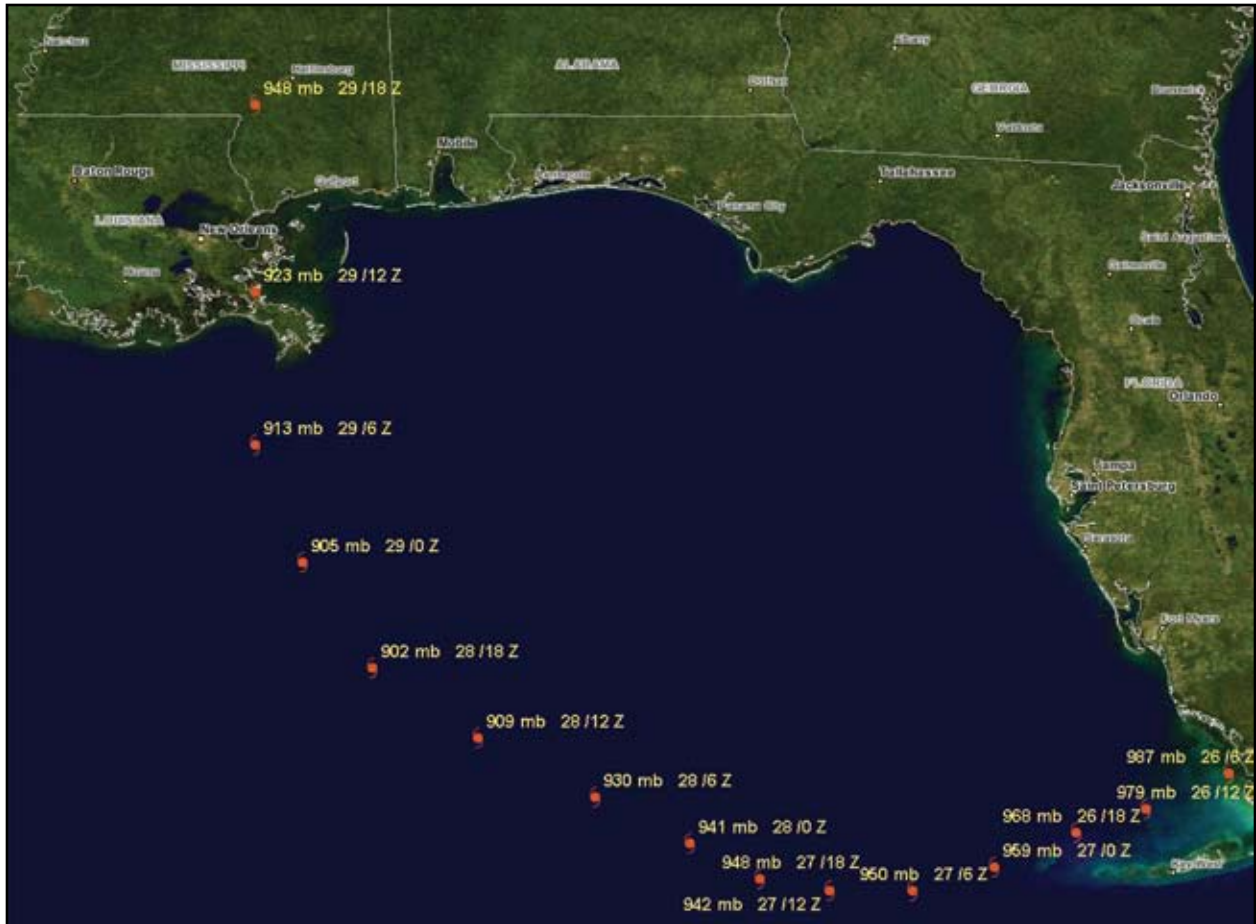
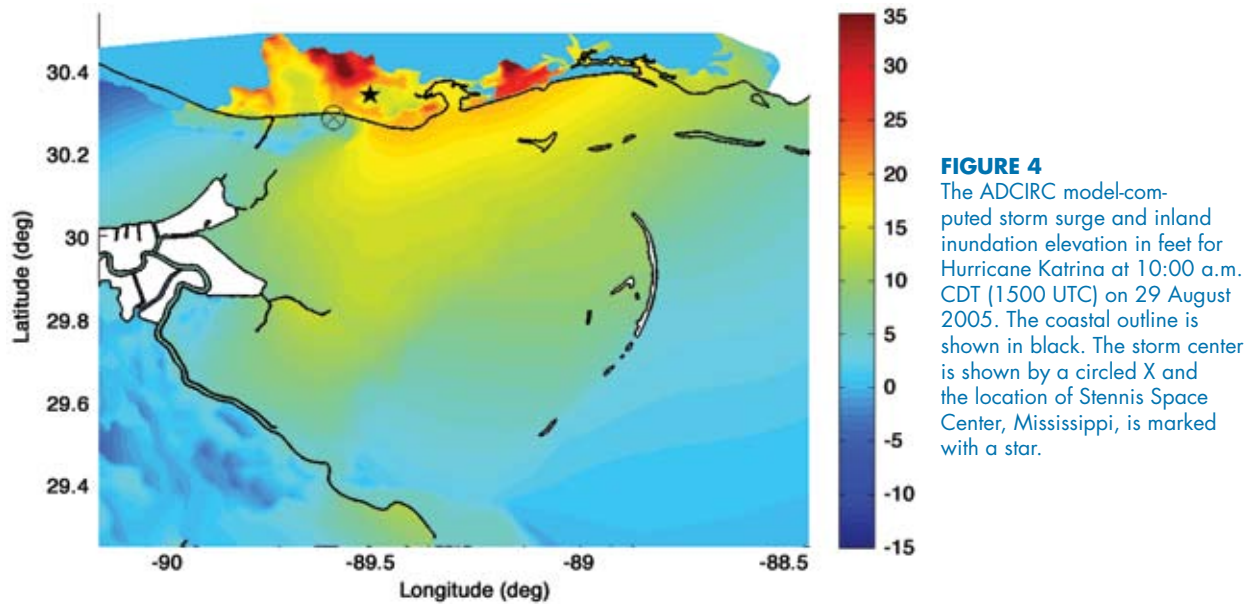
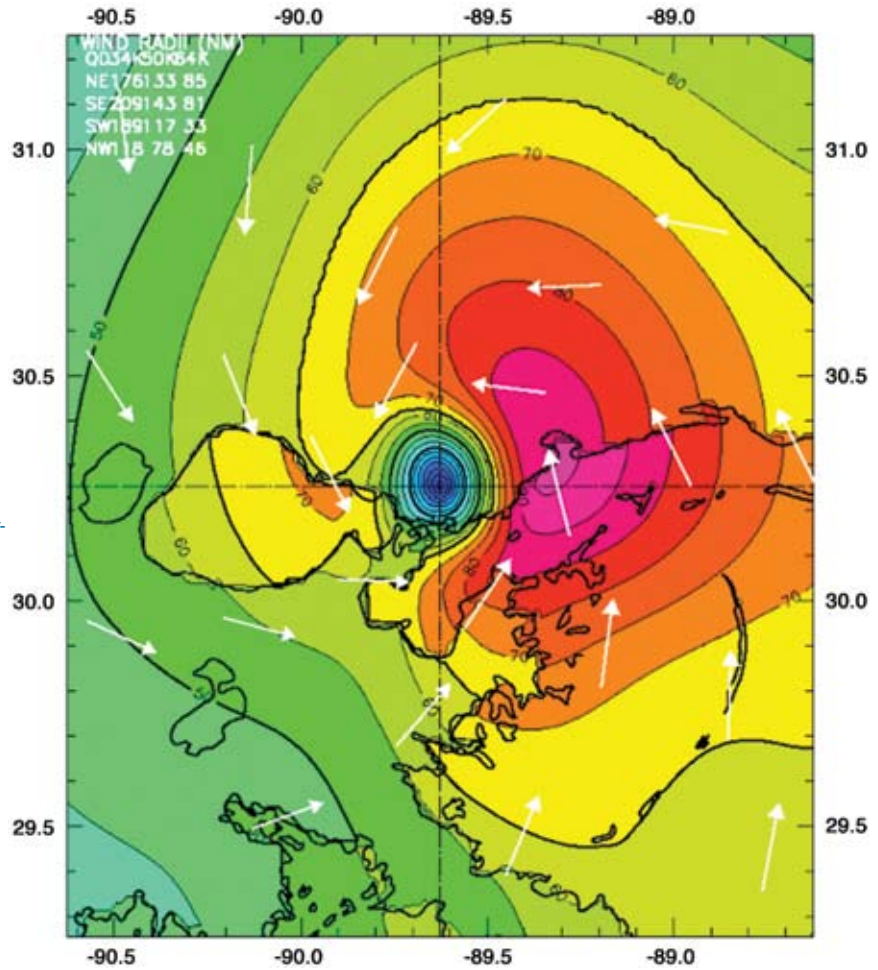


FIGURE 2
 The track of Hurricane Katrina at 6-hour intervals once the storm entered the Gulf of Mexico off the west Florida coast at 0600 UTC (6Z) on 26 August 2005 with central pressure of 987 mb. The final location of the storm at hurricane strength occurred in southern Mississippi at 1800 UTC (18Z) on 29 August 2005 with a central pressure of 948 mb.

FIGURE 3
The magnitude (color) and direction (arrows) of the maximum 1-minute sustained surface winds in knots for Hurricane Katrina at 10:00 a.m. CDT (1500 UTC) on 29 August 2005 (courtesy of the NOAA Hurricane Research Division).



on the right side of the storm reflect not only the strength of the storm winds at the time of landfall but also the buildup of surge that occurred prior to landfall. Even higher water levels are shown inland (near Waveland, Mississippi, and west of Biloxi, Mississippi) as the large radius of hurricane winds easily pushed water over the gently sloping coastal lands. Timing of the inundation indicates that areas to the west of Waveland, Mississippi, including the northern coast of Louisiana (Slidell), inundated first as hurricane winds pushed water into the bays and up the rivers. Not until landfall did the Mississippi Gulf coast west of Biloxi experience its peak flooding. Note that even after landfall (Fig. 4), sea levels remain elevated throughout the coastal waters. For some areas far inland, particularly at the wetting front, excessive inland flooding (over 30 feet) is computed. Analyses of these hindcast results have revealed limitations in the inundation mechanism within the ADCIRC model that prevent rapid advancement of a wetting front and complete drainage of the flood water following peak storm winds (evidence of this is northwest of Stennis Space Center, Mississippi).

Timing of the wetting front is difficult to validate since observations are often limited. However, the modeled water heights are compared to recorded elevations at three observing stations that survived the storm: Pilot Station East, Southwest Pass, Louisiana; Waveland, Mississippi; and Dauphin Island, Alabama (Fig. 5). In each case, the agreement between the modeled and observed water levels is quite reasonable. The phasing of the tides and peak surge computed by the model are lagging the observed values by no more than a couple of hours and the model's underprediction as the storm nears its landfall position is likely due to the neglect of surface wave effects.

Evaluation of the modeled magnitude and extent of surge and inundation is accomplished by comparing computed high water mark values to high water marks measured by the U.S. Geological Survey (USGS) shortly after the storm. At each location in the mesh, the highest water level from the model (evaluated at every 1-second model time-step) is recorded and shown in Fig. 6. Of 458 high water mark stations, 315 were wetted in the model. Red dots on the map in Fig. 7(a) indicate 143 locations that did not experience inundation during the hindcast simulation of Hurricane Katrina. It is likely that a number of factors contribute to this type of error, such as erroneous values for local water depth and land height, not accounting for the decreased wind drag over water, or limitations in the inundation mechanism as previously cited. Despite the non-wetting of certain locations, the model-computed water elevations at the remaining 315 high water mark locations had an average error of only 1.2 feet (Fig. 7(b)). Stations with the largest errors underpredict water levels and are found near those same locations

that remained erroneously dry. These results are extraordinary, given the intent of the hindcast to use an available predictive capability and information on water depth, land height, and wind strength at a level of detail typical for Navy operations in non-U.S. waters.

DEVELOPMENT OF A SURGE AND INUNDATION PREDICTION CAPABILITY

The proximity of Katrina's landfall to the Navy's Oceanographic Operational Center at NAVOCEANO, Stennis Space Center, Mississippi, reignited Navy interest in a robust capability for storm surge prediction. Different from a hindcast exercise, Navy applications require *forecast* hurricane wind fields. While real-time H*Wind products are available for storms impacting U.S. waters, this product cannot address inundation events along foreign coasts. Operationally available Navy-generated wind products such as the Navy Operational Global Atmospheric Prediction System (NOGAPS) and the Coupled Ocean Atmospheric Prediction System (COAMPSTM) do not contain an embedded hurricane model, so do not provide accurate storm track and/or intensity of a hurricane. To address the need for realistic forecast hurricane winds, the parametric cyclone model of Holland was selected.³ While not perfect, the cyclone model contains to first order the physical mechanisms of tropical storm generation and propagation. Forecast wind fields from the Holland model, based on known or projected track information, replicate with reasonable fidelity the intensity, size, and forward speed characteristics of a landfalling hurricane. This model can be exercised worldwide at the first indication of threatening tropical storm activity.

With the parametric wind model in hand, a hurricane storm surge prediction system has been developed to automate the forecast of surge and inundation in coastal regions (Fig. 8). The system, initially based on the hindcast of Hurricane Katrina, can address storms poised to strike the Mississippi Gulf Coast. Analysis and forecast data from the NOAA National Weather Service National Hurricane Center/Tropical Prediction Center forecast/advisory files are automatically read and processed. Extracted data, such as time and date information, tropical storm position, estimates to the radius of maximum winds, and the central pressure of the storm for analysis and forecast time periods, initializes the generation of forecast cyclone winds using the Holland model. These wind fields are then interpolated onto the finite element mesh providing the meteorological forcing for execution of the ADCIRC storm surge model. This system, presently designed for Gulf Coast applications by virtue of the mesh location, was transitioned to NAVOCEANO on May 10, 2006, in time for the 2006 Atlantic hurricane season.

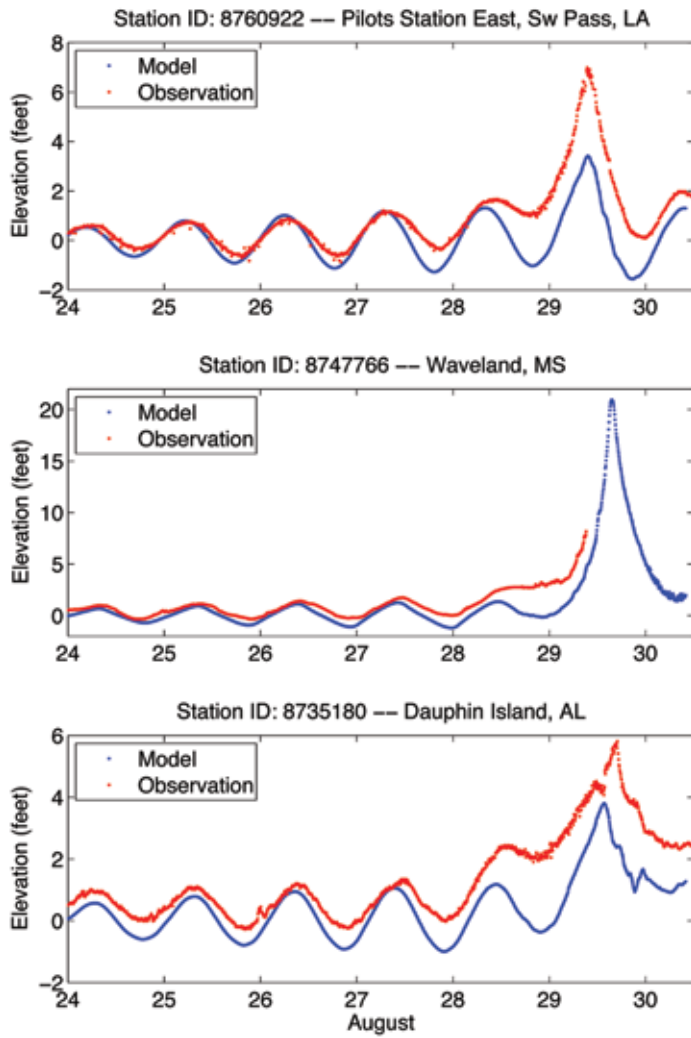


FIGURE 5
Time series of model-computed (blue) and observed (red) water elevations in feet at three NOAA coastal stations, Pilot Station East, SW Pass, Louisiana, Waveland, Mississippi, and Dauphin Island, Alabama.

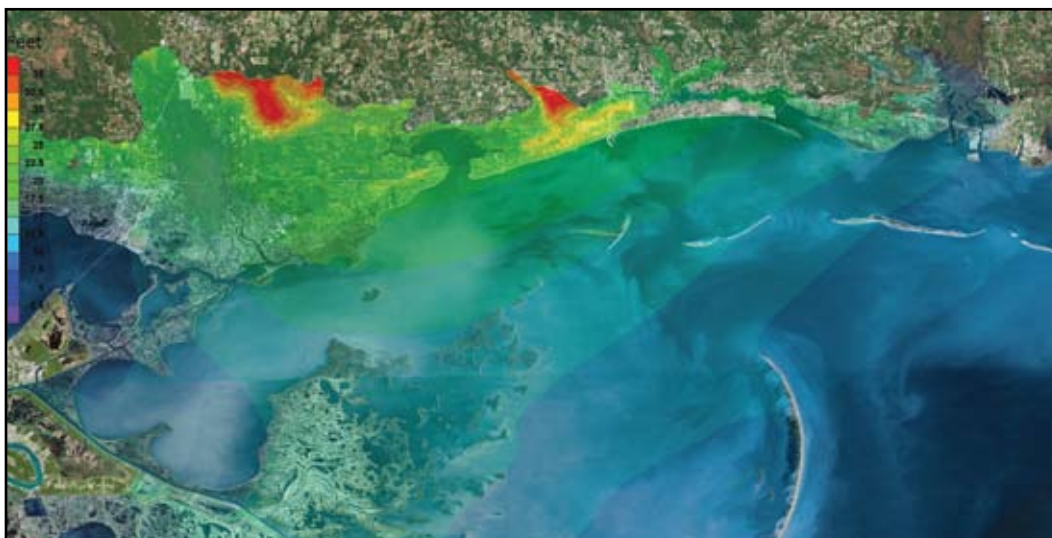


FIGURE 6
A map of modeled high water mark values (feet) obtained from evaluations at every 1-second model time-step during the hindcast of Hurricane Katrina.

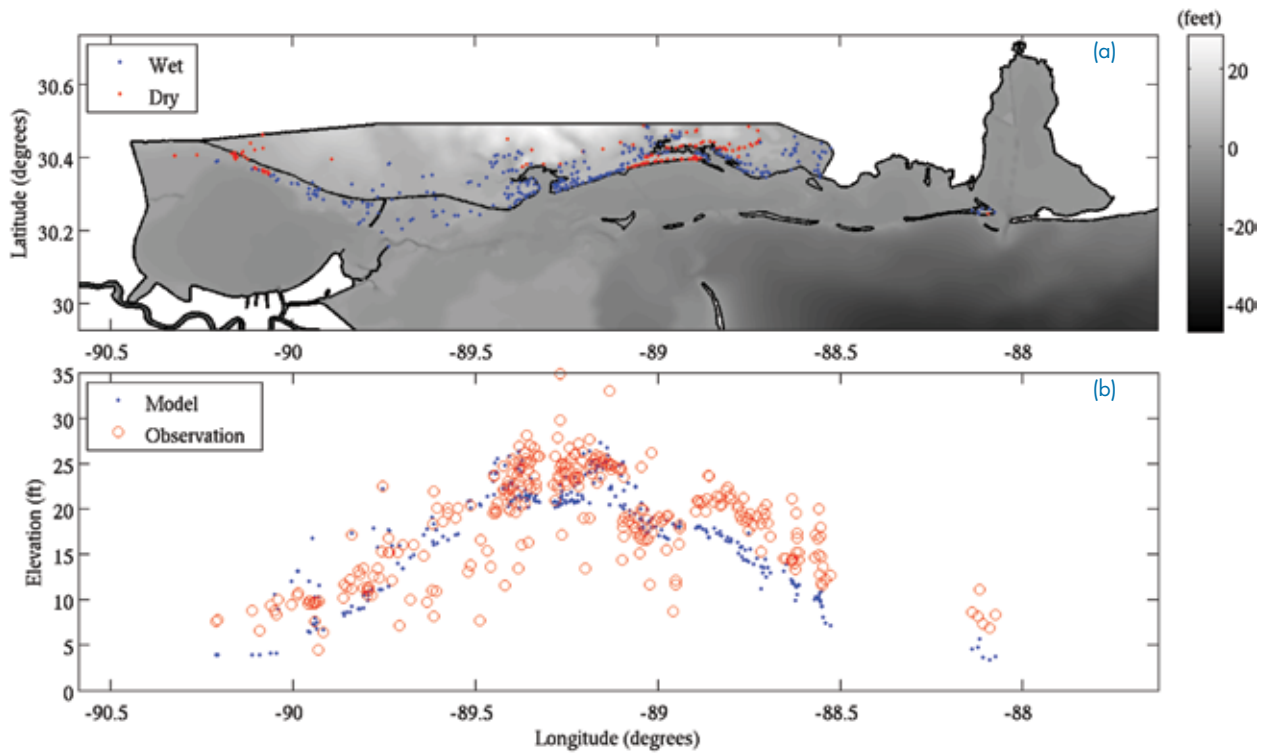


FIGURE 7 (a) A map of inundated (blue) or dry (red) USGS high water mark locations as computed by the model. (b) Comparisons of the modeled (blue) and measured (red) high water elevations in feet at 315 USGS stations.

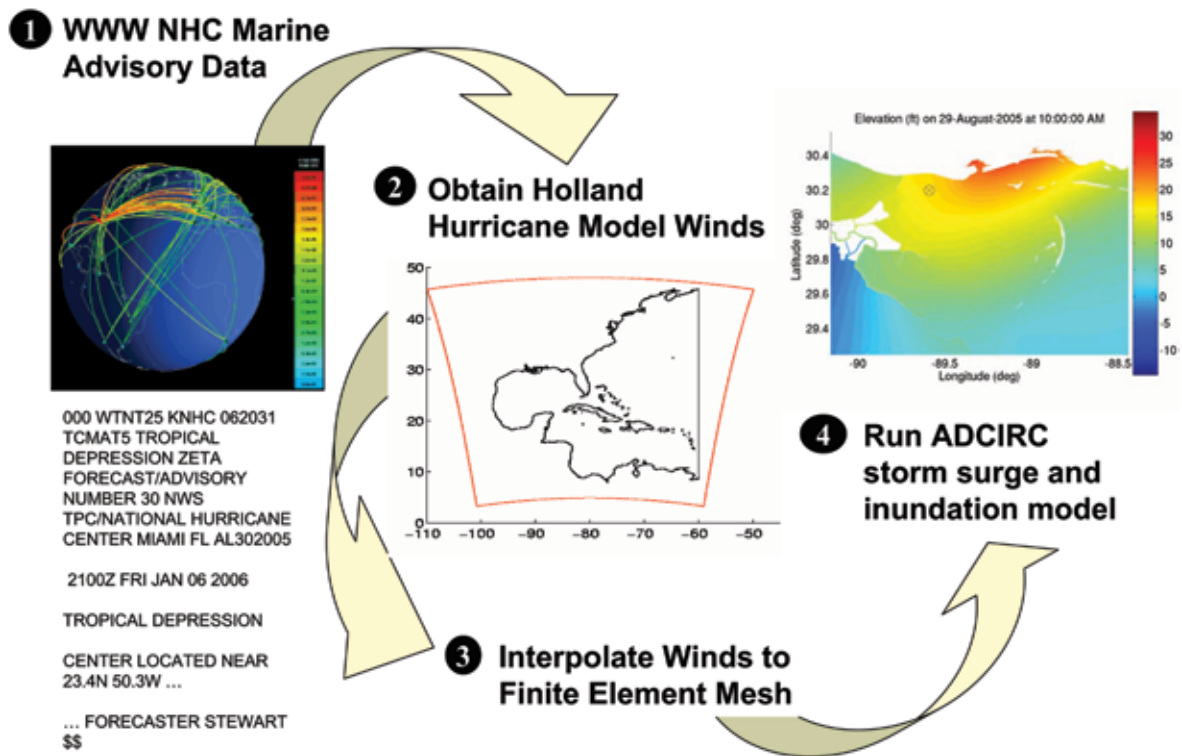


FIGURE 8 A schematic of the developed storm surge and inundation prediction system transitioned to the Naval Oceanographic Office at Stennis Space Center, Mississippi, in May 2006.

The ability to rapidly apply the ADCIRC surge model to any location globally is the ultimate goal of a surge forecast prediction system. Continued refinement of the mesh generation tool created at NRL into a fully automated operation is making that goal possible. Experience gained during the hindcast of Katrina has motivated a number of improvements in the mesh generation capability. A multi-stage mesh generation approach is often advantageous to balance resolution requirements and computational limitations in different regions of the mesh. For this approach, the ability to “stitch” together different meshed regions was developed. A series of mesh quality adjustments are now automatically applied to a created mesh to eliminate poorly constructed triangular elements that may cause model instabilities. Furthermore, an estimate of model computational time is provided based on the size of a created mesh. The user can decide if iterations on the mesh design are needed, knowing current operational constraints.

Our experience, and that of others, modeling the inundation from Katrina indicates that fine-scale information on overland elevation, vegetation type, and frictional characteristics are all very important for accurate representation of a wetting front. Methods are now being developed to automatically extract such information from remotely sensed imagery and utilize it in the mesh generation process. Achieving a fully automated mesh generation capability will expand application of our developed storm surge and inundation prediction system to worldwide inundation events.

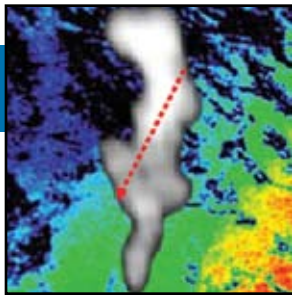
Apart from the mesh generation process, our analyses of Hurricane Katrina surge and inundation hindcasts highlight improvements to the inundation methodology that could result in even more accurate, robust forecasts. For example, the movement of water inland would be better represented as a response to not only water elevation and frictional effects but also wind forcing. The conservation of water in overland regions that are wet, dried, and rewet is another important aspect. In addition, tracking and resolving the wet-dry interface would further enhance fidelity of the inundation forecast.

The challenge at NRL is not only to develop the most advanced and accurate modeling technology but also to facilitate its transition into an operational framework whose priorities are often ease of use and quick turnaround of operational products. The hindcast of Hurricane Katrina’s storm surge and inundation provides the opportunity for progress in both realms.

[Sponsored by ONR]

References

- ¹C.A. Blain, R.H. Preller, and A.P. Rivera, “Tidal Prediction using the Advanced Circulation Model (ADCIRC) and a Relocatable PC-based System,” *Oceanography* **15**(1), 77-87 (2002).
- ²M.D. Powell, S.H. Houston, L.R. Amat, and N. Morisseau-Leroy, “The HRD Real-time Hurricane Wind Analysis System,” *J. Wind Engineer. and Indust. Aerodyn.* **77 & 78**, 53-64 (1998).
- ³G. Holland, “An Analytic Model of the Wind and Pressure Profiles in Hurricanes,” *Mon. Wea. Rev.* **108**, 1212-1218 (1980). ★



By the Light of the Sea

S.D. Miller,¹ S.H.D. Haddock,² T.F. Lee,¹ and C.D. Elvidge³

¹Marine Meteorology Division

²Monterey Bay Aquarium Research Institute

³NOAA/National Geophysical Data Center

January 25, 1995: On a dark evening in the Arabian Sea off the coast of Somalia, a merchant vessel was steaming southward when its crew began to notice a strange glow in the distance. Within minutes, and for six hours thereafter, the S.S. *Lima* found herself cutting through waters producing a radiant white glow reminiscent of a boundless snowfield. Ten years later, scientists learning of *Lima*'s surreal encounter sought out the date and time within an archive of low-light satellite data. The match found between the ship's position and an "anomalous" light source in the satellite data — spanning an area exceeding 15,000 km² and morphing over several night's time in a way consistent with the known sea surface currents — marked the first confirmed remote-sensing of the legendary "milky sea," a poorly understood phenomenon thought to be linked to population explosions of luminous bacteria. Here, we detail the unusual circumstances and important implications of this discovery.

INTRODUCTION

Most maritime cultures hold a rich tradition of folklore and legends of The Deep. Whether tales of ship-eating sea monsters and beautiful mermaids are purely the wild fabrications of weary-minded sailors consumed by superstition and prone to exaggeration, or whether they may sometimes harbor an inkling of truth, is the irresistible question that captures the imagination. Our role as scientists is to seek out physically plausible, natural explanations for what might appear to others as supernatural phenomena. In some cases, the truth revealed can be stranger than the fiction we originally sought to dispel.

For centuries, the "milky sea" was just another in a long list of improbable tales spun by colorful seafarers. As suggested by the name, milky seas describe vast expanses of seemingly white water. Since milky seas are strictly nocturnal phenomena, occurring particularly under very dark, moonless conditions, the light observed from them is not the reflection of a down-welling source of radiation (e.g., moonlight) but instead a true emission from something within (or perhaps floating atop) the water. Long before their scientific acknowledgment, milky seas were a well-entrenched part of maritime folklore. Eventually they found their way into classic sea-adventure fiction novels of the mid-19th century such as Jules Verne's *Twenty Thousand Leagues Under the Seas* and Herman Melville's *Moby Dick*, the authors no doubt drawing from the many ship reports available to them at the time.

For example, in 1832 the crew of the *Clive* felt they were in mortal danger when between Bombay and the Arabian Gulf their ship entered white waters that obscured the line of horizon and eliminated all visual indications of forward movement (due to the complete uniformity of the glow and associated loss of depth perception). The crew of the *Moozuffer*, transecting these same waters in 1849, described the ship "forcing her way through molten lead" while the stroke of the paddle wheel churned liquid resembling patches of "thick milk or cream." In 1854, the *Shooting Star* reported crossing an ocean surface shining bright enough to illuminate objects on deck and to produce on the horizon the appearance of an aurora borealis. En route to Bombay in 1856, the steamship *Singapore* encountered an ocean glowing with such brilliance that its captain was fooled into thinking that distant clouds (being illuminated by the sea) were in fact land features, and that they had somehow drifted far off course!

According to Herring and Watson,¹ at least 235 similar encounters have been logged by captains and crew since 1915, predominantly in the waters of the northern Indian Ocean (171 reports) and off Indonesia (40 reports). Despite being based on layman observations, the accounts are surprisingly consistent. It was not until 1985 that a research vessel operating in the western Arabian Sea happened upon a milky sea and collected samples for analysis.² Water samples from the three-day-long event suggested the cause to be a bloom of the luminous bacteria *Vibrio harveyi*, which were found to be colonizing upon the brown/green alga *Phaeocystis*, perhaps in the form of a surface slick.

This study remains the lone scientific encounter with a milky sea, due largely to the remote, episodic, and transient nature of these events. Now, with the help of low-light satellite observing systems, we may finally have a means for detecting, tracking, and characterizing the elusive milky seas remotely.

BIOLUMINESCENCE AS THE “LACTOSE” OF MILKY SEAS

Before presenting the satellite results, it is worth expanding here on the leading hypothesis for milky seas. Bioluminescence is a special class of chemical luminescence (chemiluminescence) that takes place within a living organism. Light is produced as the by-product of a luciferase-catalyzed oxidation of reduced flavin mononucleotide and a long-chain aldehyde. Quite unlike the familiar dinoflagellate-produced bioluminescence events, characterized by local flashes of light in the immediate vicinity of disturbed waters (e.g., breaking waves along the seashore during red tide blooms, or in the turbulent wakes behind ships), the glow emanating from a milky sea is reportedly constant, opaque, widespread, and entirely independent of mechanical stimulation.

For this reason, the most likely scientific explanation for milky seas is luminous bacteria (consistent with the observations of Lapota et al.²), which are known to produce a faint but steady glow (Fig. 1) when their populations reach a critical concentration. Requirements for this process to occur are (i) an abundance of oxygen in the water, (ii) sufficiently high



FIGURE 1
Laboratory sample of the luminous bacteria strain *Vibrio fischeri* grown in a photobacterium broth. The central emission wavelength of ~500 nm gives the appearance of blue/green light.

concentrations of a chemical called *autoinducer* that is produced and detected by the organism (a cell-to-cell communication process referred to as “quorum sensing,” which tells the colony when to begin emitting light), and (iii) an extremely high concentration of bacteria (e.g., about 10^8 cells \cdot mL⁻¹).

By standards of human vision, the light levels produced by the most intense of milky seas are considered to be rather faint. Under low-light viewing conditions (scotopic vision), the rod cells of the human eye’s retina operate as the primary photodetectors. Unlike the cone cells we use under brighter illumination, which provide three distinct visible band-passes (blue/green/red), the rods do not provide this same color discrimination capability. For this reason, even though the central wavelengths for most bioluminescent light emissions are near 500 nm (blue/green light), a milky sea would still appear white (or in the most extreme cases, perhaps having a hint of cyan as in Fig. 1). Although the absolute value of luminescence is very low, its contrast against dark, moonless skies would be perceived by the dark-adjusted eye as brilliant.

The reason bacteria would want to produce light — a costly practice from an energy standpoint — is rather interesting in its own right. In contrast to dinoflagellate organisms, which produce a bright and transient flash of light to ward off predators (ironically enough, by attracting still larger predators, higher in the food chain, to the area), prokaryotes such as luminous bacteria are thought to glow for precisely the opposite purpose—they *want* to be ingested. It so happens that the gut of a fish is a preferred habitat for these bacteria, so when they gather in a sufficient concentration (e.g., colonization upon organic matter) they take advantage of their ability to emit light in order to solicit themselves to potential hosts who are capable of sustaining that population. Under normal conditions, this might occur on an isolated piece of material, making it stand out from its surroundings. In the case of milky seas, the uniqueness factor would be lost for the sheer numbers of colonized substrata.

AN UNLIKELY PATH TO AN UNLIKELIER DISCOVERY

The series of events leading to the first detection of a milky sea from space began, strangely enough, as a lunchtime chat among colleagues attending a meteorology conference in Seattle. The discussion centered on the anticipated capabilities of the Day/Night Band (DNB), a new sensor being developed for the National Polar-orbiting Operational Environmental Satellite System (NPOESS) Visible/Infrared Imager/Radiometer Suite (VIIRS). We knew about the unique nighttime imaging capabilities of the DNB’s heritage sensor, the Defense Meteorological Satellite Program (DMSP)

Operational Linescan System (OLS), which employs a photomultiplier tube (PMT) to amplify extremely low levels of light (occurring at four to five orders of magnitude below the limits of other visible-light detectors designed for daytime observations). This high sensitivity enables detection of cloud and snow cover at night by way of reflected moonlight. It also can detect both natural (e.g., forest fires, lightning, aurora) and artificial (e.g., city lights, oil refinery gas flares, fishing fleets) sources of light. We were curious as to whether the NPOESS VIIRS/DNB, with its superior spatial and radiometric resolution, would find other kinds of weak/fine-scale light features.

To our knowledge, there were no documented cases of OLS-detected bioluminescence, presumably due to the small spatial extent and low levels of light produced by typical events. Could the DNB do better here? Stepping back, and perhaps naively so, we wondered whether certain bioluminescent events ever occurred at scales sufficient to “fill” a typical satellite pixel (i.e., of order 1 km², thereby increasing their odds of detection), such that even the OLS might stand a chance of spotting them.

And so, as any noble scientists of the 21st century might do, we ran a “Google” search on the words “bioluminescence” and “widespread.” The results led us almost immediately to a report submitted by James P. Briand, then captain of the British merchant vessel S.S. *Lima*, to the journal *The Marine Observer*:

25 January 1995: At 1800 UTC on a clear moonless night while 150 n.mile east of the Somalian coast a whitish glow was observed on the horizon and, after 15 minutes of steaming, the ship was completely surrounded by a sea of milky-white colour with a fairly uniform luminescence. The bioluminescence appeared to cover the entire sea area, from horizon to horizon [...] and it appeared as though the ship was sailing over a field of snow or gliding over the clouds [...] The bow waves and the wake appeared blackish in colour and thick black patches of oil were passing by. Later, the Aldis lamp revealed that the ‘oil patches’ were actually light green kelp, amazingly black against the white water.³

In addition to supplying specific information on the date, time, and location of the event, Capt. Briand’s report went on to include the *Lima*’s course and temperature/pressure/wind data. Realizing that the National Geophysical Data Center (NGDC) began archiving OLS data (“smooth” format or approximately 2.8 km spatial resolution) in 1992, we were optimistic about the prospects of obtaining coverage over the *Lima*’s location by one or more of the contemporary DMSP constellation members.

Our Internet search tactic proved faithful once again in guiding us to several bioluminescence experts whose input would add both substance and context to our observations. Also among those contacted were experts in the field who had dismissed altogether, based on previous failed attempts, the prospect of any possible detection with current satellite technology. Realizing the many challenges we faced from an observing system standpoint, it would be nearly impossible for us to counter their arguments with anything short of clear and definitive proof to the contrary.

AGAINST ALL ODDS

As luck would have it, several candidate OLS orbits were indeed available in the NGDC archive for the days surrounding the *Lima* report, including one evening pass collected within an hour of the initial sighting. Another thing going in our favor was the relative absence of moonlight during this period, meaning that the OLS sensor would be operating very close to its highest gain setting. Even so, we knew that our chances of detecting above the noise the very low light signals of a milky sea remained slim, hinging on an opportune positioning of the feature within the sensor’s 3000 km swath.

The OLS implements a pendulum-like cross-track scanning motion to image a scene, meaning that its footprint (the projection of the detector element onto the surface of the Earth) grows with increasing angle off nadir (similar to the spot-size of a flashlight pointed at the ground). In an attempt to preserve a near constant spatial resolution across the entire swath, the OLS mechanically decreases the size of its detector (and hence, its footprint) with increasing scan angle. At about ± 766 km off nadir, the first of these discrete deflections is clearly evident when viewing the imagery in a low-end enhancement. The regions of the imagery swath just prior to the first mechanical deflection offer the largest detector footprints, greatest signal-to-noise ratios, and hence best opportunities to detect a low-light signal. Put in terms a tennis player might understand, there exists on the OLS swath a narrow “sweet spot” offering reduced noise and therefore enhanced detection capability.

In what seemed to be a case of extreme serendipity, our target area fell repeatedly within this sweet spot on four consecutive nights, beginning with the night of the *Lima* milky sea observation. What’s more, the unprecedented level of detail in Capt. Briand’s account allowed for assignment of boundaries on the event that would prove invaluable to the data analysis to follow. The best of all possible scenarios in terms of timing and placement had stacked the odds of detection squarely in our favor. Murphy’s Law as it typically applies to scientific data gathering had never failed so miserably.

A SMUDGE ON THE SCREEN

Even with such good fortune, we would still need to rely on some amount of digital enhancement to isolate any features of interest from the considerable PMT noise present on the low end of the detector’s sensitivity range. The enhancement consisted of first subtracting out the mean intensity of each scan line (removing striping), then applying along-track and cross-track filters. This retained the slightly brighter/coherent structures while tending to remove random noise.

At first glance, the faint features in the January 25–27, 1995, imagery sequence (Fig. 2(A–C)) could easily have been mistaken for run-of-the-mill finger smudges found on most computer monitor displays. It became evident only after digital enhancement (Fig. 2(D–F)) that the coherent feature, approximately 50 km

wide by 300 km long (roughly the size of Connecticut), was not an artifact of random noise (or oily fingertips) but was a recurrent feature in the data that retained its general structure for at least three consecutive nights. A colleague once said that a career in science was 99% frustration and 1% sheer exhilaration. At the moment we overlaid the reported positions of the *Lima* at both entrance and exit from the glowing waters (Fig. 2(D)), showing a nearly perfect match with the boundaries of the peculiar comma-shaped feature appearing in the enhanced OLS imagery, it became perfectly clear that this 1% made everything else worthwhile.

UPON FURTHER REVIEW

Several milky sea accounts mention accompanying phenomena. Though mysterious to early shipboard

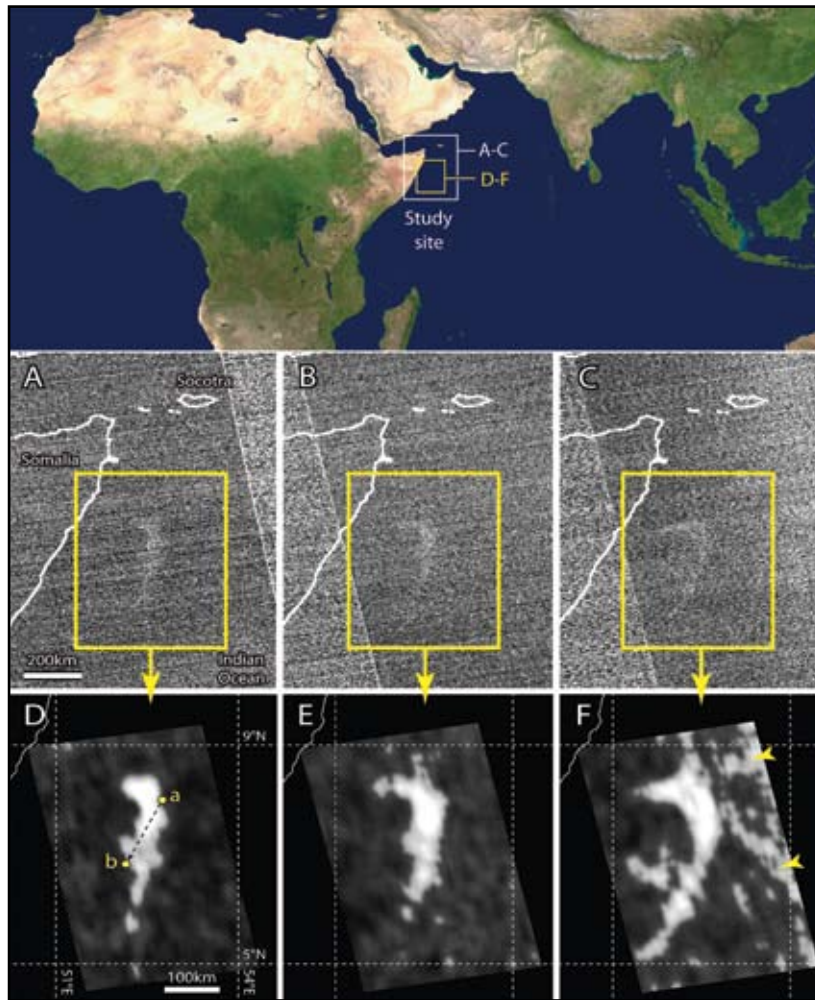


FIGURE 2 DMSP/OLS unfiltered (A–C) and digitally filtered (D–F) nighttime visible imagery for the date of the S.S. *Lima* observation (A, D: 25 Jan 1995, 1836 GMT) and the following two days (B, E: 26 Jan 1995, 1804 GMT; C, F: 27 Jan 1995, 1725 GMT), depicting a coherent bright structure just above the instrument noise. Yellow arrowheads in (F) denote noise contamination. (Figure from Ref. 4.)

observers, they now offer us clues to understanding the underlying environmental state. For example, several reports cite large sea surface temperature (SST) gradients and a sudden calming of winds when entering milky seas. Such gradients often demarcate oceanic fronts, with the cooler sides of these fronts inducing a stable boundary layer in the lower atmosphere which can decouple the surface from stronger winds aloft, resulting in a potentially rapid decrease of winds when crossing into the cooler waters. It so happens that a strong boundary exists in the region of the *Lima* milky sea encounter, formed between warmer waters transported northward by the Somali current, and the cooler, nutrient-rich waters upwelling off the Horn of Africa.

Although the *Lima* did not report any noteworthy SST or wind speed changes along its milky sea transect, we pursued nonetheless a spatial analysis of SST retrieved from Advanced Very High Resolution Radiometer (AVHRR) data and sea surface currents from the NRL Layered Ocean Model (NLOM; 1/16° resolution, courtesy of our colleagues at NRL Stennis Space Center) in order to better understand the broader environmental conditions. Figure 3(A) depicts the NLOM sea surface current field, revealing the presence of a large cool-water gyre just off the Horn of Africa. Knowledge of this eddy's existence proved key to understanding the temporal evolution of the milky sea feature (Figs. 3(B–D)), whose northern “head” appears to wrap in a counterclockwise fashion around the eddy—linking the glowing feature unequivocally to the

ocean surface. Figure 3(E) depicts the AVHRR-derived SST field (black patches correspond to clouds masked out prior to conducting the retrieval). Overlaying the *Lima*'s track upon the milky sea feature, we note that despite the presence of a strong northwest/southeast gradient in SST, the ship's course ran parallel to it. Thanks to the satellite data, we can explain the lack of an observed SST gradient for this particular case while not discounting in general the potential importance of oceanic fronts to the formation of milky seas.

Despite the fact that the OLS data were not calibrated, the known minimum detectable signal (MDS) for the sensor allowed for a conservative estimate on total light production, and by extension, the total bacteria population involved. Because the OLS sensitivity range and the bacterial light emission spectra (Fig. 4(A)) do not overlap completely, we determined an adjustment factor (i.e., how much more would need to be produced by the bacteria in order to register the same signal as an emission source having perfect overlap with the OLS response curve). Then, knowing the per-cell light emission rate for luminous bacteria (measured in the laboratory), we could compute the minimum population of cells in the near-surface water column required to produce light levels equaling this adjusted MDS. Finally, using the satellite-inferred spatial extent we computed the total bacterial population.

Following the above procedure, the MDS and adjusted MDS values were $4 \times 10^{-5} \text{ W} \cdot \text{m}^{-2} \cdot \text{sr}^{-1}$ and $1.8 \times 10^{-4} \text{ W} \cdot \text{m}^{-2} \cdot \text{sr}^{-1}$, respectively; the per-cell emis-

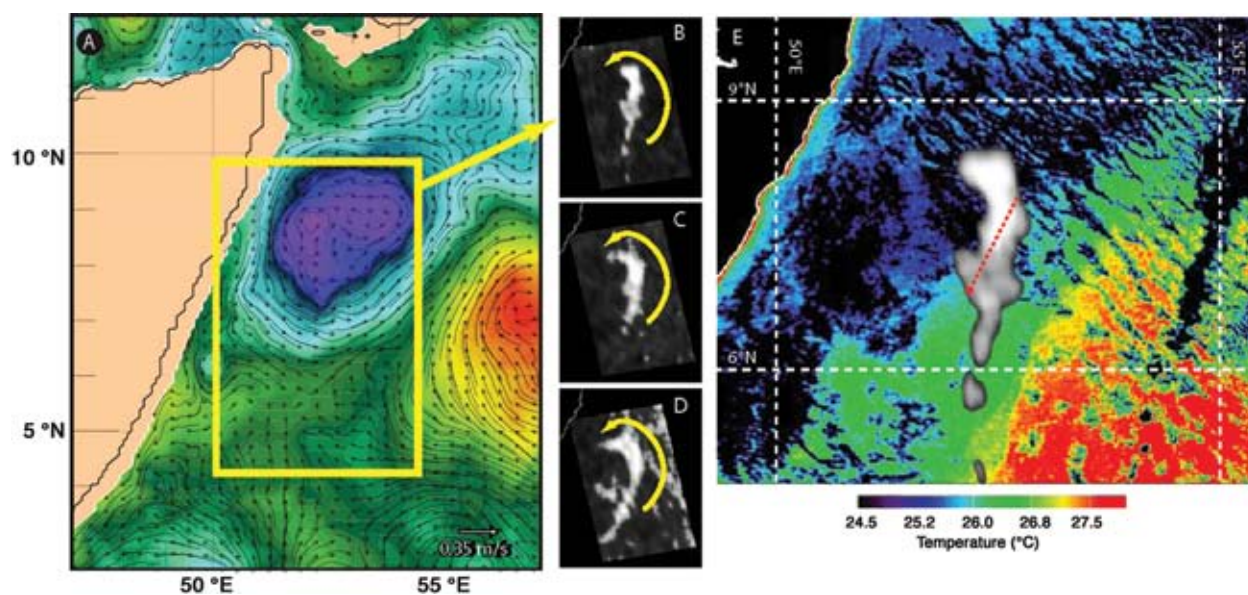


FIGURE 3

NLOM sea surface currents (A) for date of the S.S. *Lima* observation. Yellow box corresponds to the study area at right (B: 25 Jan 1995, 1836 GMT; C: 26 Jan 1995, 1804 GMT; and D: 27 Jan 1995, 1725 GMT). Blue/purple colors correspond to low values of surface height anomaly, depicting cold eddy. AVHRR-retrieved SST (E) reveals orientation of the milky sea with respect to a gradient, with S.S. *Lima* transect shown as a red dashed line. (Figure from Ref. 5.)

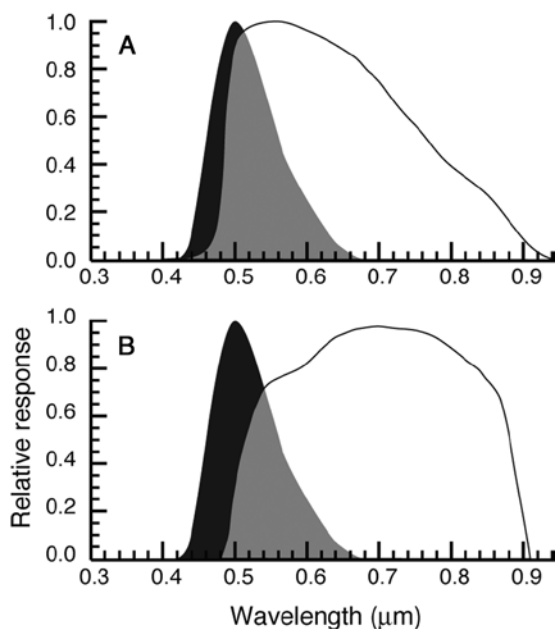


FIGURE 4
Laboratory emission spectra of bioluminescent bacteria (solid black) compared with spectral response functions for (A) the DMSP OLS nighttime visible band of the sensor used in this study, and (B) the NPOESS VIIRS day/night band. Spectral overlap areas shown in gray. (Figure from Ref. 4.)

sion was $1.2 \times 10^3 \text{ phot} \cdot \text{s}^{-1} \cdot \text{cell}^{-1}$; minimum detectable population was $1.9 \times 10^8 \text{ cells} \cdot \text{mL}^{-1}$ (within the top 10 cm of water); and the milky sea surface area (for January 25, 1995) was $15.4 \times 10^3 \text{ km}^2$. This resulted in a conservative total population estimate of 4×10^{22} bacteria. The sheer enormity of this figure, representing nearly the same number of bacteria as are estimated to occupy the upper 200 m of the all the world's open oceans (non-coastal) under normal conditions, might be put into context in the following way: if each cell were scaled to the size of a grain of sand, one could form a 10 cm thick layer covering the *entire Earth!*

THE QUEST CONTINUES

There are still far more questions than answers surrounding milky seas, foremost among them: what chain of events could lead to such a massive bacteria population explosion, and do these special circumstances tell us something important about the current/future states of the marine ecosystem or climate? Equally vague is our understanding of whether milky seas occur exclusively in association with algal blooms, or whether other sources of nutrients (e.g., deep water upwelling common in these highly productive waters) may play an important role. Laboratory work ongoing at NRL in Washington, DC, and at the University of Maryland, including the setup of *Vibrio harveyi*/*Phaeocystis* cocultures, may help determine preconditioning requirements and the nature of bacterial “super blooms.”

As outlined above, the ability of contemporary satellite sensors like the DMSP/OLS to observe the weak signal of milky seas requires serendipitous circumstances almost as uncommon as the events themselves. Among planned satellite observing systems, the VIIRS/DNB offers the only realistic hope for pursuing this research further. The primary challenge, depicted in Fig. 4(B), is that despite the improved fidelity of the DNB compared to the OLS, its spectral band pass provides even less overlap with the bioluminescent emission spectra for bacteria thought to be responsible for milky seas. By arguments stated earlier, the light production would need to be roughly a factor of two greater to be detected with this red-shifted band pass. Since the DNB will not offer an improved MDS over that of the OLS, we can only hope that reduced noise levels will mitigate the lower detector responsivity.

Until then, we will continue pursuing new leads on possible milky sea events. The maritime record, based on a sparse sampling and biased predominantly toward major shipping routes, gives little insight into the full spatial extent, global distribution, and temporal variability of milky seas. The phenomena apparently are not limited to the Arabian Sea — there have been sightings from cruise liners off the coast of Brazil, in the waters west of central Mexico, throughout the Arabian Gulf, and in the Mergui Archipelago of Indonesia. It is entirely possible that milky seas occur in other regions, less frequented by sea vessels, as well. We encourage those who believe they may have encountered a milky sea during their travels to contact us.

SUMMARY AND CONCLUSION

In retrospect, 2005 was something of a banner year for novelist Jules Verne. Within weeks of publication of these milky sea findings,⁴ news broke of the first confirmed photograph of a live giant squid, similar to the one that mistook Verne's *Nautilus* vessel for food in *Twenty Thousand Leagues Under the Seas*. Ironies linking the milky sea findings to this novel and to history itself are at times striking: (i) according to Buist,⁶ in the early 1830s a real ship called *Nautilus* crossed a milky sea near the same location as the *Lima*, (ii) encounters by the fictional *Nautilus* and the actual *Lima* and *Moozuffer* occurred within days of each other (January 25–27), (iii) the scale of the novel's milky sea was similar to the one observed in 1995, and (iv) the story's protagonist, Prof. Aronnax, discards the possibility of ever being able to compute the number of “infusoria” responsible for such an event — a calculation afforded for the first time by the satellite observations.

While unfortunately the lost city of Atlantis was not discovered in time to round out the emerging “*Twenty Thousand Leagues...*” newsreel, we have perhaps seen enough to have a modest epiphany: the

Earth remains a place brimming with natural mysteries. Stories such as these in many ways transcend the science, touching the lives of all peoples and cultures. Even as we look to other planets, solar systems, and the cosmos beyond as the new frontiers of science discovery, it is somehow both refreshing and humbling to be confronted with evidence that such frontiers still exist in our own back yard. By the light of the sea we have gained a new sense for how very little indeed we really know about the place we call “home.”

ACKNOWLEDGMENTS

We thank Ole Martin Smedstad and Jan Dastugue (NRL-SSC) for NLOM analyses, Denis Klimov for radiometric assistance, Lynne Christianson for laboratory help, James Case, Peter Herring, and Woody Hastings for mentoring this work, and Linda Norton for assistance in literature review. Research supported by the Office of Naval Research under PE-062435N and the David and Lucile Packard Foundation.

[Sponsored by ONR and the David and Lucile Packard Foundation]

References

- ¹ P.J. Herring and M. Watson, “Milky Seas: A Bioluminescent Puzzle,” *The Mar. Obsvr.* **63**, 22-30 (1993).
- ² D. Lapota, C. Galt, J.R. Losee, H.D. Huddell, J.K. Orzech, and K.H. Nealon, “Observations and Measurements of Planktonic Bioluminescence in and Around a Milky Sea,” *J. Exp. Mar. Biol. Ecol.* **119**, 55-81 (1988).
- ³ J.P. Briand, “Bioluminescence,” *The Mar. Obsvr.* **66**, 12-13 (1996).
- ⁴ S.D. Miller, S.H.D. Haddock, C.D. Elvidge, and T.F. Lee, “Detection of a Bioluminescent Milky Sea from Space,” *Proc. Nat. Acad. Sci.* **102**, 14181-14184 (2005).
- ⁵ S.D. Miller, S.H.D. Haddock, C.D. Elvidge, and T.F. Lee, “Twenty Thousand Leagues Over the Seas: The First Satellite Perspective on Bioluminescent ‘Milky Seas,’” *Int. J. Rem. Sens.*, in press (2006), DOI:10.1080/01431160600554298.
- ⁶ G. Buist, “Notes on Certain Coloured Appearances Met with on the Surface of the Sea in Warm Latitudes,” *Proc. Bombay Geogr. Soc.*, 108-125 (1855). ★



A Multi-Sensor Aerogeophysical Study of Afghanistan

J. Brozena,¹ V. Childers,¹ J. Gardner,¹ R. Liang,¹ J. Jarvis,¹ and J. Bowles²

¹Marine Geosciences Division

²Remote Sensing Division

A multi-sensor, multidisciplinary aerogeophysical survey over much of Afghanistan was recently conducted by investigators from NRL and the U.S. Geological Survey. The survey was flown aboard an NP-3D Orion aircraft operated by VXS-1. Sensor systems installed on the P-3 included dual gravimeters, scalar and vector magnetometers, a digital photogrammetric camera, a hyperspectral imager, and an L-band polarimetric synthetic aperture radar. Data from all sources was precisely co-registered to the ground by a combination of interferometric-mode Global Positioning System and inertial measurements. The data from this integrated mapping mission supports numerous efforts in Afghanistan: combat operations, economic exploration for oil, gas, and minerals, humanitarian missions, development of civil infrastructure, and agriculture resource management. This mission has also advanced the state of the art in integrated multi-sensor airborne remote sensing.

INTRODUCTION

Afghanistan is one of two active combat zones in the global war on terrorism (GWOT). The country faces dual challenges: suppressing Taliban and al-Qaeda operations and developing the basis of a legal and sustainable economy that minimizes popular support for terrorist activity. A major airborne remote sensing and mapping project conducted by the Naval Research Laboratory (NRL), the U.S. Geological Survey (USGS), and Scientific Development Squadron One (VXS-1), covering more than half of Afghanistan, contributed to both these objectives. The project marked a technological milestone in the integration and successful operation of the largest set of diverse airborne geophysical sensors ever flown. It is also noteworthy in that it was the first deployment of NRL scientists into a combat theater since World War II.

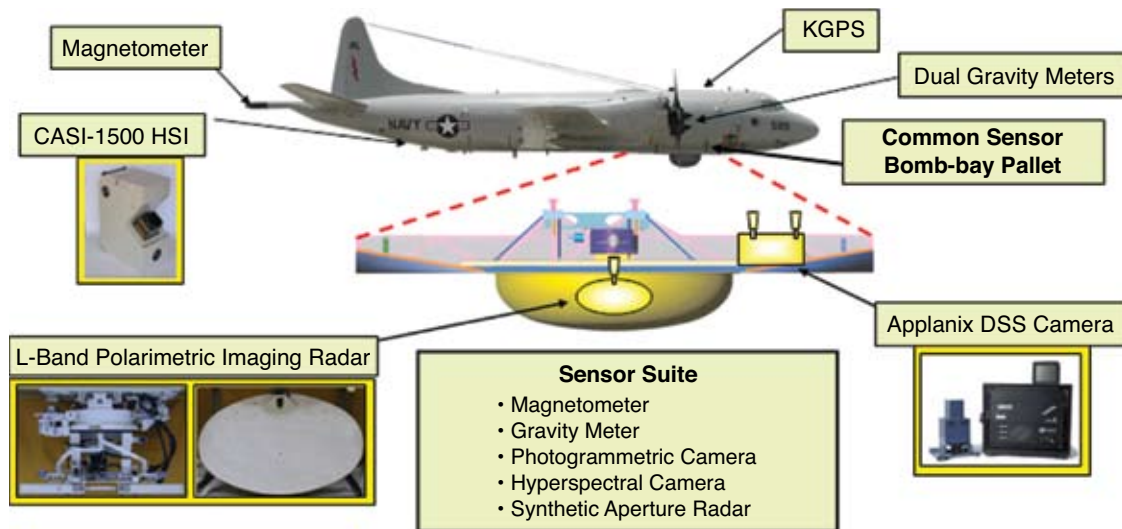
Sensors aboard the aircraft included digital true-color photogrammetric and hyperspectral optical imaging, imaging synthetic aperture radar (SAR), and both gravity and magnetic potential-field mapping systems. Rapid-turnaround photogrammetric imagery was provided to the International Security Assistance Force (ISAF) for use in current combat operations. To date, more than 150 combat missions have made significant use of these data. The rapid delivery was enabled by the use of new techniques in digital image processing and precise internal georegistration without ground control. This technology is revolutionizing aerial photogrammetric mapping by reducing both costs and processing time. Some of these data have been provided to the Riverine Analysis Team at the

Naval Oceanographic Office (NAVOCEANO) for support of Special Operations Forces. The integrated mapping mission similarly enhances economic and national development. Areas of application include reconnaissance geologic exploration for oil, gas, and mineral resources. The mission also supports civil infrastructure needs such as cadastral surveying, urban planning and development, and pipeline/powerline/road routing and construction. The data can be used for agriculture and hydrologic resource management, earthquake hazard analysis, and base-maps for humanitarian relief missions. The data sets also support basic research by NRL scientists working in the areas of sensor fusion, automated analysis techniques, riverine support, and geodesy.

SURVEY METHODS

The survey was flown aboard a research NP-3D Orion aircraft operated by the U.S. Navy's scientific development squadron VXS-1, formerly the Flight Support Detachment of NRL. Sensor systems installed on the P-3 (Fig. 1) included the following:

- dual ZLS air-sea gravimeters;
- a Geometrics 823A scalar magnetometer coupled with an Applied Physics 539 3-axis fluxgate magnetometer for compensation of the aircraft field;
- an Applanix DSS 301 digital photogrammetric camera with an integrated POS-AV 410 Inertial Measurement Unit (IMU)/Kinematic-mode Global Positioning Systems (KGPS) positioning system;

**FIGURE 1**

Sensor systems installed on the Orion NP-3D research aircraft for the Afghanistan aerogeophysical survey.

- an ITRES Corporation CASI-1500 hyperspectral imager (HSI); and
- an L-band polarimetric SAR built by NRL.

Several Ashtech geodetic-quality GPS receivers were also installed, but the primary positioning and attitude data for the various sensors were provided by the POS-AV system.

The aircraft and the science party were based at Kandahar Airfield. Logistics and flight operations were challenging, as Afghanistan is an active war zone and combat operations for much of southern Afghanistan are staged out of Kandahar. The P-3 aircraft required extensive modifications to operate in the combat theater including the addition of a flare/chaff dispenser and optical launch warning systems to counter surface-to-air missiles, infra-red strobes, secure communications channels, a low-observable paint scheme, and foamed fuel tanks to reduce the danger of ground fire. Combat takeoff and landing procedures were also required because of the potential for ground attacks. Differing optimal survey conditions for the various sensor systems combined with the dangerous operating conditions made survey planning and execution particularly difficult. Flight restrictions specified that data legs be flown at relatively high altitudes above ground level due to the threat of surface-to-air fire. While this restriction reduced the resolution of the gravity and magnetic measurements, it did allow collection of data over an approximate 4 km wide swath for the optical sensors, and a circa 15 km left of flight track nadir swath of SAR imagery. Flight ceiling limits for the aircraft limited coverage of the country to areas with elevations less than about 3,700 m, making it impossible to survey over the highest areas of the Hindu Kush

and Pamir mountains (these mountain ranges extend over the central and northeastern portions of the country, as seen in Fig. 2). However, this still allowed coverage of more than half of the country. Each line was flown at a constant barometric altitude with the survey line altitudes stepping generally upward from west to east along with the topography.

The project was laid out as three essentially distinct blocks: the northern, western, and eastern blocks (Fig. 2). Primary track spacing was 4 km, but was increased to 8 km in the northern block due to time and financial constraints. Several tie line flights and data transits of opportunity helped to maximize data coverage. Aircraft ground speed averaged between 300 and 380 kts, which is faster than considered optimal for high-resolution gravity, hyperspectral, or photogrammetric data collection. However, the increased speed allowed the survey of approximately 125,000 line-km of data tracks and more than 330,000 km² of imagery coverage in the 220 mission flight-hours allotted for the survey.

DATA COLLECTION AND PROCESSING

Photogrammetry

More than 65,000 high-resolution photogrammetric images were collected using an Applanix Digital Sensor System (DSS) Model 301 airborne digital camera mounted in the bomb bay of the aircraft. The DSS incorporates a 4 Kpixel × 4 Kpixel three-color sensor digitized with 12-bit resolution. The 55-mm lens used for this survey provides a 37° field of view. The camera can be cycled as fast as 2.5 seconds (although rates of 7–9 seconds were sufficient for operational altitudes and speeds) to produce 60% image overlap

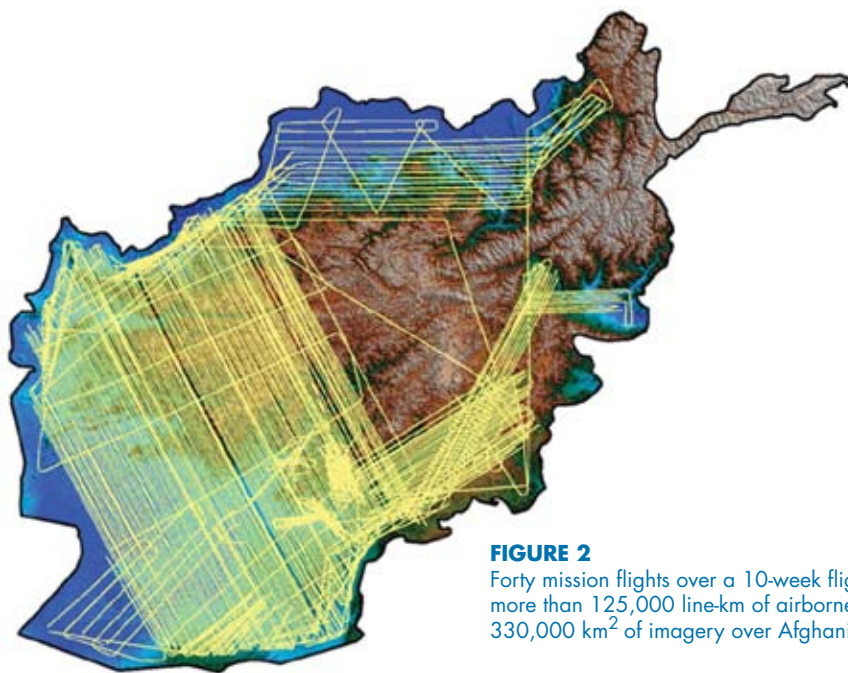


FIGURE 2
Forty mission flights over a 10-week flight period produced more than 125,000 line-km of airborne survey tracks and 330,000 km² of imagery over Afghanistan.

allowing for stereo analysis. Pixel size, or ground sample distance, varied between 85 and 135 cm. Photogrammetric images are corrected for camera calibration factors and dark pixel noise before being georeferenced using positioning data collected by the integrated POS-AV system. The POS-AV IMU provides measurements disciplined by differential dual-frequency, differential carrier-phase GPS (KGPS) to directly georeference each image pixel, thus providing precise photogrammetry without ground control. GPS positioning for this survey was particularly difficult because of the long flight baselines required by the geographic extent of the survey. Stationary differential GPS base stations were maintained at Kandahar Airfield, Kabul, Herat, and Sheberghan during survey operations in order to support multi-base station reduction of the KGPS data. The remote base stations improved the aircraft trajectories significantly during the flight segments since some baselines were more than 600 km from Kandahar. We estimate that the final rms 3-D aircraft positioning accuracy is better than 30 cm overall, with better than 10 cm over shorter flight baselines (< 300 km). Ortho-corrections are applied to the images to account for parallax errors caused by imaging variable topography at oblique angles. A 30-m posting digital elevation model (DEM) from the National Geospatial-Intelligence Agency (NGA) Shuttle Radar Topographic Mission (SRTM) was used for this correction. Data collected during a high-altitude boresight calibration flight over the airfield demonstrated sub-pixel absolute horizontal positioning (< 1 m) by comparison with precisely surveyed ground control points, and about twice this in the vertical from stereo analysis. Absolute

pixel positional accuracy degrades somewhat on the long straight tracks (up to 500 km) since turns are required to separate gyro and accelerometer bias drift in the IMU. This translates primarily into an increasing yaw error along the track with time. However, image tie-point aerotriangulation between successive images and in adjacent image strips (if there is sufficient sidelap) allows correction of much of this error. Absolute pixel position errors are estimated to be < 2 m on average, and relative positioning within mosaiced aerotriangulated images is on the order of 1 m.

Hyperspectral Imagery

Hyperspectral imagery was collected with a CASI-1500 system mounted in the bomb bay of the aircraft. The camera collects a 1500-pixel-wide push-broom swath through a 40.5° field of view with up to 288 spectral bands (0.4–1.0 μm) that were averaged down to 72 bands to improve signal-to-noise, and a dynamic range of 14 bits. The image pixel size was approximately 3 m (cross-track) × 5 m (along-track) and an integrated CMIGITS GPS (non-differential)/IMU provided attitude data for the camera. There is ongoing experimentation using the higher-resolution attitude data collected from the more accurate Applanix POS-AV IMU used for the photogrammetric data processing in order to increase the data accuracy.

Gravity

A pair of ZLS Corporation air-sea gravimeters were mounted in the center of the aircraft fuselage. The

airborne gravimeter data were corrected for aircraft vertical acceleration, Eötvös effect (correction for horizontal velocity over a curved, rotating earth), and normal reference gravity field based on aircraft positioning from the POS-AV system. High-frequency noise is attenuated by a low-pass filter resulting in along-track resolution of approximately 20–25 km (half-wavelength) at the average survey speed. The 4-km track spacing over-samples the field at survey altitudes, but improves the signal-to-noise characteristics of the gridded data set. Averaging data from the two gravimeters further reduces the noise.

Free-air anomalies corrected for the survey altitude were employed as the basic data set during preliminary analysis. Simple and complete Bouguer maps were produced from SRTM topography, calculating slab Bouguer and terrain corrections, and upward-continuing the corrections to the average survey elevation before combining with the at-altitude free-air anomalies. For final processing, all profiles are upward-continued to a constant altitude to eliminate any track-to-track discrepancy in signal content caused by the different measurement altitudes; they are then adjusted based on crossover analysis, and the Bouguer anomalies are recalculated. Crossover analysis on the initial free-air anomaly data indicates an rms measurement error for the survey of approximately 2 mGals ($1 \text{ mGal} = 10^{-3} \text{ cm/sec}^2$).

Magnetic Data

Scalar and vector magnetometers were mounted in the non-magnetic tail boom of the aircraft. Aircraft magnetic field effects on the scalar magnetometer were corrected using information from the vector magnetometer and removed in post-processing using standard compensation procedures. This compensation proved very effective (rms residual of $< 0.1 \text{ nT}$) considering that the P-3 is a large four-engine turboprop aircraft with a gross weight of more than 50,000 kg. Diurnal solar variations were obtained from ground magnetic base stations operated at Kandahar, Kabul, Herat, and Faizabad. For initial processing, the only accessible station was the Kandahar base station; this improved data quality significantly, but fairly large diurnal effects were still visible in some areas, particularly over the mountainous areas that could be surveyed. In the coming months, several different strategies of multi-base station correction will be tried prior to re-leveling the data.

Synthetic Aperture Radar (SAR)

SAR data was collected using a prototype unit designed by the Radar Division at NRL to collect L-band polarimetric phase data. The SAR antenna, also

designed for specific requirements by the Radar Division, was mounted in a large radome attached to the bomb bay of the aircraft. Center frequency was 1300 MHz with a bandwidth of 10 MHz. The data collection system was designed to handle more than double this bandwidth, but time and financial constraints precluded upgrading the RF section to the desired higher bandwidth, resulting in an effective pixel size of 3 m (along-track) \times 15 m (cross-track). Even at this reduced bandwidth, typically more than 300 GBytes of phase-data per flight were collected, totaling more than 10 TBytes for the entire survey.

RESULTS

Photogrammetric Data

Digital true-color photomosaics are currently being produced from the 65,000 photogrammetric images collected during the airborne mapping mission. Figure 3 shows a piece from a photomosaic of Kajake dam that was provided in the field to ISAF forces. ISAF troops used the photomosaics for planning a major campaign against Taliban forces attacking the dam and nearby villages during the deployment. In addition to the basic imagery products, elevations and slopes calculated from the stereo imagery models proved to be extremely useful for planning troop and vehicle movement trafficability, planning helicopter landing zones, and performing line-of-sight analysis for determination of cover and visibility. Products from the Kajake dam flight were produced and delivered to combat personnel within 48 hours of landing, a dramatic contrast to the months usually required for conventional photogrammetric operations. Both hard and soft copies of the imagery were loaded onto hand-held GPS units and provided to combat troops. The unclassified nature of the imagery proved to be a significant operational advantage for combat forces in the field who typically are not allowed to carry classified maps and images.

Orthorectified photomosaics of the Kajake reservoir and Helmand river area were also provided to the Riverine Analysis Team at NAVOCEANO to support Special Operations Forces. Although the turnaround times demonstrated in this project were considered extremely rapid, real-time kinematic (RTK) GPS positioning techniques and prototype image calibration and ortho-correction software now being tested have the potential to allow product delivery in near real-time.

As the photogrammetric mosaics of the remainder of the country are processed, they are being provided to USGS for economic analysis projects, to NGA for incorporation into DoD's imagery library of the country, to USAID for construction and development projects, and to the government of Afghanistan for



FIGURE 3

This image shows part of a digital photogrammetric mosaic produced over the Kajake dam and reservoir. Pixel ground sampling distance and absolute georegistration accuracy were approximately 1 m and 2 m, respectively. Stereo models for elevation and slope estimates were also produced for the region. These imagery data were provided to ISAF troops engaged in combat with Taliban forces in the area.

myriad uses. At the same time, the pipeline of imagery products to ISAF forces in Afghanistan is continuing to support current and future combat operations.

Hyperspectral Data

Analysis of the hyperspectral imagery is processing-intensive and is only in the initial stages. Spectral classification software allows automated identification of features such as vegetation, water, buildings, roads, and some soil and mineral types. Figure 4 shows a few such classifications for the area of Kandahar Airfield. Water depth (bathymetry) can also be estimated from the hyperspectral data should the water clarity be sufficient to allow the return of some photons from the bottom. The hyperspectral data are being provided to the Riverine Analysis Team at NAVOCEANO for bathymetry estimation, river trafficability, and other operational joint analysis with the photogrammetric data. The data will also be used to support exploration for minerals and studies in agriculture and hydrology for economic development of the country.

Gravity Data

Gravity measurements are indicative of local mass distribution and are used operationally for corrections to high-end inertial navigation units on some strategic weapons systems, for definition of local vertical

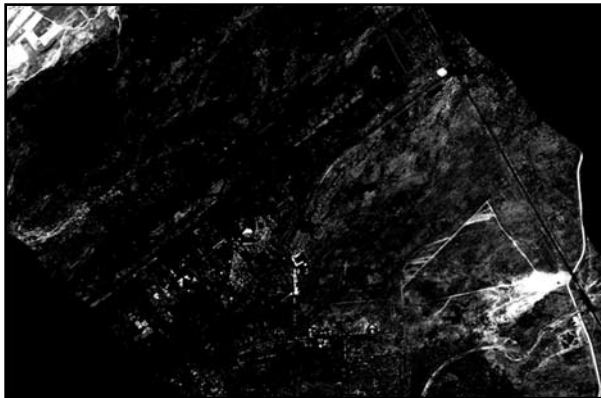
datums, for global earth gravity models, and for economic geology in oil, gas, and mineral exploration. As final data reduction is completed, the gravity data are being supplied to NGA for weapon-systems products and the WGS2006 gravity model, and to USGS and the government of Afghanistan for use in exploration geology for economic resources. The free-air gravity anomaly map (Figure 5(a)) is dominated by the extreme topography of the mountains that, even at survey altitude, produced a signal spanning more than 150 mGals. The complete Bouguer anomaly map (Figure 5(b)) removes first-order topographic effects and reveals the segmentation of Afghanistan into the large Helmand basin to the southwest separated from the Tadjik basin to the north by the folded and thickened crust of the central mountains. The Katawaz basin in the southeast is characterized by alternating parallel lineated Bouguer anomaly highs and lows that are anti-correlated with fault-parallel topography. The easiest way to generate such a non-isostatic pattern is large-scale compressional bowing of relatively constant thickness crust such that the topographic highs overlie upwarped higher density mantle, and the downwarped crust displaces mantle. The Kabul basin to the northeast near the Pakistani border appears to be out of isostatic equilibrium to an even greater extent with a relatively large negative Bouguer gravity anomaly (generally indicative of thickened crust) over a topographically depressed region. It is likely that the sedimentary sections in these relatively Bouguer-low areas are abnormally thick, and a possible source for oil and gas resources for the country. Magnetic depth-to-source calculations (see below) also provide estimates of the sedimentary thickness within these basins, showing large possible sedimentary sections. The existence of these basins was known prior to the survey, but the extent, shapes, and estimated depths were previously unknown.

Magnetic Data

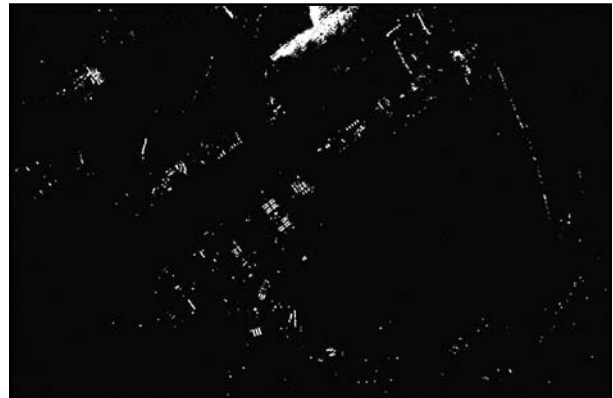
The local magnetic field in the region is created by the bulk induced and remnant magnetization of the source rock in the vicinity. As such, magnetic measurements yield useful information about local geologic structures and mineralogic assemblages of interest for economic geology. The spatial frequency content of the magnetic field variations at the aircraft altitudes flown also provide information about the distance to the causative magnetic source material since higher frequencies attenuate more rapidly with distance. Since sediments are largely non-magnetic, distance estimates based on frequency content can provide an estimate of sedimentary thickness overlying more magnetic basement rock. Additionally, there are operational requirements for magnetic data, primarily for magnetic



(a)



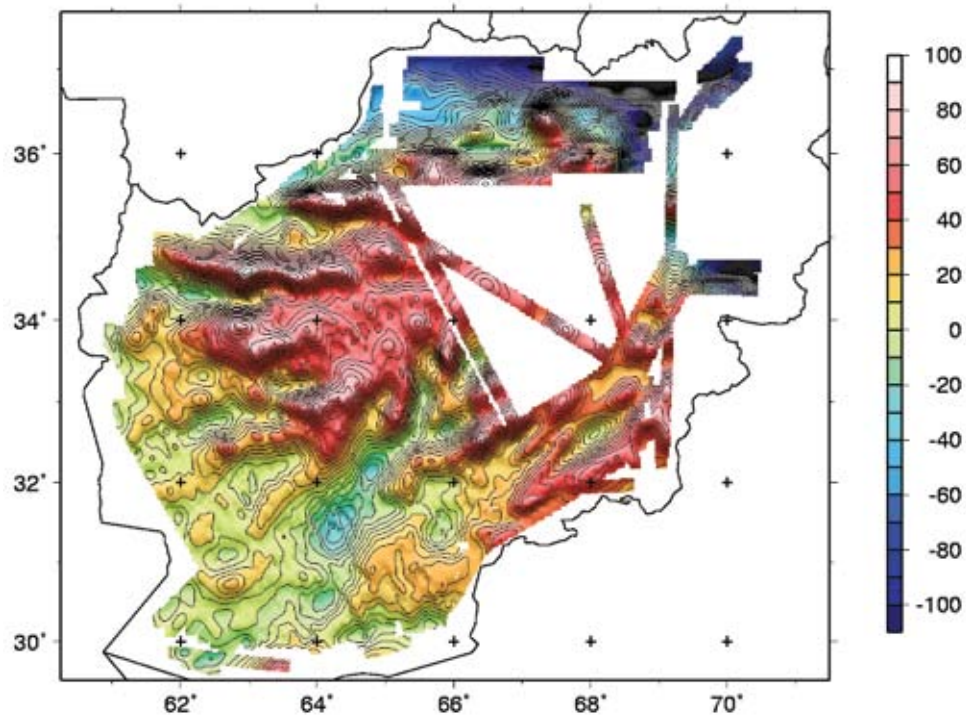
(b)



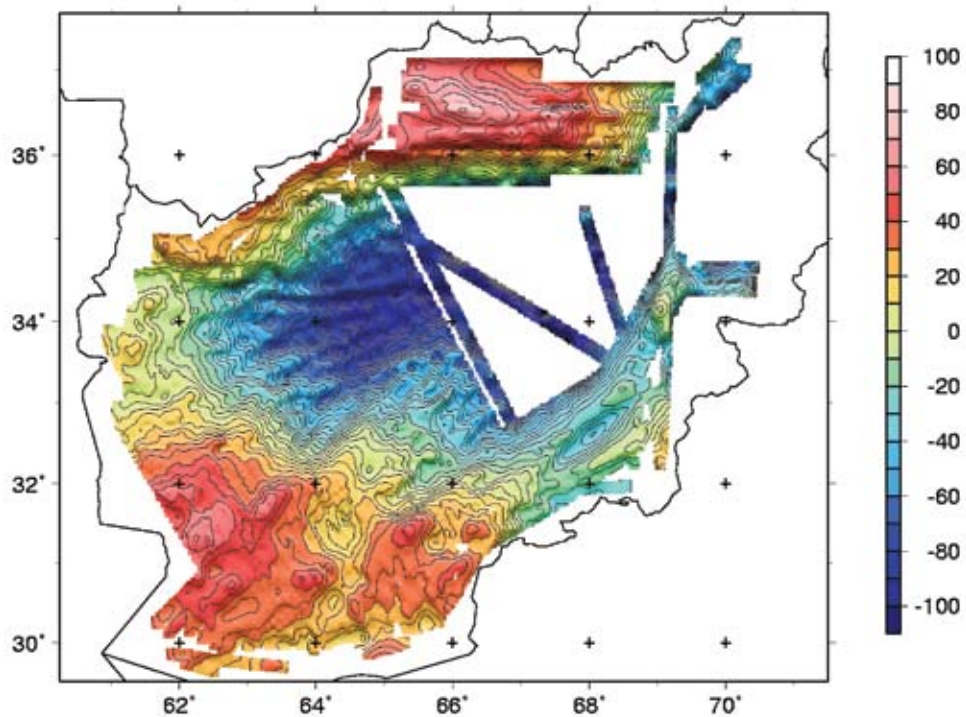
(c)

FIGURE 4

(a) Synthetic true-color imagery of Kandahar Airfield synthesized from the 288 band (0.4–1.0 μm) CASI-1500 hyperspectral imager. (b) Automated feature analysis for vegetation in the area of Fig. 4(a) produced from the hyperspectral data by calculating similarity to spectral signature of chlorophyll. (c) Same as (b) but matching the spectral signature of buildings in the area of the airfield.



(a)



(b)

FIGURE 5

(a) Free-air gravity anomaly map showing the relative gravity highs produced by the mountains (warm colors) compared to the relative lows of the plains. Units are mGals ($1 \text{ mGal} = 10^{-3} \text{ cm/sec}^2 \sim 1 \mu\text{g}$). (b) Complete Bouguer gravity anomaly map produced by removing an estimate of the mass effects of topography and elevation. The residual anomaly is indicative of subsurface mass variations and deviations from the assumptions used in the modeling. At this scale, the largest effects can be attributed to crustal thickening over the mountainous regions (cool colors) and to thick sections of less dense sediments that fill the crustal depressions of basin regions (warm colors). The sedimentary basins are of great interest for oil and gas exploration.

compass variation corrections. The information content of the magnetic data collected for this survey was limited by the high-altitude flights required for safe operation. However, it is expected that the final result will be a very good quality regional survey because of the low measurement noise, over-sampled track spacing, careful use of distributed base stations, and consistency of the survey parameters of the large area. Useful geologic information can be observed even in the preliminary data (Fig. 6). The final processed data will provide an excellent medium- to long-wavelength basis for the selection and control of future low-altitude aeromagnetic surveys. Several commercial historical data sets were obtained by USGS prior to deployment to Kandahar. In general these data, when upward-continued to flight altitudes, fit well with the new data after adjustment. The exception to this is a survey over the mountainous central region. It is believed that residual discrepancies in this case are related to errors in the reported altitudes of the historical data set.

SAR Data

The primary use of the SAR data will be in inversion to mineral types and properties from radar reflectivity. The data will also be used to supplement the optical imagery in geologic analysis of faulting, bedding, and rock foliation. Feature analysis for man-made objects and buildings may also be possible.

Since some ground penetration is possible at L-band frequencies, there may also be some visible signatures of buried streambeds and perhaps old roads for hydrologic and archeological research. At this time, only unfocused (uncorrected for aircraft attitude and trajectory) SAR images have been produced for verification and quality control of the data set (Fig. 7).

CONCLUSION

Despite the difficulties of first-time integration of a large component of complex and diverse sensors, and operation in a combat environment, the aerogeophysical project is considered to be a complete success. The Navy flight and ground maintenance personnel safely completed 100% of desired missions with no mishaps or significant problems. Nearly 20 Tbytes of raw data were collected from the various systems, with literally no data lost to hardware or software problems over the course of the 40 mission flights. Analysis of the enormous data set will occupy scientists at numerous institutions for some time, but even at this stage, the contributions to operational support of GWOT and to advances in the state of the art in airborne remote sensing are substantial. Additionally, the environmental data collected from the suite of sensors is invaluable to the economic redevelopment of Afghanistan.

[Sponsored by the government of Afghanistan, ONR, and NGA] ★

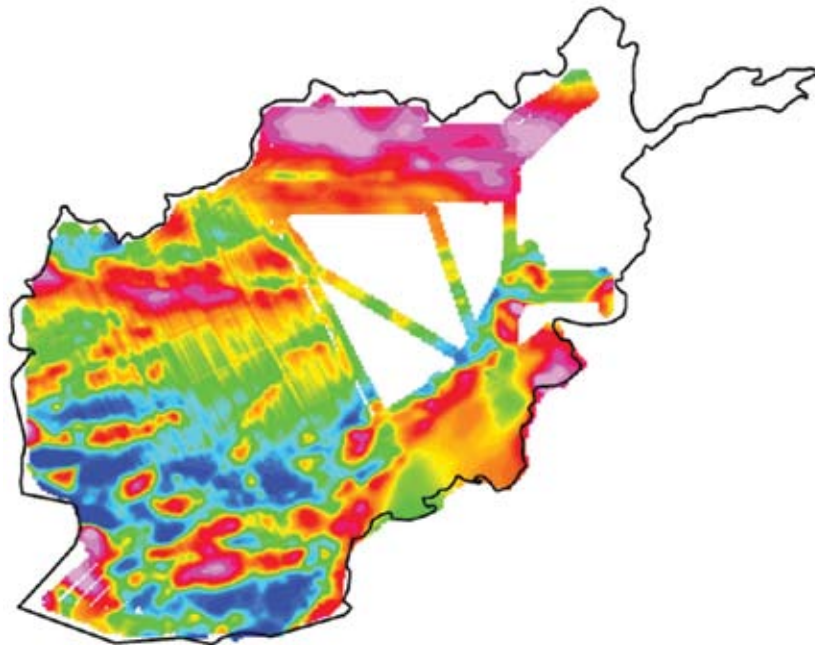


FIGURE 6

Magnetic anomaly map corrected for diurnal variation at Kandahar Airfield. Note the residual diurnal artifacts (streaks following the flightlines) over some high areas of the Hindu Kush mountains. The magnetic data are useful for calculating bulk estimates of the magnetic properties of the local rocks and the depth to the magnetic source material, both useful in oil, gas, and mineral exploration.

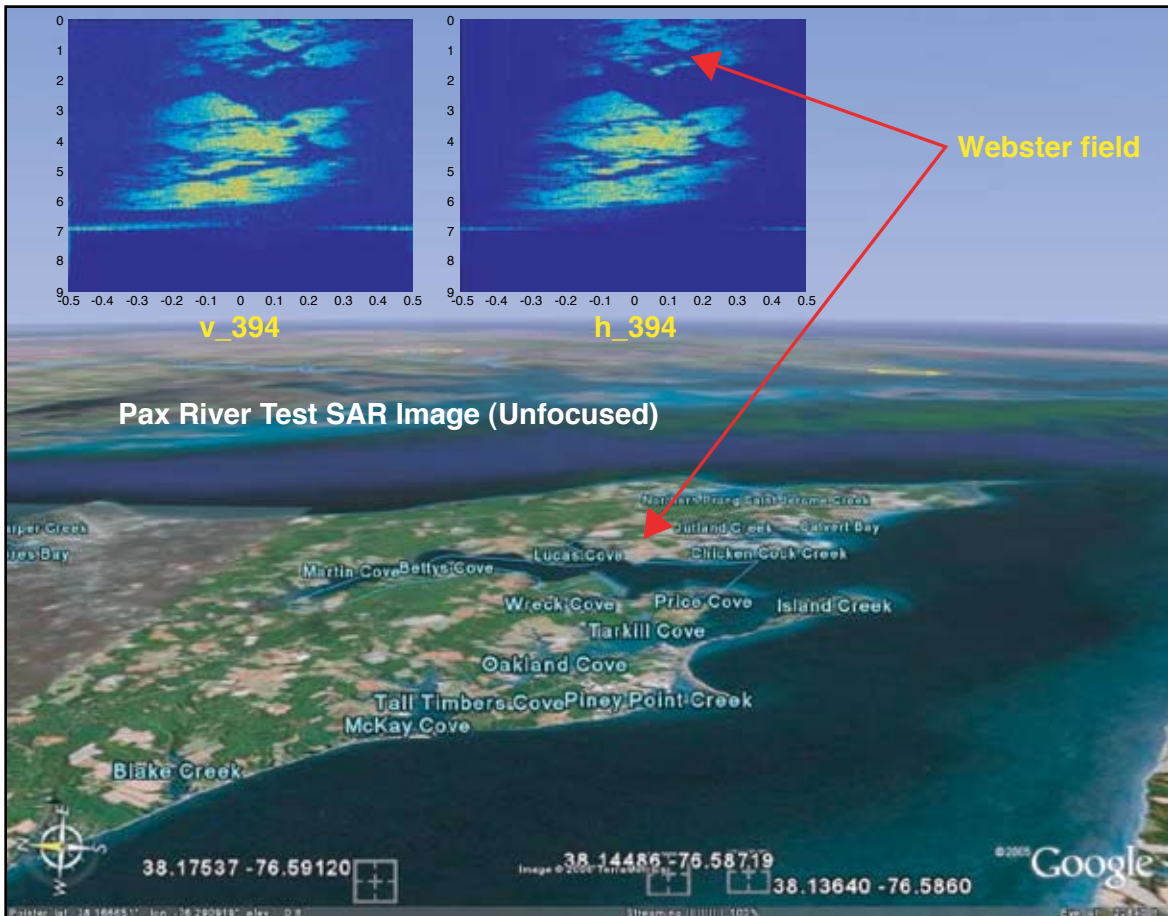


FIGURE 7
 Test SAR imagery produced in the vicinity of Patuxent River Naval Air Station prior to deployment to Kandahar. The images have not yet been focused to compensate for variations in aircraft motion and attitude.

ACOUSTICS





121 Modeling Reverberation Time Series for Shallow Water Clutter Environments

K.D. LePage

125 Remote Intense Laser Acoustic Source

T.G. Jones, A. Ting, J. Peñano, P. Sprangle, and L.D. Bibee

127 Fiber Optic Towed Arrays

C. Kirkendall, T. Barock, A. Tveten, and A. Dandridge

Modeling Reverberation Time Series for Shallow Water Clutter Environments

K.D. LePage
Acoustics Division

Introduction: The phenomenon of clutter in shallow water environments can be modeled from several approaches. One approach we have taken is to model reverberation time series for heterogeneous environments with a variety of scattering mechanisms to compare the resulting characteristics to those of experimentally observed clutter. Here we show R-SNAP¹ reverberation time series estimates for the Malta Plateau region in the Straits of Sicily that seem to capture some of the clutter behavior observed during the SCARAB 98 experiment conducted in conjunction with the NATO Undersea Research Centre (NURC), Italy.² Of particular interest is the appearance of coherent time-frequency striation patterns in both the modeled and observed reverberation, with spatially compact, broadband clutter features superimposed by the presence of environmental discontinuities.

Malta Plateau Reverberation Characteristics: The Malta Plateau is a shallow (70–200 m) site in the Straits of Sicily north of Malta. It is characterized by a muddy bottom lying over consolidated sediment/rock that becomes exposed as the Ragusa Ridge, which runs north-south between Malta and eastern Sicily. In Fig. 1, reverberation in the 100 Hz to 2 kHz band for a 91 m impulsive SUS charge is shown superimposed on the bathymetry for the site. These data were collected during the SCARAB 98 trial conducted by SACLANT-CEN (now NURC) on a conventional (ambiguous) array towed in the north-south direction.^{2,3} Clearly evident is reverberation clutter associated with a region of shoaling bathymetry and thinning sediment cover on the Ragusa Ridge to the east of the ship track. Also evident are strong scattering events from certain known wrecks to the south and east of the source and from the Campo Vega oil production platform to the NNW (approximate locations are indicated by black crosses).

Figure 1 shows that there are at least two types of clutter in the SCARAB 98 data set: environmental clutter characterized by increased reverberation from the exposed ridge, and target-like clutter events associated with anthropogenic sources such as shipwrecks and oil production facilities. Figure 2 shows the spectrogram of the SUS reverberation seen on the bearing of 116 true from Fig. 1. Here one can observe the broadband nature of both the discrete clutter event seen at 15 s caused by a sunken ship, and the extended clutter return from the Ragusa Ridge from 19 to 24 s. One also observes many other smaller clutter events,

probably associated with smaller environmental discontinuities, which are most energetic between 1 and 2 kHz. Superimposed on these features is the time-frequency structure of coherent round-trip propagation to the scatterers in the waveguide, characterized by a clearly visible striation pattern typically associated with passive acoustics in shallow water waveguides⁴ but here clearly evident in the active acoustic reverberation.

Malta Plateau Environmental Description: A detailed geoacoustic and scattering description of the environment between Sicily and Malta has been prepared by Charles Holland at the Applied Research Laboratory at the Pennsylvania State University (ARL/PSU) based on measurements of propagation, scattering strength, and reverberation.³ The results are shown in Table 1. Notice that both the sediment attenuation and the scattering strength grow linearly with frequency. Using the values in Table 1 gives good agreement between the data and the range-independent model results for the background levels of reverberation on the sediments of the Malta Plateau, away from the Ragusa Ridge. We use these background environmental parameters, along with detailed measurements of the bathymetry and sediment thickness on the Malta Plateau collected by Osler and Algan,⁵ to model environmental clutter from the Ragusa Ridge.

Malta Plateau Simulation Results: Using the environmental parameters in Table 1, the detailed bathymetry and sediment thickness measurements of Osler and Algan, and the SUS source spectrum and towed array beamwidth, we exercised the time series generation capability of R-SNAP to simulate environmental clutter for the 337.5–362.5 Hz band over the Ragusa Ridge from the sediment-water and sediment-basement interfaces. Figure 3 compares the measured data, shown in blue, and the simulation (minus 30 dB), shown in red. Agreement is quite good, up to and including the clutter enhancement associated with the ridge, which in the model is captured by the exposure of the sediment-basement interface to acoustic energy where the sediment cover thins dramatically. Figure 4 shows the spectrograms of the data and the model. Note the time-frequency striations visible in the data (b) are replicated in the simulations (a). Overall, many aspects of the clutter caused by the Ragusa Ridge are faithfully replicated in the simulations.

Conclusions: The R-SNAP code has been exercised to model environmental clutter caused by an exposed ridge on the Malta Plateau south of Sicily. Model-data comparisons at 350 Hz show favorable agreement between the reverberation data from the ridge and the simulations using average environmental parameters

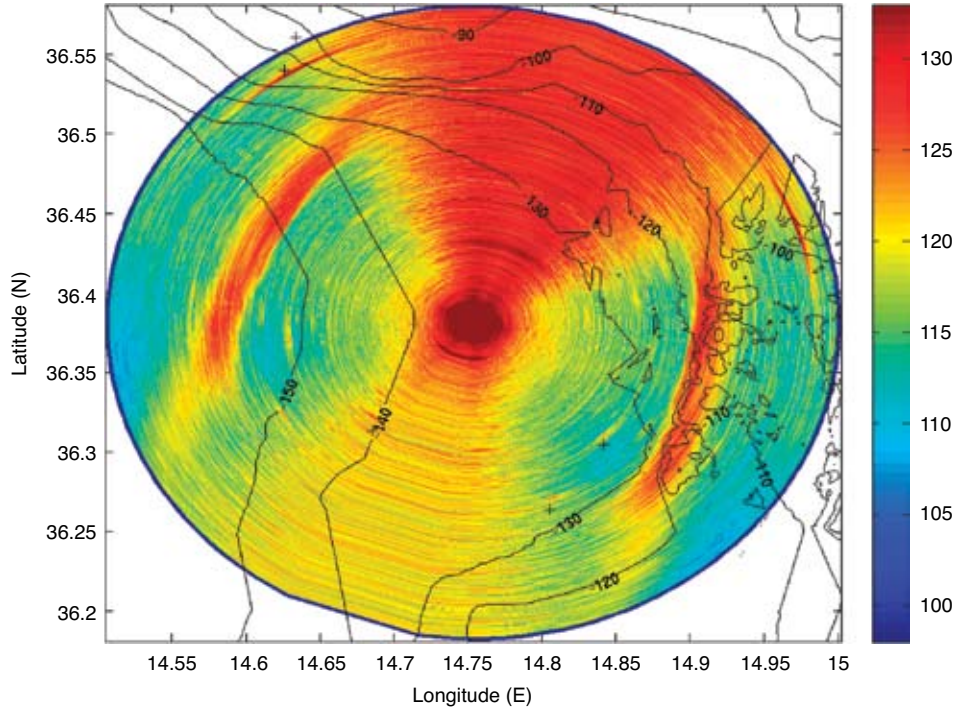


FIGURE 1 Reverberation data collected on the Malta Plateau. Ambiguous clutter returns from the Ragusa Ridge are clearly visible. Clutter from wrecks (south of the receiver) and the Campo Vega oil production platform (northwest of the receiver) is also visible. Known approximate positions of these objects are indicated with crosses.

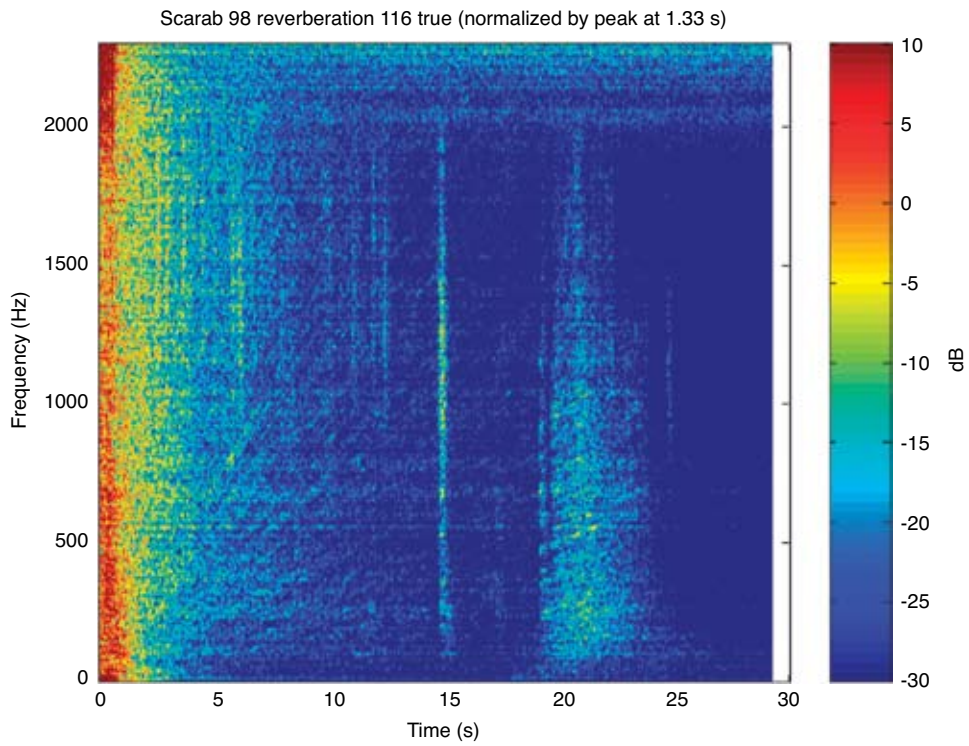


FIGURE 2 Time-frequency spectrogram of SUS reverb looking towards shipwreck (15 s) and Ragusa Ridge (18–25 s).

TABLE 1
Background Environmental Properties for Malta Plateau

PROPERTY	VALUE
Sediment Sound Speed Ratio	1.05
Sediment Density	1.80 gm/cm ³
Sediment Attenuation (dB/l)	0.70 f (f in kHz)
Sediment Scattering Strength (Lommel-Seeliger)	-47 + 14.8 f (f in kHz) dB
Basement Scattering Strength (Lommel-Seeliger)	-15 dB

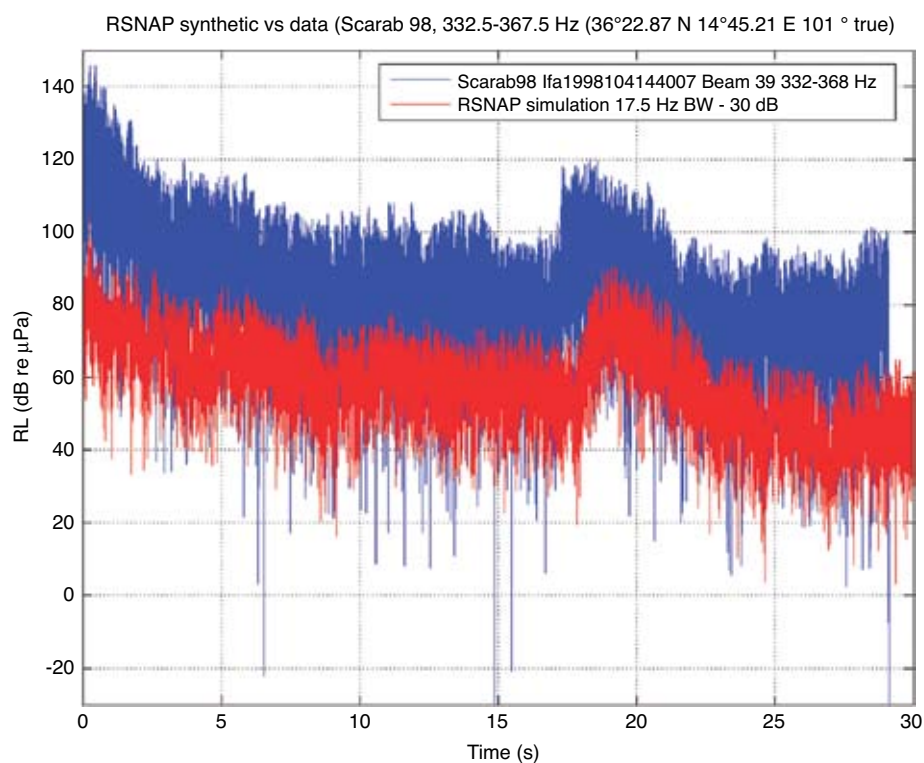


FIGURE 3
Narrowband reverberation time series in the 332–368 Hz band measured from the Ragusa Ridge on the Malta Plateau during SCARAB 98 (blue), and simulated by R-SNAP for the same frequency band (red, offset by 30 dB) using environmental parameters measured in situ. The simulation captures many of the characteristics of the measured data.

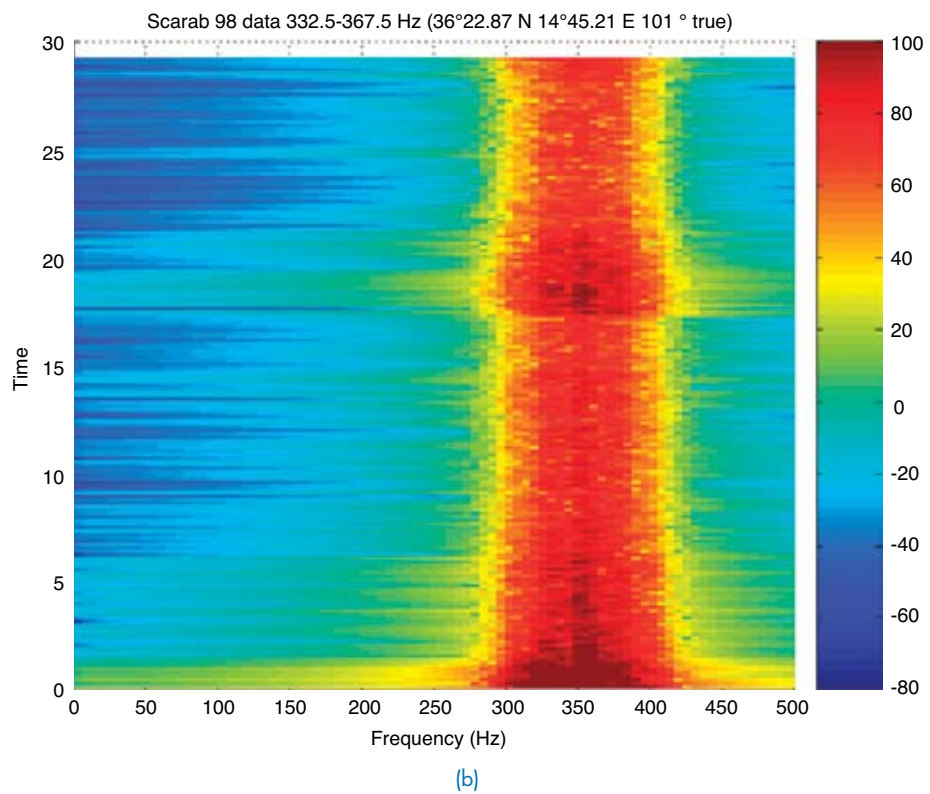
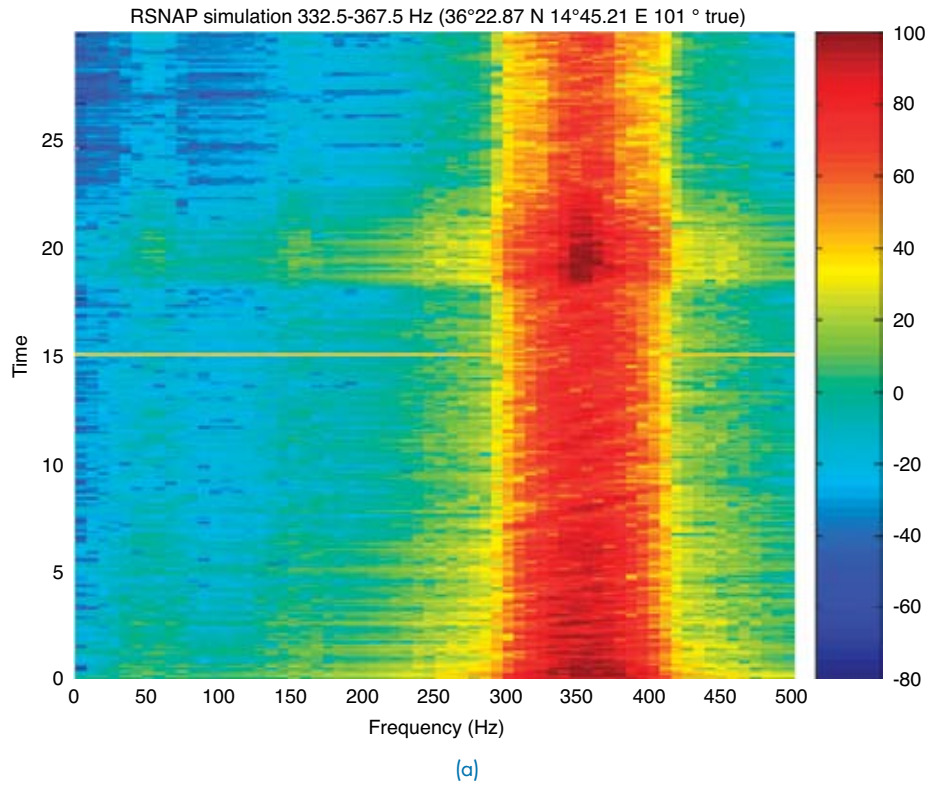


FIGURE 4
Spectrograms of (a) 350 Hz R-SNAP simulation shown in Fig. 3, and (b) SCARAB 98 data. Many of the characteristics of the data are captured by the simulation, including coherent time-frequency striations of positive slope and the clutter return from the Ragusa Ridge starting at 18 s.

supplied by an independent analysis. This agreement includes both the presence of coherent time-frequency striations in the data, and strong clutter enhancements over the Ragusa Ridge. The results illustrate that with sufficient environmental knowledge, certain clutter characteristics of shallow water reverberation associated with large environmental inhomogeneities may be predicted. The R-SNAP tool is at the vanguard of a new generation of reverberation models that are capable of predicting coherent reverberation time series for well-characterized shallow water waveguides. Time series simulation allows the estimation of sonar clutter for notional systems of interest.

[Sponsored by ONR]

References

- ¹ K.D. LePage, *Monostatic Reverberation in Range Dependent Waveguides: The R-SNAP Model*, SR-363, SACLANT Undersea Research Centre, La Spezia, Italy, 2003.
- ² K.D. LePage, P. Neumann, and C.W. Holland, "Broad-band Time Domain Modeling of Sonar Clutter in Range Dependent Waveguides," *Proc. of IEEE/MTS OCEANS '06, Boston, MA, September 18-21, 2006*, in press.
- ³ C.W. Holland, "Mapping Seabed Variability: Rapid Surveying of Coastal Regions," *J. Acoust. Soc. Am.* **119**(3), 1373–1387 (2006).
- ⁴ G.L. D'Spain and W.A. Kuperman, "Application of Waveguide Invariants to Analysis of Spectrograms from Shallow Water Environments that Vary in Range and Azimuth," *J. Acoust. Soc. Am.* **106**(5), 2454–2468 (1999).
- ⁵ J. Osler and O. Algan, *A High Resolution Seismic Sequence Analysis of the Malta Plateau*, SR-311, SACLANT Undersea Research Centre, La Spezia, Italy, 1999. ★

Remote Intense Laser Acoustic Source

T.G. Jones,¹ A. Ting,¹ J. Peñano,¹ P. Sprangle,¹ and L.D. Bibee²

¹Plasma Physics Division

²Marine Geosciences Division

Introduction: NRL is developing a novel underwater acoustic source, in which a tailored intense broadband laser pulse propagates many meters underwater and generates an acoustic pulse at a predetermined remote location. Such a new acoustic source could enable or improve several critical Navy and commercial applications, including acoustic imaging, undersea communications, and navigation. As part of this work we are exploring intense laser propagation physics through both air and water. Air propagation of the laser pulse will be useful for applications where airborne lasers generate underwater acoustic signals. Controlled underwater compression of these optical pulses is achieved using a combination of group velocity dispersion (GVD), which provides longitudinal compression, and nonlinear self-focusing (NSF), which provides

transverse compression. The resulting high-intensity laser pulse then causes photoionization, intense localized heating, and shock generation.¹ Recent experiments included the first demonstration of underwater acoustic generation using an intense broadband laser pulse. Intense acoustic source levels were measured, and are in the range of useful levels for some Navy applications. Optical GVD was precisely measured, and characterization of this acoustic source, including power spectrum and radiation pattern, is under way.

Potential Applications: Several applications would make use of a high-repetition-rate pulsed laser. The repetitively pulsed laser can be steered with rapidly movable mirrors. Such a laser, which can be compact and is commercially available with appropriate bandwidth and pulse energy, could be placed on an underwater platform and used for generating phased acoustic arrays. This arrangement can also provide rapid oblique-angle acoustic scattering data for imaging and identifying underwater objects (as depicted in Fig. 5), a significant addition to traditional direct backscattering data. The ability to put the laser on an airborne platform opens many other potential applications, including undersea communications from aircraft, and navigation via remotely generated acoustic beacons. The relative strength of the GVD and NSF effects in water and air are such that a properly designed laser pulse can travel many hundreds of meters through the air relatively unchanged, then quickly compress upon entry into the water.

First Broadband Acoustic Generation Demonstrated: Using lens-assisted focusing, we recently demonstrated the first laser acoustic generation using

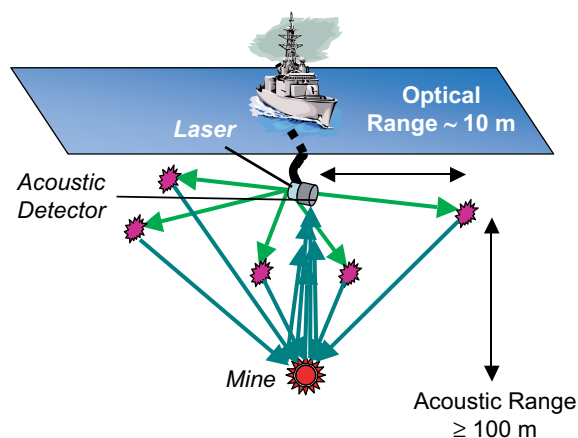


FIGURE 5 A schematic of a laser-based acoustic imaging application shows laser light (light green) propagating to predetermined acoustic generation locations (purple), and the resulting acoustic pulses propagating to and scattering from a target (blue-green).

a broadband laser pulse. The Plasma Physics Division Intense Laser Interaction Laboratory features a 10-terawatt ultrafast broadband laser, operating at a wavelength of 800 nm (deep red). This light was first converted to 400 nm (blue), which propagates underwater, using a nonlinear harmonic generation crystal. We then directed and focused this light into our newly constructed acoustic characterization chamber, shown in Fig. 6, which was outfitted with an array of high-frequency hydrophones. These hydrophones recorded intense pressure traces of the resulting acoustic pulses, a sample of which is shown in Fig. 7. Sound pressure levels (SPLs) up to 170 dB were measured, with pulse durations on the order of 1 μ s, and a corresponding peak in the power spectrum near 1 MHz. We also observed strong optical dispersion in water due to rapid stretching and power reduction of the pulse during propagation, as was apparent from the narrow range of underwater propagation distances for which the water was photoionized. The relatively novel use of photoionization and shock generation in our scheme provides several orders of magnitude improvement in photo-acoustic energy conversion efficiency over previous schemes using slow laser heating and thermal expansion. Ongoing experiments aim to increase the SPL as well as increase the acoustic power at lower frequencies.

Precise GVD Measurement: A recently constructed 8-meter-long underwater laser propagation chamber,

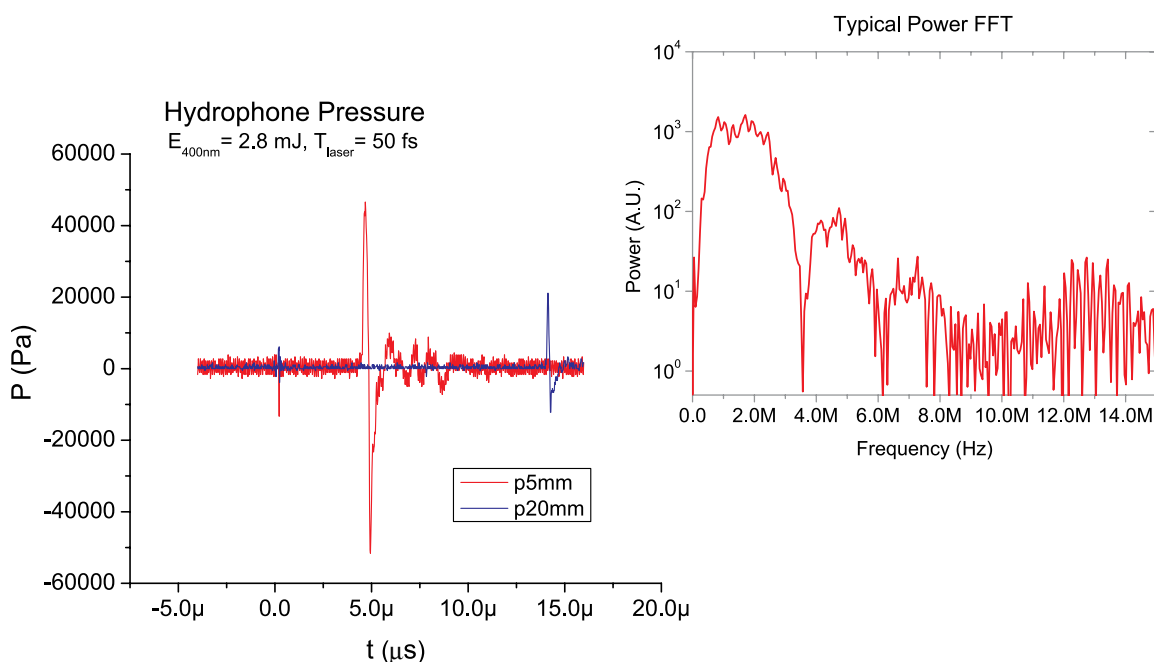
shown at right in Fig. 6, provided a path for studying long-distance underwater propagation effects, including GVD. A custom-tailored optical pulse with a time-varying wavelength can be longitudinally compressed at a predetermined remote location using GVD, in which different wavelengths of light propagate at different velocities. The variation in the speed of light with wavelength is characterized by the GVD parameter β_2 , which governs remote optical pulse compression. After several passes through the chamber, an ultra-short, 400 nm broadband laser pulse becomes stretched in time due to the GVD-induced variation in propagation speeds of its different wavelength components. We measured the pulse length after such propagation with a 10-picosecond-resolution streak camera, yielding a value of $\beta_2 = 1.0 \times 10^{-27} \text{ s}^2/\text{cm}$, in good agreement with the calculated value. This is the first direct measurement of β_2 underwater.

Simulation: The Beam Physics Branch has several years of research experience in atmospheric propagation of intense lasers, and has developed a comprehensive laser propagation simulation code, HELCAP, to simulate the relevant physics. This code has now been adapted to simulate intense underwater propagation. Recent 3D simulations predict controlled underwater optical pulse compression. These simulations also identified a fundamental underwater propagation power limit at approximately 20 MW, due to onset of beam filamentation instabilities.



FIGURE 6

The transparent acrylic acoustic characterization chamber (left) provides a clear view of underwater laser-induced breakdown, and fixtures for mounting an array of hydrophones. The 8-meter-long underwater laser propagation chamber (above) allows study of intense light propagation and remote optical compression.

**FIGURE 7**

A hydrophone trace shows intense acoustic generation with modest laser pulse energy. The red trace shows the pressure evolution at 5 mm from the laser source, and the blue trace shows pressure at 20 mm. The inset shows a power spectrum of the trace at 5 mm. These NRL experiments are the first acoustic generation demonstration using broadband ultra-intense laser beams.

Summary: The novel underwater laser acoustic source under development at NRL provides the first laser acoustic generation at a predetermined and variable remote underwater location. A driving laser pulse can propagate through water only, or through both air and water, so that a compact laser on either an underwater or airborne platform can be used for remote acoustic generation. This source promises to open an array of potential applications for both Navy and commercial use.

[Sponsored by ONR]

References

¹T.G. Jones, A. Ting, P. Sprangle, L.D. Bibee, and J. Peñano, "Remote Intense Laser Acoustic Source," U.S. Patent App. 11/268,400, Nov. 2005. ★

Fiber Optic Towed Arrays

C. Kirkendall, T. Barock, A. Tveten, and A. Dandridge
Optical Sciences Division

Introduction: Towed arrays were one of the first application areas considered for fiber optic acoustic sensors. The concept of having only the low-cost, passive components (fiber optic elements) in the "wet" end of the system, while the lasers and expensive components were located in the tow vessel, addressed

the increasing costs of Navy towed arrays. The earliest demonstration of this technology was made in 1983: the fiber interferometric sensor was formed with fiber couplers (to split the light), with the sensing fiber wrapped on a solid plastic mandrel. For this demonstration, the laser and the demodulation electronics were collocated with the fiber interferometer. In 1984, smaller-diameter sensors and interrogation approaches suitable for remote sensor interrogation were developed. The 48-channel All Optical Towed Array (AOTA) demonstration in December 1990 positioned this technology for production of fatline arrays, but the end of the Cold War resulted in cancellation of the program. There were continuing efforts funded by ONR to develop the technology for small-diameter (thinline) fiber optic towed arrays through the 1990s. In the late 1990s there was renewed interest in producing a fiber optic towed array to address the cost and reliability issues of the TB-29 conventional thinline towed array.

TB-33 Towed Array: The current effort to bring the fiber optic towed array to production (designated the TB-33) is a joint effort involving Naval Undersea Warfare Center (NUWC), Chesapeake Sciences Corporation, General Dynamics, and NRL. NRL has played a critical role in developing the hydrophone design for this array and the interrogation/multiplexing approach used in the system. Unlike the AOTA demonstration and the Navy's fiber optic LightWeight Wide Aperture

Array (currently in production), which are coupler-based systems, the TB-33 array uses low-reflectivity fiber Bragg gratings written in the fiber to define the sensors by forming low-reflectivity Fabry-Perot interferometers. The hydrophones are passively multiplexed both in time and in wavelength to allow hundreds of channels to be carried over just four optical fibers. This architecture is ideally suited to the towed array — it minimizes the number of optical components in the array, which is critical to minimizing the diameter of the hydrophone core, and in turn allows a thicker hose wall to be used, thus increasing the durability and reliability of the array.

Performance: During testing, the fiber optic hydrophones both in calibration and under tow have shown excellent uniformity in responsivity. Figure 8(a) shows the relative responsivity of an array of 24 channels under static ensonification; in the frequency band of interest, the spread is ~ 0.2 dB. Figure 8(b) shows the raw output of an array of 84 hydrophones under tow; the uniformity is excellent.

Until recently, much of the testing of the fiber optic array concept involved arrays with rather low channel counts; the results were then scaled up to arrays with hundreds of elements. During this type of testing, NRL measurements indicated that the system architecture was susceptible to a number of noise terms that would appear identically on multiple channels (known as coherent noise, which results in an apparent target broadside to the array). One noise term was associated with the thermally induced phase noise of the fiber in the compensating interferometer associated with the interrogation system (referred to as a compensator). This was easily addressed by simply increasing the number of compensators from one to eight, thus lowering the coherent component. Another coherent noise term observed was due to strains in the optical signal

path between the compensators and the hydrophones, which resulted in a small phase shift (noise term) in each channel. For a full-scale TB-33 array this would give a noise ~ 60 dB above the coherent noise specification.

NRL proposed three basic approaches to solving this noise problem in the array architecture. The first solution was to move the compensators from the tow platform into the array. This move resulted in an ~ 30 dB decrease in signal path coherent noise. The second solution was to develop a signal path strain cancellation system to reduce the apparent strain in the tow cable; this system and its performance are shown in Fig. 9. This also gave an ~ 30 dB reduction in noise. The final technique to improve the signal-to-noise ratio of the array was to increase the responsivity of the hydrophone by 6 dB. To achieve this, the hydrophone had to be made more compliant, and thus would experience greater deformation due to hydrostatic pressure. Several approaches to this new hydrophone were proposed by the design team. The NRL design, incorporating an internal stop to suppress buckling of the hydrophone mandrel up to the survival pressure, was the only design to survive. The results of the pressure tests of several of the designs are shown in Fig. 10. Although 6 dB is a relatively modest improvement, this design reduced not only the coherent noise, but also the incoherent noise contribution. Chesapeake Sciences Corporation has taken this basic design and productionized it for the TB-33 system. The combination of these three approaches lowered the coherent noise term by ~ 70 dB, thus allowing the fiber optic system to meet the coherent noise requirement.

Acknowledgments: This work was sponsored in part by NAVSEA's (PMS-401) TB-33 program.

[Sponsored by NAVSEA] ★

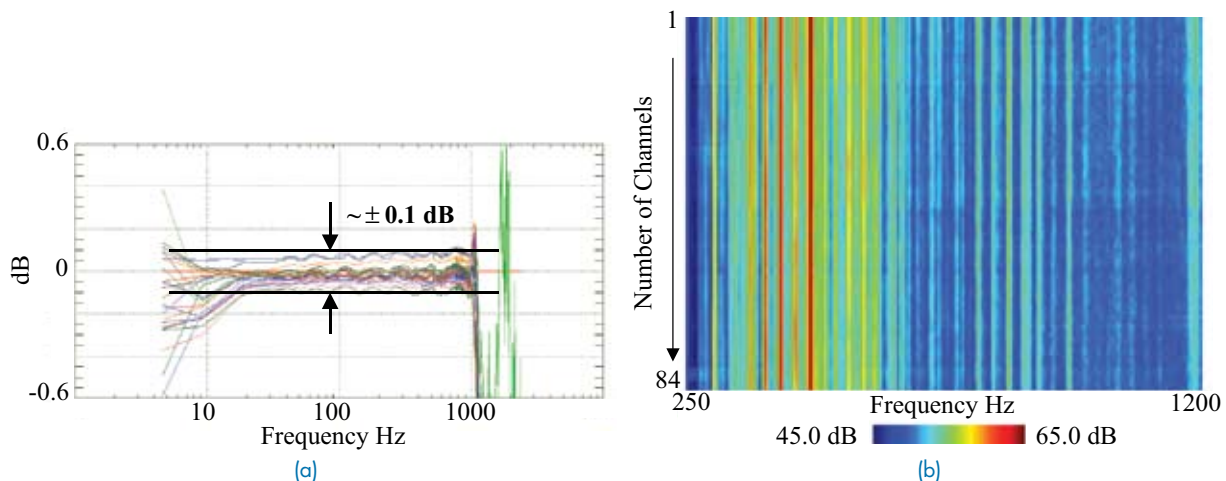


FIGURE 8 Examples of fiber optic hydrophone response uniformity from the Fiber Optic TB-16 (FOTB-16) program (Northrop Grumman, NUWC, NRL). The calibration uniformity of 24 channels is shown in (a) while the spectra for 84 channels under tow are shown in (b).

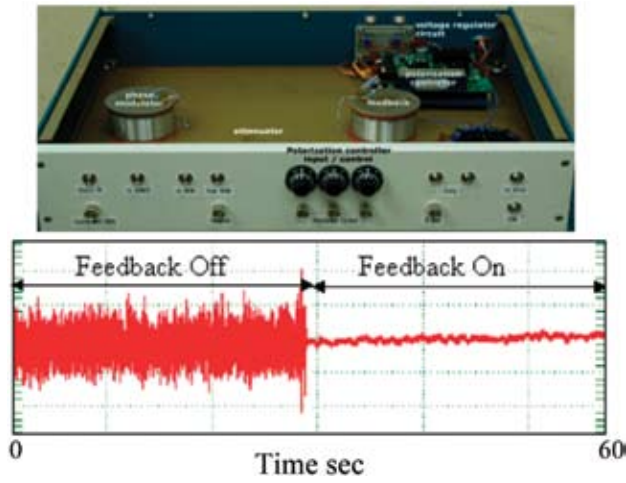


FIGURE 9
Signal path strain cancellation hardware and noise reduction results.



High Responsivity Fiber Hydrophones for TB-33

Initial Baseline, 0dB, **Failed**

NRL Concept, +6 dB, **Fully Successful**

Industry Concept, +5 dB, **Failed**

Industry Concept, +6 dB, **Failed**

Industry Concept, +5 dB, **Failed**

Industry Concept, + 5 dB, **Failed**

FIGURE 10
Fiber optic hydrophone crush results for six design concepts.

ATMOSPHERIC SCIENCE AND TECHNOLOGY





133 The Terrain-Induced Rotor Experiment (T-REX)

J.D. Doyle and V. Grubišić

136 Polar Clouds from Space Shuttle Exhaust

M.H. Stevens and C.R. Englert

137 An Advanced Framework for Battlespace Environment Data Assimilation

L. Xu, T. Rosmond, N. Baker, and J. Goerss

139 Understanding and Forecasting the Sun's Impact on the Battlespace Environment

J.L. Lean, J.M. Picone, J.T. Emmert, and J.P. Dahlburg

142 Understanding the Effect of Atmospheric Turbulence on Optical and Infrared Propagation using Hilbert Phase Analysis

C. Font, G.C. Gilbreath, M.P.J.L. Chang, and E.S. Oh

The Terrain-Induced Rotor Experiment (T-REX)

J.D. Doyle¹ and V. Grubišić²

¹*Marine Meteorology Division*

²*Desert Research Institute*

Introduction: The Terrain-induced Rotor Experiment (T-REX) is a coordinated international effort focused on exploring the structure and evolution of atmospheric rotors and associated phenomena in complex terrain.¹ Atmospheric rotors are intense low-level horizontal vortices that form along an axis parallel to and downstream of a mountain ridge crest in association with large-amplitude mountain waves. High levels of turbulence characterize rotors, which are known to pose a great hazard to aviation. Recent numerical, theoretical, and observational studies of rotors^{2,3} show that rotors are strongly coupled to both the structure and evolution of overlying mountain waves and to the underlying boundary layer. Consequently, the overarching objective of T-REX is to study synergistic interaction between rotors, mountain waves, and boundary layer dynamics. The T-REX field campaign was centered on the Owens Valley in the lee of the southern Sierra Nevada in eastern California. This portion of the Sierra Nevada is the tallest, quasi-two-dimensional topographic barrier in the contiguous United States; it includes the highest peak in the lower 48 states (Mt. Whitney 4,418 m) and the steepest lee slopes.

Experimental Design: The T-REX experimental design reflects the need to document a coupled system of deep vertical extent, reaching from the ground to upper tropospheric–lower stratospheric altitudes. The major portion of the ground-based instrumentation was deployed within the focus region in the Owens Valley. Four major groups of instruments were present during T-REX: (i) the surface station network, (ii) ground-based remote sensors, (iii) flux measuring instruments, and (iv) radiosondes. The ground-based instrumentation included scanning and dual-Doppler lidars and three radar profiler systems (Fig. 1(a)).

In order to document the mesoscale structure and evolution of the wave/rotor part of the coupled system over Owens Valley, and the kinematic and thermodynamic structure of airflow through the depth of the troposphere upstream and downstream of the Sierra Nevada, three research aircraft were involved in the T-REX campaign: the National Science Foundation (NSF)/National Center for Atmospheric Research (NCAR) High-performance Instrumented Airborne Platform for Environmental Research (HIAPER); the UK Facility for Airborne Atmospheric Measurements (FAAM) BAe146; and the University of Wyoming King Air (Fig. 1(b)). The three aircraft covered the range of

altitudes from nearly 150 m above ground within the Owens Valley to about 14 km in the lower stratosphere. In addition to the probes for in situ kinematic and thermodynamic measurements, the special instrumentation carried by the aircraft included (i) a cloud radar (King Air), (ii) in situ chemical tracer instruments and microphysics probes (HIAPER and BAe146), and (iii) dropsonde systems (HIAPER and BAe146) (Fig. 1(b)).

Real-Time Numerical Model Forecasts: The T-REX field operations were supported by a real-time forecasting effort that included a number of mesoscale, medium-range global, and mountain wave prediction models. The special real-time models and output provided in support of T-REX were augmented by the widely available forecast models from U.S. and international operational centers. High-resolution mesoscale forecast models were executed by various groups to specifically support the T-REX forecasting operations. The NRL Marine Meteorology Division provided high-resolution forecasts (horizontal grid increment of 2 km) for T-REX using the atmospheric module of the Coupled Ocean/Atmosphere Mesoscale Prediction System (COAMPS®).^{*} The NRL COAMPS effort was the backbone of the T-REX high-resolution mesoscale real-time forecasting capability. The initial conditions for COAMPS were obtained through mesoscale data assimilation, which were used for twice-daily 48-h forecasts, with lateral boundary conditions from the Navy Operational Global Atmospheric Prediction System (NOGAPS). Other supporting mesoscale model efforts included the WRF-NMM, WRF-ARW, and MM5 forecasts performed by NOAA/NCAR, the Army Research Laboratory (ARL), the National Weather Service (NWS), and the Air Force Weather Agency (AFWA). Because of timeliness and availability issues, the T-REX forecasters primarily relied on the 2-km resolution COAMPS, a 4-km resolution WRF-NMM, and the 12-km National Centers for Environmental Prediction (NCEP) Eta for mesoscale model guidance. Real-time forecasts from linear theory models produced by NRL-Monterey and the UK Met Office augmented the short guidance for T-REX mission planning.

A comparison of the real-time COAMPS forecast vertical velocity with the HIAPER observations at 13.1 km (above sea level) is shown in Fig. 2 for six of the T-REX Intensive Observation Periods (IOPs). The IOPs 4, 6, and 13b were considered among the strongest during the field campaign, while IOPs 9, 10, and 13a were the weaker events. The HIAPER flew a series of cross-mountain-oriented race track patterns above the Sierra in the upper troposphere and lower stratosphere. The results are stratified into northern and southern

^{*}COAMPS® is a registered trademark of the Naval Research Laboratory.

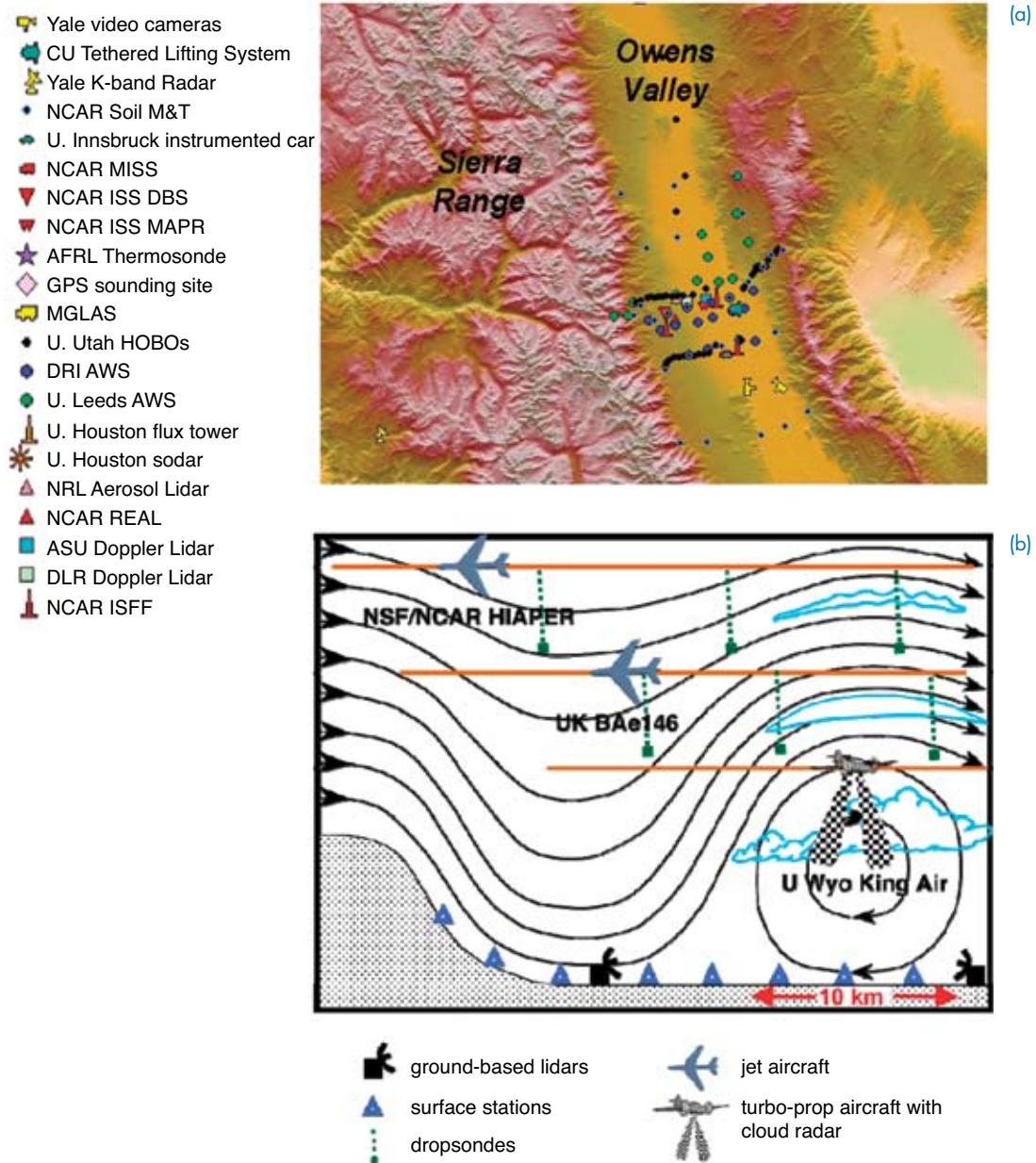


FIGURE 1
 (a) Color relief map of the southern Sierra Nevada showing the T-REX field campaign ground-based instrumentation network. (b) A schematic view of the composite T-REX airborne observing network comprising three aircraft along with other major instrumentation in approximate relation to rotor type of phenomena.

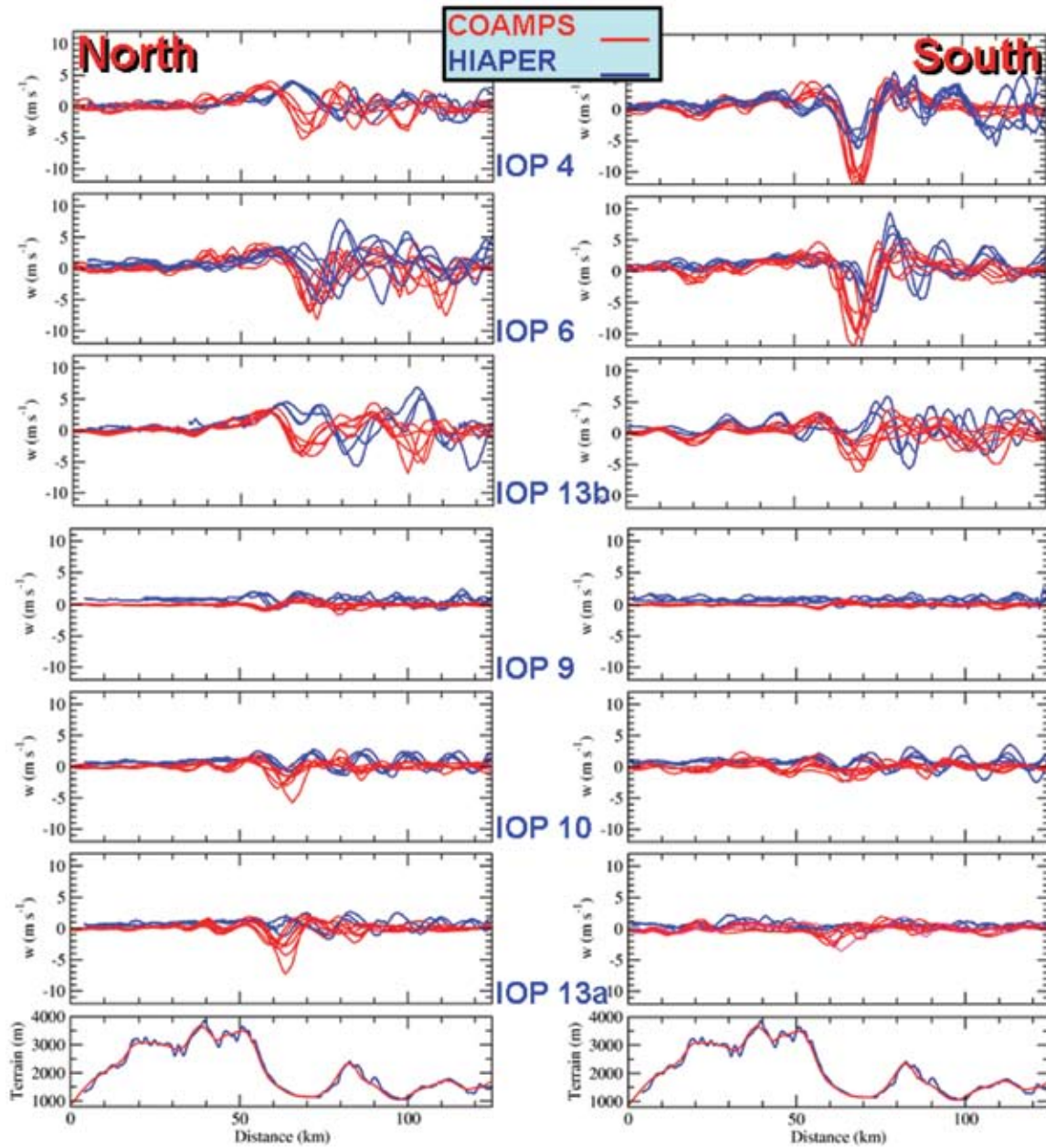


FIGURE 2

Vertical velocity (m s^{-1}) derived from the real-time COAMPS forecasts (red) and HIAPER observations (blue) at 13.1 km ASL. The data are stratified for the northern and southern cross-mountain flight segments. Terrain (m) is interpolated to the aircraft transect derived from a digital elevation model (blue) and from the COAMPS model terrain (red).

segments in Fig. 2. The real-time forecasts were able to consistently distinguish the strong and weak events and were generally able to characterize the gravity wave amplitudes and wavelength differences between the north and south segments.

Summary: Spring 2006 was a very active period of mountain waves over the Sierra Nevada. A large number of mid-latitude weather systems, greater than the climatological average, passed over the T-REX target area, yielding many opportunities for special observations of the coupled rotor system. This was

also a very moist period in the Sierra Nevada, bringing the effect of moisture on mountain waves and rotors more strongly into focus. Fifteen IOPs were conducted during the two-month field campaign including 12 HIAPER, 25 King Air, and 11 BAe146 research flights. More than 350 dropsondes were deployed along with more than 400 radiosondes. Preliminary results indicate that the T-REX observations reveal new insights into the interactions of internal waves, rotors, and boundary layer properties over complex topography. The emergence of a new generation of observing platforms and high-resolution numerical models such as

COAMPS represents an unprecedented opportunity for fundamental studies of gravity waves and rotors.

Acknowledgments: T-REX investigators and participants come from several U.S. and European universities, research institutes, and agencies. The outstanding efforts of the T-REX field campaign participants, including the NCAR Field Project Support (FPS), the NWS Las Vegas Forecast Office, and the T-REX staff, are gratefully acknowledged. Primary funding for T-REX was provided by NSF.

[Sponsored by ONR and NSF]

References

- ¹ V. Grubišić, J.D. Doyle, J. Kuettnner, G.S. Poulos, and C.D. Whiteman, "Terrain-induced Rotor Experiment (T-REX) Overview Document and Experiment Design," 72 pp. (2004). Available at <http://www.eol.ucar.edu/projects/trex/documents/>.
- ² J.D. Doyle and D.R. Durran, "The Dynamics of Mountain-Wave Induced Rotors," *J. Atmos. Sci.* **59**, 186-201 (2002).
- ³ J.D. Doyle and D.R. Durran, "Recent Developments in the Theory of Atmospheric Rotors," *Bull. Amer. Meteor. Soc.* **85**, 337-342 (2004). ★

Polar Clouds from Space Shuttle Exhaust

M.H. Stevens and C.R. Englert
Space Science Division

Introduction: The Earth's mesosphere lies above the stratosphere in the region between 50 and 90 km altitude, far above where airplanes or balloons can fly. In the unique polar summer mesosphere, the temperature plummets below 150 K (−190 °F), making this region the coldest on Earth, so inaccessible that it is sometimes like studying the atmosphere of another planet. In this extremely rarefied and dry place, water ice particles are found in narrow layers near 82 km altitude called polar mesospheric clouds (PMCs). PMCs are not known in the published record until 1885.

The specific processes leading to the formation of PMCs are disputed. However, some evidence indicates that they became brighter and more frequent in the late 20th century, leading some scientists to argue that they are indicators of global climate change. One hypothesis reasons that increasing amounts of methane (CH₄) emitted at the Earth's surface by industrial and agricultural processes increase the humidity of the upper atmosphere as the methane is broken down by ultraviolet sunlight to form water vapor.

Recently, NRL's Space Science Division scientists have complicated this hypothesis by identifying a new source for PMCs, challenging long-held beliefs about the meteorology of the upper atmosphere. Using satel-

lite observations from NRL's Middle Atmosphere High Resolution Spectrograph Investigation (MAHRSI), Stevens et al.¹ showed that the exhaust plume from the space shuttle can be transported all the way from the east coast of the United States to the Arctic summer mesosphere to form PMCs. Additional data from other experiments now reveal that this phenomenon has occurred over both poles. Here we present the initial observations leading to the discovery, and discuss its scientific impact.

The Discovery: MAHRSI was an experiment designed to measure hydroxyl (OH) in the Earth's mesosphere on a satellite deployed and retrieved by the crew of the space shuttle. It flew on two one-week missions in November 1994 (STS-66) and August 1997 (STS-85). MAHRSI observed near-ultraviolet light (~309 nm) from the atmosphere at high spectral resolution (0.02 nm), which allowed for the discrimination of OH solar fluorescence from the bright Rayleigh scattered background. PMCs were never considered as a science objective of MAHRSI, but were unexpectedly detected while analyzing data at the Kennedy Space Center during the late summer mission in 1997.²

OH is created when water vapor is destroyed by solar ultraviolet radiation and it is therefore sometimes used as a proxy for water vapor. Water vapor is the primary effluent of the shuttle's main engines and is copiously injected in a relatively narrow layer between 105 and 115 km altitude off the east coast of the United States as the shuttle accelerates to orbit.

As shown in Figs. 3(a) and 3(b), one to two days after the launch of STS-85, unexpectedly bright OH intensities were observed by MAHRSI in the upper mesosphere at Arctic latitudes (circled in red). Figure 3(c) shows that about a week after launch, PMCs were also observed over much of northern North America by MAHRSI, as indicated by the red crosses. Using observations from a German companion experiment called Cryogenic Infrared Spectrometers and Telescopes for the Atmosphere (CRISTA), Stevens et al.¹ found that the water content of these clouds (~100 t) was consistent with the amount available in the shuttle plume (~300 t). This was the first evidence that a launch vehicle plume injected in the subtropics could create Arctic PMCs. To our knowledge, the global scale transport of this exhaust plume had never been considered before.

The Scientific Impact: We have since assembled more data from a variety of ground-based and satellite experiments. For example, we found that another shuttle exhaust plume (STS-107) created polar clouds, but this time they were in the Antarctic summer, contributing 10-20% to the total ice content of PMCs observed that season.³ Proposed trends in cloud bright-

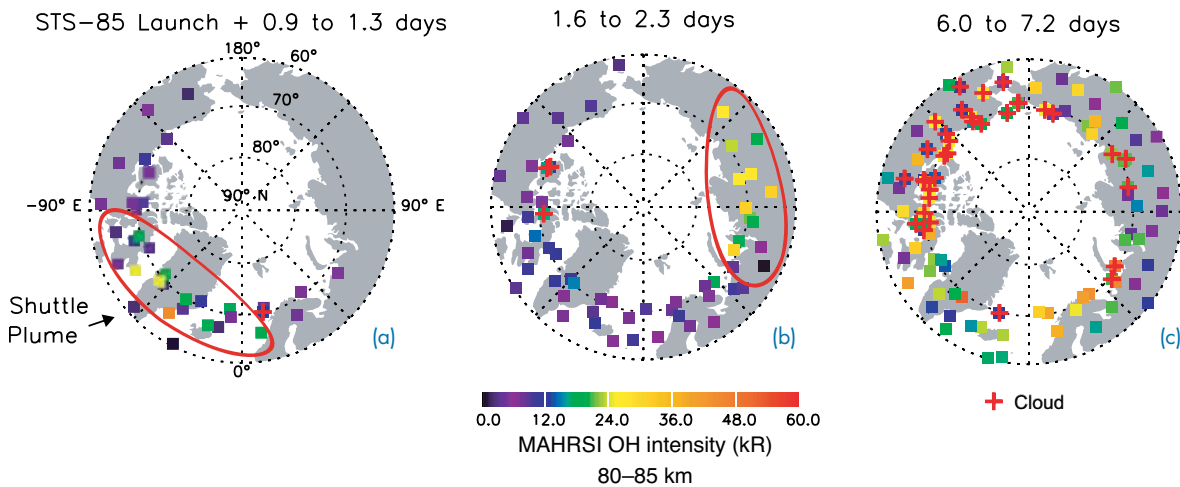


FIGURE 3

STS-85 carried the Middle Atmosphere High Resolution Spectrograph Investigation (MAHRSI) into orbit in August 1997. MAHRSI observed the shuttle's exhaust plume in the Arctic (circled in red) by measuring solar resonance fluorescence of OH, where 80–85 km radiances are referenced to the color bar. MAHRSI scans the limb of the Earth, so that OH observed viewing toward 80–85 km can originate at altitudes higher than this along the line of sight. A week after launch, MAHRSI observed polar mesospheric clouds over northern North America (red crosses, Fig. 3(c)). The amount of water in the observed PMCs is consistent with the amount injected by the shuttle.

ness since 1980 are not larger than this. This calls into question the interpretation of late 20th-century PMC trends solely in the context of global climate change.

The Upper Atmospheric Physics Branch at NRL's Space Science Division is poised to build on the success of MAHRSI with a new instrument called the Spatial Heterodyne IMager for MESospheric Radicals (SHIMMER). This instrument uses innovative technology called spatial heterodyne spectroscopy that allows for higher spectral resolution and throughput while minimizing mass and volume. SHIMMER is scheduled to launch in 2007 on a much longer, one-year mission to measure OH in the middle atmosphere.

Acknowledgments: The authors are grateful to Jörg Gumbel, Klaus Grossmann, Paul Hartogh, Markus Rapp, Robert Meier, Xinzhaoh Chu, Matthew DeLand, and John Plane for providing data and model results in valuable support of this work. We are also grateful to David E. Siskind for many productive discussions and suggestions.

[Sponsored by ONR and NASA]

References

- ¹M.H. Stevens, J. Gumbel, C.R. Englert, K.U. Grossmann, M. Rapp, and P. Hartogh, "Polar Mesospheric Clouds Formed from Space Shuttle Exhaust," *Geophys. Res. Lett.* **30**(10), 1546 (2003). doi: 10.1029/2003GL017249
- ²M.H. Stevens, "Heavenly Harbingers," *Smithsonian*, November, 2001, 20-23.
- ³M.H. Stevens, R.R. Meier, X. Chu, M.T. DeLand, and J.M.C. Plane, "Antarctic Mesospheric Clouds Formed from Space Shuttle Exhaust," *Geophys. Res. Lett.* **32**, L13810 (2005). doi: 10.1029/2005GL023054

★

An Advanced Framework for Battlespace Environment Data Assimilation

L. Xu,¹ T. Rosmond,² N. Baker,¹ and J. Goerss¹
¹Marine Meteorology Division
²SAIC

Introduction: Battlespace environment data assimilation is a key element of the DoD's strategic plan to ensure information superiority and battlespace dominance in the 21st century. It is used to provide all the necessary initial conditions for making atmospheric/oceanic forecasts and to produce the common operational picture required by the warfighter. This environmental picture is critical for the safety of ships, aircraft, personnel, and other assets, for sea-basing and ship fuel economy, for accurate delivery of precision ordnance, for theatre air and missile defense, for transformational communications, and for homeland security. Battlespace environmental data assimilation is a process that infers the atmospheric/oceanic state through an optimal combination of previous numerical model forecasts, in situ and remotely sensed observations, and theoretical information. The Navy's current operational data assimilation systems are three-dimensional (3D) and provide the warfighter with a snapshot of the battlespace environment at a single point in time, several times a day. To provide the warfighter with a continuous picture of the battlespace environment over the time window of the observations used to generate the initial conditions, a highly advanced and efficient four-dimensional (4D) data assimilation algorithm

suitable for both atmospheric and oceanic applications is essential. To meet the warfighter’s requirement in the 21st century, scientists at NRL-Monterey have recently developed an advanced framework for battlespace environment data assimilation, called NAVDAS-AR: NRL Atmospheric Variational Data Assimilation System – Accelerated Representer. Here we give a brief description of the current operational system, then describe the NAVDAS-AR framework and its current and future applications.

Current Operational System: The Navy’s current operational data assimilation system is based on the observation-space three-dimensional variational (3DVAR) algorithm, NAVDAS: NRL Atmospheric Variational Data Assimilation System. 3DVAR is widely used in intermittent cycling atmospheric/oceanic data assimilation for the analysis of global and synoptic scales around the world. NAVDAS has been quite successful in handling slowly evolving flows and observation platforms that sample heterogeneously in space. Two major assumptions were made in developing NAVDAS and the 3DVAR data assimilation system in general. First, all the observations collected over a 6-hour data assimilation window are assigned to the middle of the time window (Fig. 4(a)) due to the lack of a time dimension in the theoretical formulation of the 3DVAR. Second, the analyzed fields are required to satisfy only simple geophysical relationships with each other due to the fact that a dynamic model is not used to constrain the fields during the minimization step. Also, from an efficiency perspective, the computational cost of NAVDAS is proportional to the square of the number of observations (Fig. 5), which creates an insurmountable barrier in assimilating the huge volume of remotely sensed observations expected to be available in the near future.

NAVDAS-AR Framework: NAVDAS-AR is based on the latest scientific research in estimation theory and computational technologies and provides a flexible framework for a wide variety of applications, including global and mesoscale atmospheric and oceanic data assimilation.^{1,2} It consists of three major components: data quality control and pre-processing, four-dimensional variational (4DVAR) data analysis, and post-processing. The centerpiece of NAVDAS-AR is an accurate and efficient observation-space 4D variational minimization algorithm. It is used to produce the best fit to the observations and the numerical model forecasts simultaneously over a 6-hour data assimilation window. Due to the inclusion of the time dimension, NAVDAS-AR is a natural framework for the assimilation of observations that are not made at the standard synoptic observing times, but are taken more frequently in time over the data assimilation window (Fig. 4(b)). Because

of the use of the numerical forecast model as a dynamic constraint, NAVDAS-AR is also capable of properly assimilating single-level data such as aircraft winds and temperatures (commercial and military), satellite feature-tracked winds, and sea-surface wind retrievals from satellite instruments such as NRL’s WindSat or scatterometers. Moreover, the computational cost for NAVDAS-AR is proportional to the model grid density and is not impacted by the amount of data to be assimilated, a highly desirable benefit for operational efficiency, as shown in Fig. 5.

Concluding Remarks: NAVDAS-AR, a highly advanced framework suitable for 4D battlespace environmental data assimilation, has recently been developed at NRL-Monterey. Like the Navy’s current operational data assimilation systems, NAVDAS-AR is

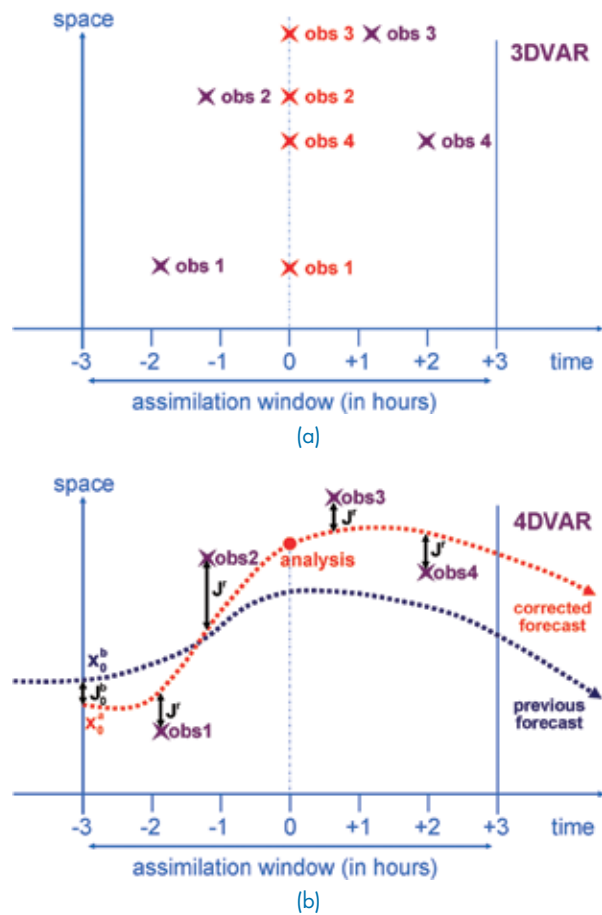
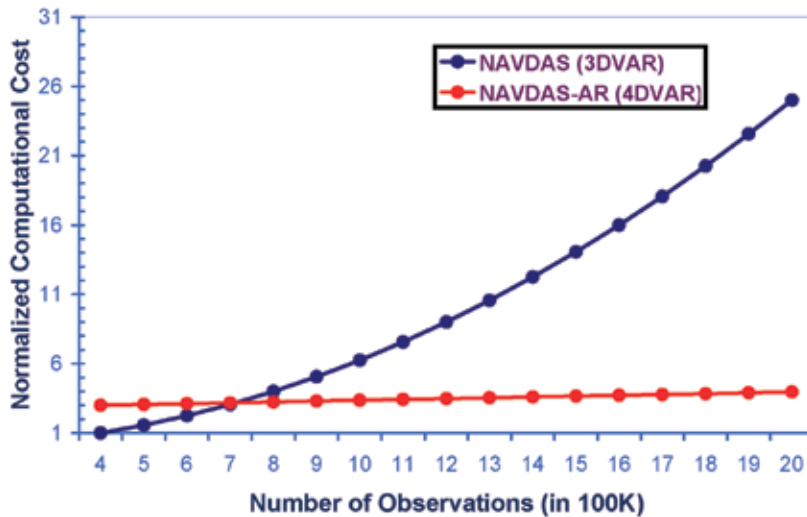


FIGURE 4 A schematic of 3DVAR (a) and 4DVAR (b). The abscissa represents time of the data assimilation. The ordinate indicates the observation locations in three-dimensional space. Four observations (obs 1 – obs 4) are scattered at different temporal and spatial locales over the 6-hour data assimilation time window. (a) In 3DVAR, all observations are assimilated at “0” hour and the results are constrained by simple geophysical relationships. (b) In 4DVAR, all observations are assimilated at the “observed” hours and the dynamical model is used to constrain the results.

**FIGURE 5**

The ordinate is the computational cost normalized by the cost of assimilating 400K observations using operational NAVDAS. The abscissa is the number of observations to be assimilated (scaled by 100K). The computational cost of NAVDAS is a quadratic function of number of observations to be assimilated, while the computational cost of NAVDAS-AR increases very little with an increase in the number of observations.

theoretically cast in observation-space. It possesses all the advantages that the observation-space algorithm can provide, such as its ability to produce the adjoint of the data assimilation system with minimal effort. But unlike the operational observation-space 3DVAR algorithm, NAVDAS-AR preserves the time information in the observations, uses a dynamical model to constrain the analyzed fields, and does not limit the total number of observations to be assimilated. Because of these advantages, NAVDAS-AR has recently been chosen as the basis for the Navy's next-generation atmospheric and oceanic data assimilation systems.

Acknowledgments: The support of the Naval Research Laboratory and the Office of Naval Research, through program element 0602435N, and the support of SPAWAR PMW180, through program element 0603207N, is gratefully acknowledged.

[Sponsored by ONR and SPAWAR]

References

- ¹ T. Rosmond and L. Xu, "Development of NAVDAS-AR: Non-linear Formulation and Outer Loop Tests," *Tellus* **58A**, 45-58 (2006).
- ² L. Xu, T. Rosmond, and R. Daley, "Development of NAVDAS-AR: Formulation and Initial Tests of the Linear Problem," *Tellus* **57A**, 546-559 (2005). ★

Understanding and Forecasting the Sun's Impact on the Battlespace Environment

J.L. Lean, J.M. Picone, J.T. Emmert, and J.P. Dahlburg
Space Science Division

Introduction: The battlespace environment extends far above the surface of the Earth. Of special

importance are the outer layers of the Earth's atmosphere, from altitudes 100 to 1000 km, where there is sufficient mass to impede the motion of Earth-orbiting spacecraft, and where layers of charged particles control the propagation of radio waves. Changes in atmospheric "drag" alter the orbits of the thousands of space objects in low Earth orbit (LEO) that are tracked by the U.S. Space Command. The ionosphere transmits, reflects, retards, and refracts kHz to MHz radio wave frequencies. As a result, fluctuations in the neutral and ionized environment can negatively impact Naval operations by disrupting communications and navigation and by degrading radar accuracy, targeting precision, and orbit prediction.

The Sun is the primary source of variations in the neutral and ionized upper atmosphere. A suite of new solar and atmospheric databases that extend over the Sun's 11-year activity cycle are now refining our understanding of the intricately interconnected Sun-Earth system, thereby improving the ability to predict this region's impact on DoD systems. The new databases include solar imagery from NRL instruments aboard the Solar Heliospheric Observatory (SOHO),¹ daily thermospheric mass density derived from spacecraft drag via a new NRL algorithm,² and total electron content obtained from analyses of GPS timing by the Center for Orbit Determination in Europe (CODE).³

Changing Solar EUV Radiation: The Sun's extreme ultraviolet (EUV) radiation waxes and wanes continuously throughout the 11-year solar activity cycle, as bright active regions emerge, evolve, and decay in the outer solar atmosphere. The Sun's rotation on its axis further modulates the EUV radiation on a cycle of approximately 27 days by altering the population of active regions on its hemisphere visible at Earth. The sequence of solar images in Fig. 6, made at 28.4 nm by

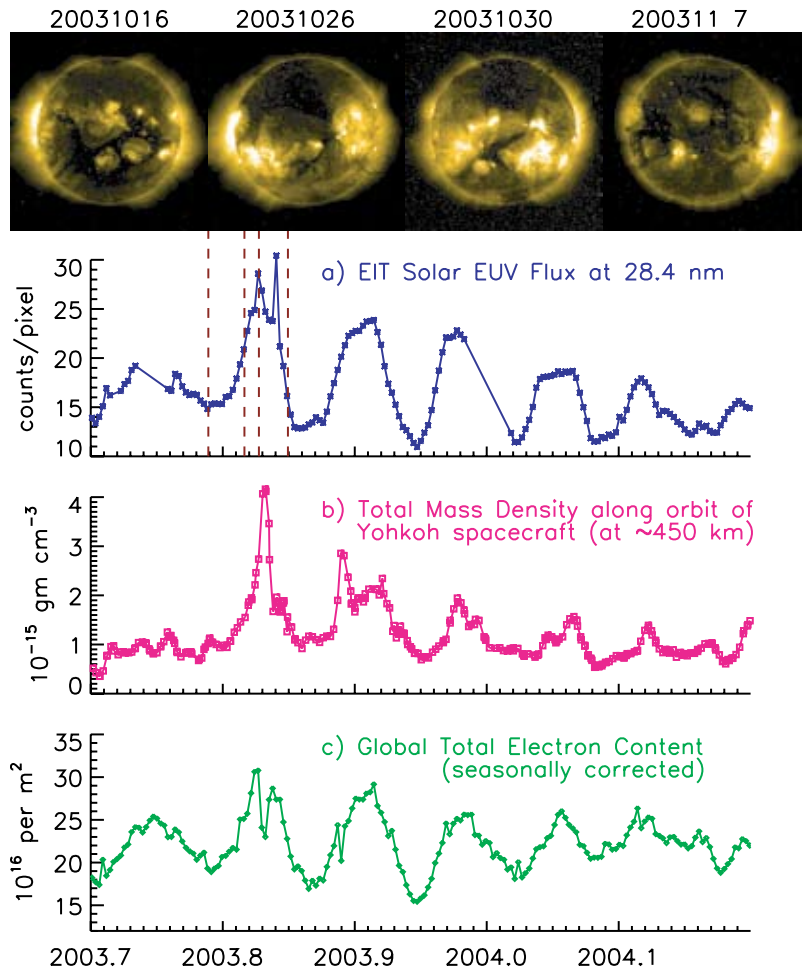


FIGURE 6 Images of the Sun made by SOHO EIT¹ at 28.4 nm show the movement of bright active regions across the Sun’s disk as a result of its rotation on its axis. Shown in (a) are the resultant changes in the net solar EUV radiation obtained by summing all pixels in each image during a period of six solar rotations. During the same period, total mass densities in the upper atmosphere estimated along the track of the Yohkoh spacecraft (altitude ~450 km) from TLEs² varied as shown in (b). The total electron content variations shown in (c) are derived from GPS by CODE.³

SOHO's Extreme Imaging Telescope (EIT),¹ illustrates the passage of large active regions across the solar disk. These cycles cause Earth-directed EUV radiation (irradiance) to vary by a factor of ~two over each 27-day period, as shown in Fig. 6(a).

Impacts on the Upper Atmosphere and Ionosphere: Since solar EUV radiation supplies the energy that heats the upper atmosphere and creates the ionosphere, its fluctuations directly impact neutral and ion compositions. Spacecraft in low Earth orbit decay more rapidly when solar activity is high because the upper atmosphere is hotter and denser. Ionospheric transmission of radio waves decreases because there are more electrons, and higher-frequency radio waves are reflected because peak electron densities are larger.

As Fig. 6 illustrates, neutral densities (b) and total electron content (c) change significantly during the Sun's rotational cycle. Along the track of the Yohkoh spacecraft (USSPACECOM object 21694) at about 450 km altitude, mass density (derived from two-line element sets, TLEs, using NRL's new algorithm²) can increase by factors of two, with concomitant increases in spacecraft drag. During the last rotational cycle of 2003, for example, the decay rate of Yohkoh (mass $M = 390$ kg, cross-sectional area $A = 1$ m²) increased from 0.07 km/day to 0.2 km/day. Since drag acceleration is proportional to A/M , the decay rate of a picosat ($M = 0.5$ kg, $A = 0.01$ m²) in a similar orbit would be an order of magnitude larger.

Forecasting Solar EUV Radiation: Because of the impact of space weather on civilian and military space

operations, utilization, and assets, the National Weather Service and Air Force Weather Agency jointly issue 1- to 3-day and longer forecasts of the 10.7 cm radio flux. This index of solar EUV radiation is used for input to a variety of space weather models, such as the NRLMSIS⁴ neutral density specification model. Analysis of time series of solar EUV radiation and atmospheric densities, such as in Fig. 6, aid in characterizing and understanding changes in the battlespace environment that are driven by solar activity, and in validating and improving space weather models. Solar imagery such as in Fig. 6 promises to enhance near-term forecasting capability by identifying the impending impact of large active regions that emerge on the Sun's east limb, prior to rotating to the center where their contribution to Earth-directed flux maximizes. Figure 7 shows that the east limb flux leads the net flux by about 5 days.

[Sponsored by ONR and NASA]

References

- ¹J.-P. Delaboudiniere et al., "EIT: Extreme-Ultraviolet Imaging Telescope for the SOHO Mission," *Solar Phys.* **162**, 291-312 (1995).
- ²J.M. Picone, J.T. Emmert, and J.L. Lean, "Thermospheric Densities Derived From Spacecraft Orbits. I. Accurate Processing of Two-Line Element Sets," *J. Geophys. Res.* **110**, A03301 (2005). doi: 10.1029/2004JA010585
- ³S. Schaer, G. Beutler, and M. Rothacher, "Mapping and Predicting the Ionosphere," in J.M. Dow et al., eds., *Proceedings of the IGS 1998 AC Workshop, Darmstadt, February 9-11, 1998*, ESA/ESOC, Darmstadt, Germany, 307-318 (1998).
- ⁴J.M Picone, A.E. Hedin, D.P. Drob, and A.C. Aikin, "NRLMSISE-00 Empirical Model of the Atmosphere: Statistical Comparisons and Scientific Issues," *J. Geophys. Res.* **107**(A12), 1468 (2002). doi:10.1029/2002JA009430

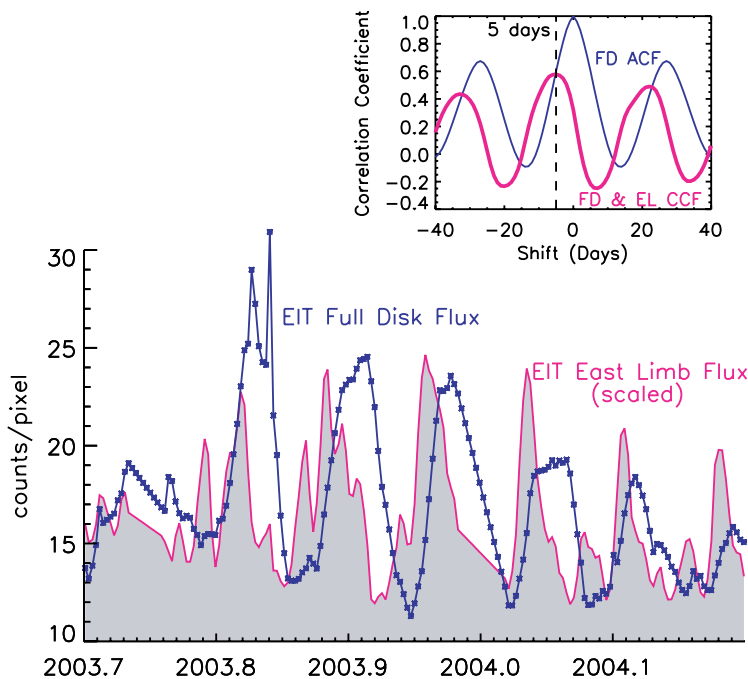


FIGURE 7
The net, disk-integrated solar EUV radiation at 28.4 nm from Fig. 6(a) is compared with the radiation from the east limb (left side of each image in Fig. 6). As the cross-correlation function in the inset figure shows, the east limb (EL) flux peaks approximately five days prior to the full disk (FD) flux.

Understanding the Effect of Atmospheric Turbulence on Optical and Infrared Propagation using Hilbert Phase Analysis

C. Font,¹ G.C. Gilbreath,¹ M.P.J.L. Chang,² and E.S. Oh³

¹Information Technology Division

²University of Puerto Rico, Mayagüez Campus

³Remote Sensing Division

Introduction: The refractive index structure parameter C_n^2 is a figure of merit used to describe the magnitude of the effect of turbulence in the atmosphere. Understanding the influence of different local climate parameters upon C_n^2 is an important step toward developing a prediction model for in-field laser interrogators. The layered structure of the atmosphere and its random behavior present unique challenges to theoretical and experimental studies in propagation research. This article presents a novel technique termed Hilbert Phase Analysis (HPA) to provide insights into the physical interactions. We explore the technique's use in analyzing the dependence of C_n^2 on local climate variables using data recently obtained from campaigns conducted in Puerto Rico.

The Method: HPA is a new technique that consists of Empirical Mode Decomposition (EMD) and the Hilbert Transform (HT). EMD is an instantaneous frequency filter bank that generates a family of empirical eigenmodes called Intrinsic Mode Functions (IMF) from a non-linear, non-stationary time series.¹ By transforming the IMFs with HT, we produce physically interpretable instantaneous phase angles, ϕ_i . These values are akin to Fourier phase angles, except that they apply per sample point. This feature now enables

the study of the temporal phase relationship for many measurables in a point-wise manner. This is not possible using standard Fourier techniques. Legacy time series tools such as wavelets provide relatively poor temporal resolution. Figure 8 illustrates how, by using HPA, the phases ϕ_1 and ϕ_2 of two interdependent signals can be shown to be related. On the left, Signal 1's vector rotates clockwise, while that of Signal 2 on the right rotates counter-clockwise. The time-dependent phase angles of these signals are clearly inversely correlated. The relationship can provide insight into how climatic parameters might affect C_n^2 .

Experiment: A series of campaigns to collect C_n^2 and simultaneous climate data are being performed at the University of Puerto Rico at Mayagüez.² The results described here are from a campaign conducted in February and March 2006. Scintillometers were placed on the roofs of buildings at the main campus of the university. The transmitter and receiver were separated by 90 meters over land. Climate data was acquired at a nearby weather station.

Data Analysis: Figure 9(a) compares meteorological data with C_n^2 over time. This data is from a very clear and sunny day. We can see close tracking between the measured solar radiation flux (SR) and the temperature (T), which is expected, since the solar flux controls the heating of the atmosphere. We also observe similar tracking of C_n^2 with T, validating that temperature plays a major role in defining optical turbulence. From the relative humidity (RH) record, we see an inverted relationship to T and therefore to C_n^2 . If we directly cross-correlate C_n^2 and a climate variable, the resulting function is very difficult to interpret, since C_n^2 is highly variable with time.

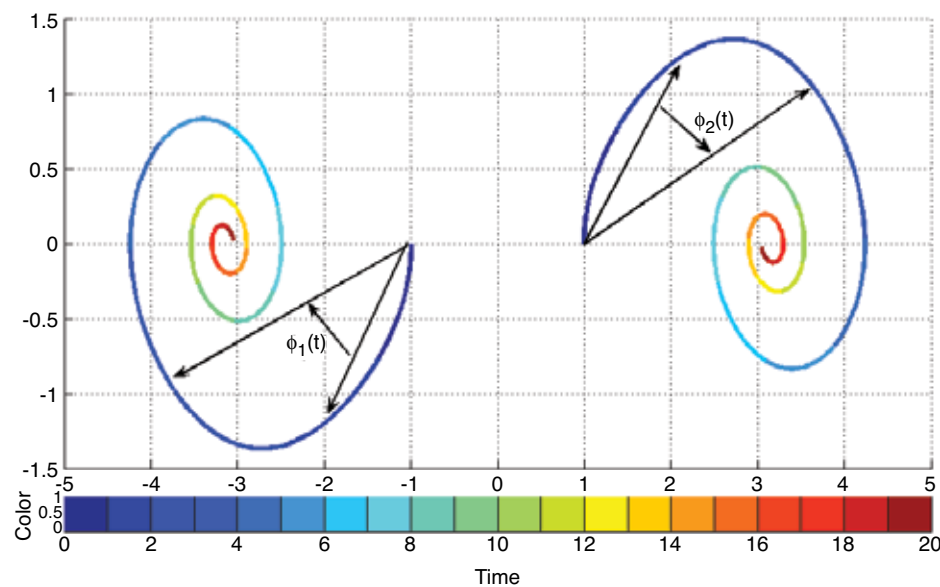
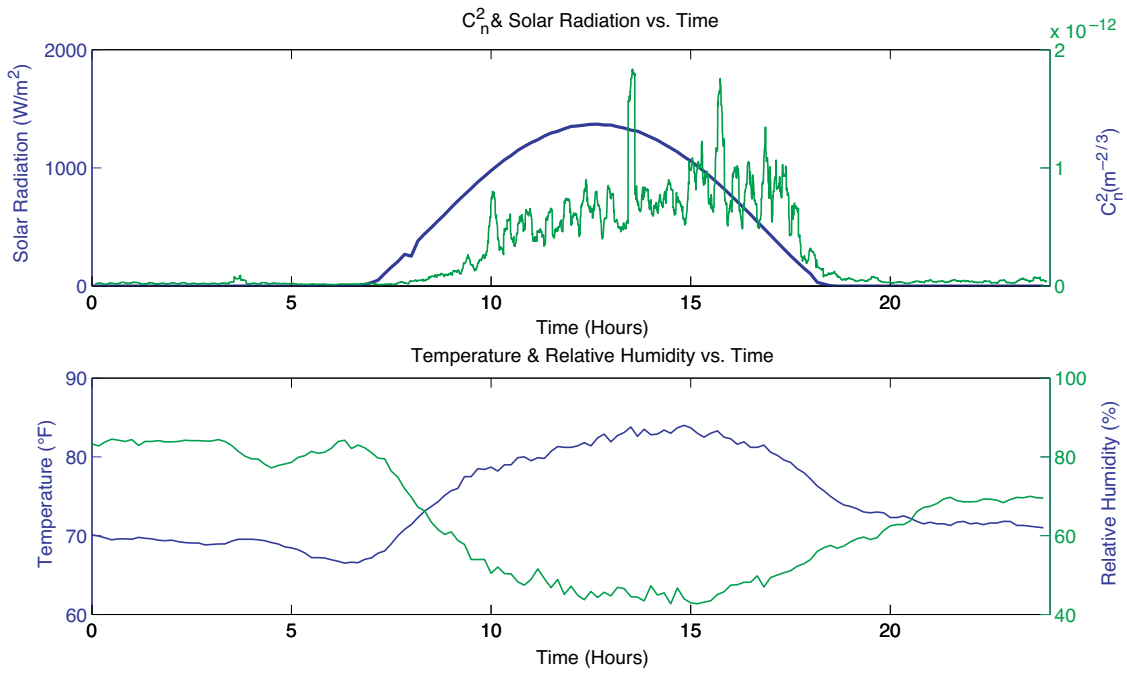
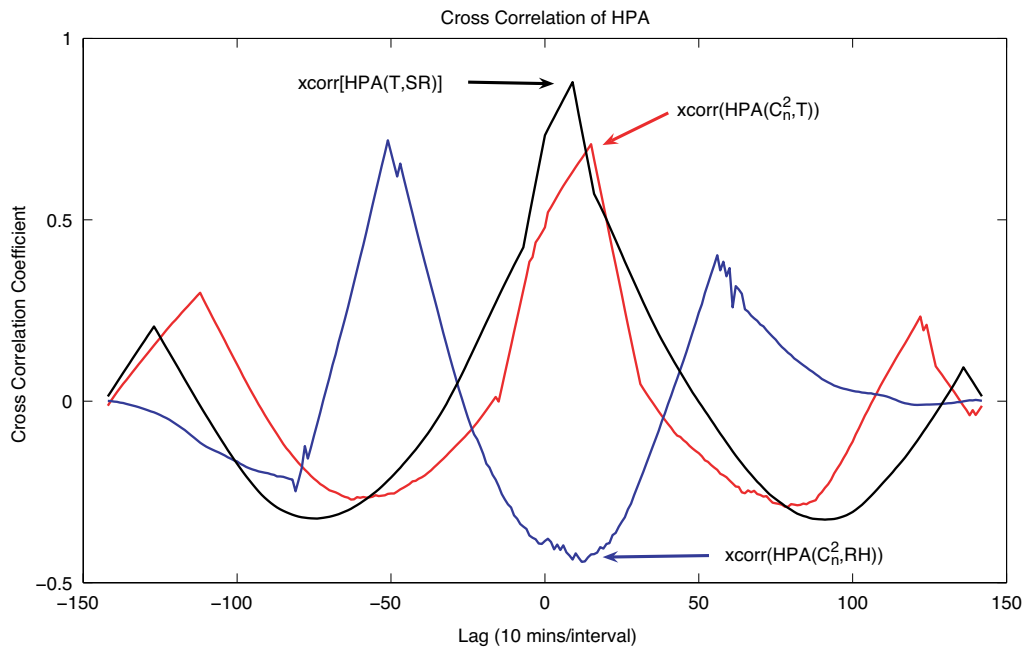


FIGURE 8 Illustration of HPT phase angles where the colors represent the changes in time. The arrows show the signal vectors, which change over 20 time steps.



(a)



(b)

FIGURE 9
 (a) Data for March 9, 2006; (b) Cross-correlations of the instantaneous phase angles of the different measurements within ±500 minutes of the zero lag position. Black: The correlation function between solar radiation flux (SR) and temperature (T) phase angles, showing a strong positive correlation. Red: The correlation function between C_n² and temperature (T) also showing a strong positive correlation. Blue: The correlation function between C_n² and relative humidity (RH), showing a negative correlation.

Applying HPA to this family of measurements provides us with the time-varying phase angles. Since we expect correlations between our raw parameter records, we calculated cross-correlations of the HPA-determined phase angles, as shown in Fig. 9(b). The curve plotted in black is the cross-correlation function of the instantaneous phase angles SR and T; it shows that T faithfully follows SR, with an approximate ten-minute lag. The cross-correlation function of C_n^2 and T indicates that the turbulence parameter follows a similar relationship. These results support the conventional theory that temperature strongly influences C_n^2 , thereby calibrating the HPA technique against known atmospheric behaviors. Finally, the cross-correlation function between C_n^2 and RH shows an inverse dependence, which corroborates the first-order approximation of an inverse relationship existing between temperature and relative humidity.

Conclusions: HPA provides the ability to study the time-varying phase angles of non-linear signals.

In this research, the technique was tested with optical turbulence data and its simultaneous local climate record taken in a recent campaign in Puerto Rico. The technique demonstrated consistency with conventional physics. That is, the direct influence of temperature on C_n^2 was verified. Additionally, the technique reveals an approximate inverse relationship between C_n^2 and relative humidity. The experiment is being extended to over-the-water ranges of up to 600 meters between Magueyes Island and the Villa Parguera Hotel in La Parguera, Lajas, Puerto Rico, as shown in Fig. 10.

[Sponsored by ONR]

References

- ¹M.P. J. L. Chang, E. Roura, C.O. Font, G.C. Gilbreath, and E. Oh, "Applying the Hilbert-Huang Decomposition to Horizontal Light Propagation C_n^2 Data," *Proc. of the SPIE* **6268**, 62683E (2006).
- ²M.P.J.L. Chang, C.O. Font, G.C. Gilbreath, and E. Oh, "Humidity's Influence on Visible Region Refractive Index Structure Parameter C_n^2 ," *Applied Optics* **46**, 2453-2459 (2007). ★



FIGURE 10

Propagation path shown for C_n^2 experimental studies for 2006–2007 campaigns.

CHEMICAL/BIOCHEMICAL RESEARCH



147 Polymeric Protection of Navy Fighter Jet Towlines

M.K. Kolel-Veetil and T.M. Keller

148 Single-Domain Antibodies: Rugged Recognition Elements

E.R. Goldman, J.L. Liu, J.B. Delehanty, G.P. Anderson, and A. Hayhurst

Polymeric Protection of Navy Fighter Jet Towlines

M.K. Kolel-Veetil and T.M. Keller
Chemistry Division

An Introduction to Towlines: Towed decoys are used to protect military fighter and transport aircraft against radar-guided air-to-air and surface-to-air missiles (Fig. 1). A towed decoy provides an aircraft-like target that draws an oncoming missile away from the aircraft that is being protected. The towline in general consists of a set of conducting and communication members, which is ensheathed by a structurally protective envelope (strength member) made of a high-performance organic fiber. A towline can “burn through” when exposed to a fighter jet’s afterburner plume, resulting in the loss of the decoy. This “burn through” is a result of the initial thermo-oxidative degradation of the protective sheath and the subsequent breakdown of the conducting and communication members. The Naval Research Laboratory is part of an undertaking of

the U.S. Navy Integrated Defensive Electronic Countermeasures (IDECM) and Radio Frequency Countermeasures (RFC) programs, who share a central objective, which is the development of advanced towline systems that can function at high temperatures and for longer durations. The developmental effort is a collaborative venture that includes teams of chemists, physicists, engineers, and military personnel.

Protective Polymers: Siloxane polymers that contain carborane clusters, developed simultaneously by Olin Laboratories and Union Carbide in the 1960s, have exceptional thermal stability in air. The thermal stability stems from the synergistic electron-withdrawing effect of the carborane clusters that strengthen the Si-O bonds in these polymers more than in siloxane polymers. Research at NRL has furthered the chemistry of these thermo-oxidatively stable polymers by incorporating crosslinkable diacetylene units.¹ The improved polymers, collectively known as poly(carborane-siloxane-acetylene)s or PCSAs (Fig. 2), produce extended network structures through the



FIGURE 1
Photograph of a misdirected missile heading towards a decoy attached to a towline behind a military fighter aircraft.

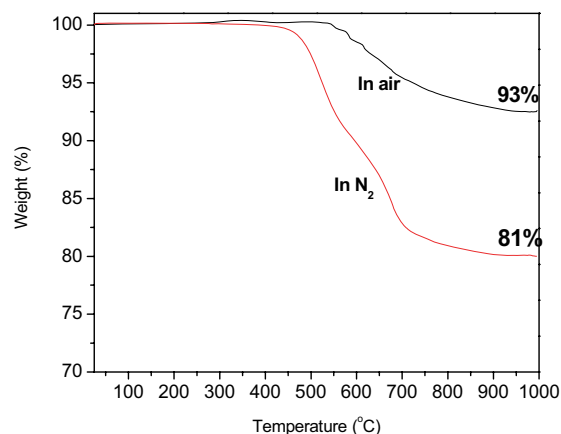
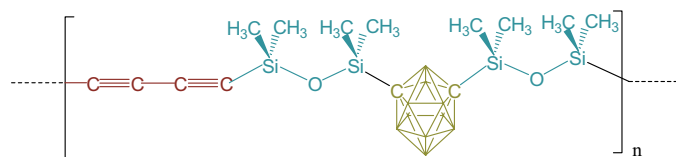


FIGURE 2
Schematic representation of a PCSA polymer (left) and TGA thermograms of its stabilities in air and in N₂ to 1000 °C (right).

thermally initiated crosslinking reactions of the diacetylene groups. The manipulation of the concentration of the diacetylene crosslinking units in the PCSAs allows improvement in their processability and enhancement of their elastic properties.² These highly processable PCSAs are ideally suited to protect high-performance organic fiber strength members used in the Navy fighter jet towlines against oxidation.

Protection of High Performance Organic Fibers:

The common strength members used in the Navy fighter jet towlines made of materials such as Kevlar, Zylon, and carbon fibers suffer catastrophic thermo-oxidative degradation in the 400° to 700 °C temperature range (Fig. 3). This limits the use of the towlines to temperatures below this range and to very short durations (on the order of seconds). A possible means to extend the operational temperature and the duration of deployment of the towed decoy is to inhibit the oxidative degradation of the towline strength member. Ongoing research at NRL on various organic strength members (Kevlar, Zylon, and carbon fibers) that were coated with PCSAs has demonstrated that the time to degradation, and hence, to failure, of the strength members can be improved by almost 100% under oxidative conditions at high temperatures. The improvement is a direct consequence of the formation of an oxidatively protective sheath on the *strength* member by the PCSAs. Studies have also indicated that a towline *conducting* member can be protected when it possesses a coat of the PCSAs as a protective barrier. This can result in the improvement of the conducting member's insulative properties, thereby enhancing its breakdown voltage and temperature. The protection of the organic fibers by the PCSAs can also have significant impact on the stability of the fibers used in armored vests and in other applications that use high-performance organic fibers.

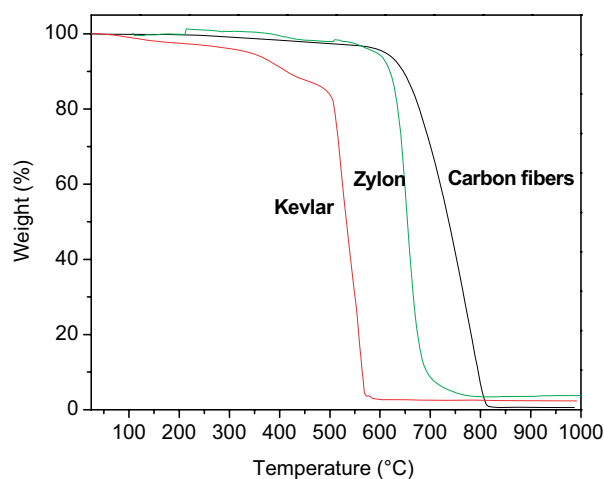


FIGURE 3
TGA thermograms of common towline strength members in air.

Summary and Acknowledgments: Ongoing research at NRL indicates that thermo-oxidative protection of the organic strength member is a viable means of developing improved towlines for use in Navy fighter jets. The benefits of such a protection may be translatable to the case of towline conducting members, which could vastly enhance the utility of this approach. These encouraging findings have led to the initiation of improved towline fabrication for actual flight test simulations. Towards this end, the transitioning of the PCSA technology to industry has been achieved, thereby facilitating the production of PCSAs in bulk quantities. Industrial facilities have also been tasked with applying PCSA coating on strength and conducting members and then assembling improved towlines. The new towline, an example of NRL research for tomorrow's Navy, is slated to be completed in FY2007. The time-to-failure studies and the insulative breakdown studies have been performed at the Materials Science and Technology Division and at the Tactical Electronic Warfare Division, respectively.

[Sponsored by ONR].

References

- ¹L.J. Henderson and T.M. Keller, "Synthesis and Characterization of Poly(carborane-siloxane-acetylene)," *Macromolecules* **27**(6), 1660-1661 (1994).
- ²M.K. Kolel-Veetil, H.B. Beckham, and T.M. Keller, "Dependence of Thermal Properties on the Copolymer Sequence in Diacetylene-containing Polycarboranylenesiloxanes," *Chem. Mater.* **16**(16), 3162-3167 (2004). ★

Single-Domain Antibodies: Rugged Recognition Elements

E.R. Goldman,¹ J.L. Liu,¹ J.B. Delehanty,¹
G.P. Anderson,¹ and A. Hayhurst²

¹Center for Bio/Molecular Science and Engineering

²Southwest Foundation for Biomedical Research

Introduction: The ability to quickly and accurately detect potential bio-threat agents is a priority for the Department of Defense and for homeland security. Most rapid diagnostic and detection immunoassays rely on monoclonal or polyclonal antibodies (IgG) as the recognition elements. Although sensitive and specific, these "conventional" antibodies are time-consuming to develop and have limited stability. In order to form the antigen binding site, conventional IgG require the pairing of variable (V) heavy and light domains. Cloned derivatives of conventional IgG that comprise just these V domains form a minimal antigen binding site. These derivatives have long been used to develop recognition elements for biosensor applications. However, these single-chain antibodies (scFv) are

often less stable than the parental full-length antibodies and aggregate irreversibly at elevated temperatures due to their two-domain structure. Ideally, development of a one- or single-domain structure capable of antigen binding may avoid aggregation upon heating and would facilitate the application of biosensors at elevated environmental temperatures or for continuous use over long periods of time.

In the mid 1990s, it was discovered that certain animals, such as camels, llamas, and sharks, possess a class of “unconventional” immunoglobulins consisting of heavy-chain homodimers where antigen binding is mediated through a single V domain (Fig. 4). These V domains, when cloned as single-domain antibodies (sdAb), comprise the smallest known antigen binding fragments (13-15 KDa). SdAb can refold to bind antigen after chemical or heat denaturation, enabling them to retain the ability to bind antigen after exposure to elevated temperatures. Our goal was to develop recombinant libraries of sdAb to permit the selection and evaluation of these unique biomaterials for the benefit of future biodefense requirements.

Libraries and Selections: In a collaborative effort, NRL and the Southwest Foundation for Biomedical Research have developed large libraries of sdAb, derived

from llama (1 billion representatives) and spiny dogfish shark (60 million representatives), which are displayed on filamentous phage M13. We selected the llama-derived library for binding to a variety of real and surrogate bio-threat agents and then isolated binders in each selection. Llama-derived sdAb were isolated against model protein hen egg lysozyme (HEL), cholera toxin, staphylococcal enterotoxin B (SEB), ricin, and live vaccinia virus (a smallpox surrogate). The spiny dogfish sdAb library was useful for the delivery of cholera toxin-binding sdAb.

Characterization: We demonstrated that our isolated binders were specific, binding to cognate target and not irrelevant antigens. We further showed that binding of the anti-toxin sdAb to a toxin-coated surface could be countered by the addition of soluble target. This is important, since it demonstrates that the sdAb can recognize toxin in solution and not merely bind to immobilized antigen, which may be partially denatured.

To test for improved heat stability, isolated sdAb were heated to elevated temperatures for 5 minutes, cooled, and then assayed for target binding and interaction with an irrelevant antigen. These tests were done in parallel with conventional antibodies, and in nearly

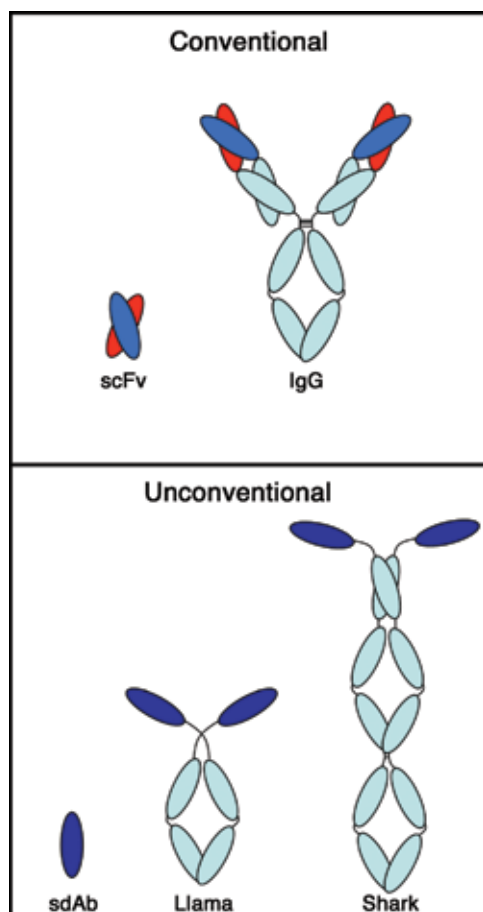


FIGURE 4

Schematic representation of (top) a conventional antibody (IgG) and its cloned minimal antigen binding fragment (scFv), and (bottom) shark and llama antibodies and their cloned minimal binding fragment (sdAb).

all cases the sdAb retained specificity and activity upon heating to the highest temperatures (95° to 100 °C) while the conventional antibodies lost their binding ability. As a further test of thermal stability and an indicator of improved shelf life, sdAb were heated to 95 °C for various lengths of time (Fig. 5). Again, these experiments were done side-by-side with conventional antibodies. All examined sdAb proved more stable than conventional antibodies when subjected to prolonged heating. Some retained 100% of their binding ability even after heating to 95 °C for 45 minutes. Other sdAb retained close to 100% binding activity for the first ~10 minutes and then slowly lost activity over the course of 60 to 90 minutes. The majority of conventional antibodies lost ~90% of their binding activity after the first 5 minutes of heating, while the best conventional antibody lasted no more than 20 minutes at 95 °C prior to losing ~90% of its binding activity.

The sandwich assay format employed by many biosensors uses an immobilized antibody together with a labeled antibody to form an antibody-antigen-antibody sandwich. We have demonstrated the ability of our sdAb to be used in this format for the detection of toxins (Fig. 6), demonstrating the applicability of the sdAb for detection and to diagnostics-type assays.

Conclusions: Our developed sdAbs represent a new generation of durable detection reagents that can be integrated into any antibody-based biosensor. The libraries we developed are renewable and available to be rapidly mined for recognition elements for current and future bio-threat agents. SdAb will benefit the DoD and homeland security by permitting the fielding of biosensors with rugged recognition elements selective against a wide range of targets.

[Sponsored by DTRA and NRL]

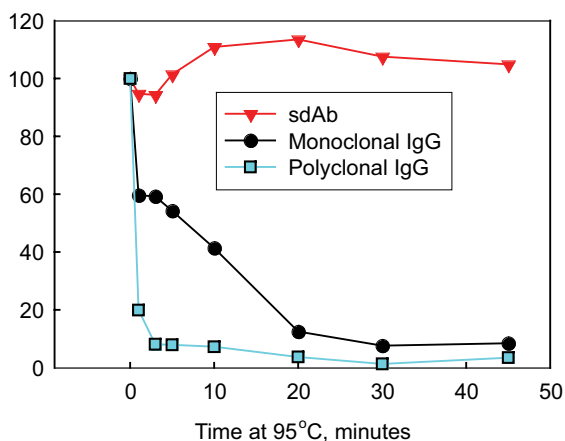


FIGURE 5 Thermal stability of anti-ricin reagents; sdAb (red) and conventional monoclonal (black) and polyclonal (blue) antibodies.

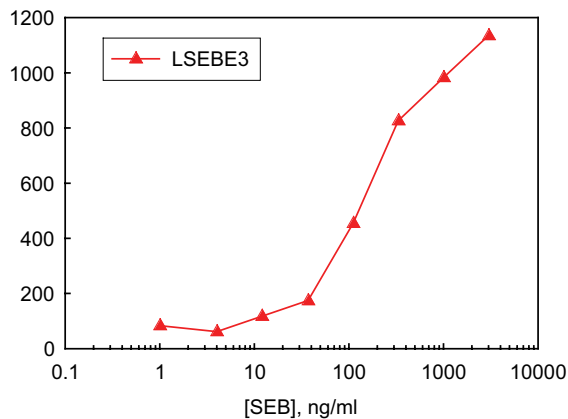
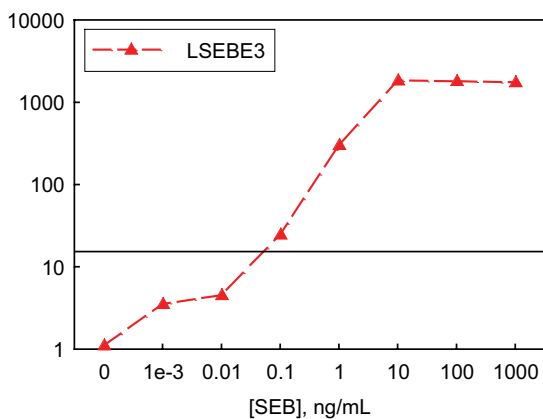
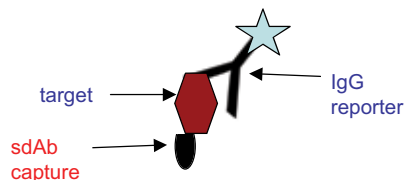
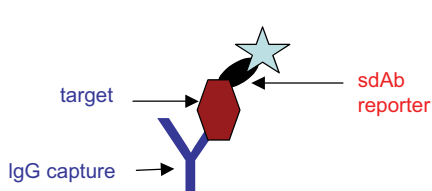
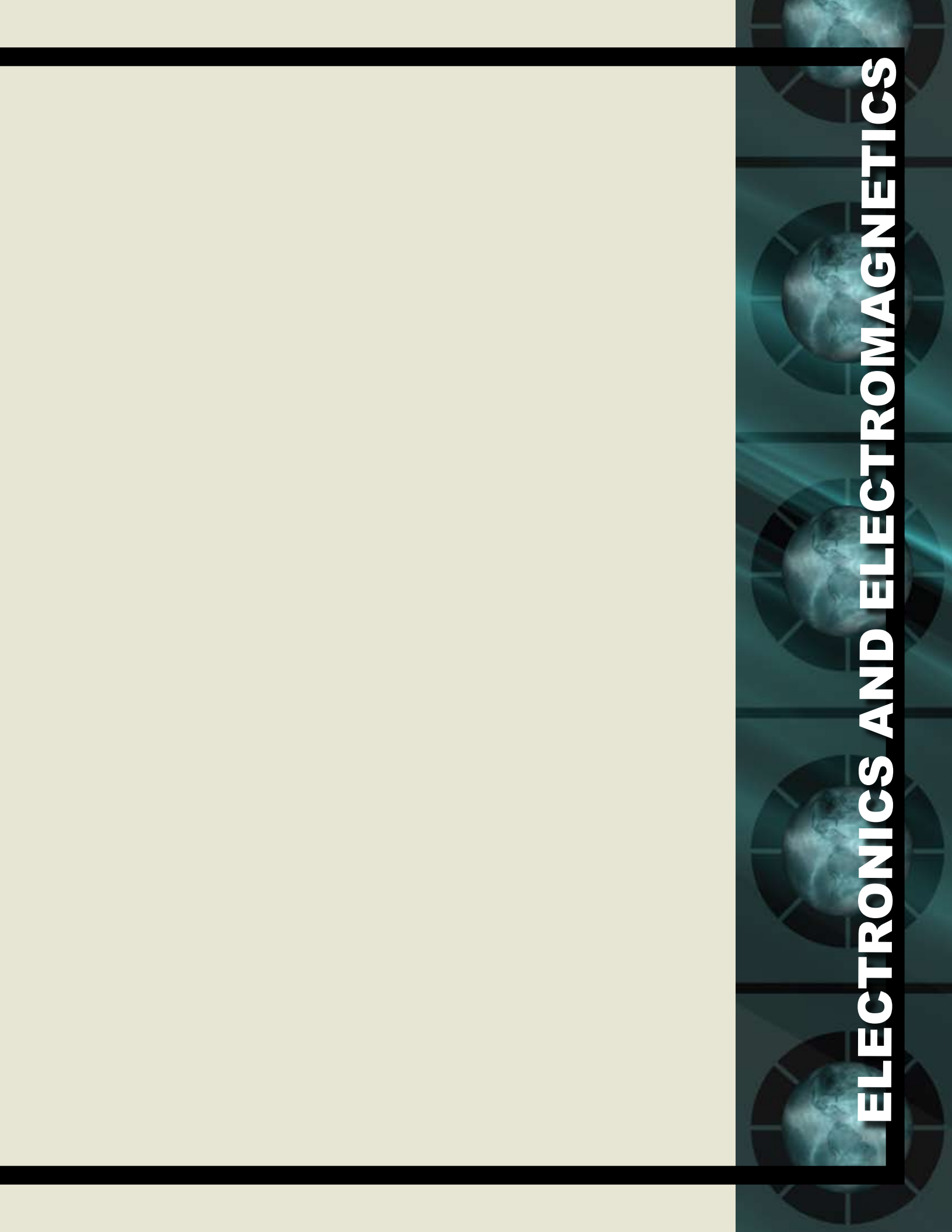


FIGURE 6 Performance of anti-SEB sdAb as a reporter (left) and capture (right) in sandwich assays for SEB.



ELECTRONICS AND ELECTROMAGNETICS



153 Numerical Analysis of Electromagnetic Bandgap Structures

S.-T. Chun and R.S. Schechter

155 Broadband Over Power Lines (BPL) and Its Impact on Spectrum Allocation

L.S. Cohen and A. Light

156 Near-Earth Radio Frequency Propagation

R.A. Wert and A.K. Goroch

159 Unmanned Sea Surface Vehicle Electronic Warfare

D. Trempfer and J. Heyer

Numerical Analysis of Electromagnetic Bandgap Structures

S.-T. Chun and R.S. Schechter
Radar Division

Introduction: Electromagnetic bandgap (EBG) structures¹ and negative index of refraction (NIR) meta-materials are periodic dielectric or metallic material structures that allow greater control over electromagnetic waves than has previously been possible. Man-made versions of these materials block the propagation of electromagnetic waves within particular frequency bands and allow propagation only in certain spatial directions (Fig. 1). They are scalable and operate over a wide range of frequencies. These qualities are very desirable for a variety of applications such as radar, communication devices, and sensors.

Traditionally, the analysis of the electromagnetic properties of EBG materials relied heavily on the mathematics of infinite periodic structures, similar to that used to describe crystal diffraction. However, for real applications, the finite dimensions, lattice defects, and boundaries have to be included in the analysis to account for their impact on the bandgap characteristics. To accomplish this requires a direct numerical simulation of the finite EBG structure.

We have used a Finite-Difference Time-Domain (FDTD) numerical code to design and characterize EBG structures and to analyze the electromagnetic performance of finite EBG structures at microwave frequencies. This code allows us to directly view the time evolution of the fields in these materials. The FDTD approach is useful for optimization of EBG parameters and can facilitate the design in many emerging applications.

FDTD Method: The FDTD method^{2,3} is a numerical technique commonly used in the electromagnetic

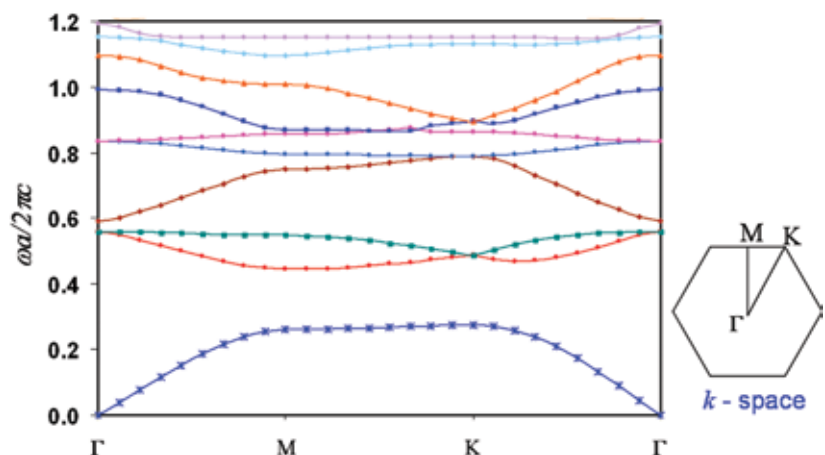
and optical communities. It is a finite difference solution of Maxwell's differential equations in a bounded computational region. The approach simulates the time evolution of the electromagnetic fields in a spatial volume. It is ideally suited for wave propagation and scattering in complex media and permits visualization of the resulting wave fields as a function of time. Since the computational domain is finite, the method requires the use of absorbing boundaries at the edges of the domain, called perfectly matched layers (PMLs), to permit waves to exit the grid without reflecting back, similar to the absorbing walls of an anechoic chamber.

The FDTD simulations for this work require the use of large parallel computers at various DOD High-Performance Computer (HPC) sites. Our code employs parallel programming techniques based on OpenMP and the Message Passing Interface (MPI) so that very large numerical grids may be used to model electromagnetic phenomena in very large computational domains. Typical simulations may use from 100 million to over a billion FDTD cells and require 8 to 64 processors to model EBG structures in three dimensions.

Simulation of EBG Structures: The Radar Division has used the FDTD method to simulate various EBG structures for possible radar applications. As an example, consider an EBG structure consisting of a hexagonal lattice of dielectric rods made of aluminum oxide with a dielectric constant of 12. By removing two rows of rods from the lattice, a waveguide channel is formed by creating a line defect. The effect of this on the electromagnetic properties of the EBG lattice is that localized modes with propagating frequencies inside the bandgap may exist. Figure 2 shows just this situation where a propagating waveguide mode is created in an EBG lattice. A narrow band pulse is introduced at one end of the defect waveguide. Since the pulse center frequency lies in the forbidden bandgap, no waves may propagate at any angle into the surrounding lattice. The

FIGURE 1

Dispersion properties of transverse magnetic (TM) mode in triangular EBG structure made of dielectric rods, $\epsilon_r = 12$, with radius 0.2σ where σ is the lattice spacing. This structure exhibits both bandgaps and directionally dependent electromagnetic wave propagation.



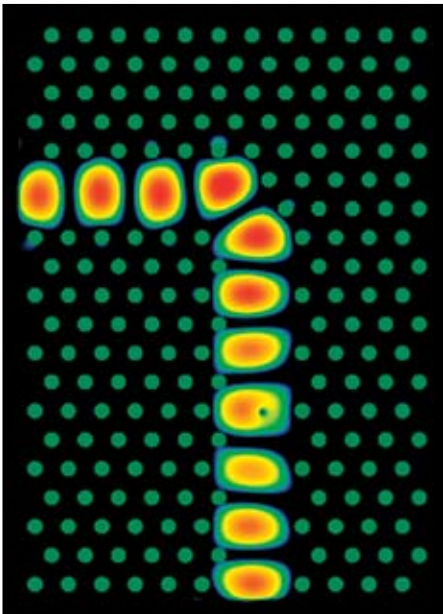


FIGURE 2
EBG waveguide showing a narrow-band transient bending around a sharp corner.

energy is confined, similar to the conventional metallic waveguide. The parameters of the waveguide may be optimized to decrease the losses caused by propagation around a sharp bend.

Other structures are also simulated that are important in controlling microwaves. For example, by removing a circular region and introducing a point defect, a cavity resonator is created. This resonator will have a resonant frequency and quality factor, or Q factor, that depends on the size of the cavity and the properties of the surrounding EBG lattice. EBG structures can also be used in antennas as a substrate to suppress surface waves. These surface wave modes tend to degrade the performance of patch antennas. Suppressing these modes is accomplished by introducing a bandgap at the frequency of the surface wave mode.

Left-Handed Materials: Another class of periodic structures or meta-materials that is becoming important in microwave applications is left-handed material (LHM). These materials have a periodic arrangement of scatterers like EBG structures. A LHM that we have modeled is composed of a periodic array of split-ring resonators (SRRs) that produces an effective negative magnetic permeability, and an array of thin wires to provide an effective negative electric permittivity. At frequencies where both the effective permeability and permittivity are negative, the index of refraction will be negative and the group and phase velocities will have opposite signs. Snell's law requires that for negative index materials, refracted waves be bent to the same

side of the normal as the incident waves, unlike right-handed materials (RHM), which bend waves to the opposite side of the normal. These unusual characteristics have the potential of enabling LHMs to be used for super lenses, cloaks of invisibility, and filters.

We have modeled a finite array of rectangular SRRs on the top side of a circuit board along with the wires on the opposite side of the board. Figure 3 shows the electric field in a region containing 16 LHM boards of varying length and stacked to form a wedge. Every other board is a wires-only board. Plane waves are incident from the left. Waves leaving the wedge undergo negative refraction since they are bent down from the normal (indicated by the dashed line). The higher amplitude areas in red, over the circuit boards, are indications of resonances in the SRR elements. These simulations illustrate the power of the FDTD method when combined with parallel processing to study electromagnetic wave propagation in complex structures. They will be useful in designing and optimizing unit cell geometry and lattice parameters that determine stop/pass-bands of EBG and other meta-material structures. This type of research represents an important step towards the use of EBG structures in microwave circuits.

[Sponsored by ONR]

References

- ¹J.D. Joannopoulos, R.D. Meade, and J.N. Winn, *Photonic Crystals: Molding the Flow of Light*, Princeton University Press (1995).
- ²R.S. Schechter, S.T. Chun, M.S. Kluskens, M. Kragalott, and D.A. Zolnick, "Introducing a Sub-cell Tensor Technique into a (2, 4) FDTD Method," *Appl. Comp. Electromag. Soc. Journal* **21**, 45-50 (2006).
- ³S.T. Chun and J.Y. Choe, "A Higher Order FDTD Method in Integral Formulation," *IEEE Trans. Antennas and Propagat.* **53**, 2237-2246 (2005). ★

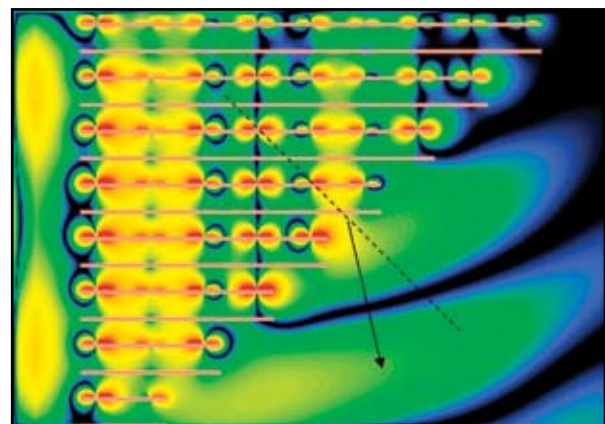


FIGURE 3
Computed electric field clearly showing negative refraction by an LHM wedge.

Broadband Over Power Lines (BPL) and Its Impact on Spectrum Allocation

L.S. Cohen¹ and A. Light²

¹Radar Division

²Sentel Corporation

Introduction: For many years the electric utility companies have employed power lines to transmit signals in the tens of kHz range for the control of switches and relays on electric power transmission systems. The electric utility companies and internet providers have become interested in employing existing power lines for providing residential and commercial internet access, using frequencies from 1.6 to 30 MHz in order to attain data rates of 1 or more Mbits/s. Initially intended to provide high-speed internet service to consumers in rural areas, Broadband Over Power Lines (BPL) is of great interest to service providers as power lines reach virtually every home and community in the country. A major concern with BPL is that the data signals impressed upon power transmission lines can emit disruptive electromagnetic interference (EMI) to communications and high frequency (HF) radar receivers residing in the 2–30 MHz band. The NRL Radar Division and the Space and Naval Warfare Systems Center (SPAWAR) Charleston was tasked by the Naval Sea Systems Command to determine what changes in the ambient background noise levels might result from a BPL installation.

Description of a Typical BPL System: With the employment of digital signal processing (DSP) hardware and embedded software, BPL transmissions utilizing digitally modulated carriers in the frequency range of 2–30 MHz are a reality. As shown in Fig. 4,¹ the BPL concept relies on impressing computer data on medium voltage (MV) power lines carrying 1,000 V to 40,000 V and is supported by the following: (1) PC; (2) modem; (3) extractor, which is the transition from the residential/commercial low voltage (LV) power lines to one of the three phases supplying the residential or commercial establishment; (4) repeaters providing amplification and correction for phase distortion; and (5) injector supporting the transition from the power line phase to the fiber optic link.

Typically, BPL uses orthogonal frequency division multiplexing (OFDM). OFDM is a technique for transmitting data whereby parallel data streams digitally modulate multiple carrier frequencies with a frequency spacing equal to $1/T$ Hz where T is the duration of the data symbol in seconds. The digital modulation scheme to modulate these data streams can range from bipolar phase shift keying (BPSK) to quadrature amplitude modulation (QAM). The PC BPL modem thus converts a serial data stream into successive parallel streams that digitally modulate one of a group of orthogonal carriers. These modulated orthogonal carriers transition from the LV line to the MV overhead phase line either through an inductive coupler that bypasses the transformer, or through a Wi-Fi transponder and modem

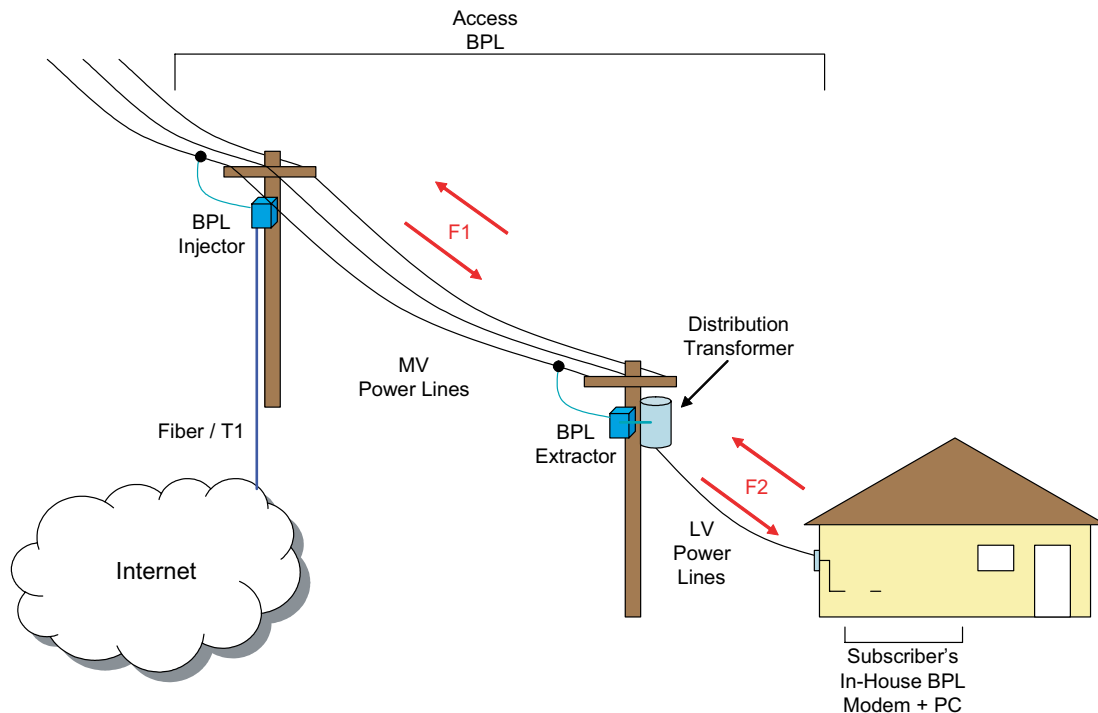


FIGURE 4
Basic BPL system.¹

that resides adjacent to the PC and transmits the data signal to a transponder on the utility pole connected to the phase through an inductive coupler.

BPL Testing: A commercial BPL test site was chosen on the east coast of the United States. Measurements were conducted over a period of three days, October 26–28, 2004 (see Fig. 5). Measurements were taken using a spectrum analyzer with a 10.0 kHz resolution bandwidth and a calibrated loop antenna. The loop antenna was situated 1.8 meters above the ground and at a slant distance of 17.7 meters from the BPL energized power line phase. Table 1 provides a comparison of ambient noise levels that would occur in a rural environment (a natural setting to operate an HF radar or communications system) and the measured BPL emissions corrected for a 1.0 MHz bandwidth. BPL emissions can definitely degrade the operation of HF radar or communications receivers due to the significant rise in the noise floor. In fact, numerical modeling using a method of moments (MOM) electromagnetic simulation program indicates that the measured power line would be a source of EMI to a sensitive HF receiver beyond 183 meters.

Conclusions: Issues that need to be considered when performing BPL measurements are (1) the unsymmetrical radiation characteristics of power lines; (2) the changing load impedances resulting in different emissions characteristics; (3) the presence of structures such as buildings in the vicinity of the power lines; and (4) changes in BPL signal amplitude that maintain a given signal-to-noise ratio insuring reliable data transfer. Based upon measurements and modeling, it is our opinion that BPL in the 2–30 MHz band is a cause for concern when operating HF radar and communications receivers in close proximity to BPL excited power lines. The received power impinging on an HF radar antenna array is proportional to $1/R^4$, where R is the distance the electromagnetic wave traverses from the array to the target and back to the array, whereas the

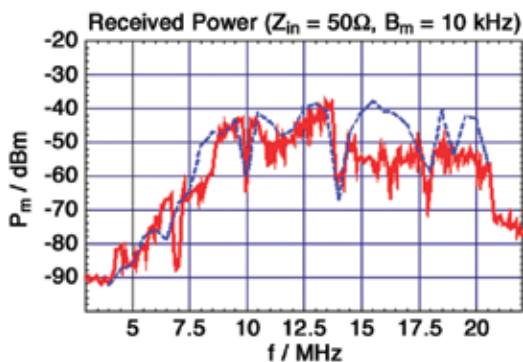


FIGURE 5
Corrected spectrum analyzer (red) and MOM (blue) data.

TABLE 1

Measured Versus Rural Ambient Noise Levels in a 1.0 MHz Receiver Passband

Frequency (MHz)	Rural (dBm/MHz)	Measured (dBm/MHz)
10	-86	-44
15	-89	-34
20	-92	-32

interference energy from BPL signals is only attenuated by space as $1/r^2$, where r is the separation between the power line and the radar antenna. Thus BPL signals that raise the noise floor of an HF receiver may greatly compromise performance.

Acknowledgments: The authors would like to acknowledge Mr. Mark Johnson of the Naval Sea Systems Command and Mr. Joe Thomason of the Naval Research Laboratory for their support in making this work possible.

[Sponsored by ONR]

References

- ¹Potential Interference From Broadband over Power Line (BPL) Systems to Federal Government Radiocommunications at 1.7–80 MHz, National Telecommunications and Information Administration (NTIA) Report 04-413, April 2004. ★

Near-Earth Radio Frequency Propagation

R.A. Wert¹ and A.K. Goroeh²

¹Tactical Electronic Warfare Division

²Marine Meteorology Division

Introduction: The Near-Earth Propagation (NEP) program at NRL is investigating the unique radio frequency (RF) phenomena that occur within one meter of the Earth's surface. In the past, researchers have generally focused their propagation analysis on signals that propagate significantly above the Earth's surface.¹ However, with tomorrow's distributed and integrated micro-sensors, long-range, medium-altitude communication will not necessarily be the norm.

This article discusses some of the physical phenomena associated with near-Earth propagation. When radiating near the Earth, a communications link is subjected to a number of physical impairments, including Fresnel region encroachment and multipath reflections. The NEP program collected a variety of RF propagation observations in a controlled anechoic chamber at NRL, and in the open atmosphere in a variety of environmental conditions at Marine Corps Base Quantico,

VA, and White Sands Missile Range, NM. The signal variation was measured in the 400 MHz, 1.78 GHz, and 2.4 GHz RF spectral regions with monopole and horn antennas at several heights above the surface and as a function of antenna-receiver separation. In this way we observed the influences of surface roughness, heating, and cooling on changes in the radiation pattern of the emitted RF signal.

Temperature and Moisture Gradients: The near-Earth atmosphere is characterized by heat and moisture exchanges that result in strong temperature and humidity gradients that vary locally and diurnally. At the Earth's surface, gradients are strongest and turbulent effects dominate, as defined by Garratt.² Traditional propagation analysis and models do not generally account for these rapidly varying microclimate perturbations—rather they use a stochastic model of near-surface flux. Our near-Earth propagation observations include the detailed characterization of the turbulent mixing regime immediately adjacent to the Earth's surface. The turbulent exchange results in small air parcels of varying temperature and humidity, termed micro air parcels, with length scales similar to the wavelengths of the RF signals studied here. These varying micro-air parcels translate to varying index of refraction parcels, which in turn cause dynamic ray bending, resulting in scattering of the original signal (Fig. 6).

Refractivity and Refractive Index: In the standard atmosphere, refraction causes RF energy propagating in the forward direction to bend downward. Depending on frequency, the bending allows the radio horizon to propagate well beyond the traditional line of sight.

Only minor changes in refractive index are necessary to cause a significant change in energy propagation. Near the Earth's surface the refractive index values range from 1.000250 to 1.000400 as described by Goldhirsh and Dockery.³ This refractive index value typically decreases with height but may decrease quickly or increase with height if local weather anomalies occur. By using the relationship between refractivity and the refractive index, the refractive index is derived in terms of total pressure, temperature, and water vapor concentration, as shown in Eq. (1). Variations of temperature and moisture in the propagation path cause local refraction of the signal, resulting in signal loss and increase of noise.

$$n = 77.6 \times 10^{-6} \left(\frac{P}{T} \right) - 5.6 \times 10^{-8} (\rho) + 1.7305 \times 10^{-3} \left(\frac{\rho}{T} \right) + 1 \quad (1)$$

n : index of refraction
 T : temperature (Kelvin)
 P : localized atmospheric pressure (mb)
 ρ : water vapor concentration (g/cm^3)

Distributed Sensor Setup: During multiple experiments, distributed autonomous nodes were placed in a field to measure inter-node signal loss. The field was prepared grass cut to a height of approximately 4 cm. The terrain between the nodes was primarily flat. Nodes were placed and tested with new batteries that were characterized under similar conditions. The monopole antennas were placed perpendicular to the surface of the Earth and at a height of 7 cm measured

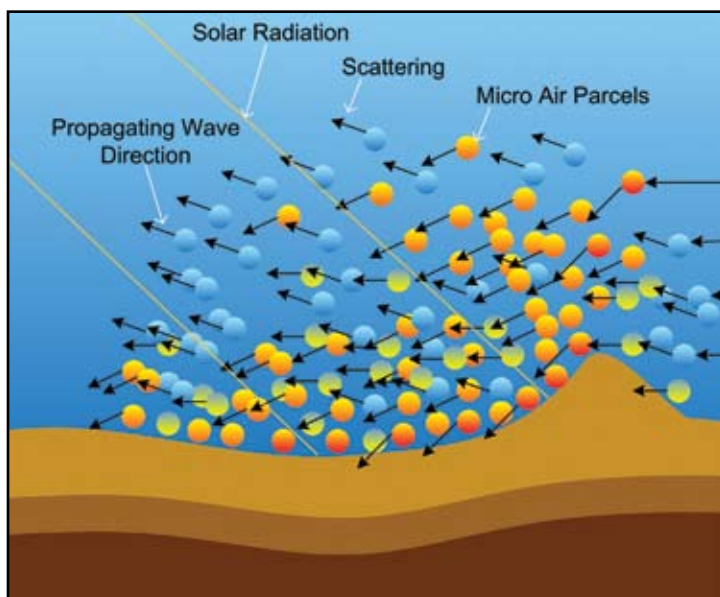


FIGURE 6
 Micro air parcel concept: temperature and moisture gradients in the near-Earth environment result in a turbulent mix of micro air parcels. The micro air parcels with varying indexes of refraction cause turbulent wave bending.

at the base. The controller node autonomously polled each of the sensor nodes sequentially. After receiving the polling request, the sensor nodes transmitted data packets back to the controller node for thirty seconds. While receiving the data packets the controller node packaged the radio signal strength indicator (RSSI) information as seen by the controller node and forwarded it to the recording node. The recording node was placed at a height of 91 cm and connected to a laptop to record this RSSI data. While the information was transmitting from one of the sensor nodes to the controller node, the recording node monitored the transmission and recorded the RSSI as seen by the recording node. The controller node polled each sensor node independently, once per hour, for 48 hours. In addition to the RSSI data, meteorological data was also collected and time stamped to examine the correlation between surface temperature, flux, and propagation path signal strength loss.

Distributed Sensor Analysis: The node data were collected over a period of 48 hours. As expected, the data demonstrates that the greater the distance between the receiving and transmitting nodes, the lower the power received. In addition, as the temperature and heat flux increase, the overall signal strength decreases. Thirty seconds of data was collected for each node every hour. Further analysis of the data reveals that during the 30-second collection period the signal strength varies rapidly when insolation is at its peak, but minimally during the early morning hours. Of par-

ticular interest, the slant path was observed to exhibit higher short-term variability than the flat near-Earth link. Signal strength was much lower for both paths when compared to a link several wavelengths above the Earth (see Fig. 7 for results from a separate experiment). Additionally, both paths exhibited increased diurnal cycle fluctuations compared to paths at standard propagation heights.

Summary: Several experiments were conducted of the propagation environment within one meter of the Earth's surface using distributed nodes, horn antennas, and monopole antennas with high-fidelity data collection. The experiments recorded both rapid perturbations and diurnal changes in the propagation signal strength over short periods of time with stationary antennas and no moving reflectors in range of the equipment. The microclimate of the near-Earth atmospheric boundary layer is a contributing factor to the signal strength changes.

[Sponsored by NRL]

References

- ¹ S. Shibuya, *A Basic Atlas of Radio-Wave Propagation*, Wiley-Interscience, New York (1987).
- ² J.R. Garratt, *The Atmospheric Boundary Layer*, Cambridge Atmospheric and Space Science Series, Cambridge University Press (1994).
- ³ J. Goldhirsh and D. Dockery, "Propagation of Radio Waves in the Atmosphere," Vol. 1, Johns Hopkins University Whiting School of Engineering and Applied Science, unpublished course materials, Baltimore (2005). ★

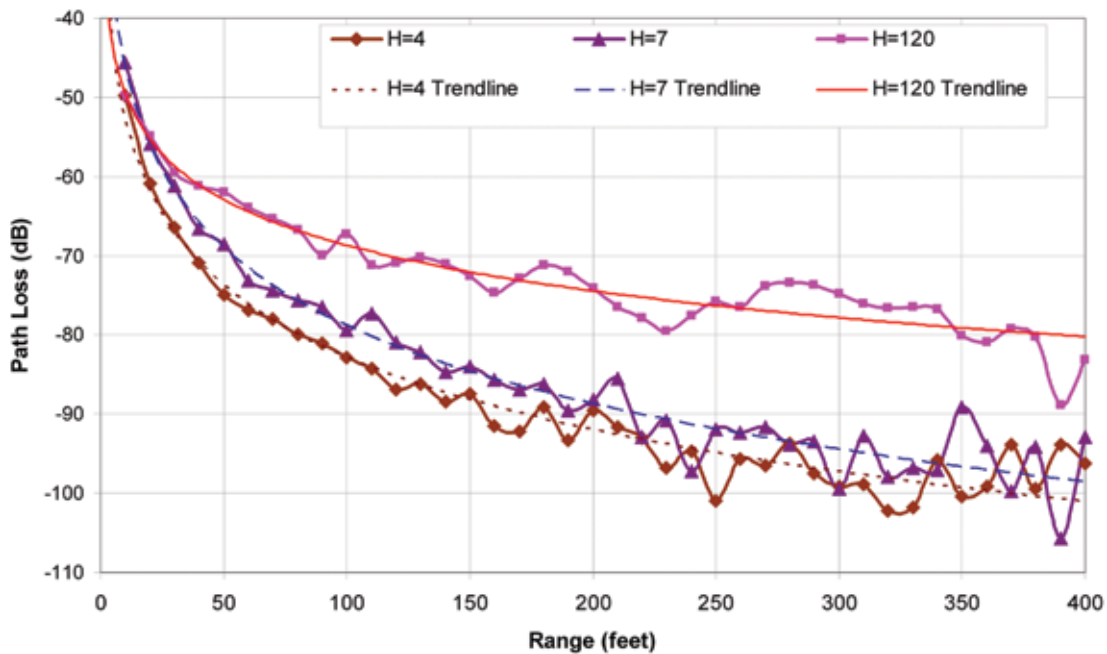


FIGURE 7

RF pathloss graph. This graph depicts RF pathloss observed from a monopole transmitter and corner reflector receiver. The three collection heights were 4 inch, 7 inch, and 120 inch.

Unmanned Sea Surface Vehicle Electronic Warfare

D. Tremper and J. Heyer

Tactical Electronic Warfare Division

Introduction: The use of tactical unmanned vehicles provides a means to accomplish a wide variety of combat missions without risk to operators' lives and without loss of expensive platforms. In addition, these vehicles offer an opportunity to rapidly field advanced warfighting capabilities at relatively low cost simply by developing payload systems that seamlessly integrate with the vehicle's onboard control network. With the emergence of open control system standards, such as the Joint Architecture for Unmanned Systems (JAUS), the ability to build so-called plug-and-play payloads is approaching reality.

To exploit the opportunity of fielding advanced capabilities using unmanned platforms, the Tactical Electronic Warfare Division at NRL is developing an advanced electronic attack (EA) payload for surface ship defense that is suitable for unmanned vehicles like those planned for use with the Littoral Combat Ship. This development, sponsored by the Office of Naval Research, is designed to provide capabilities to counter late-generation sea surface surveillance and targeting radars found in maritime patrol aircraft and multi-role fighters, and to provide the capability to attack anti-ship missiles during their initial target survey scans. Used singly, the unmanned vehicles provide a long-duration self-protection countermeasure system. Used in multi-vehicle constellations, the unmanned vehicles with EA payloads can be used to provide an area defense capability over large sectors.

To demonstrate the utility of unmanned vehicles for surface ship defense, NRL has teamed with the

Naval Sea Systems Command, Carderock Division, to integrate an electronic warfare (EW) payload onboard a sophisticated unmanned surface vehicle called the High Speed Unmanned Sea Surface Vehicle (HS-USSV). The HS-USSV is a remote-controlled 11 m hydrofoil, shown in Fig. 8. Its design provides a stable jamming platform that can maintain mission performance in high sea-state conditions and at speeds commensurate with large USN combatant ships.

USSV-EW System Overview: The EW payload for the HS-USSV leverages the wideband digital radio frequency memory (DRFM)-based EA system developed under the ONR Advanced Multifunction Radio Frequency (RF) Concept Future Naval Capabilities program. In addition to the standard playbook of jamming techniques, this DRFM-based system, shown in Fig. 9, has the capability to generate high-resolution false targets with realistic amplitude and Doppler modulations, engage multiple threats simultaneously, and generate sophisticated multi-component waveforms that combine false targets with various kinds of obscuration jamming. A novel, low-cost direction finding system has also been developed for the HS-USSV. High transmit power is achieved through use of high-gain antennas and high-power microwave power modules developed for tactical aircraft.

Payload command and control and system monitoring are provided by an interactive EW module developed for the NRL SIMDIS visualization tool shown in Fig. 10. SIMDIS provides operators with a real-time 3D visualization of platform positions and motions. The new EW module adds graphic representations of threat emitters as they are detected by the payload's electronic support receiver and EA engagement activity. Using a computer running SIMDIS with the EW module, operators can remotely control all payload functionality,



FIGURE 8
USSV during EW payload testing.



FIGURE 9
COTS-based digital RF memory (DRFM) waveform generator prototype.

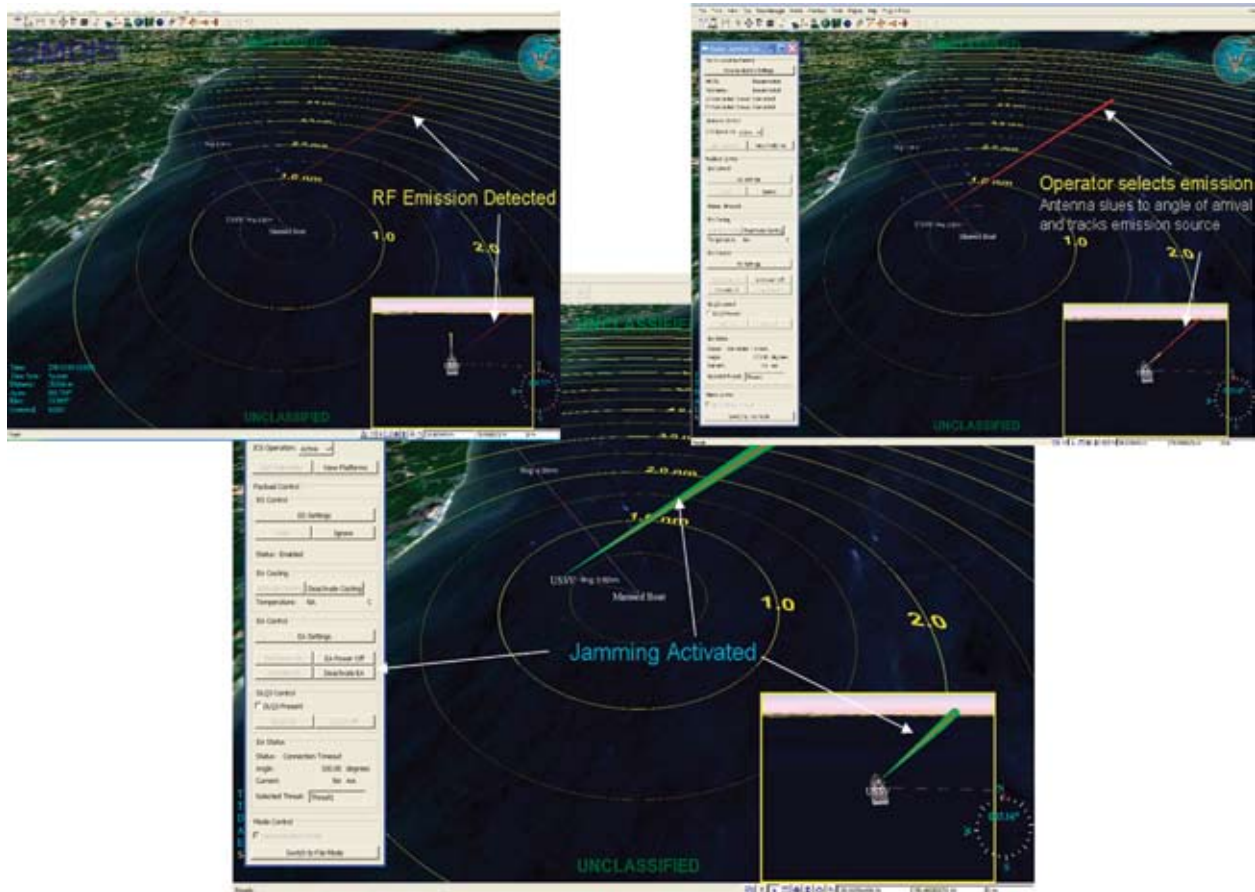


FIGURE 10
SIMDIS-based EW payload control interface. Top Left: Red beam denotes presence and direction of hostile RF emissions detections. Top Right: Operator selects RF transmission to be tracked by the EA antenna. Bottom: Operator activates EA against selected hostile emission.

specify search and threat parameters, and monitor the payload's activity. Payload control includes the capability to conduct preemptive jamming against known emitter locations, or reactive jamming against known threat emitters within designated geographic sectors. Friendly, neutral, and hostile RF signals are color-coded in the SIMDIS display to provide operators with rapid situational awareness. Any detected RF transmission within the bandwidth of the payload can be selectively tracked and jammed by the payload operator. Multiple payloads can be controlled by a single SIMDIS terminal, providing the capability to execute coordinated multi-vehicle EW concepts.

HS-USSV EW Experimentation: Experiments with the HS-USSV are planned through fiscal year 2008 to evaluate selected EA mission capabilities. These include operational deception to deceive synthetic aperture and inverse synthetic aperture radars, creating overwhelming numbers of decoy targets within an area to confuse airborne targeting platforms, and as a long-duration anti-ship missile (ASM) decoy.

The initial EA experiment was conducted in August 2006 and focused on the ASM decoy mission. Using

a shore-based ASM simulator to track the ship target, the experiment examined the set of effective HS-USSV station positions that prevent the ASM seeker from successfully tracking the target vessel. The experiment revealed that a HS-USSV performing EA could deny ASM radar tracking of the target vessel using generic jamming waveforms. Additional experiments are planned for 2007 aimed at demonstrating other EA missions.

Summary: The use of unmanned surface and air vehicles is a promising avenue for delivering advanced electronic warfare capabilities to defend surface ships. The Tactical Electronic Warfare Division at NRL is aggressively developing EW payload technologies that provide low-cost, sophisticated electronic attack capabilities that can be rapidly transitioned to unmanned vehicles that utilize open architecture standards such as the Joint Architecture for Unmanned Systems. The effort is leveraging technologies developed under multiple ONR Future Naval Capabilities programs and NRL basic research programs to build a robust EW system with capabilities not currently found in the Fleet.

[Sponsored by ONR]



**INFORMATION TECHNOLOGY
AND COMMUNICATIONS**





165 High Altitude Relay and Router

M. Rupar, J. Doffoh, and R. Mereish

167 Comprehensive Maritime Awareness (CMA) Joint Capabilities Technology Demonstration (JCTD)

C.T. Dwyer

169 Efficient Linearization of Microwave Power Amplifiers

J.X. Qiu, D.K. Abe, T.M. Antonsen, Jr., B.G. Danly, B. Levush, and R.E. Myers

High Altitude Relay and Router

M. Rugar, J. Doffoh, and R. Mereish
Information Technology Division

Introduction: The Satellite and Wireless Networking Section of NRL's Transmission Technology Branch has been tasked with determining the feasibility of the use/development of communications relays held aloft by balloons at high altitude (~65,000 ft above mean sea level, or MSL). The objective of this High Altitude Relay and Router (HARR) program is to extend the range of line-of-sight (LOS) communication links, particularly those compromised by terrain. The HARR project objectives are to

- develop payloads capable of doing on-board routing of network traffic between multiple ground nodes within and out of line-of-sight, and
- develop payloads capable of extending tactical communications in the UHF band for both data and voice communications for point-to-point links.

NRL has developed two candidate relay platforms. The first operates in L-band using the 802.11b protocol, and incorporates a router in the sky that can direct traffic from ground site to ground site, either directly or via another balloon-based relay. Converter/amplifiers allow these routers and associated ground terminals to operate at ranges exceeding 100 miles.

The second payload simulates a UHF FLTSAT payload, providing 25-kHz "bent-pipe" relays that can operate at SATCOM channels or LOS channels, transponding the signal to avoid self-interference. Voice at 240 miles and data at 80 miles were demonstrated using legacy UHF military systems.

The payloads were integrated with a telemetry package developed by the Air Force Research Laboratory (AFRL) of Kirtland AFB, NM. Two sets of launch testing were conducted, the first in Roswell, NM, in November 2005, and the second outside of Lubbock, TX, in June 2006. At each location, testing took place over an approximate 100 mile range and took advantage of the prevailing seasonal winds at 65,000 ft. The launch of the entire package is shown in Fig. 1. The payload shown has a UHF package with dual antennas.

Payload 1: UHF Transponder: The UHF transponder was tested using standard military radio sets: the AN/PRC-117F, and the standard Navy UHF radio, the AN/WSC-3 transceiver. Testing in Roswell focused on voice communications, achieving links between PRC-117F radios at 245 miles. Data communication was also successful with both radio sets, but over a more limited range.

In the second phase of testing in Lubbock, the emphasis was more on data throughput and performance as a function of slant range to the relay. Data sets were collected for the 117F operating in IP mode at slant ranges up to 80 miles, for both directional and omni-directional antennas (as shown in Fig. 2), and for uni-directional data using satellite modems at slant ranges up to 40 miles.

A dual transponder design was also tested on one of the launches in Lubbock, with each channel sharing the same antennas. This was to validate the design for the future payload, which will accommodate up to four channels simultaneously. Both channels were occupied simultaneously with digital waveforms, resulting in good performance and no interference issues, regardless of mode of operation.

Data throughputs for the PRC-117F radios were 9600 bps maximum, due to limitations in the radio's IP



FIGURE 1
Launching of NRL payload by AFRL personnel in Roswell, NM, November 2005.

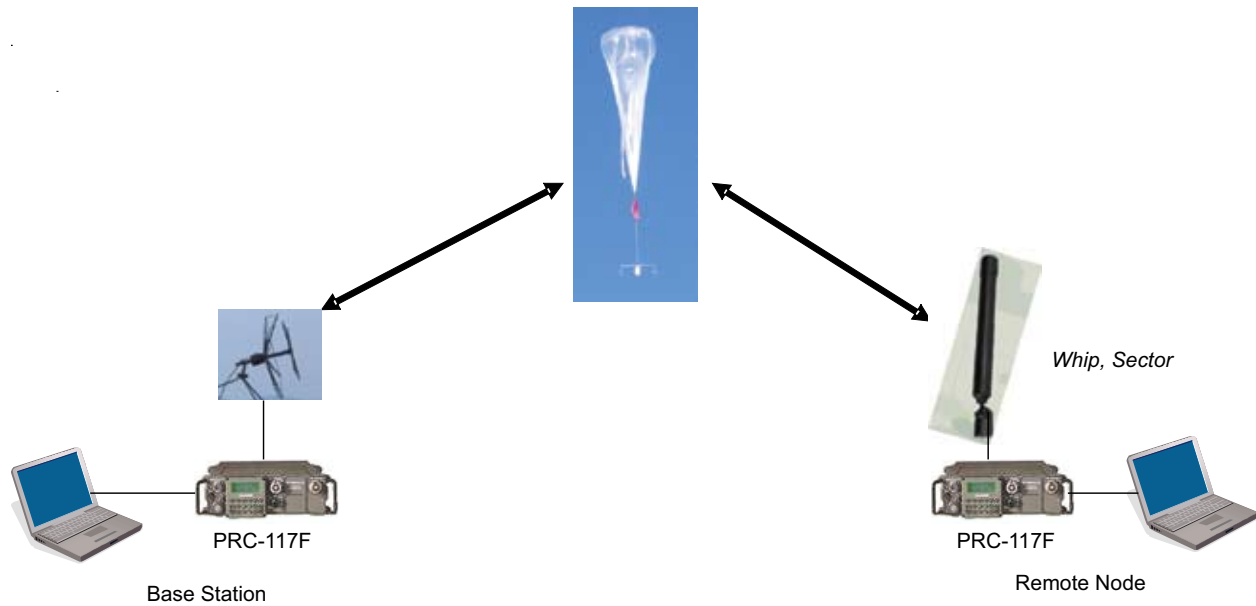


FIGURE 2
Test configuration, UHF high altitude transponder.

implementation, while 19.2 kbps were achieved using the WSC-3 radios in simplex mode.

Payload 2: 802.11b Transponder: The 802.11b payload was a Linux-based router in a hardened PC104 platform that was programmed by NRL to route information according to the destination, accommodating both unicast and multicast traffic. NRL commissioned Shireen, Inc., to build a set of amplifiers that would also do frequency translation of the standard 802.11b waveform to a frequency band near 1.8 GHz. These lightweight amplifiers were first successfully demon-

strated in Roswell, and supported three very successful flight tests in Lubbock.

During the 802.11b testing, ground nodes were set no more than 30 miles apart. Data was taken during the entire duration of each flight, with a maximum slant range of 130 miles achieved. Data was collected in the form of UDP packets, utilizing NRL's Multi-Generation Tool Kit (MGEN).

Testing encompassed a number of scenarios: multicast and unicast traffic, uni-directional and bi-directional, all with two and three ground nodes in the network. An example of one test is illustrated in Fig. 3.

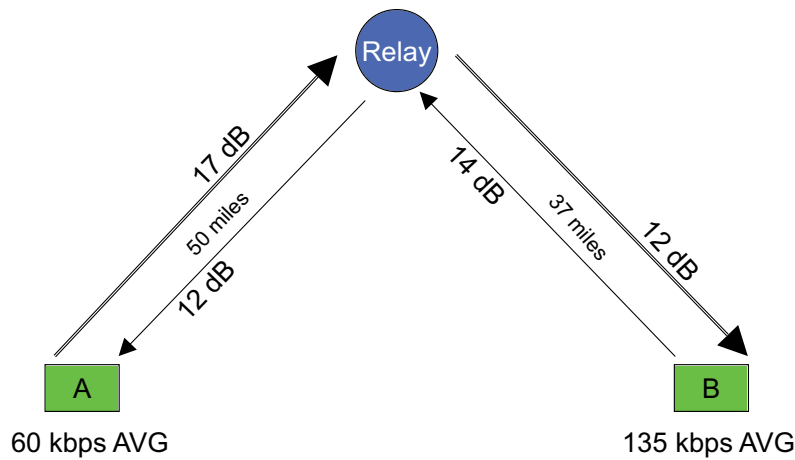


FIGURE 3
Example of 802.11b relay/router testing for two nodes conducting bi-directional multicast. The S/N ratios (expressed in dB) were collected at the receive point at each node in the link.

Scripts were generated to fill the path with as much data as possible, and the signal-to-noise ratio (S/N) was measured at each receive point to correlate networked performance with RF performance.

Conclusion: NRL has successfully demonstrated two communications payloads borne aloft by a high altitude balloon, one a UHF relay, the other a router in the sky operating with the 802.11b waveform. Each of these payloads can interface immediately or with minimal hardware investment with existing tactical communications in the fleet and Marine Corps ground units. The High Altitude Relay and Router can provide a line-of-sight extension of over 100 miles to existing tactical communications for periods in excess of ten hours as currently designed.

Future efforts will involve performance improvements, miniaturization of the payloads, and testing of multiple common applications.

[Sponsored by ONR]



Comprehensive Maritime Awareness (CMA) Joint Capabilities Technology Demonstration (JCTD)

C.T. Dwyer
Space Systems Development Department

Background: The Comprehensive Maritime Awareness (CMA) Joint Capabilities Technology Demonstration (JCTD) is a program to improve Maritime Domain Awareness (MDA). The CMA JCTD vision is to share maritime shipping information throughout the world to deter use of commercial maritime shipping for terrorism, WMD proliferation, drugs, piracy, and human trafficking. CMA serves as an exemplar for a “culture of sharing” of maritime information between the U.S. and international partners. The project takes advantage of ongoing efforts, proven technologies, and current information-sharing agreements. CMA has two main focus areas: 1) demonstrate the importance of interagency and international information-sharing for improved maritime awareness; and 2) demonstrate improved information management techniques — such as application of the U.S. Department of Defense Net-Centric Data Strategy — to enable effective management of large volumes of shared data. CMA is working cooperatively with the Republic of Singapore. Singapore’s position as a nexus for shipping in Southeast Asia provides a unique opportunity for sharing information.

Problem to be Addressed: Effective homeland defense relies on ensuring air and maritime shipping

is not used to transport WMD, other terrorist mechanisms, or terrorists. Resource limitations force the U.S. to inspect and interdict only a fraction of all maritime shipping due to the high volume of shipping coming into U.S. ports and the economic requirements to maintain rapid flow of goods. This is a global problem, shared by our international friends and allies.

U.S. and international information resources — some unclassified, some classified — help to focus inspection assets on the most probable threats. Much of the available information is exploitable, but only through painstaking correlation approaches that can require hours of an analyst’s time for a single vessel. Also, much of the information developed by the U.S. and the international community is not shared. The current labor-intensive processes and lack of sharing create inefficiencies and missed opportunities to address threats as early as possible, prior to threats entering our ports. See Fig. 4.

Serious gaps exist in identifying and prioritizing worldwide maritime threats:

- Maritime forces lack the tools to provide timely and accurate maritime situational awareness.
- Automatic tools to identify and prioritize relevant and actionable information are lacking.
- The inability to acquire, fuse, and manage disparate information limits timely cueing and focus.
- Information-sharing barriers (technical, cultural) limit the effectiveness of partner entities.

Proposed Solution: CMA addresses the problems listed above by developing a culture of sharing between international partners and the U.S., and between U.S. agencies. See Fig. 5. CMA’s goals are to (1) track maritime movements, to include vessels, people, and cargo; (2) identify which movements are potential threats; and (3) prioritize them for action. This will improve maritime security by acquiring, integrating, and exchanging relevant maritime activity information, identifying possible threats using available information, and then focusing limited interdiction and inspection assets on the most probable threats.

Draw information from multiple sources: The U.S. is not alone in desiring to obtain a more complete maritime picture. Many of our friends rely on maritime shipping for their existence. Information is to be obtained from multiple sources, including a Common Operational Picture (COP), Automated Information Systems (AIS), Department of Defense systems, Department of Commerce databases, and Department of Homeland Security information. Singapore’s sources of information may include Port Authority information, Singapore AIS information (to include Singapore’s AIS-like system for 100% of its maritime traffic), and others.

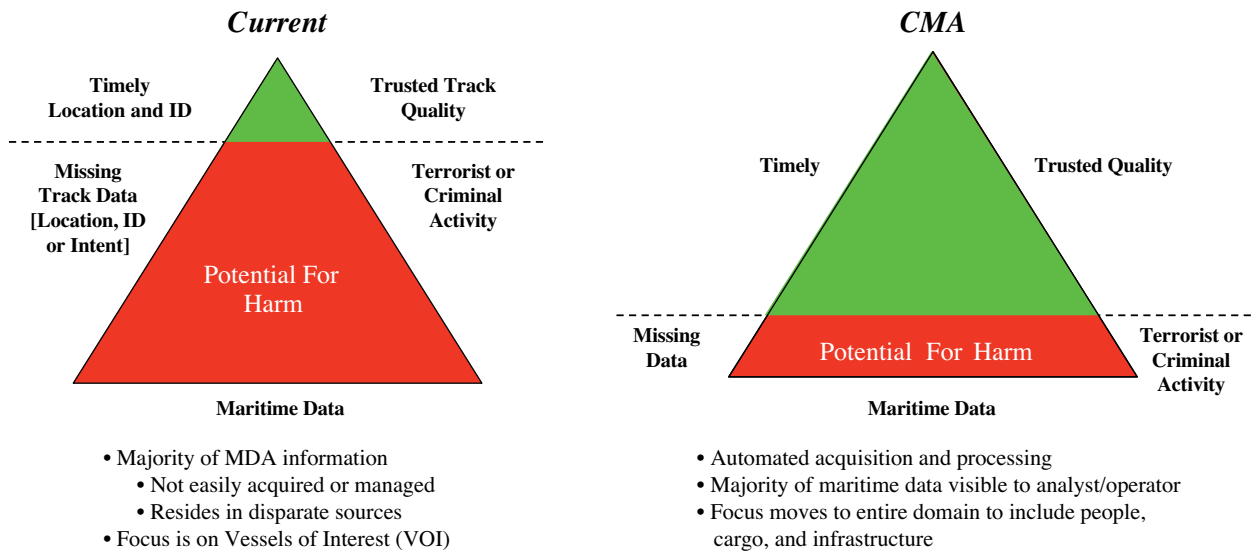


FIGURE 4
Knowledge level: current and CMA.

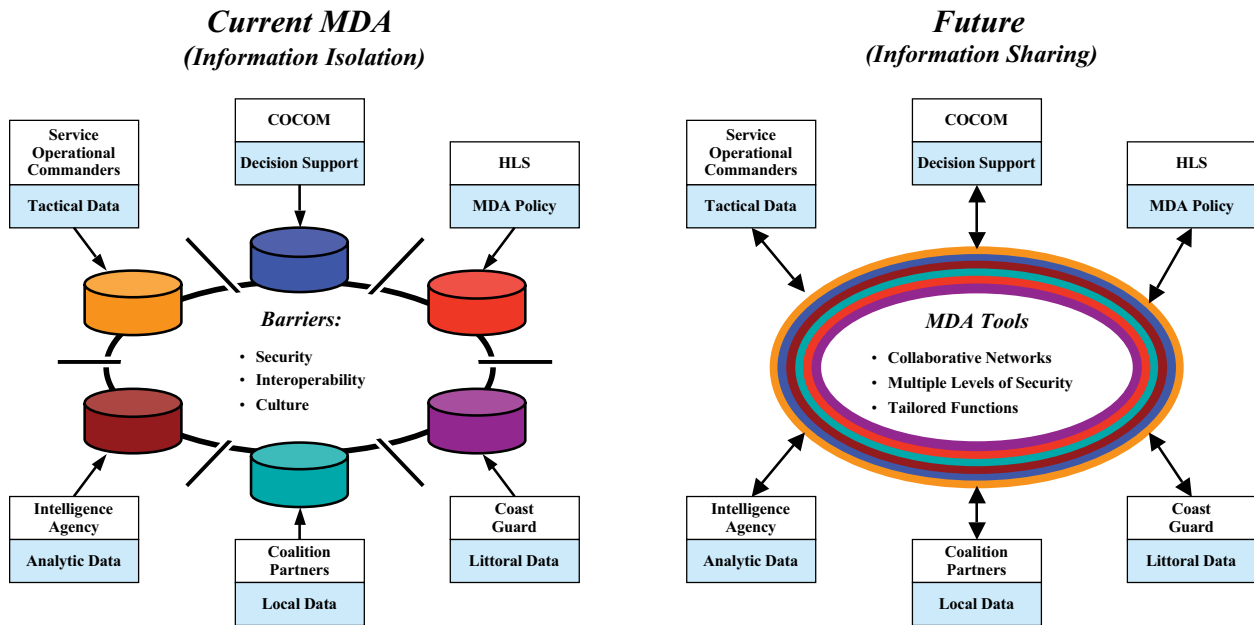


FIGURE 5
Reducing technical/cultural barriers. Policy modifications are necessary to allow information flow across technical and geographic boundaries.

Correlate multi-source information to maritime contacts: Adding more sources of information will overwhelm maritime security forces and analysts searching for threats unless the sources of information can be correlated. CMA automates this effort to reduce the workload for maritime analysts.

Identify Anomalies and Threats: Once disparate sources of information are correlated and fused, the information is used to identify anomalies and threats. Identification of anomalies might be as simple as automatically finding discrepancies between various data sources. For instance, as a ship approaches Long Beach, its AIS indicates the ship name is the Tokyo Maru. However, the automated tool searches databases and shows the Tokyo Maru was seen in Rotterdam one day earlier. The track would be flagged automatically. Another case could be a ship approaching Long Beach with an Advanced Notice of Arrival indicating crew size of 34, when the last port of call in Singapore shows crew size of 30. An automated report would flag the ship for investigation.

Define and Demonstrate Sharing Practices and Policies: Because maritime threats are a concern to all maritime nations, sharing the identified anomalies and threats (within already established information-sharing restrictions) is critical. Circuits for sharing classified information are available on the Coalition Enterprise Regional Information Exchange System (CENTRIXS). In addition, automated security guards are used to ensure that only releasable information is exchanged, in accordance with existing disclosure policies.

[Sponsored by Deputy Under Secretary of Defense Advanced Systems and Concepts] ★

Efficient Linearization of Microwave Power Amplifiers

J.X. Qiu,¹ D.K. Abe,¹ T.M. Antonsen, Jr.,^{2,3} B.G. Danly,¹ B. Levush,¹ and R.E. Myers⁴

¹*Electronics Science and Technology Division*

²*University of Maryland*

³*SAIC*

⁴*ATK*

Introduction: The growing use of multiple-carrier, complex (multi-level, multi-phase), spectrally efficient waveforms such as quadrature-amplitude-modulation (QAM) and code division multiple access (CDMA) in communication systems is placing a growing demand on the power efficiency and linearity of microwave power amplifiers. Continuing reliance on vacuum elec-

tronics amplifiers such as traveling-wave tube amplifiers (TWTA) in space-based transponders and ground terminals requires tube designers to constantly develop new techniques to improve the efficiency and linearity of devices. To satisfy performance requirements, there is an increasing trend of designers incorporating pre- or post-linearization modules with the power amplifiers to improve overall system efficiency and linearity.¹ Signal predistortion is a simple and effective linearization technique that has been used successfully for both solid-state power amplifiers (SSPA) and TWTAs.

The most commonly used predistortion linearization scheme is an analog predistortion linearizer utilizing a third-order nonlinearity. The nonlinearity is usually realized with either two anti-parallel diodes, an FET channel, or a low-power solid-state amplifier driven into compression. Third-order linearizers are reasonably effective at suppressing nonlinear distortion at low drive powers. Close to saturation, however, a higher-order nonlinearity is necessary for effective linearization. Predistortion linearizers with individually adjustable coefficients up to the fifth-order have been reported in the literature, but they are considerably more complex than third-order linearizers. Furthermore, it is prohibitively difficult to extend such a configuration much beyond a fifth-order implementation. We have developed a novel technique for realizing predistortion linearizers with orders greater than or equal to five using cascaded third-order linearizers.² The advantage of this approach is the relative simplicity of the third-order modules and the extensibility of the technique to cost-effective, arbitrarily higher-order nonlinearities.

Cascaded Third-Order Linearization: A baseband block model for a predistortion linearizer with both third- and fifth-order nonlinearities is shown in Fig. 6(a). A third-order linearizer has only the third-order term. A fifth-order linearizer has both the third- and fifth-order terms, which are independently adjustable. The challenge in construction of a fifth- or higher-order linearizer is to obtain the corresponding independently adjustable nonlinear components. The degree of difficulty increases exponentially with the degree of nonlinearity.

To simplify the realization of a fifth-order linearizer, two third-order linearizers can be placed in cascade to obtain both a third-order nonlinearity and a fifth-order nonlinearity (Fig. 6(b)). The appropriate amplitudes and phases of the third- and fifth-order components can be obtained by simultaneously adjusting the third-order coefficients of the two cascaded linearizers. To realize functions with nonlinearities higher than fifth-order, three or more third-order linearizers can be cascaded.

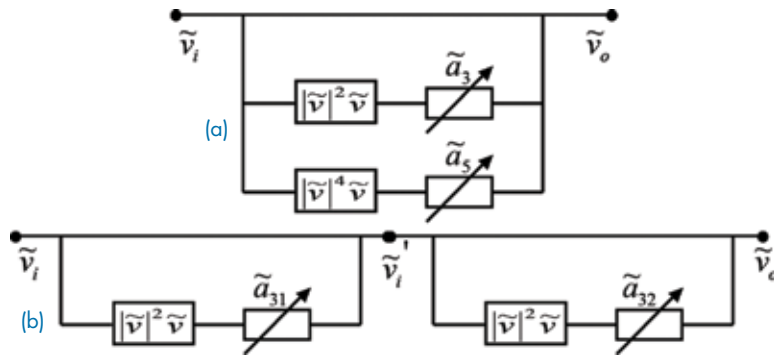


FIGURE 6 Baseband block model of predistortion linearizers. (a) A conventional parallel path linearizer with up to a fifth-order nonlinearity; (b) two cascaded third-order linearizers.

Experimental Verification: The effectiveness of cascaded third-order linearization was tested with five TWTs covering L-, C-, Ku- and Ka-band frequencies:

- L-band: Hughes 8537H helix TWT, 80 W CW, 1.53–1.65 GHz.
- C-band:
 - NRL/Northrop Grumman helix TWT, 140 W, 4–6 GHz.
 - Varian VZC6961K1 helix TWT, 40 W, 4–8 GHz.
- Ku-band: CPI VTU-6397 helix TWT, 13–14.75 GHz, 600 W.
- Ka-band: CPI VTA-6430 coupled-cavity TWT, 28–30 GHz, 500 W.

With the exception of the C-band Varian VZC6961K1, all of the TWTs were designed for communication applications (Fig. 7). The nonlinear code CHRISTINE was used to simulate the helix TWTs and CHRISTINE-CC was used to simulate the coupled-

cavity TWT. The measured small- and large-signal performance of all the TWTs was in good agreement with the simulations.

Different types of waveforms relevant to communications applications were used for testing. They included single-tone, two-tone, and digitally modulated waveforms. The waveforms were generated in baseband with an Agilent E4438C vector signal generator. Predistortion was applied to the baseband waveforms before they were up-converted to the appropriate in-band microwave frequencies of the TWTs.

Depending on the test waveform, different metrics were used to evaluate the performance of the linearization schemes. These metrics include AM/AM conversion (characterizing the change in the amplitude of the output power as function of the amplitude of the input power) and AM/PM conversion (characterizing the change in the phase angle of the output waveform as a function of the amplitude of the input power) for single-tone waveforms; intermodulation distortion

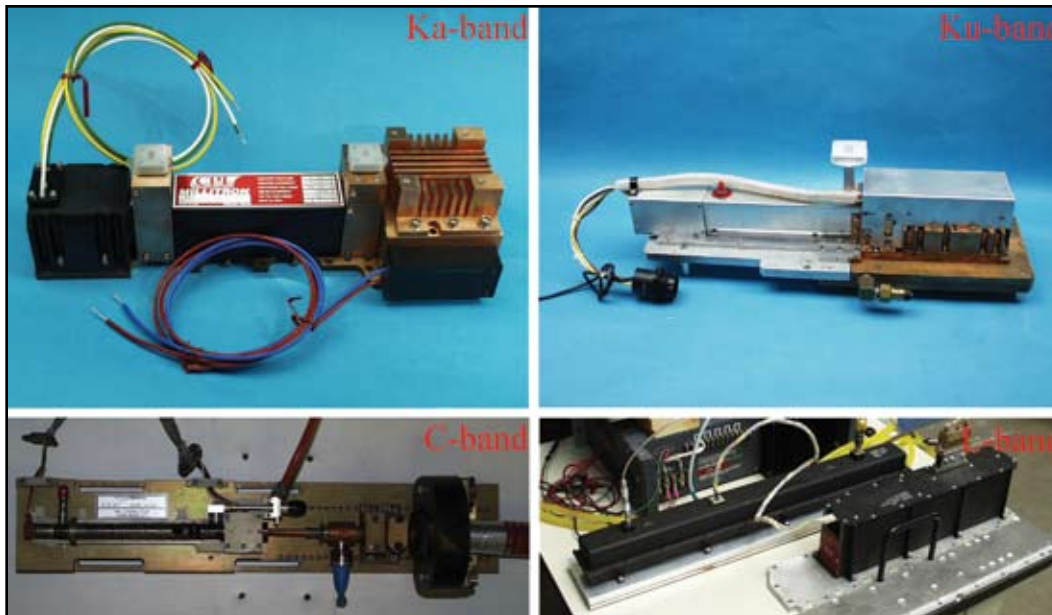


FIGURE 7 The four communication TWTs used in the evaluation of different predistortion schemes.

(generation of unwanted frequency components corresponding to the sum and difference of the driven frequencies) for two-tone waveforms; and adjacent-channel-power-ratio and error-vector-magnitude for digital waveforms. For all of the evaluation metrics, the improvement in gain compression through the use of linearization, in general, and the further improvement of fifth-order relative to third-order linearization are clearly demonstrated. Also note that there is almost no difference in performance between the fifth-order and cascaded third-order linearization functions, verifying that the cascaded third-order nonlinearity implementation functions as an efficient fifth-order nonlinearity generator.

Digital communication systems use advanced digital modulation techniques to increase spectral efficiency, to provide multiple access, and to improve reliability and anti-jamming capability. The presence of nonlinearities in the system not only degrades system performance but also generates spectral re-growth that can cause interference with neighboring systems. In Fig. 8, the spectra of 32-QAM waveforms measured at the output of the Varian C-band TWT are shown for the un-predistorted case and the third-order, fifth-order, and cascaded third-order predistorted cases. The presence of pedestals on the sides of the main lobe is an indication of spectral regrowth leading to potential interference with adjacent communications bands. In the figure, one can see the benefit of applying third-order predistortion, as it lowers the height of the pedestals by about a factor of ten. An additional factor of ten improvement can be observed for both the fifth-order and cascaded third-order linearization making a total of a hundred-fold improvement over the un-predistorted case.

Conclusion: We have developed a simple and efficient technique for realizing fifth- or higher-order predistortion linearization functions using cascaded third-order nonlinearities. The performance of two cascaded linearizers was experimentally demonstrated to be similar to that of a pure fifth-order implementation. The use of third-order modules has the potential advantage of being simpler to implement in hardware, and the cascading technique is, in principle, readily extensible to the implementation of cost-effective, arbitrarily higher-order linearizers.

[Sponsored by ONR]

References

- ¹ A. Katz, "Linearization: Reducing Distortion in Power Amplifiers," *IEEE Microwave Magazine* 2(4), 37-49 (2001).
- ² J.X. Qiu, D.K. Abe, T.M. Antonsen, Jr., B.G. Danly, B. Levush, and R.E. Myers, "Linearizability of TWTAs Using Predistortion Techniques," *IEEE Transactions on Electron Devices* 52(5), 718-727 (2005). ★

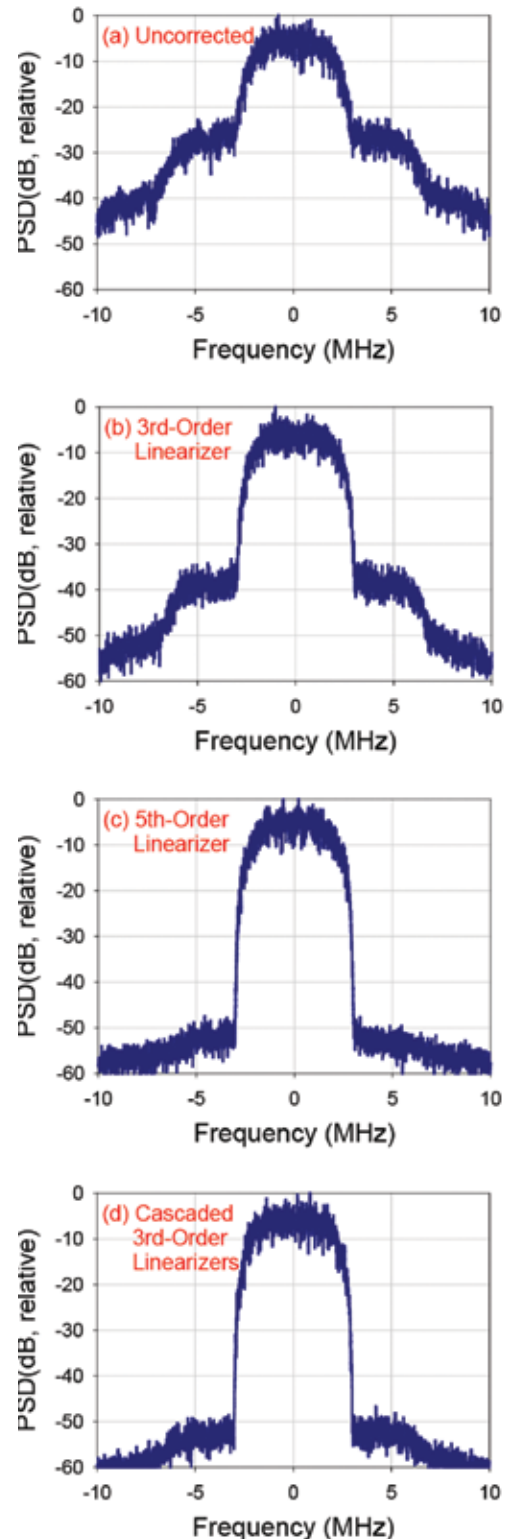


FIGURE 8 32-QAM spectra for the Varian C-band TWT at saturation. (a) No linearization; (b) third-order linearization; (c) fifth-order linearization; (d) cascaded third-order linearization. Note that while the fifth-order and cascaded third-order schemes have similar performance, the cascaded linearizer is simpler to implement.

MATERIALS SCIENCE AND TECHNOLOGY





175 Initial Microstructural Evolution during Friction Stir Welding

R.W. Fonda, J.A. Wert, A.P. Reynolds, and W. Tang

177 3D Unsteady Computations of Flapping Flight in Insects and Fish

R. Ramamurti and W.C. Sandberg

180 Highly Efficient Surface Enhanced Raman Scattering (SERS) Nanowire/Ag Composites

S.M. Prokes, O.J. Glebocki, and R.W. Rendell

Initial Microstructural Evolution during Friction Stir Welding

R.W. Fonda,¹ J.A. Wert,² A.P. Reynolds,³ and W. Tang³

¹Materials Science and Technology Division

²Center for Fundamental Research: Metal Structures in Four Dimensions, Risø National Laboratory,

Roskilde, Denmark

³University of South Carolina

Introduction: Friction stir welding (FSW) has become an important new technique for joining aluminum alloys. In FSW, a rotating tool is plunged into the solid metal, heating it sufficiently (without melting) that the surrounding metal can be “stirred” together into a solid joint. Despite the commercial success of this technique, many fundamental aspects of this welding process remain poorly understood. To address this lack of understanding, we have made the first-ever friction stir welds in a single crystal and quenched the end of the weld to “freeze-in” a static representation of the dynamic deformation field surrounding the tool. The single crystal starting material ensures that the FSW process is directly responsible for all the grain boundary generation and crystallographic texture evolution observed in the weld (except that from conventional recrystallization). Thus, this study is uniquely designed to reveal the initial stages of grain boundary development and texture evolution that occur during FSW.

The Friction Stir Weld Samples: An aluminum single crystal was friction stir welded in four different directions for this study (see Fig. 1). Upon completion of the welds, the tool was withdrawn and the end of the weld was immediately quenched in an attempt to preserve the microstructure surrounding the tool. The regions ahead of the welding tool were polished at the plate mid-thickness and examined in a scanning electron microscope using electron backscattered diffraction. This analysis focused on the evolution of grain structure and texture during FSW and thus excluded

the large conventionally recrystallized grains, which are not typically observed in friction stir welds.

Texture Evolution: The stirring action of the rotating welding tool introduces a corresponding rotation in the surrounding material, as shown in the pole figures at the bottom of Fig. 2. Small rotations develop in a continuous manner from the original single crystal orientation. These rotations continue until a specific terminal orientation, indicated with a star, is achieved. This terminal orientation aligns the $\{111\}$ crystal planes, which are the most densely packed planes and thus the planes along which slip occurs, with the shear plane of the deformation field. For this weld, a rotation of about 50° was required to align these planes. Once the $\{111\}$ planes are aligned with the shear field, further deformation can be accommodated by repeated slip of those planes without the necessity for any further crystal rotation. This texture evolution was observed in all the weld orientations.

The texture evolution in a weld made perpendicular to the one discussed above exhibited an additional and surprising characteristic (see Fig. 3). Most of the initial texture evolution was similar to that discussed above, with the pink single crystal orientation evolving towards a darker pink and eventually a blue terminal orientation. However, thin deformation bands with a different pink orientation developed *by rotating counter to the prevailing deformation field* until achieving a green terminal orientation. This counter-rotation aligns the $\langle 110 \rangle$ crystal direction, the prevalent slip direction for face-centered cubic materials such as aluminum, along the shear direction of the deformation field.

The texture observed near the tool is characteristic of high-temperature, high-strain deformation of aluminum and has previously been observed in friction stir welds. The severe conditions that produced this texture have also removed any correlation to the texture from which it developed.

Grain Boundary Generation: The deformation introduced during FSW is inhomogeneous, causing

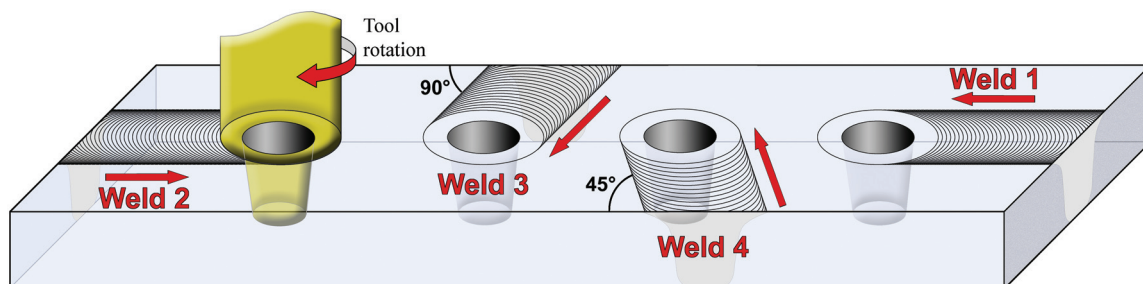


FIGURE 1

Schematic of the FSW process and the four weld orientations examined in this study.

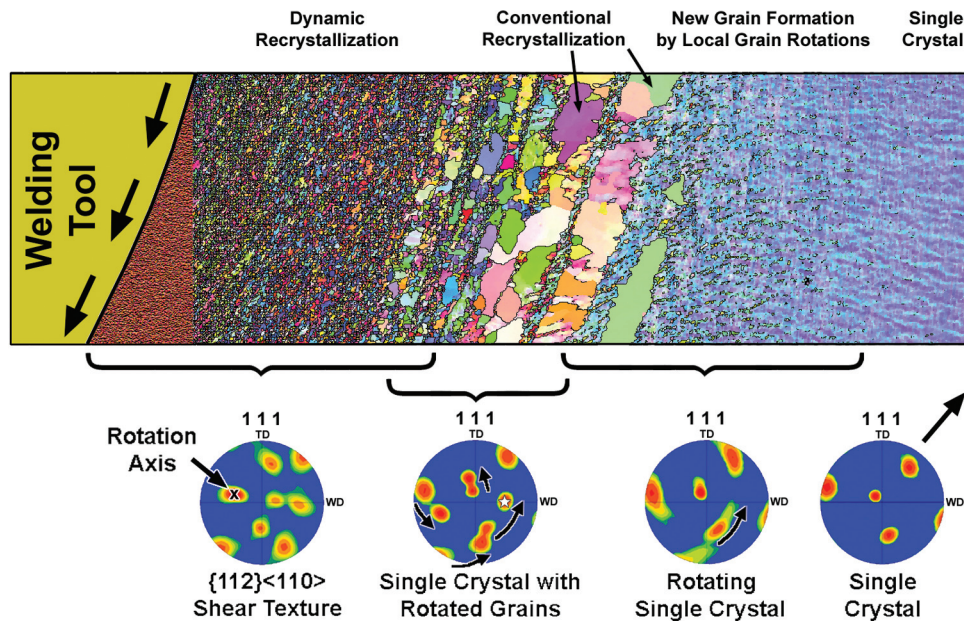


FIGURE 2 Electron backscattered diffraction scan of the region ahead of the tool in Weld 3. Colors represent crystal directions and black lines indicate grain boundaries with at least 15° misorientations. Pole figures at the bottom reveal the crystallographic texture evolution of the small grains; labels at the top indicate different regions of grain/texture evolution.

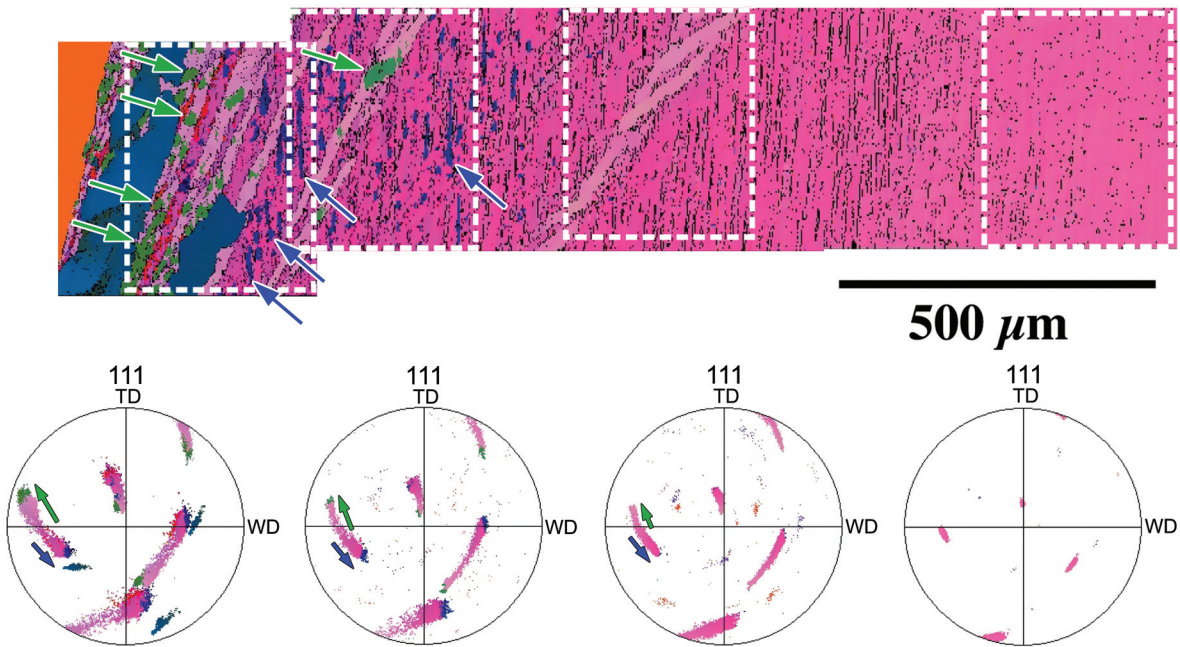


FIGURE 3 Electron backscattered diffraction scan of the outer weld-affected regions ahead of the tool in Weld 2 and pole figures from the boxed regions. Colors indicate orientations and are consistent between image and pole figures, while black lines indicate misorientations $\geq 15^\circ$. Blue arrows indicate terminal orientations from the normal rotation while green arrows indicate the terminal orientations from the counter-rotation.

some regions to rotate relative to others and thus develop misorientations between those regions (see Figs. 2 and 3). These small misorientations give rise to a modulated appearance of the single crystal. The rotated regions continue to develop in both size and misorientation as the tool approaches and the welding deformation increases, generating distinct grains within the single crystal. If these new grains are not already aligned with the shear deformation field (e.g., as in Fig. 2, where the grains are perpendicular to the deformation field), the grains rotate in response to that deformation in order to align with the deformation field.

Summary: This study represents the first-ever investigation of friction stir welds in a single crystal material, and is crucial for understanding the fundamental processes that occur during this welding process. By “freezing-in” the microstructure surrounding the welding tool, we were able to determine the initial mechanisms of texture evolution and grain boundary development that occur during FSW. The shear deformation generated by the welding process gradually rotates regions of the single crystal, which grow in size and misorientation as the welding deformation continues. This rotation continues until these new grains achieve an easily-sheared orientation. Some regions of the weld may even rotate counter to the prevailing deformation field in order to achieve such an orientation. As the tool advances, the new grains gradually rotate to align with the deformation field.

Further development of this grain structure and texture has been obscured by conventional recrystallization and severe deformation near the tool. Additional studies are required to determine the processes of grain boundary evolution and texture evolution that occur after these initial stages.

[Sponsored by NRL and ONR]



3D Unsteady Computations of Flapping Flight in Insects and Fish

R. Ramamurti and W.C. Sandberg
Laboratory for Computational Physics and Fluid Dynamics

Introduction: The flight of insects and birds and the swimming of fish have been sources of continuous fascination throughout the ages. Observation and controlled experimentation have historically been the main sources of information on performance. The mathematical description of the performance of flying creatures has been limited, due to the previously insurmountable difficulties associated with describing

flapping wings with changing shape. Typical analytical descriptions are generally for steady flight only. Recent computational technology developments have enabled three-dimensional unsteady computations^{1,2} to be successfully completed for flapping wings and deforming shapes. 3D unsteady computations, coupled with appropriate experiments, can now provide a more complete view of the fluid dynamics underlying the remarkable aerodynamic and hydrodynamic feats observed in insects, birds, and fish. If we seek to attain that level of performance in our designed vehicles, we still have much to learn. This paper briefly summarizes some attempts we have made at the Naval Research Laboratory (NRL) to gain insights into the unsteady aerodynamic performance of flying insects and swimming fish, and to incorporate that understanding into the design of unmanned underwater vehicles and unmanned air vehicles.

Underwater Flight: Our choice for a computational investigation of fin swimming was the bird wrasse (*Gomphosus varius*), shown in Fig. 4. This fish is reported to have excellent low-speed maneuverability and good high-speed propulsion—characteristics we are very interested in having in our vehicles. These fishes have been observed to fly underwater by flapping their pectoral fins with a motion that resembles the wing kinematics of certain flying insects. 3D unsteady computations were carried out for the wrasse with its pectoral fins executing the shape deformation time-history obtained from the measured fin kinematics. Figure 5 shows an instantaneous pressure distribution and the time history of lift and thrust production throughout several stroke cycles. An important objective, as we study the flow field evolution about the flapping fin and attempt to gain insights into the force production mechanism underlying the impressive dynamic performance of these living creatures, is to understand how variation of major design parameters changes the force production dynamics. For example, how important is the precise deformation time history of the fin for acceptable force production? Since the underwater vehicle design community has an aversion to deformable materials we need to understand what performance is sacrificed if we significantly alter the ability of the fin to deform. Our computations show that substantial penalty is incurred if we restrict the deformation of the fin. Detailed discussion of these results can be found in Ref. 3.

Maneuvering Insects: In addition to underwater vehicles we are also interested in the development of small unmanned air vehicles, referred to as Micro Air Vehicles (MAVs). We chose to pursue the fruit fly, *Drosophila*, for computational investigations since detailed wing kinematics and corresponding force data

FIGURE 4
Bird wrasse in natural environment.

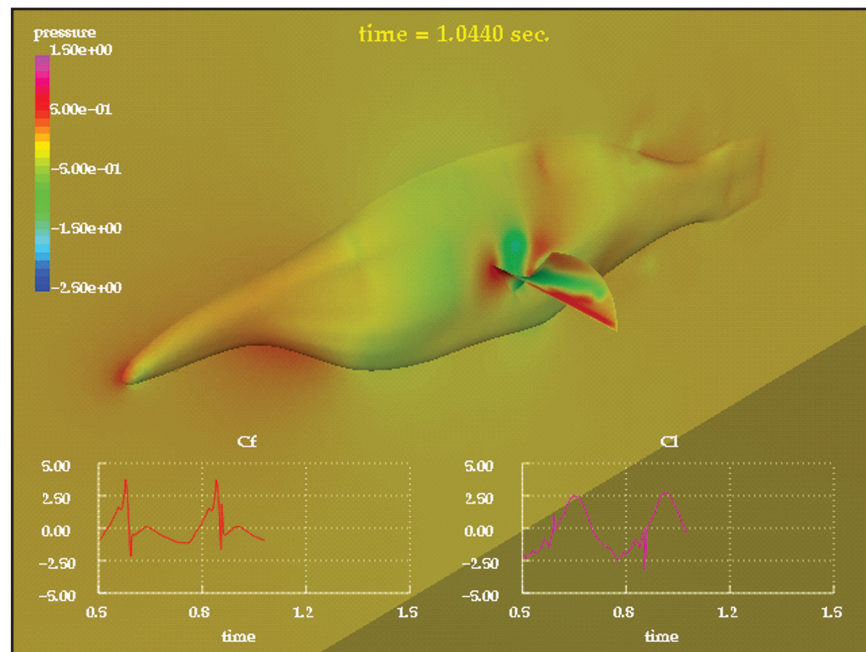


FIGURE 5
Surface pressure distribution, thrust, and lift time histories for a swimming bird wrasse.

were available. The lift, thrust, and drag time histories and wing flow field evolution were computed about a single wing executing specified kinematics. The results of these computations were compared with experimental data and were extremely good. Since we must not be content with only good hovering or straight-ahead flight, we also considered the vehicle's ability to avoid obstacles. The motion of the fruit fly *Drosophila* involves several successive sharp turns called *saccades*. Since detailed kinematics and force measurements also exist for the *Drosophila* undergoing these turning maneuvers, we computed the flow over the wing and the body during the maneuver for the complete two-wing and body, with specified kinematics. The differences in the kinematics between the right and left wings show that subtle change in stroke and deviation

angles can result in the yaw moment required for the turning maneuver. The origin of the yaw moment is investigated by computing the center of pressures on each wing and the individual moment arms. This investigation⁴ leads to the conclusion that it is the forward force and a component of the lift force that combine to produce the turning moment while the side force alone produces the restoring torque during the maneuver. The vorticity shed from the wing's leading edge and the tips (Fig. 6) show a loop-like structure that during stroke reversals pinches off into Λ -like structures that have not been previously observed in the wakes of flapping fliers.

Unmanned Vehicles: We have computed the unsteady dynamics about the rigid wing of a flapping

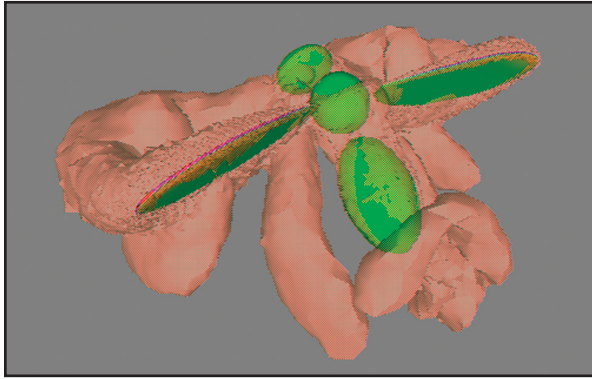


FIGURE 6
Contours of iso vorticity shed from the wings of *Drosophila* during maneuver.

fruit fly and about the deforming pectoral fin of a swimming bird wrasse. The unsteady computations have been compared with experimental data and found to be in excellent agreement. Based on these computations and realizing that birds and insects do not have substantial fixed lifting surfaces unrelated to propulsion and control, the Tactical Electronic Warfare Division at NRL developed a vehicle, the Biplane Insectioid Travel Engine (BITE), that has no fixed lifting surface but uses two tandem sets of clapping pairs of reversing camber wings. The reversing camber flapping wing has proven to be a versatile mechanism for producing thrust/lift without copying the insects' flying configurations directly. Computational studies (Fig. 7) show that the BITE-wing configuration is capable of producing sufficient thrust and lift using four reversing-camber tandem clapping wings. This configuration is amenable

to some form of vortex capture mechanism, as seen in fruit flies and other two-winged insects. An underwater counterpart with flapping deforming fins is also being developed at NRL in collaboration with Dr. B. Ratna of the NRL Center for Bio/Molecular Science and Engineering.

Acknowledgments: This work was supported by the Office of Naval Research through the NRL Undersea Warfare Focus Area Swimming Vehicles Project with Dr. Edward Franchi as the Technical Monitor, and the NRL Tactical Electronic Warfare Division Micro Air Vehicles Program with Dr. Jim Kellogg as the Technical Monitor. The authors would like to thank Prof. Rainald Löhner of George Mason University for his support. The computations were supported in part by a grant of HPC time from the DoD HPC centers ARL MSRC SGI-O2K and NRL SGI-O2K.

[Sponsored by ONR]

References

- ¹R. Ramamurti and W.C. Sandberg, "A 3-D Computational Study of Aerodynamic Mechanisms of Insect Flight," *J. Exp. Biol.* **205**, 1507-1518 (2002).
- ²R. Ramamurti, W.C. Sandberg, R. Löhner, J.A. Walker, and M.W. Westneat, "Fluid Dynamics of Flapping Aquatic Flight in the Bird Wrasse: Three-dimensional Unsteady Computations with Fin Deformation," *J. Exp. Biol.* **205**, 2997-3008 (2002).
- ³R. Ramamurti and W.C. Sandberg, "The Influence of Fin Rigidity on the Force Production in the Bird-Wrasse: A Computational Study," NRL Memorandum Report 6410--04-8840, November 2004.
- ⁴R. Ramamurti and W.C. Sandberg, "A Computational Investigation of the Three-dimensional Unsteady Aerodynamics of *Drosophila* Hovering and Maneuvering," *J. Exp. Biol.* **210**, 881-896 (2007). ★

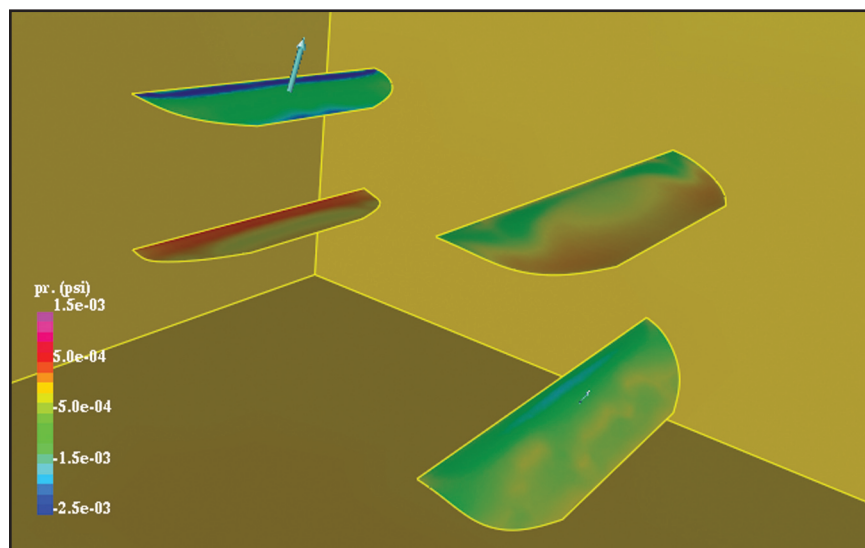


FIGURE 7
Surface pressure on the wings of the BITE vehicle at maximum lift.

Highly Efficient Surface Enhanced Raman Scattering (SERS) Nanowire/Ag Composites

S.M. Prokes, O.J. Glembocki, and R.W. Rendell
Electronics Science and Technology Division

Introduction: Optically based sensing provides advantages over electronic sensing because optical spectra can uniquely fingerprint a chemical compound, significantly reducing false alarms and simplifying the detection process. In addition, light can easily be directed over long distances, enabling remote sensing. One of the most promising optical sensing techniques is surface enhanced Raman scattering (SERS). In Raman scattering (RS) of light from a chemical of interest, the vibrational modes in the chemical red-shift the frequency of the scattered light, producing a spectrum characteristic of that molecule. Ordinary Raman scattering cross-sections are very small, resulting in low sensitivity (10^{-8} of the intensity of the exciting laser); this is not a problem for most solids and liquids, because of the large numbers of molecules or atoms exposed to the laser light, but in the case of trace amounts of molecules in gases or liquids, detection through ordinary Raman scattering is virtually impossible. However, SERS enhances the Raman signal by many orders of magnitude by the use of a substrate of metal nanoparticles.¹ The SERS enhancement of molecules adsorbed on the roughened metal surface is caused by local electromagnetic fields that are created by the laser excitation of surface plasmons at the metal surface. Even larger SERS effects can be produced by local “hot spots” in the electric fields, produced by interactions of localized plasmons on adjacent or neighboring nanoparticles.² Although the SERS effect has been recognized for a long time, a full understanding of the phenomenon has not yet been achieved. This lack of understanding limits its application potential, as it is difficult to produce highly sensitive, inexpensive, and repeatable SERS substrates. To address these issues, we have developed a new SERS substrate material consisting of dielectric/Ag metal shell nanowires that exhibit high SERS sensitivity due to their plasmonic coupling. These nanowires are sensitive at low concentrations, quite repeatable, and inexpensive to produce.

Technical Approach: The growth of the Ga_2O_3 nanowires was performed by vapor-liquid-solid (VLS) growth in a tube furnace, using Si(100) and Si(111) substrates and a 20 nm Au film.³ Ga (99.995% purity) and oxygen were used as the source materials and the growth was performed at 900 °C at a vacuum of 10^{-2} Torr. The Ag shell coating was deposited via e-beam evaporation under high vacuum conditions. The SERS sensitivity of the nanowire substrates has been determined using Rhodamine 6G/methanol and

DNT/methanol dilutions. The $\text{Ga}_2\text{O}_3/\text{Ag}$ nanowire composite substrates are shown in Fig. 8(a). As can be seen, they consist of a dense random 3D network of crossed wires. A comparison of the SERS signal from 0.2 picograms of Rh6G for the nanowire composite substrates and a commercially available SERS substrate (Klarite) from Mesophotonics Ltd is shown in Fig. 8(b). As shown, no SERS signal is evident in the case of the commercial Mesophotonics sample, while a strong SERS signal is clearly seen for the nanowire composites. From these results, the nanowire/Ag composite substrate can repeatedly exhibit an enhancement which is roughly two orders of magnitude higher than the commercially available SERS substrate.

The SERS of Rh6G, using the nanowire/metal random 3D arrays, has also been measured to be several orders of magnitude more sensitive than other SERS substrates, such as Ag nanosphere arrays produced by the Tollen’s reaction, SiO_2/Ag nanosphere composites, polystyrene/Ag nanosphere composites, and roughened metal surfaces. In addition, these wires have exhibited sensitivity to DNT—which has a very low vapor pressure and is thus difficult to detect—better than picograms (shown in Fig. 9); this is the first reported SERS measurement of DNT using Ag metal nanostructures.

Furthermore, these nanowire composites can easily be removed from the substrate by sonication in an ethanol solution, and show an enhanced SERS signal even when deposited in a significantly dilute form. This opens up the possibility of covert tagging and tracking applications.

The most intriguing result from this work indicates that randomly crossed wires increase the SERS enhancement in the vicinity of the regions where wires cross, as shown in Fig. 10(a). The effect on the plasmon resonance by wire crossings can be modeled using a finite element Comsol⁴ simulation of the electric field near two 45-nm-diameter Ag crossed wires in response to light polarized in the x-direction (Fig. 10(a)). The crossing of the nanowires leads to coupled plasmon behavior that spatially extends the sensitivity of the nanowires to encompass the regions between the wires and significantly beyond the wires. This would not only enhance the SERS effect due to the strong coupling, but also allow more molecules to enter this high electric field region, thereby enhancing the SERS sensitivity. In the case of two Ag nanospheres of the same diameter, the enhancement spatial extent is significantly smaller, as shown in Fig. 10(b). In addition, the nanosphere geometries require a very specific spacing in order to maximize the enhancement due to coupling, which is not the case in crossed wires, since an optimal spacing is always present for every crossing angle due to the wire geometry. As a simple rule of thumb, the sensitivity regions for the wires are within a sphere whose diameter is the length of the longest wire, which is a

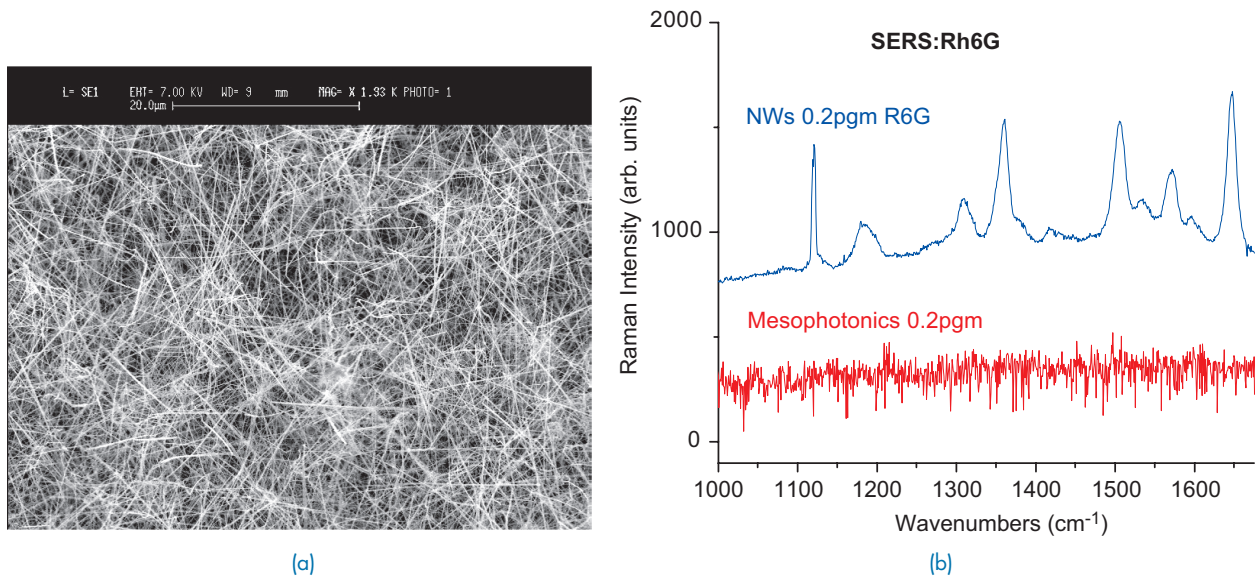


FIGURE 8 (a) Ga₂O₃ core/Ag shell nanowire composite and (b) comparison of SERS signal for Mesophotonics “Klarite” commercial substrate and Ga₂O₃/Ag nanowires.

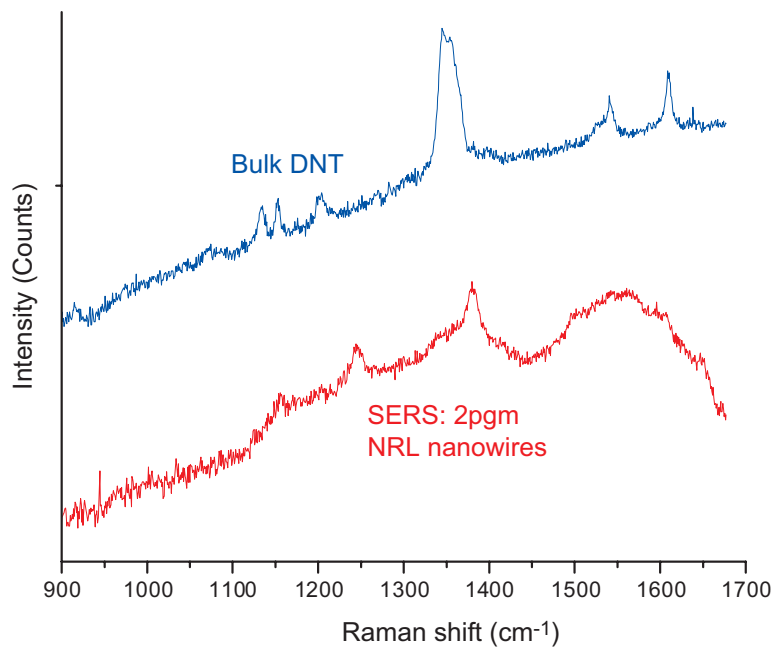
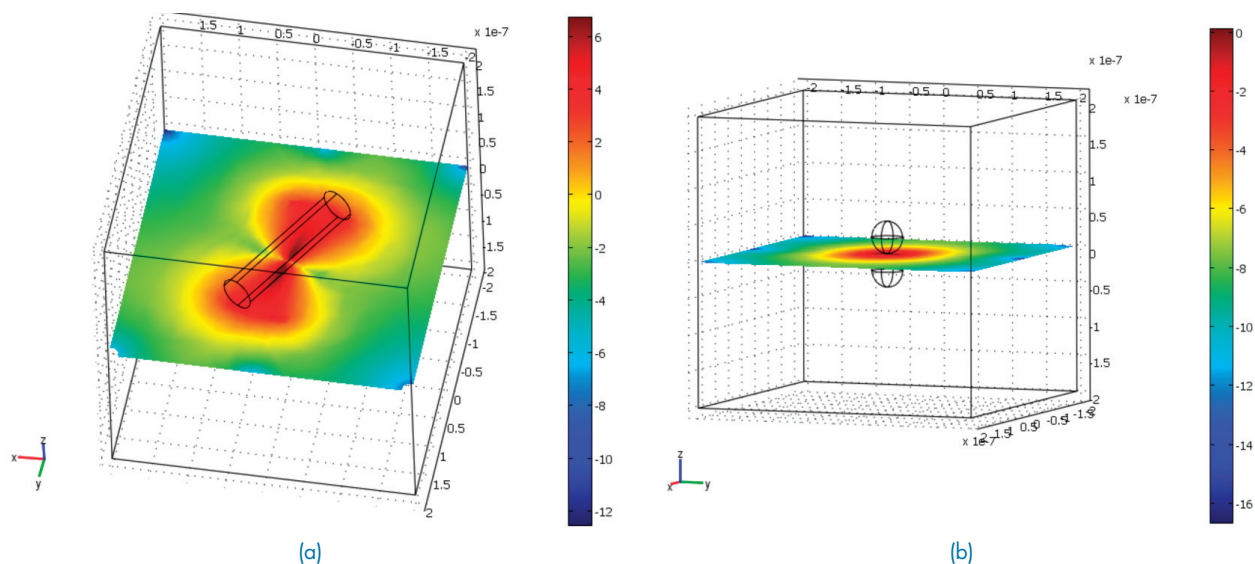


FIGURE 9 Raman spectrum of bulk DNT and a SERS spectrum of 2 picograms of DNT obtained from the dielectric/Ag nanowires.

**FIGURE 10**

Comsol electric field simulations for (a) Ag crossed nanowires and (b) same diameter Ag nanospheres. Note the much larger area of enhancement in the case of the nanowires.

significant improvement over nanosphere-type SERS substrates.

Conclusion: Randomly oriented $\text{Ga}_2\text{O}_3/\text{Ag}$ nanowire networks have been formed and we have shown that these substrates result in highly sensitive SERS signals using Rhodamine 6G as well as DNT. It is suggested that this SERS sensitivity is due to the formation of a large number of “hot spots” (enhanced electric fields due to plasmon coupling) when arranged in a random crossing geometry. Finite element calculations show significantly enhanced electric fields in the regions of the wire crossing, as well as surrounding the crossed wires, in support of the experimental results.

Due to these highly efficient hot spot regions formed by the crossing of the nanowires, we have also

demonstrated that large SERS enhancements are possible even when the density of the nanowire network is significantly reduced. Since these wires can be deposited at low concentrations on any substrate and any size area, they have potential in applications such as large area sensor arrays, covert tagging, and remote sensing.

[Sponsored by ONR]

References

- ¹ M. Fleischman, P.J. Hendra, and A.J. McQuillen, *Chem. Phys. Lett.* **26**, 163 (1974); D.L. Jeanmaire and R.P. van Duyne, *J. Electroanal. Chem.* **84**, 1 (1977).
- ² J.B. Jackson, S.L. Westcott, L.R. Hirsch, J.L. Wet, and N.J. Halas, *Appl. Phys. Lett.* **82**, 257 (2003).
- ³ S.M. Prokes, W.E. Carlos, and O.J. Glembocki, *Proc. of SPIE* **6008**, 60080C-1 (2005).
- ⁴ Comsol Multiphysics, Comsol, Inc., www.comsol.com. ★

OCEAN SCIENCE AND TECHNOLOGY





185 Measuring Undersea Noise from Breaking Waves

S.L. Means and M.A. Sletten

187 Real-Time Coastal Monitoring and Prediction for Operations and Research

J.W. Book, P. Martin, M. Rixen, J. Dykes, D. Wang, S. Ladner, M. Tudor, and J. Chiggiato

191 A Roughness Estimation Algorithm for Sidescan

M.L. Gendron, M.C. Lohrenz, G. Layne, and J. Sample

Measuring Undersea Noise from Breaking Waves

S.L. Means¹ and M.A. Sletten²

¹*Acoustics Division*

²*Remote Sensing Division*

Introduction: Breaking waves are ubiquitous on the Earth's oceans and play an important role in air-sea interactions, which are important to global climatological effects. Of particular interest to the Navy, breaking waves can be a dominant source in the undersea ambient noise field. Although breaking waves have been known to be the source mechanism of this sound for some time, most predictive models have been limited to simply associating sound levels to wind speeds. Recently NRL has undertaken simultaneous measurements of the surface expression of breaking waves, via radar and video, and their subsequent acoustic emissions to understand the relationships between characteristics (size, duration, etc.) of individual breaking waves and the generated acoustic noise spectra.

Experimental Setup: The Navy operates a range of offshore towers as a part of a Tactical Air Combat Training System (see Fig. 1). One of these towers, R2, serves as a platform from which we deployed a number of experimental sensors. The tower is located in the shallow waters (25 m) approximately 75 km off the coast of Savannah, Georgia, and extends 50 m above the water surface. The tower is equipped to supply power through solar panels, wind turbines, and a diesel generator. Additionally, it is equipped with two-way microwave communication back to shore. These features allow us to make long-term measurements while controlling the data acquisition from our offices at NRL via the Internet.

In early January 2006, we placed a bottom-moored vertical array of 32 hydrophones 100 m north of the tower. A cable connecting the array to the tower supplied power and transmitted the acoustic signals for acquisition. In addition to the hydrophone array, a high-resolution digital video camera and a dual-polarized, coherent, X-band radar were mounted on the tower to observe the ocean surface above the array.

Acoustic-Video-Radar Associations: To date, measurements have been made when wind speeds ranged from 5 to 21 m/s and when wave heights were between 1 and 3.4 m. The acoustic array data were processed to listen to the waves breaking directly overhead. Figure 2(a) shows an image from the video camera mounted atop the tower. The water surface above the array is visible along with the 20-m² helicopter pad. The region outlined in red represents a 100-m × 100-m area centered over the hydrophone array. The image pixels

within this area are rectified (see Fig. 2(b)) to form a bird's-eye view such that quantitative measurements of the breaking waves can be obtained. We then used detection and tracking algorithms to capture the location and size of the actively breaking portions of individual breaking waves as a function of time. It is this active portion of the breaking waves that gives rise to acoustic radiation. Figure 3(a) shows a time-frequency surface of the sounds generated by the overhead breaking waves. Each breaking event produces a broadband burst of energy that lasts less than a couple of seconds. At the top and bottom of this figure, the occurrences of the breaking waves, as obtained through video processing, have been inserted as white lines. Although not perfect, a good agreement can be seen between the acoustic and video occurrences of breaking events. Further analysis will allow us to develop empirical relationships between the acoustic energy and the size of the surface expression of the breaking waves.

Comparison of the radar backscatter cross-sections from the two polarizations of the radar (transmit and receive antennas vertically polarized, VV; and transmit and receive antennas horizontally polarized, HH) allows the detection of sea spikes, which are radar backscatter events indicative of breaking waves. A sea spike is a scattering event for which the horizontal cross-section is greater than the vertical cross-section, so that their ratio, σ_{HH}/σ_{VV} , is greater than 1. A large body of research conducted over the past three decades has established a strong correlation between sea spikes and hydrodynamically nonlinear features, such as breaking waves, so the sea spike percentage can be used as a good, radar-based indicator of breakers. Similarly, we can process the video images to obtain a measure of the average active whitecap coverage of the actively breaking waves. Both measurements are analogous to the whitecap coverage ratio that is often reported as an indication of breaking wave activity. Both of these measures of breaking wave activity are plotted in Fig. 3(b) for a day in which the wind speed decreased from 13 m/s to 8 m/s. The blue dots show the average active breaking wave coverage obtained through video analysis. The red circles indicate the percentage of occurrences in which the cross-section ratio exceeds 1 for the same time period. Both of the measurements indicate the same general trend as the wind speed decreased over the day.

Summary: The capability to make long-term measurements of breaking waves allows us to obtain empirical relationships that will improve undersea noise predictions under a range of wind speeds and sea states. Additionally, the video measurements will serve to calibrate the radar measurements for better detection of actual breaking waves instead of sea spikes. The

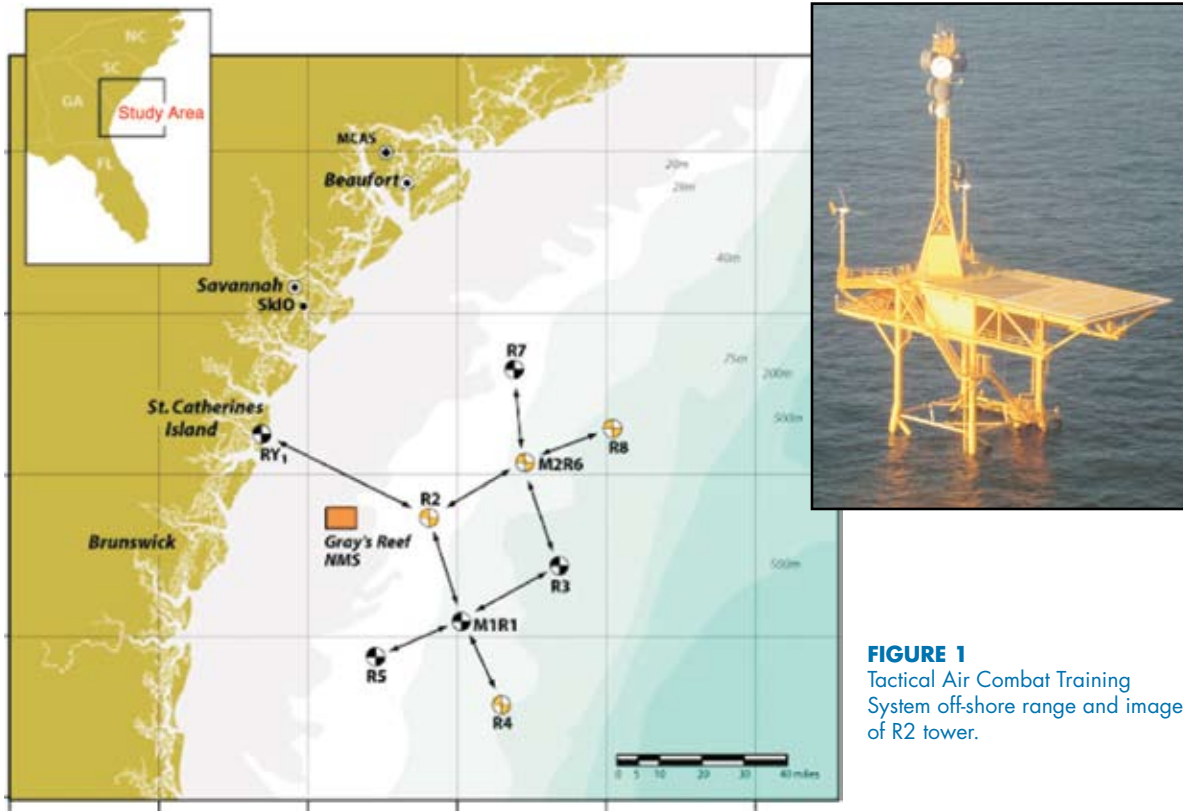


FIGURE 1
Tactical Air Combat Training System off-shore range and image of R2 tower.

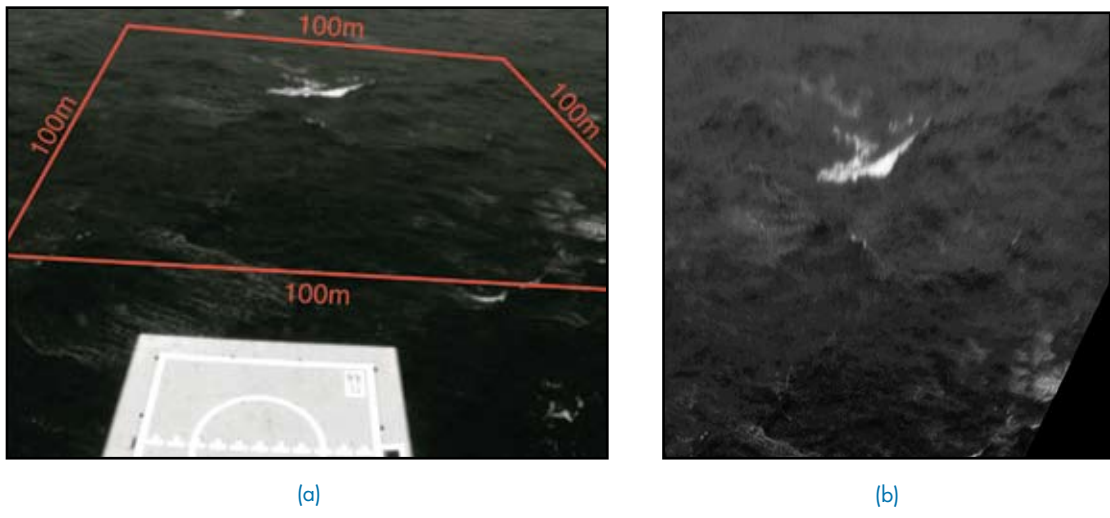


FIGURE 2
(a) Video image snapshot from atop tower. (b) Rectified video image of individual breaking wave.

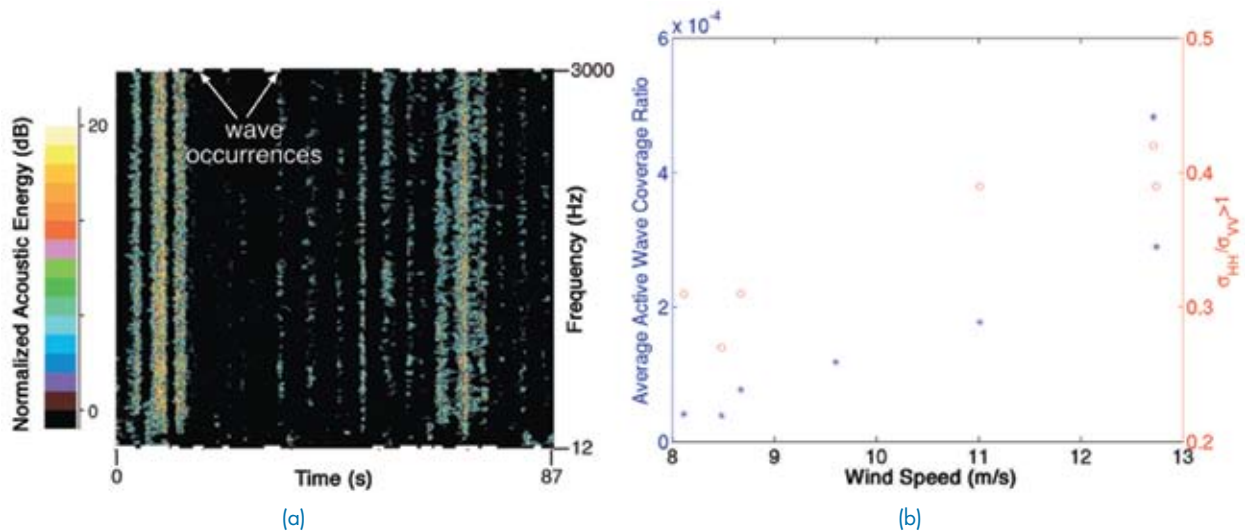


FIGURE 3 (a) Time-frequency surface of breaking wave-generated acoustic signatures and occurrences obtained from video. (b) Average active wave coverage ratio, obtained from video, and percentage of occurrences of sea spikes, obtained from radar backscatter.

improvement of breaking wave detection via radar will serve to improve our understanding of the importance of breaking waves in air-sea interactions.

[Sponsored by ONR]



Real-Time Coastal Monitoring and Prediction for Operations and Research

J.W. Book,¹ P. Martin,¹ M. Rixen,² J. Dykes,¹ D. Wang,¹ S. Ladner,³ M. Tudor,⁴ and J. Chiggiato⁵

¹*Oceanography Division*

²*NATO Undersea Research Centre*

³*Planning Systems Inc.*

⁴*Croatian Meteorological and Hydrological Service*

⁵*Regional Agency for Environmental Prevention in Emilia-Romagna*

Introduction: The coastal ocean is often characterized by vigorous, swiftly evolving fronts and eddies. These features bound waters of different characteristics and can have a high impact on operations and sensor performance. However, their complex dynamics make monitoring and prediction challenging. These features and other environmental conditions must be identified or forecast in near real time so that sampling can be designed to study them and operations can be modified to optimize performance based on their impact. This topic was one of the main research thrusts of a recent Joint Research Project (JRP) between the Naval Research Laboratory (NRL) and the NATO Undersea Research Centre (NURC). In the framework of this JRP, an international, collaborative research effort was developed involving more than 20 different research

groups from seven countries. The research focused on winter and summer experiments in the central Adriatic Sea, an archetypal coastal area for fronts and eddies. NRL, in collaboration with the other institutions, implemented and tested a complete, real-time, coastal monitoring and prediction system during three “Dynamics of the Adriatic in Real-Time” (DART) cruises. Here we describe some tangible results and implications of the real-time monitoring and prediction thrust of this work.

Real-Time Coastal Monitoring: For the DART experiments, a near-real-time, in situ measurement and reporting system was used for adaptive sampling, forecast validation, and demonstration of real-time operational capabilities. The system consisted of satellite remote sensing products, surface drifting floats, and new Shallow-water Environmental Profiler in Trawl-resistant Real-time (SEPTR) configuration moorings. The SEPTRs sit on the ocean bottom with a shape and weight distribution (lower left panel of Fig. 4) designed to resist damage from fishing equipment. A profile is made by a buoy from the SEPTR base to the ocean surface at programmable intervals to transmit previous measurements and then make new measurements throughout the water column while returning to the protective SEPTR base. The SEPTR technology enabled near-real-time monitoring of waves and profiles of ocean velocity, temperature, salinity, and optics in a heavily fished frontal zone.

All the real-time data were collected, processed, and posted to password-protected NURC ftp and web sites accessible to scientists both at land-based laboratories and aboard the NURC ship with a high bandwidth satellite link. In particular, during the first summer

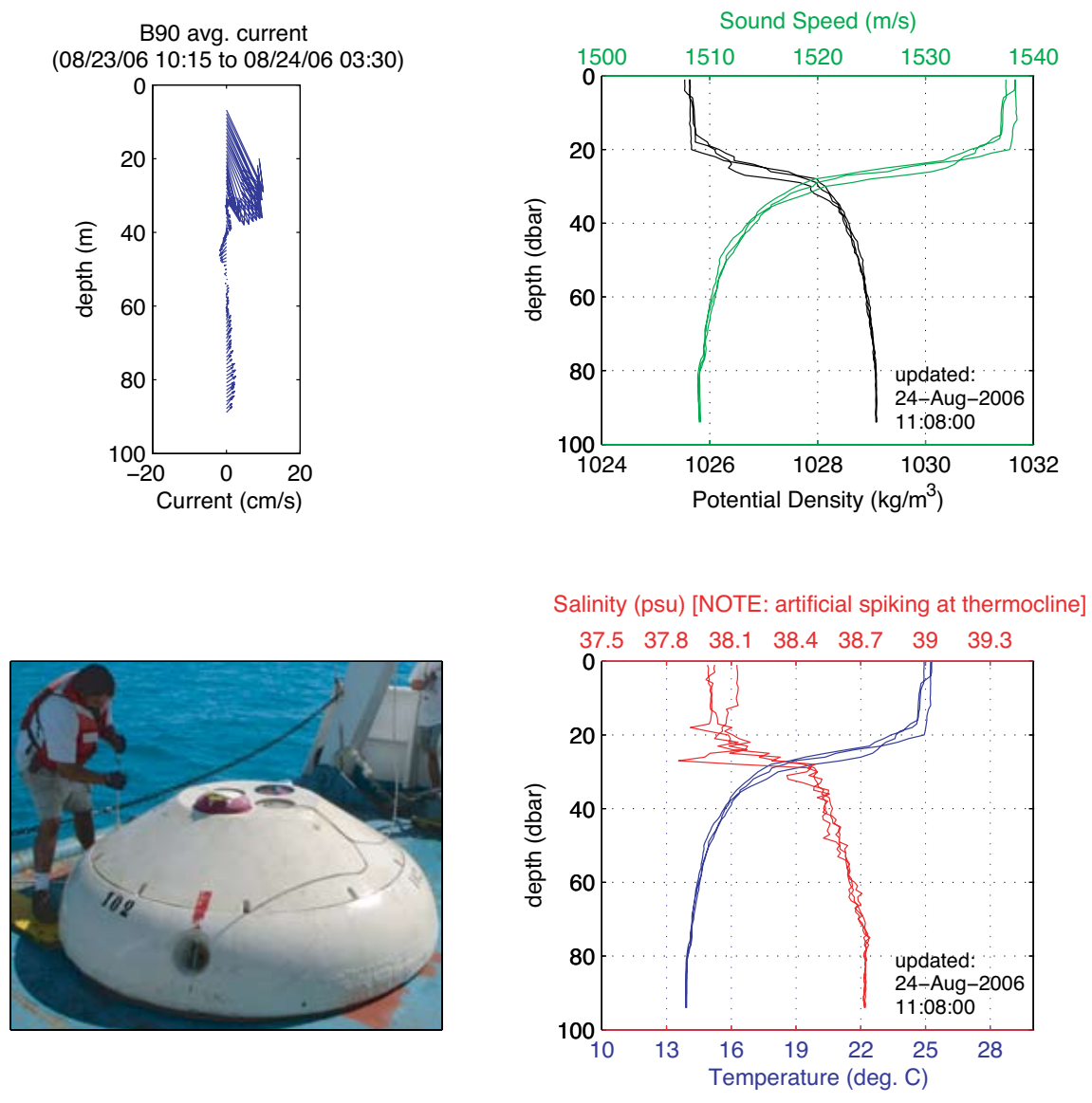


FIGURE 4

A SEPTR mooring and examples of near-real-time data display. Upper left panel and both right panels show the most recent 48 hours of measured and transmitted profiles of ocean velocity, temperature, salinity, density, and sound speed from one SEPTR as of August 24, 2006, 11:08 UTC, in the same form as displayed on the experiment web page. Lower left shows the SEPTR in its trawl-resistant configuration as used on the ocean bottom.

cruise, graphics (e.g., Fig. 4) from three SEPTRs were prominently featured on the experiment web page and updated every measurement cycle (6 hours) showing the last 48 hours of transmitted velocity, sound speed, density, temperature, and salinity profiles. Multiple SEPTR moorings made it possible to track significant mixed-layer depth changes both in time and space.

The real-time measurements successfully improved scientific sampling during the research cruises. Examples include the NURC real-time processing of Advanced Very High Resolution Radiometer sea surface temperature (SST) and Moderate Resolution Imaging Spectroradiometer (MODIS) thermal and ocean-color images used during the winter cruise to identify a rapidly evolving frontal filament for focused sampling. Also, the automatic ftp posting of processed MODIS Terra (AM Orbit) and AQUA (PM Orbit) SST and chlorophyll concentration images by NRL was used to identify several different eddy and current meander events and verify numerical model predictions. In another example, the transmitted velocity data from a SEPTR showed a clear daily pattern of high and low vertical shear caused by the interaction of a mean current and an inertial oscillation, which was an environmental consideration for microstructure turbulence measurements.

Real-Time Coastal Prediction: The second component of the real-time-support thrust of the DART

experiments was the implementation, use, and validation of a wide variety of meteorological, ocean, and wave prediction systems (more than a dozen were used). The products most used for real-time support were from the Navy Coastal Ocean Model (NCOM) and the Simulating Waves Nearshore (SWAN) model run by NRL; the Limited Area Model Italy (LAMI) meteorological model, the Adriatic Regional Ocean Modeling System (AdriaROMS), and the SWAN model run by the HydroMeteorological Service of the Regional Agency for Environmental Prevention in Emilia-Romagna (ARPA-SIM); and the Aire Limitée Adaptation Dynamique développement InterNational (ALADIN) meteorological model run by the Croatian Meteorological and Hydrological Service (CMHS). All these tools provided daily nowcasts and forecasts of the environmental state of the central Adriatic and were used for both short- and long-term planning.

Figure 5 shows an example of the scientific benefit of having accurate forecasts from numerical ocean and meteorological models. Cruise sampling was redesigned to verify the existence and capture the evolution of the predicted (boxed in red) northern anticyclone in this 48-hour ALADIN surface wind and NCOM ocean current and temperature prediction graphic (left panel of Fig. 5). The SEPTRs indeed showed anticyclonic turning (right panel of Fig. 5) and the high-resolution, in situ sampling suggested the presence of colder offshore water being advected onshore as predicted. In

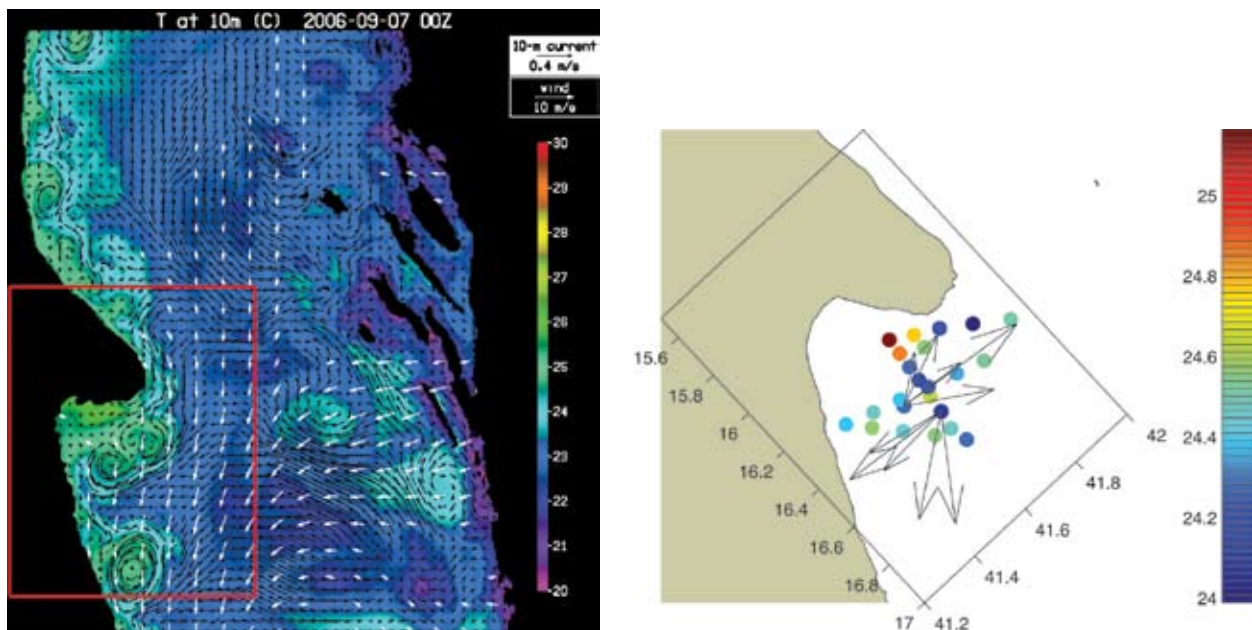


FIGURE 5

Forecast and adaptively sampled environmental conditions. Left panel is NCOM-predicted temperature (color) and ocean currents (black arrows) at 10 m depth and ALADIN surface winds (white arrows) on September 7, 2006, 00 UTC, forecast 48 hours earlier. Twenty-six hours of conductivity, temperature, and depth (CTD) data were collected from a ship (10-m temperature data shown as colored dots in the right panel) starting on September 8, 2006, 18 UTC, and two SEPTRs measured CTD data (10-m temperature data also shown) and velocities (10-m values are black arrows, right panel).

a similar event (not shown), a summer cruise measured a major meander of the coastal current system based on NCOM and AdriaROMS ocean forecasts.

During storm conditions, high-resolution wind and wave forecasts are essential for planning ship operations that are sensitive to sea state. During the final mooring recovery stage of the cruises, 48-hour wave forecasts were provided to the ship for each mooring of interest from the ARPA-SIM runs of LAMI and SWAN (Fig. 6, upper panel). Based on this figure, the ship was redirected to arrive at mooring B50 near forecast hour 27 to take advantage of the predicted short-duration lull in wave activity. As shown by the NRL-run SWAN model in the lower panel, the spatial variability in the forecast for this event was as important as the temporal variability.

Conclusions: The DART experiments showed the power and importance of reporting measurements and providing environmental forecasts to ships in near real time. Without these, the experiments would have been less successful, as many of the frontal events that were the focus of the research effort would have been missed. For operations, high-resolution predictive systems and new, in situ measurement systems can accurately quantify sound speed variations and other environmental impacts in complex frontal regions.

Acknowledgments: Pierpaolo Falco provided the photograph used in Fig. 4. We are grateful for the many and varied contributions of the entire DART international group towards the success of these experiments. [Sponsored by ONR] ★

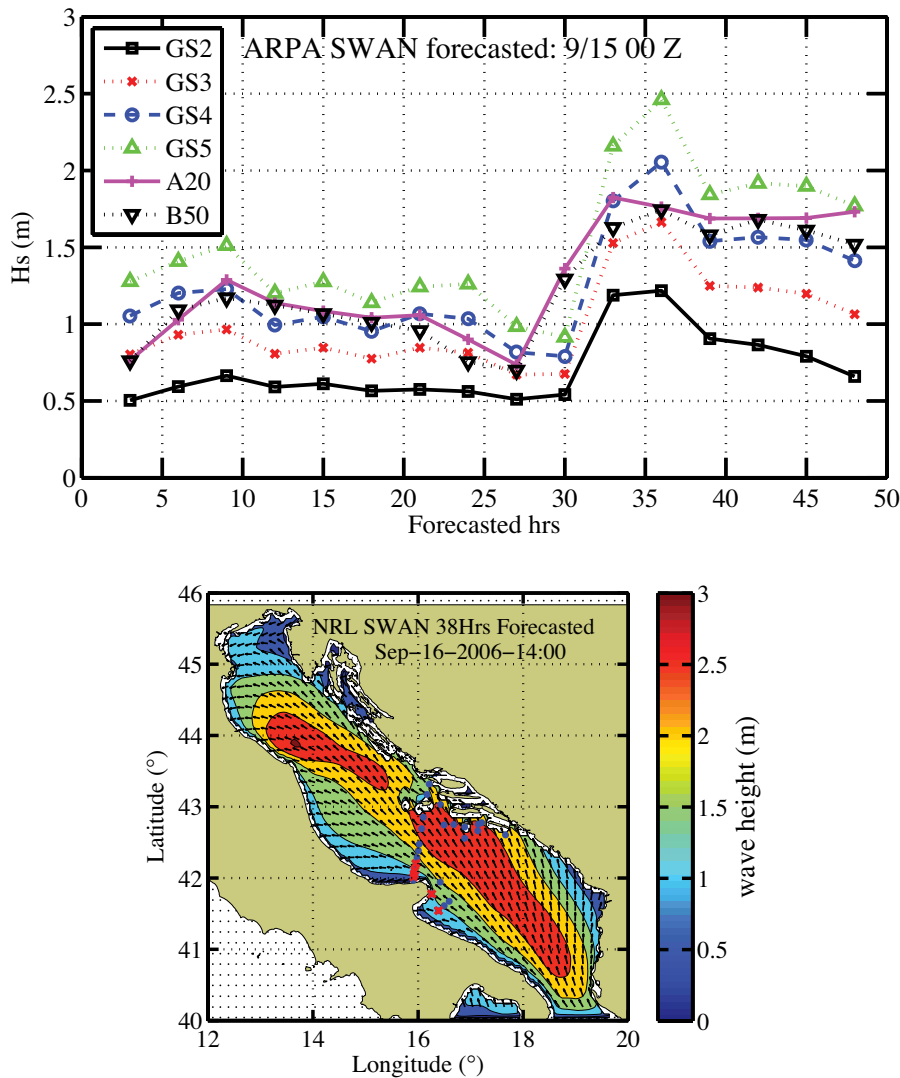


FIGURE 6 Temporal focused graphic of wave forecasts used for operation planning and the spatial pattern of waves near the storm maximum. Upper panel is forecast of significant wave height at several mooring locations during the forecast cycle starting at September 15, 2006, 00 UTC, from the ARPA-SIM SWAN run. Lower panel is NRL SWAN forecast significant wave height and mean wave direction at hour 38 for the entire Adriatic.

A Roughness Estimation Algorithm for Sidescan

M.L. Gendron, M.C. Lohrenz, G. Layne, and J. Sample
Marine Geosciences Division

Introduction: The Naval Oceanographic Office (NAVOCEANO) requires accurate estimates of seafloor roughness (bottom relief) and the density of seafloor clutter (mine-like echoes), typically derived from sidescan sonar imagery (SSI), to determine the bottom type of a geographic area for mine warfare. Determining clutter and roughness manually can be time-consuming and produce inconsistent results. Automated algorithms can derive clutter and roughness from SSI in a consistent and timely manner.

Features such as pockmarks, sand ripples, and rocks on the seafloor are visible in SSI as bright spots (“brights”) with adjacent shadows. The Naval Research Laboratory (NRL) developed a real-time clutter detection algorithm (transitioned to NAVOCEANO in 2001) that quickly and reliably identifies clutter in SSI and clusters the results into polygons. An object’s height (estimated from the length of its shadow) is one measurement used to determine whether the object is mine-like. The authors theorized that height also could be used to automatically estimate seafloor roughness.

NRL has developed a new automated roughness estimation algorithm, based on the clutter detection algorithm, to automatically derive seafloor roughness from SSI. In repeated trials, polygons generated by the new roughness algorithm correlated well (as high as 87%) with manually generated polygons for the same region. This article presents the NRL automated roughness algorithm (transitioned to NAVOCEANO in 2006), including test results and comparisons with manual methods.

Real-time Automated Clutter Detection Algorithm: The authors’ clutter detection algorithm ingests one SSI scan line at a time. Across-track bright and shadow positions and lengths are stored in two geospatial bitmaps,¹ one each for shadows and brights.

Shadows and brights in a scan line are located by first adaptively obtaining a lower intensity threshold, i_{\min} , such that all samples of intensity less than i_{\min} are considered shadows. An upper intensity threshold, i_{\max} , is set such that all samples of intensity above i_{\max} are considered brights. An appropriate gamma shift converts image intensities to fit a normal distribution, such that i_{\min} and i_{\max} are set to the quartiles of the shifted (normal) distribution.

Next, the bright and shadow geospatial bitmaps are examined from the edges of the scan lines toward the center (nadir) to detect runs of shadows followed by runs of brights. A circular lookup table is created

to “window” several scan lines at a time. This lookup table is populated with positions and run-lengths of shadows and brights. The window information is used to determine if a series of scan-line detections comprise an object, and the shadow length is one component in determining the object’s height.

Automated Roughness Estimation Algorithm: In the new roughness algorithm, the authors used sensor altitude above the seafloor, distance of the shadow from nadir, length of the shadow (determined by the clutter detection algorithm), and sonar resolution to estimate roughness (depicted as polygons representing smooth and rough areas). The algorithm was first tested on two geographic regions (I and II) and compared with manual roughness estimated by analysts at NAVOCEANO. The detected object locations for each region were clustered and categorized into smooth and rough polygons.

Figures 7 and 8 show the manual polygons (white outlines) overlaid on results of the roughness algorithm (blue-filled polygons) for Regions I and II, respectively. The percentage of agreement between manual and automated polygons for Region I is 60%. (This is the same as %correct for the automated method, assuming the manual method is ground-truth.) Interestingly, both the manual and automated methods clearly indicate a smooth “lane” running through the center of the SSI in Region I. During mine warfare operations, bottom roughness is one of the components considered when choosing which navigation lanes to

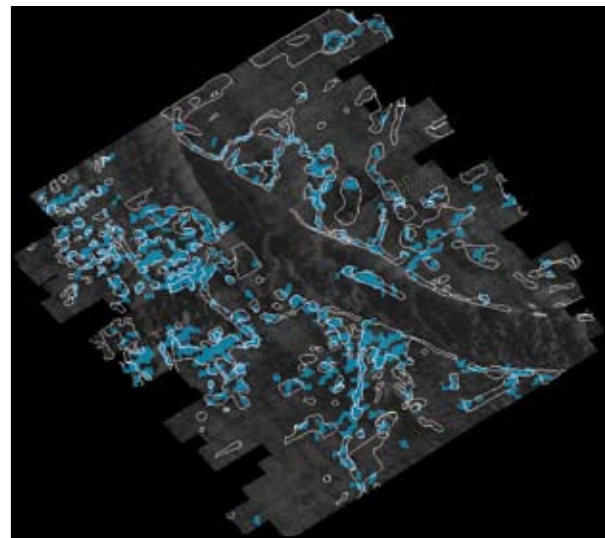


FIGURE 7
Both the manual (white outlines) and automated (blue filled polygons) roughness estimations indicate a smooth lane through the center of Region I. The percentage of agreement between the manual and automated methods is about 60%.

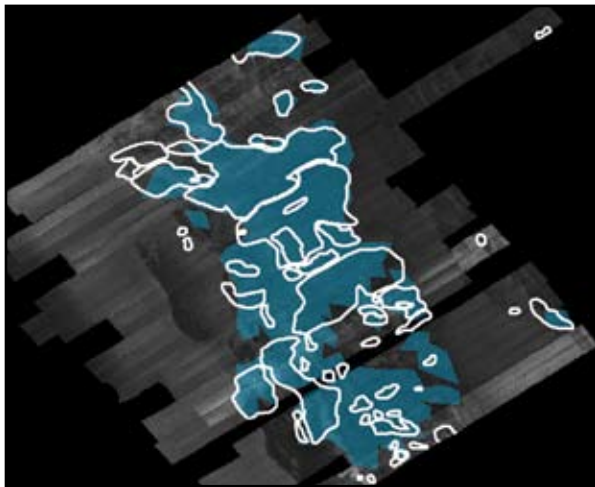


FIGURE 8
Manual roughness polygons overlaying automated roughness polygons for Region II: percentage of agreement between the manual and automated methods is about 84%.

clear of mines, since it is easier to clear a smooth sea-floor than a rough one. The percentage of agreement between manual and automated polygons for Region II is approximately 84%. A third test, over Region III in 2006, resulted in 87% agreement (Fig. 9). Table 1 shows how the authors calculated percent agreement.

Conclusion: This article describes a new real-time algorithm developed by NRL to estimate roughness. The algorithm was tested on three regions where NAVOCEANO analysts had manually estimated bottom roughness. The algorithm correctly identified a smooth lane in Region I, with 60% agreement between automatically and manually estimated roughness polygons. The algorithm was 84% correct for Region II, and 87% correct for Region III. The algorithm operates in real time, compared with weeks of post-processing time required for manual roughness estimations.

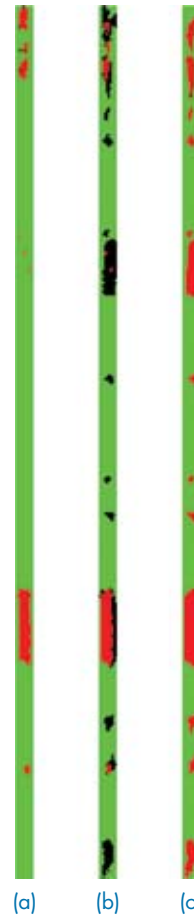


FIGURE 9
Third test of roughness algorithm, for Region III in September 2006: a) manually generated roughness polygons, b) logical AND of manual and automatically generated polygons, c) automatically generated roughness polygons. The percentage of agreement between manual and automated methods is about 87%.

Acknowledgments: This work was sponsored under Program Element 602435N by the NRL 6.2 Base Program.

[Sponsored by NRL]

Reference

¹M.L. Gendron, P.B. Wischow, M.E. Trenchard, M.C. Lohrenz, L.M. Riedlinger, and M. Mehaffey (2001). *Moving Map Composer*. Naval Research Laboratory, US Patent No. 6,218,965. ★

Table 1 — Calculation of % Agreement Between Manually Generated Roughness (Fig. 9(a)) and Automatically Generated Roughness Polygons (Fig. 9(c)). Figure 9(b) is the Binary AND Between Figs. 9(a) and 9(c), Providing a Comparison Between the Two Methods of Categorizing Roughness, Summarized in this Table.

ID	# Pixels	Image (%)	Description
	3822	79.3	Correct (smooth)
	349	7.2	Correct (rough)
	649	13.5	Incorrect (falsely categorized as rough)
	0	0.0	Incorrect (falsely categorized as smooth)
		86.5	Total correct
		13.5	Total incorrect (conservative errors only)

OPTICAL SCIENCES





195 Distributed Fiber Optic Sensing for Homeland Security

C.K. Kirkendall, R. Bartolo, J. Salzano, and K. Daley

196 Transduction of the Spin State Variable Between the Electron and Optical Polarization at Zero Magnetic Field

A.T. Hanbicki, O.M.J. van 't Erve, G. Kioseoglou, C.H. Li, and B.T. Jonker

199 Optical Manipulation of Ultracold Atoms

F.K. Fatemi and M. Bashkansky

201 Real-Time Fleet Protection

L.N. Smith and J.R. Waterman

Distributed Fiber Optic Sensing for Homeland Security

C.K. Kirkendall,¹ R. Bartolo,¹ J. Salzano,² and K. Daley²

¹Optical Sciences Division

²SFA Inc.

Introduction: The need to protect our borders and critical infrastructure, such as pipelines, power distribution, and transportation, has grown in importance over the last few years. To address this need, fiber optic sensing technology developed in the Optical Sciences Division at NRL for antisubmarine warfare applications has recently been adapted to homeland security applications. Ground-based seismic sensing applications have significantly different requirements than traditional underwater acoustic applications. As a result, new optical interrogation and signal processing techniques are needed. Border and critical infrastructure sensor systems must be able to monitor long lengths (several km to several 10's of km) with reasonable spatial resolution (5 to 100 m), and have sufficient seismic sensitivity to detect targets of interest. We have developed and recently field-tested a fiber optic distributed seismic sensor system capable of meeting these requirements and report on some initial observations below.

Fiber Optic System Description: The system concept for a border monitoring application is shown in Fig. 1. The sensor is a standard commercial off-the-shelf (COTS) optical fiber cable buried in the ground along the perimeter to be monitored. Seismic activity in the ground couples to the buried cable and induces a strain in the optical fiber within the cable. The optical interrogation system developed at NRL simultaneously monitors the entire fiber length (currently up to 5 km) for time-varying changes in strain. The interrogation system segments the optical fiber into sequential spatial channels of a fixed length (currently 10 m) as shown in Fig. 1. With this spatial aperture, the system is capable of detecting very low signal-level induced strains in the fiber. One of the goals of these field tests was to equate the strain resolution capabilities of the optical

system with real-world seismically induced strain levels observed in a buried optical cable.

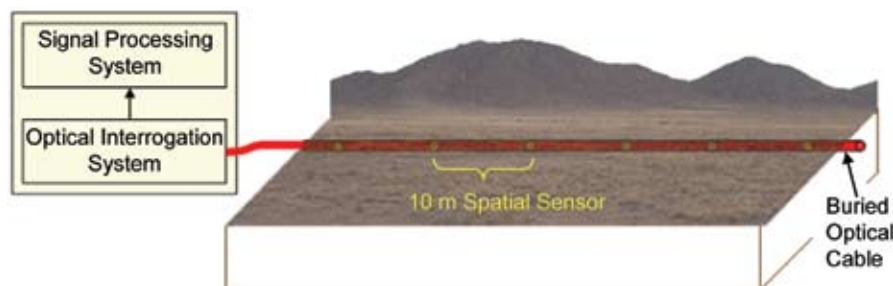
The interrogation and signal processing system shown in Fig. 1 is connected to one end of the optical cable, which would typically be placed in a secure location. The interrogation system houses the electro-optics components that optically interrogate the sensor cable and demodulate the return signal to recover the seismically induced strain. The signal processing system monitors activity along the entire perimeter and includes a real-time display and data archival functions.

Field Test Results: The system has been tested at two different locations in the southwestern United States using optical cables buried from less than one foot deep to as much as four feet deep. Several fiber optic cable designs, with different fiber protection schemes and cable armoring, have been tested. As might be expected, different burial depths and cable designs yielded different levels of sensor sensitivity, but in general, all tested configurations performed satisfactorily.

Many test scenarios were run, including individuals walking and running, digging, and a variety of vehicles both on road and off. In one of the walking test scenarios, an individual started at the buried cable and walked perpendicular to the cable. When he reached the end point, he stomped his foot ten times to mark the end of the test. The envelope of the time series data for this test from one 10-m spatial channel is shown on the top of Fig. 2. Each spike in the plot corresponds to a footfall of the walker. The bottom half of the plot shows the spectrogram of the time series envelope for the same segment of time. The cadence of the walker is clearly visible in the spectrogram and is seen to lower in frequency as the walker slowed down near the end of the test.

In one installation, a section of the cable was buried roughly 3 m from the edge of a paved roadway. During our testing, a caravan of seven Humvees drove up the road and stopped near the 350-m mark. The progress of all seven vehicles along the array can be seen in Fig. 3, which is a waterfall display of the seismic energy detected on the first 150 10-meter spatial chan-

FIGURE 1
Buried fiber optic distributed seismic sensor border monitoring concept.



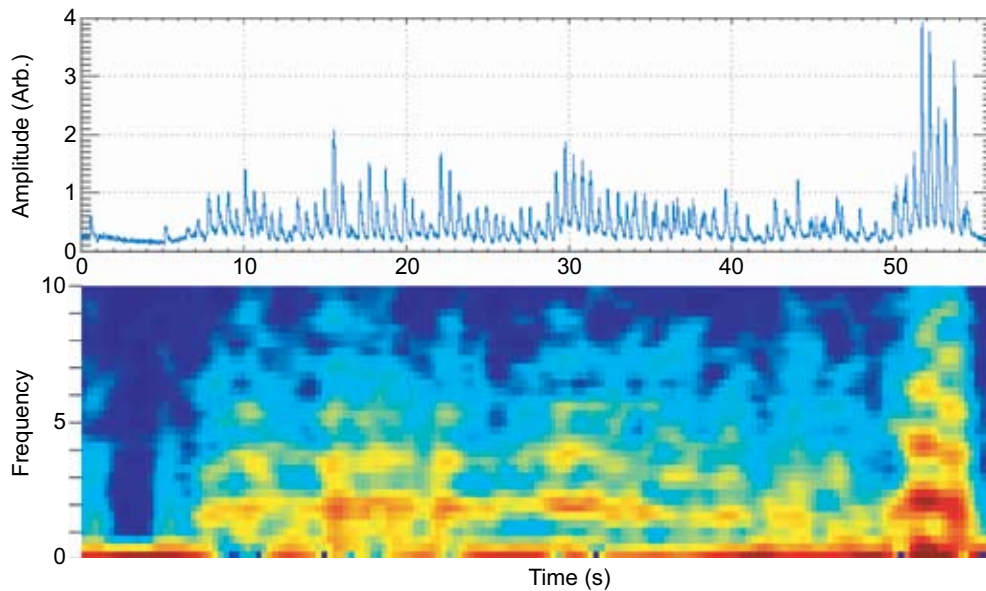


FIGURE 2

The envelope of the time series of a person walking perpendicular to the cable is shown in the top plot. The bottom image shows the spectrogram (time-frequency plot) of the time series envelope above.

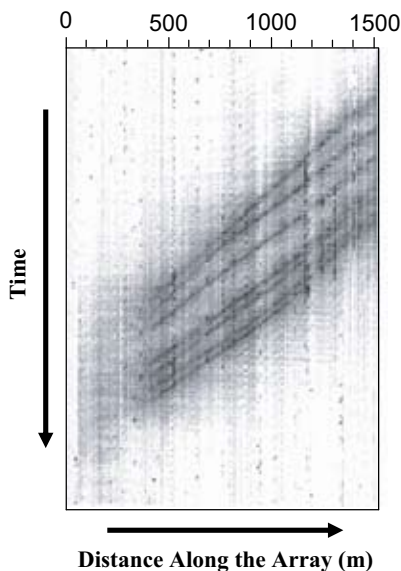


FIGURE 3

Band power waterfall display of a caravan of seven Humvees driving up the array from the distal end.

nels (1.5 km total span). The signal intensity is color-coded from white to black, covering a 50-dB variation in signal level.

Closing: The fiber optic system developed is capable of transforming a standard single mode optical fiber in a COTS cable into a sensitive seismic sensor. The achieved sensitivities and detection capabilities are in line with the requirements for trip wire border monitoring and homeland security applications. The

current system can resolve 10-m spatial regions and can interrogate up to 5-km perimeters. This system provides a new, unique sensing capability to better protect our borders and critical infrastructure.

[Sponsored by DARPA and DHS]

★

Transduction of the Spin State Variable Between the Electron and Optical Polarization at Zero Magnetic Field

A.T. Hanbicki,¹ O.M.J. van 't Erve,² G. Kioseoglou,³ C.H. Li,¹ and B.T. Jonker¹

¹Materials Science and Technology Division

²Philips Research Laboratories, Eindhoven, the Netherlands

³NRL/NRC Postdoctoral Research Associate

A New Spin on Electronics: Utilizing the spin degree of freedom of an electron in a semiconductor device is the basis for the emerging field of spin electronics, or spintronics.¹ The idea is that spin-polarized electrons can be introduced into a semiconductor host, and the electron's spin rather than charge can be used as a new state variable to produce performance and functionality not attainable by simply controlling charge motion (as is done in existing devices). To realize this new technology, it is first necessary to get spin-polarized carriers into the semiconductor, and NRL researchers are taking a lead role in this pursuit.

Our principal approach has been to electrically inject spin-polarized carriers from an Fe contact into

an AlGaAs/GaAs light emitting diode (LED). In this system, we have been able to sustain electron spin polarizations of 40% to 70% in the GaAs. Further, we have uncovered a wealth of information on spin relaxation and transport phenomena through detailed spectroscopic studies. Most recently, we have been able to modify this system so that we can efficiently transduce spin angular momentum from the electrons to the photon optical polarization at zero magnetic field, a key step toward practical device applications such as spin-pumped laser diodes.²

Lighting the Way: The test devices commonly used to investigate spin injection are called spin-LEDs. In these devices, spin-polarized electrons are injected from a ferromagnetic (FM) metal like Fe, across a heteroepitaxial interface, through a semiconductor like AlGaAs, and into a GaAs quantum well (QW). In the QW, these spin-polarized electrons radiatively recombine with holes from the p-type substrate to produce circularly polarized light. Using quantum selection rules based on the conservation of angular momentum, we can directly relate the degree of light polarization, P_{circ} , with the spin polarization of the injected electrons, P_{spin} .

Out (of-Plane) with the Old: Typical spin-LEDs (Fig. 4(a)) use a narrow (~ 10 nm) QW recombination region in which quantum confinement constrains the hole angular momentum to lie along the surface normal (z -axis). For most thin FM films, out-of-plane is a hard magnetization direction. Consequently, a rather large external magnetic field (>0.5 T) must be applied to orient some component of the FM contact magnetization (and corresponding electron spin orientation) along the z -axis so that the electron and hole spins are colinear. It would be very advantageous to use the small coercive fields (<0.005 T) and large remanent magnetizations that FM metal contacts typically exhibit *in-plane*. This would greatly facilitate spin manipulation and transduction of the spin state variable between the electron spin and optical polarization for multifunctional device applications.

Observations at the Cutting Edge: By using light emitted from the *edge* of the spin-LED, we can fully benefit from the small in-plane coercive fields and large remanent magnetizations that our Fe contact naturally provides (Fig. 4(b)). Unfortunately, the story is not so straightforward as simply collecting light from the cross section of a device. By comparing light emitted from spin-LEDs in both the surface and edge emission geometry, we have discovered that details of the material system need to be fully understood to realize devices that can supply significant optical polarizations with small fields.

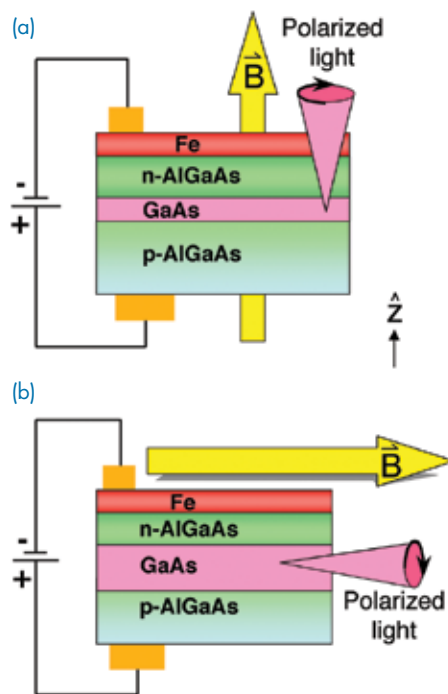


FIGURE 4
(a) Surface emitting spin-LED in the Faraday geometry, light from the active area travels through the Fe top contact. (b) Edge emitting spin-LED, light is emitted from a cleaved edge.

Figure 5 shows the circular polarization in the edge emission geometry as a function of applied field for several different QW widths. The inset is a photo of a spin-LED under test. For all fields, no circular polarization is observed from a system with a 10-nm-wide QW. This is expected because, as noted above, the hole angular momentum is constrained to lie along the surface normal and is thus orthogonal to the spin of the injected electron and light propagation direction. When wider QWs are used, the hole angular momentum can lie in-plane, colinear with the electron spin and light propagation direction. Hysteretic behavior of P_{circ} can be observed at very low fields (Fig. 6), demonstrating efficient electrical injection of spin-polarized electrons *even at zero field*.

A Wider Understanding: Even for wide QWs, the observed P_{circ} is much lower than expected at low applied fields, and the field dependence deviates significantly from the Fe magnetization data (Fig. 6), suggesting that some mechanism suppresses the optical polarization. We attribute the systematically lower polarization of the edge-emitted light to a partial out-of-plane orientation of the average hole angular momentum. In wide quantum wells, some fraction of the holes are weakly bound at the interfaces of the QW where the symmetry is reduced. This may arise from trapping at local interface potentials such as step

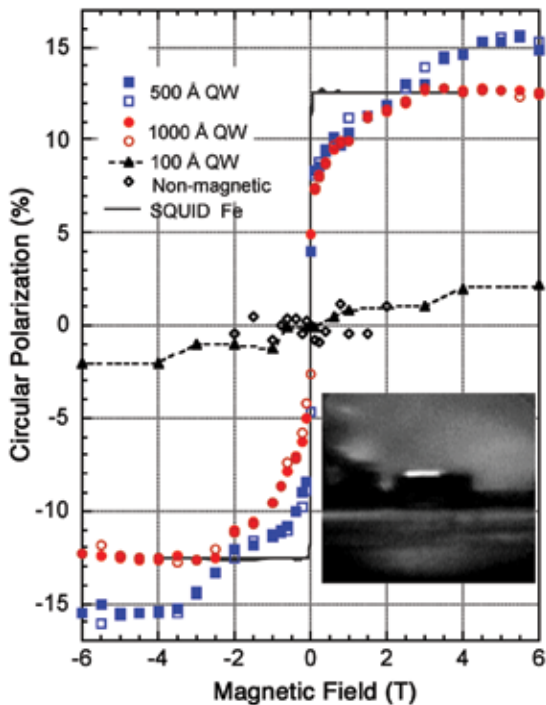
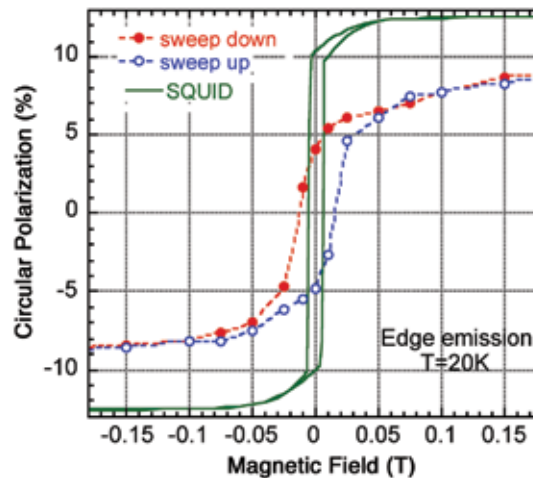


FIGURE 5 Electron spin polarization vs magnetic field at $T = 20$ K of edge emitting spin-LEDs with Fe spin injecting contacts and a 100-nm (circles), 50-nm (squares), and 10-nm (triangles) GaAs QW. The magnetic field is applied in-plane as shown in Fig. 4(b). The solid line is the in-plane magnetization measured by superconducting quantum interference device (SQUID) magnetometry at 20 K and scaled to the 100-nm QW data. The inset is a photo of a spin-LED under test.

FIGURE 6 Optical polarization vs magnetic field of an edge-emitting spin-LED with an Fe contact and 50-nm QW at 20 K for small magnetic fields. The solid line shows the magnetization of the Fe film along the light propagation direction at 20 K.



edges, a well-known mechanism for the formation of quantum dots, or band bending in the semiconductor heterostructure. The angular momentum of such holes is then constrained to lie along the surface normal, as in the narrow 10-nm QW, and they do not contribute to the circular polarization of the edge-emitted light. This is an effect felt only by the holes, not by the electrons, and will not impact the performance of future spintronic devices based on manipulation of the electron spin system.

Summary and Implications: In summary, spin-polarized electron injection has been demonstrated in remanence using edge-emitting spin-LEDs with Fe contacts and wide quantum wells. These results

demonstrate that spin-polarized injection is possible without an external magnetic field, and that the sign of the polarization achieved in the semiconductor is controllable with modest magnetic fields. These are key characteristics for spin manipulation and nonvolatile behavior in future device applications.

[Sponsored by NRL and ONR]

References

- ¹For a recent review, see I. Zutic, J. Fabian, and S. Das Sarma, "Spintronics: Fundamentals and Applications," *Rev. Mod. Phys.* **76**, 323 (2004).
- ²O.M.J. van 't Erve, G. Kioseoglou, A.T. Hanbicki, C.H. Li, and B.T. Jonker, "Remanent Electrical Spin Injection from Fe into AlGaAs/GaAs Light Emitting Diodes," *Appl. Phys. Lett.* **89**, 072505 (2006). ★

Optical Manipulation of Ultracold Atoms

F.K. Fatemi and M. Bashkansky
Optical Sciences Division

Motivation: It is well known that ultracold atoms ($T < 1$ milliKelvin) are promising candidates for next-generation inertial sensors and magnetometers. An “atom interferometer” measures accelerations and rotations in much the same way as does a laser-based interferometer, except that the recorded interferograms are due to matter wave interference rather than optical interference.

Large laboratory-based atom interferometers using thermal atom beams have demonstrated unparalleled performance, but the most promising path to making such technology practical is to use ultracold atoms: unlike room temperature atoms, cold atoms can be guided along controlled trajectories, analogous to fiber optics for light. The roles of matter and light are reversed—whereas material guides photons in fiber optics, photons guide atoms in atom optics. To realize high sensitivities with cold atoms, we must 1) obtain a large flux of cold atoms and 2) guide atoms coherently in atom waveguides. Our group is working on these issues using optical techniques with cold atoms derived from a “magneto-optical trap” that contains roughly 10^8 rubidium atoms at a temperature of $10\ \mu\text{K}$ and density of 10^{11} atoms/cm³.

Background: When an atom is exposed to an optical field, the force acting on the atom is proportional to the intensity gradient. Laser fields tuned above an atomic resonance repel atoms from regions of high intensity toward low intensity. Such “blue-detuned” atom manipulation, therefore, helps preserve coherence by lowering spontaneous emission events. One

challenge to using blue-detuned traps and guides is the requirement of creating volumes or channels in space bounded by regions of high intensity, such as a hollow laser beam. Because lasers generally produce Gaussian modes, they cannot guide atoms with blue-detuned light without modification.

Cold Atom Transport: We have developed tools for delivering a large flux of atoms through hollow optical fibers.¹ Figure 7(a) shows a schematic of a hollow optical fiber developed in our lab, designed to transfer cold atoms through its vacuum core from a source chamber of trapped cold atoms to a destination chamber. Blue-detuned light is coupled into the annulus of the fiber, and the evanescent field that extends into the core is sufficient to prevent atoms from sticking to the fiber walls. In our technique, light is coupled through the sides of the fiber using micro-prisms embedded into the cladding (Fig. 7(b)). The fiber ends are coated so that light only interacts with the atoms during transport.

Dark Optical Traps: We have also generated guides for cold atoms using spatial light modulation of freely propagating beams. By altering the phase profile across a Gaussian beam with a spatial light modulator, we create hollow laser beams (inset of Fig. 8(a)). Crossing two hollow laser beams provides full 3D confinement of the atoms in traps as small as a few tens of microns in diameter. Figure 8(b) shows a time sequence of atoms expanding into a single hollow beam, and full confinement with crossed beams is shown in Fig. 8(c). We have shown that, because the atoms are confined to the dark and are minimally exposed to the guiding light, scattering rates can be reduced by up to two orders of magnitude over conventional traps based on red-detuned light.²

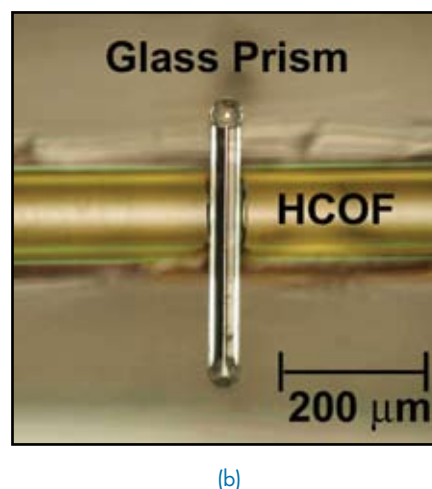
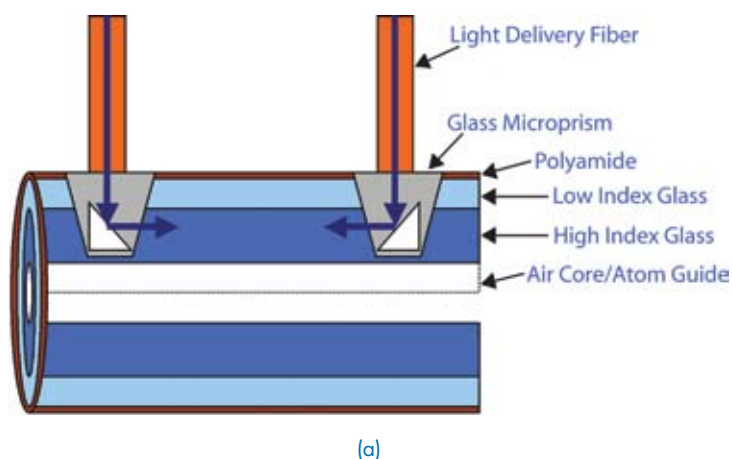


FIGURE 7
(a) Side-illuminated hollow core fiber. (b) Image of glass prism embedded in hollow core optical fiber (HCOF).

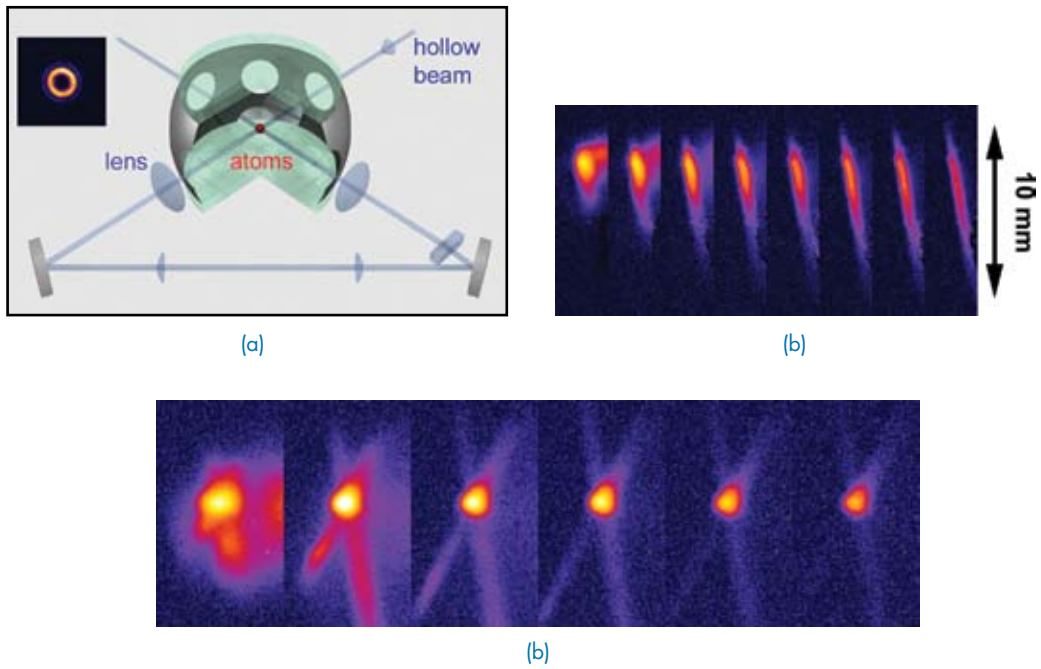


FIGURE 8
 (a) Hollow beams intersect in the center of a vacuum chamber containing a magneto-optic trap of cold atoms. Inset: 200 μm diameter hollow beam formed by spatial light modulation. (b) Cold atoms expanding into a single hollow beam over 50 ms. (c) Cold atoms confined in crossed hollow beams over 100 ms.

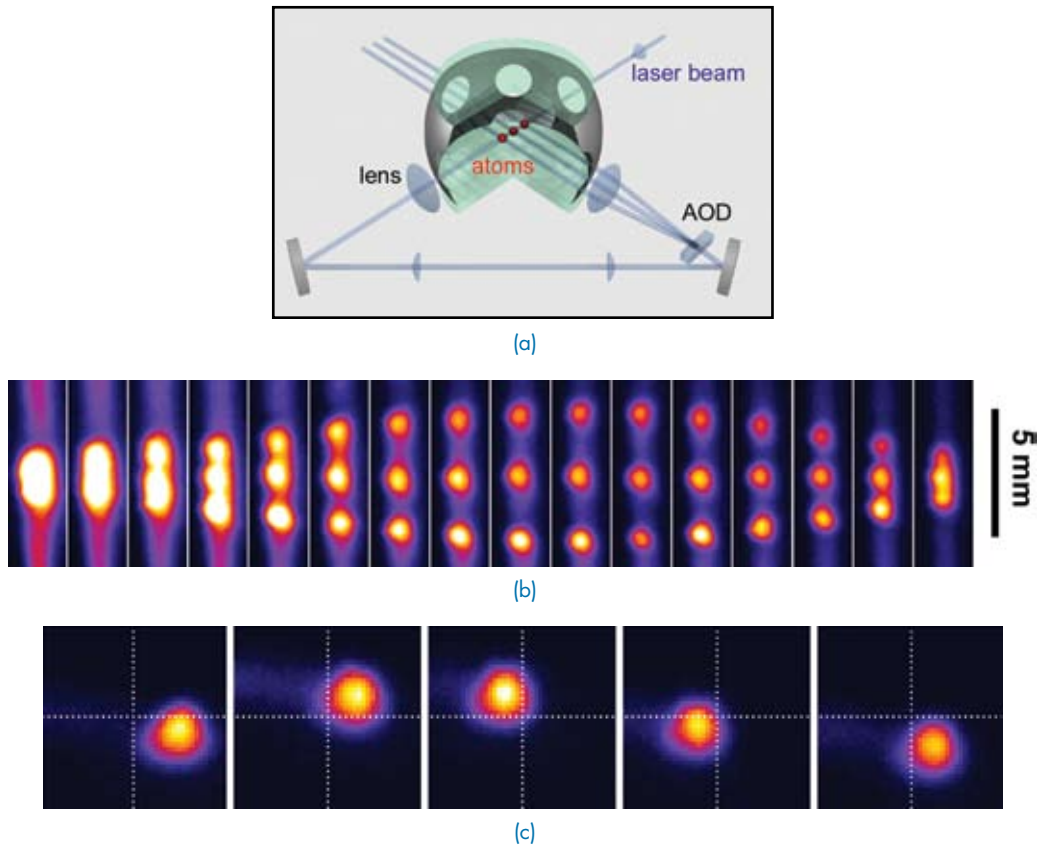


FIGURE 9
 (a) Spatial locations of atoms are controlled by acousto-optic deflection (AOD). (b) Atom cloud split into three independently controlled clouds separated by 5 mm. Images are taken every 2 ms. (c) Atoms moved in a 2 mm diameter circle using a second AOD before the chamber. Images are taken every 10 ms.

Dynamic Manipulation of Atoms: These confining traps can also be manipulated spatially. Figure 9(a) shows a schematic of our current apparatus, in which the intersection point of the crossed hollow beams is controlled with acousto-optic deflectors (AODs). These deflectors scan the beam by changing the RF drive frequency, so the spatial positions can be scanned rapidly (>50 kHz) with excellent resolution. Furthermore, the AODs can be driven with multiple drive frequencies simultaneously, generating several atom traps in parallel that can be independently controlled. We have recently demonstrated splitting of the traps into three individually controlled sites (Fig. 9(b)).³ Using multiple AODs, we have moved the atoms in 2D trajectories (Fig. 9(c)).

Summary: We have demonstrated spatial control of ultracold atoms using all-optical techniques that preserve atom coherence. In addition to applications in inertial sensing, such spatial sampling by small, dense atom clouds may allow spatially resolved magnetometry with resolutions not possible with current alkali magnetometers. The techniques shown here may be combined with magnetic atom-guiding techniques, which are most commonly pursued for these applications. Despite extensive research in cold atom physics for over two decades, interest in both applications and fundamental research derived from it continues to grow.

[Sponsored by ONR]

References

- ¹F.K. Fatemi, M. Bashkansky, and S. Moore, "Side-Illuminated Hollow Core Optical Fiber for Atom Guiding," *Opt. Express* **13**, 4890-4895 (2005).
- ²F.K. Fatemi and M. Bashkansky, "Cold Atom Guidance Using a Binary Spatial Light Modulator," *Opt. Express* **14**, 1368-1375 (2006).
- ³F.K. Fatemi, M. Bashkansky, and Z. Dutton, "Dynamic High-speed Spatial Manipulation of Cold Atoms Using Acousto-optic and Spatial Light Modulation," *Opt. Express* **15**, 3589-3596 (2007). ★

Real-Time Fleet Protection

L.N. Smith and J.R. Waterman
Optical Sciences Division

Introduction: Recent advances in infrared sensor technology, detection algorithms, and high performance commercial computing hardware have enabled powerful new approaches to autonomous day/night video imaging-based protection systems for Navy surface ships. Under the ONR Fleet and Force Protection Future Naval Capabilities program, NRL has

developed the Distributed Aperture System Infrared Search and Track (DAS IRST) system¹ for that purpose. The DAS IRST system provides situational awareness against terrorist-class threats such as surfaced divers, rafts, small boats, and light aircraft, and covert surveillance capability, including autonomous detection, tracking, and threat designation for antiship missiles. The performance characteristics of the system are superior to prior implementations as the result of the development very-large-format high-sensitivity infrared focal planes and improved real-time detection, tracking, and threat declaration algorithms.²

Antiterrorist Force Protection: The importance of shipboard situational awareness against asymmetric threats is dramatically illustrated by the October 2000 attack on the USS *Cole* during a routine fuel stop in Yemen. In that event, a small surface craft approached the port side of the destroyer and delivered explosives that put a 40-by-40-foot gash in the ship and killed 17 sailors. There is a clear need for around-the-clock, high-resolution, 360-degree continuous video imagery with computer-based detection and warning to counter such actions. Several field tests in 2005 and 2006 quantified the capability of the DAS IRST system to perform this task under a wide range of conditions, demonstrating the ability to monitor the activity of small boats, rubber rafts, and swimmers within several kilometers of the ship. Figure 10 is a view of the DAS IRST GUI (graphical user interface) with a view from the Naval Surface Warfare Center Dahlgren, VA, test range in which there are small boats. The algorithms in the system automatically find the moving objects that require additional attention, highlight them in the display, and provide track information to the ship combat system for further action.

Covert "Radar Off" Ship Operation: In today's Naval fleets, ship radars provide constant surveillance for antiship cruise missiles (ASCM), up to and even beyond the visible horizon. In tomorrow's fleets, this surveillance capability potentially will be supplemented by a "passive" surveillance system such as the DAS IRST system. Radars are "active" in that they send out a signal that informs anyone listening to the presence of the ship. An Infrared Search and Track system is "passive" in that it provides a similar ASCM surveillance capability without sending any signal. These future ships will then be able to operate covertly by turning off their radars and using their DAS IRST system for constant surveillance of the horizon.

The stringent performance requirements associated with detecting and tracking subsonic sea-skimming cruise missiles led to an extensive effort at NRL to find the best algorithms for ASCM detection, tracking, and automatic threat declaration. In realistic field tests at

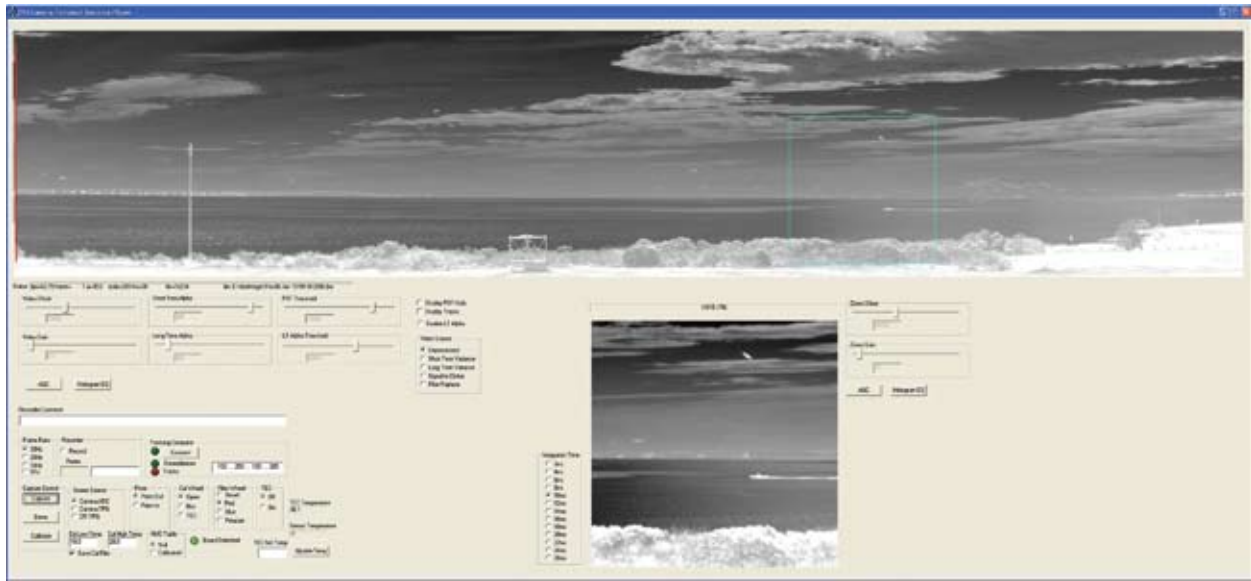


FIGURE 10
An image from the sensor taken at Dahlgren, VA, displayed on the DAS system GUI. The upper image is the full 10 x 48 degree field of view of the sensor. The lower image highlights a detected surface threat at higher magnification. The remainder of the screen is employed for user control of image display, detection, and tracking.

the Navy Surface Combatant Center at Wallops Island, VA, the decoy target shown in Fig. 11 was towed by a LearJet so that ASCM-like data could be collected by the sensor. These data were used to create Receiver Operator Characteristic (ROC) plots, such as the one shown in Fig. 11, that compare the performance of the standard 2D spatial signal-to-clutter ratio method to three new methods (absolute deviation ratio (ADR), temporal signal-clutter ratio (SCR), and combined) created here at NRL. The goal was to find all the true detections with as few false detections as possible. As illustrated in Fig. 11, the performance of all three new algorithms is significantly superior to the standard method. Furthermore, an automatic threat declara-

tion system was created that uses all available physical property information such as persistence, velocities, scintillation of the target intensity, and track history.

System Description: The DAS IRST sensor is shown in Fig. 12. It is a 30-Hz frame-rate infrared camera that employs a unique 512 x 2560 molecular-beam epitaxy (MBE)-grown midwave HgCdTe focal plane array (FPA) and an anamorphic optical system (appears green in the figure) that permits two fields of view: 3.6 x 48 degrees for distant horizon surveillance and 10 x 48 degrees for closer-in situation awareness. A combination of filters provides midwave spectral band capabilities in the 3.4 to 4.8, 3.8 to 4.1, or 4.6 to

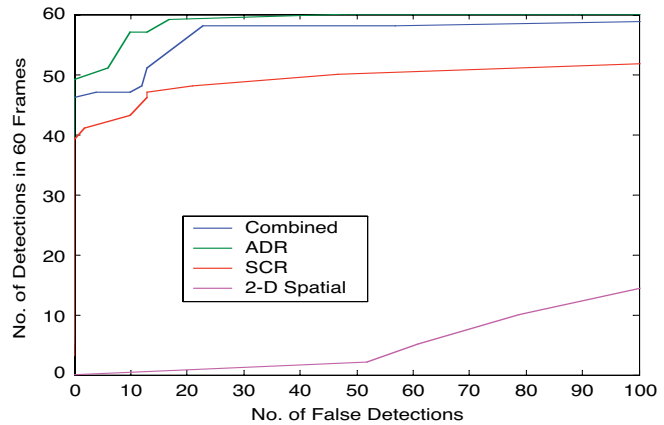


FIGURE 11
This towed target (left) provided a realistic test of the algorithms for detecting ASCMs at ranges out to 25 km. The ROC curve (right) generated from this data compares the original 2D spatial detection algorithm to three novel algorithms developed in this project.



FIGURE 12
DAS IRST sensor (bronze-colored assembly)
mounted on pan-tilt positioning system.

4.8 μm ranges. A temporal noise-limited noise equivalent differential temperature (NEDT) of ~ 20 mK has been achieved. The minimum ensquared energy for the sensor is 65%, resulting in a noise equivalent irradiance (NEI) of approximately 10^{-15} W/cm², a value commensurate with long-range missile detection.

In addition to the sensor, two subsystems are required for detection, tracking, and declaration of threats. A PC-hosted FPGA-based subsystem on the PCI bus performs real-time signal processing of this voluminous image data and finds “detections.” These detections go to a PC-based subsystem, which discerns false alarms from real tracks and correctly declares possible threats.

The DAS IRST system is the result of a coordinated effort by several groups led by NRL. The optics were fabricated by Axsys Infrared Systems, the FPA by

Raytheon Vision Systems, FPGA hardware implementations were done by Smart Logic, and software was developed by V_Systems. NRL staff was responsible for the overall specification and design of the system, sensor hardware integration and testing, algorithm development, and field testing.

[Sponsored by ONR]

References

- ¹J.R. Waterman, L.N. Smith, J. Griffith, S. Black, and A. Childs, “Performance Characterization of the Navy’s Staring DAS IRST System,” Proceedings 2005 MSS Specialty Group Meeting on Passive Sensors, Feb. 2005.
- ²L.N. Smith, J.R. Waterman, and R. Smith, “Demonstration of Novel Detection Algorithms for the Navy DAS IRST System with 2005 Shore-Based Test Data,” Proceedings of MSS Conference on Passive Sensors, Feb. 2006. ★

REMOTE SENSING





207 Pyroconvection and Climate Change

M. Fromm, S. Miller, J. Turk, and T. Lee

208 Joint Demodulation of Low-Entropy Narrowband Cochannel Signals

T. Meehan, F. Kragh, and K. Clark

211 Remotely Measuring Turbulent Coastal Atmospheres

W.P. Hooper, G.M. Frick, B.P. Michael, and R.J. Lind

Pyroconvection and Climate Change

M. Fromm,¹ S. Miller,² J. Turk,² and T. Lee²

¹Remote Sensing Division

²Marine Meteorology Division

Introduction: In March 1998, the Naval Research Laboratory (NRL) launched a satellite instrument named Polar Ozone and Aerosol Measurement (POAM) III. Just a few months after launch, POAM III started detecting mysterious clouds in the stratosphere in the sub-Arctic northern hemisphere. It was obvious that an unusual phenomenon was being recorded. We now know that these mysterious aerosol-cloud layers were smoke from forest fires that erupted like a volcano into what is now called pyrocumulonimbus (pyroCb for short). This initial discovery has been followed by more research and discovery by NRL's Remote Sensing and Marine Meteorology Divisions. In this article we summarize highlights of our pyroCb research and its importance.

Until the discovery of pyroCb, the common wisdom was that there was only one natural terrestrial force that could inject material into the lower stratosphere—a volcanic eruption. Volcanic eruptions are well known and their impact on climate can be significant. The tropopause is still considered by many to be an effective lid for any force except a strong volcano.

With the recent work at NRL we now have characterized the unique and formidable power of the pyroCb in action and even found a nuclear winter/volcano type link between stratospheric smoke layers and cooling near the Earth's surface.

The PyroCb, Up Close and Personal: On August 17, 2003, a large fire in Alberta near Conibear Lake,

Canada, erupted into deep pyroconvection. On that day, the Conibear Lake pyroCb created a large, thick, deep plume in the lowermost stratosphere.

Imagery from the Moderate Resolution Imaging Spectroradiometer (MODIS) shows the Conibear Lake pyroCb in its maturity (Fig. 1). Three visible bands give a true-color scene. A near-infrared (NIR) channel shows the flaming fires in red outline. Thermal infrared (THIR) brightness temperature (good for cloud-top height) is displayed as the blue contour, enclosing the cloud surface colder than -45°C .

Notice two dominant flaming spots in the scene. The Conibear Lake fire is upstream of the convective cloud complex, and another fire to the west is emitting a long smoke plume. The pyroCb consists of two cumulonimbus anvils. The easternmost is from an earlier pulse of intense pyroconvection. The western anvil has a sharp, perturbed texture distinct from the glaciated eastern anvil. The “older” eastern anvil has smoothed after detaching from the vigorous updrafts and by wind shear. The active western anvil shows turrets of strong tropopause-penetrating upheaval. Perhaps the most remarkable visible feature, on both anvils, is the smoky coloration in comparison to nearby pristine air mass convection. Obviously, this pyroCb has injected enough smoke to the cloud top to visibly pollute it.

The THIR component to this image shows that both anvils are dense and top out at the tropopause. The contour also signifies a temperature so low that the cloud top particles “inside” the contour are exclusively ice. Another feature of the THIR contour is a second appearance near the very center of the western anvil. Inside this contour, the cloud-top temperature actually increases. This “warm core” is a well known (albeit poorly understood) “enhanced V” signature of extreme

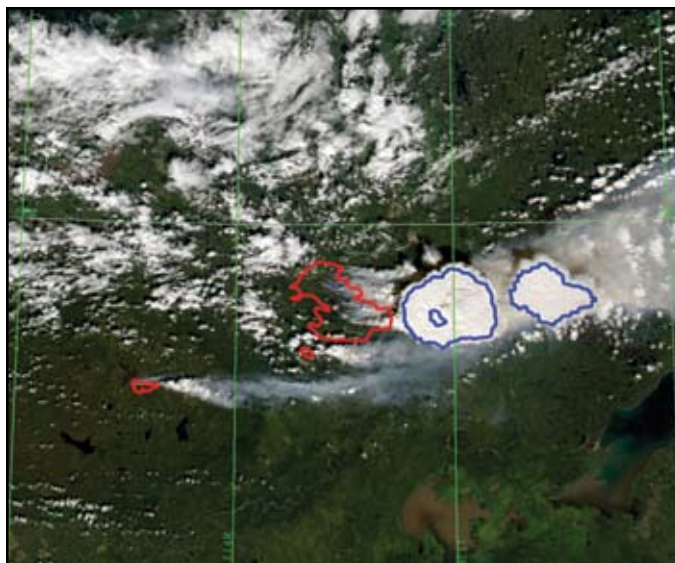


FIGURE 1

Conibear Lake pyroCb (August 17, 2003, in Canada) true-color image with fires (red) and -45°C IR temperature contour (blue).

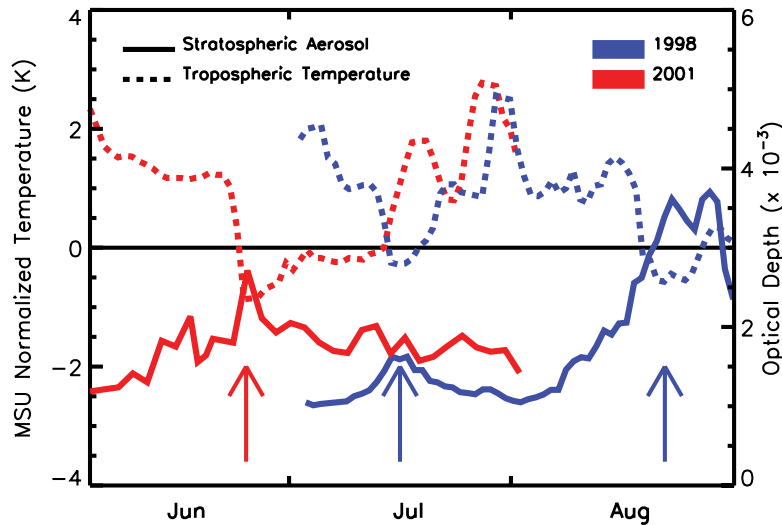


FIGURE 2
Time series of POAM III stratospheric aerosol optical depth and MSU tropospheric normalized temperature. Arrows indicate pyroCb-caused aerosol increases.

convection. Taken together, the THIR and true-color analyses reveal that this is a vigorous convective cloud with a unique smoke/ice mixture.

Climate Implications of PyroCb: A fundamental question about pyroCb is whether they have an important impact on weather or climate. We find strong circumstantial evidence that the stratospheric smoke from pyroCb cools the lower troposphere. Figure 2 shows how we determined this. We invoked an independent satellite-based temperature record from the Microwave Sounding Unit (MSU). We compare zonal average MSU temperature with POAM zonal average stratospheric aerosol optical depth (AOD). The simultaneous, strong departure of both AOD and temperature from the norm implies a hemispheric anomaly. Figure 2 shows three instances (indicated by arrows) where corresponding MSU tropospheric temperature reveals a sudden, obvious drop coincident with a spike in AOD. Each of these represents a plume we traced to pyroCb.^{1,2} In each case, the drop in temperature apparently persists on the order of weeks. This impact of a hemispheric smoke pall on the lower atmosphere is consistent with first principles—the aerosols reflect additional solar energy back to space, reducing the energy absorbed at the Earth’s surface. The multi-week persistence of this cooling underscores the important contribution pyroCbs make to hemispheric weather and climate patterns.

Climate change projections that show global warming place the largest temperature increases at high latitudes. The boreal zone will be thusly impacted. Forest fire experts project that forest fire size and frequency will increase due to this forcing. Obviously,

this provides us with great motivation to explore the pyroCb phenomenon more fully.
[Sponsored by ONR]

References

¹ M. Fromm and R. Servranckx, “Transport of Forest Fire Smoke Above the Tropopause by Supercell Convection,” *Geophys. Res. Lett.* **30**(10), 1542 (2003). doi: 10.1029/2002GL016820
² M. Fromm, R. Bevilacqua, R. Servranckx, J. Rosen, J. Thayer, J. Herman, D. Larko, and R. Servranckx, “Pyro-cumulonimbus Injection of Smoke to the Stratosphere: Observations and Impact of a Super Blowup in Northwestern Canada on 3-4 August 1998,” *J. Geophys. Res.* **110**, D08205 (2005). doi: 10.1029/2004JD005350



Joint Demodulation of Low-Entropy Narrowband Cochannel Signals

T. Meehan,¹ F. Kragh,² and K. Clark¹
¹Space Systems Development Department
²Naval Postgraduate School

Introduction to Cochannel Signals: Many receivers today operate in an interference-limited environment. In a dense signal environment, the performance of a receiver is limited by interference from multiple signals at the receiver rather than signal-to-noise ratio. In the interference-limited environment, there is a diminishing return from investing additional resources into improving traditional receiver parameters such as noise figure. Advanced processing techniques exist that can help recover information that would otherwise be

lost using a single-channel receiver.¹ This work investigates some of these techniques.

Interference may originate from many sources, such as users on the same or adjacent frequency band, unintended emissions, and intermodulation. This work investigates interference from cochannel information bearing signals. Cochannel interference is commonly defined as the reception of two or more signals at the receiver overlapping in frequency and in time.

AIS: The Automatic Identification System (AIS) is a ship- and land-based tracking and communications system operating in the very high frequency (VHF) maritime band. The primary function of AIS is to provide information for surveillance and the safe navigation of ships.^{2,3} The AIS typically sends ship-based tracking messages indicating position and state information at intervals of 2 to 10 seconds. The International Maritime Organization (IMO) has ruled that all passenger ships, cargo ships greater than 500 gross tons, and all ships greater than 300 gross tons on an international voyage must carry an AIS transceiver by July 2008.⁴ As a result, AIS provides an excellent means to monitor ship traffic entering U.S. waters and, thus, is of great interest to the Department of Homeland Security. Reception of AIS from a low Earth orbit (LEO) satellite, such as TACSAT-2, would provide an AIS monitoring capability at a greater distance than possible with coastal AIS receivers. However, because of the large field-of-view from LEO, the probability of cochannel interference while monitoring AIS is high.

This work uses the AIS signal as an example of a signal with the following properties: narrowband, cochannel, and low-entropy. The AIS signal is shown to have significant redundancy of information content from message to message. Analysis of the AIS data suggests a 168-bit AIS packet contains approximately 20 bits of new information. This research investigates the low-entropy property of the AIS signal and presents experimental results quantifying this property.

Joint Field-Based MAP: Although multiuser detection is a mature research field,¹ little prior research has focused on low-entropy signals. Optimal detection uses all the available information to make a decision. The optimal joint detection techniques are often dismissed due to the complexity of the receiver. Situations exist where this complexity is justified and is the most cost effective way to recover a signal. The field-based maximum *a posteriori* (MAP) joint detection algorithm uses the available *a priori* information to aid in jointly making a decision of what values are sent. Conceptually it is not difficult to understand; the idea is to select the combination of transmitted signals that maximize the *a posteriori* probability of a transmitted field. Let \mathbf{A} be

an $N \times N_s$ matrix of the transmitted symbol vectors $\mathbf{A} = \{\alpha_1 \alpha_2 \dots \alpha_{N_s}\}$, where N_s is the number of signals and N is the length of each vector. The optimum receiver (minimizing the probability of incorrect \mathbf{A}) is defined as the MAP receiver⁵ that selects the most probable \mathbf{A} given the received vector r . Finding the most likely set of transmitted signals, $\hat{\mathbf{A}}$, is now a combinatorics problem; try all 2^{NN_s} permutations of \mathbf{A} and select the one that maximizes the *a posteriori* probability. This method is impractical for all but the shortest of messages. This research investigates *efficient* methods of incorporating the information available at a receiver in order to make a decision.

Results: This work develops the Joint Field-Based MAP algorithm in order to achieve the goals stated above. By incorporating *a priori* information from the signal sources, this detector outperforms maximum likelihood (ML)-based joint detectors. The field error rate (FER) performance gain is highly dependent on the specific signal characteristics. Here, results are presented for representative signals that show gains of approximately 3 to 18 dB over the current state of the art (joint symbol-by-symbol detection). Figure 3 illustrates this for the reception of the longitude field of an AIS message. FER is plotted for three different correlation coefficients, ρ . Even for highly correlated signals, the field-based MAP detector has acceptable performance. This gain does come at a cost. There must be a source of *a priori* information; this may be previous signal receptions or some other source of side information. Without knowledge of one or more of the cochannel signals, there will be no gain in performance. There is also a processing cost. Implementing the Joint Field-Based MAP detector is both more computationally costly and more difficult to set up than that of the joint ML detection. The complexity of the Joint Field-Based MAP detector is exponentially dependent on both the number of users and the field length. A complexity reduction is possible by recognizing that some field values occur with negligible probability. This technique significantly reduces the computational cost while incurring a small penalty in FER performance.

Summary: Figure 4 presents a “big picture” view of the objective in this work as applied to remote reception of the AIS. The algorithm begins with some knowledge about existing ships — this could be very specific information such as a previous position report or very general, such as “Ship A left Port B at 1300 yesterday.” At the receiver, two or more signals are received overlapping in frequency and time. The signal parameters for each of the overlapping signals are estimated. This reception is passed through multiple matched filters, and each filter is matched to a specific pulse with

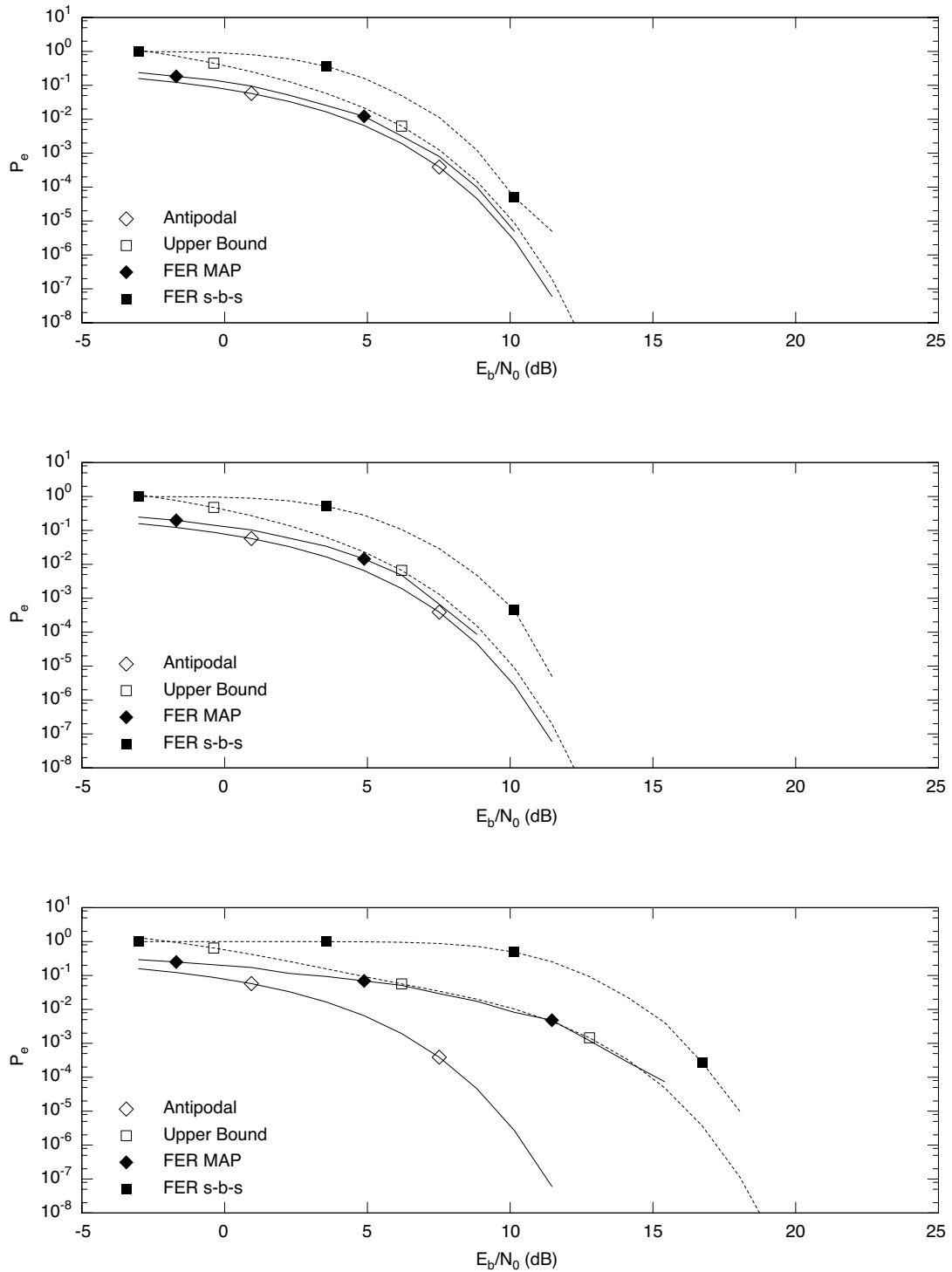


FIGURE 3
Joint field-based MAP for 28-bit field values separated by 1.

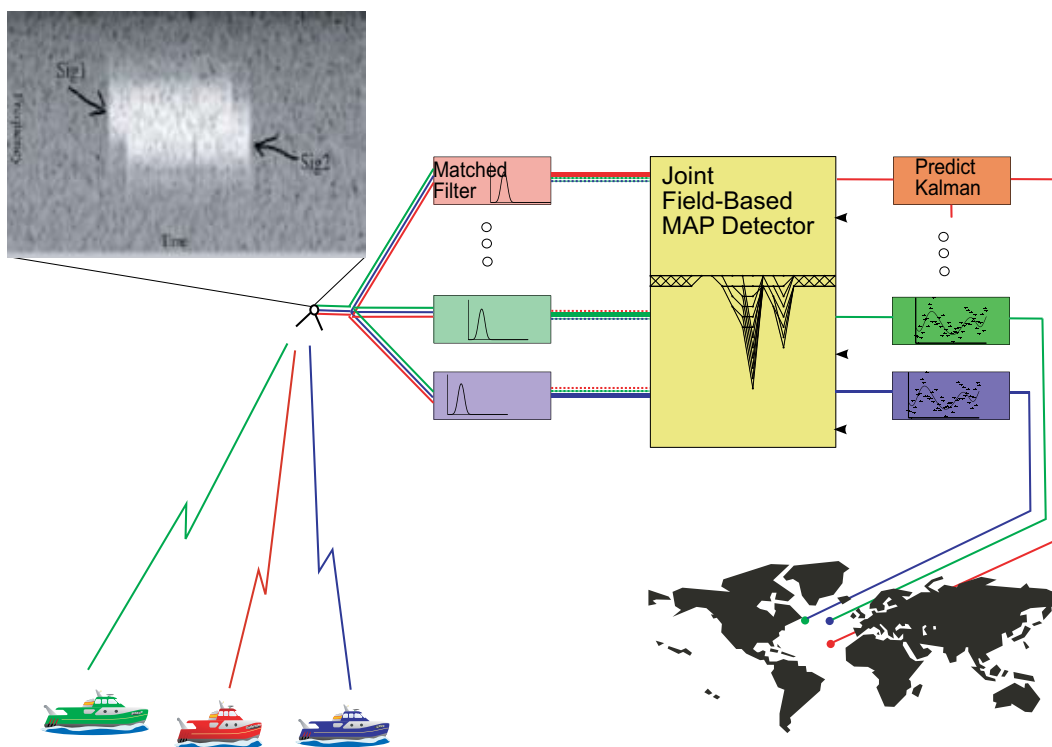


FIGURE 4
Application of joint field-based MAP.

estimated parameters. The resulting decision statistics are then passed to the Joint Field-Based MAP detector, along with *a priori* information derived from previous receptions or other sources. The output of the decisions from the joint detector is then passed to prediction algorithms for future receptions.

This work focuses on advanced reception techniques that are of particular relevance to the military. Most of these techniques are applicable when there is sufficient extra processing capability available. These techniques are tailored toward asymmetric communications; the scenario where there are existing transmitters and an advanced receiver platform. Although this work uses the AIS signal as an example, it is envisioned that with adequate processing resources, these algorithms can be used to improve the bit error rate (BER) performance of many other systems. This work presents simulation and analytical bounds demonstrating the benefit of using these advanced detection techniques on cochannel signals.

[Sponsored by USAF]

References

¹S. Verdú, *Multuser Detection*, Cambridge University Press, 1st ed. (1998).
²“Technical Characteristics for a Universal Shipborne Automatic Identification System Using Time Division Multiple Access in the VHF Maritime Mobile Band,” ITU-R M.1371-1, 2001.
³“IALA Technical Clarifications on ITU Recommendation,” ITU-R M.1371-1, 2003.

⁴“Adoption of Amendments to the International Convention for the Safety of Life at Sea, 1974, as amended,” 2000. Resolution MSC.99(73).

⁵H. L. Van Trees, *Detection, Estimation, and Modulation Theory Part I*, Wiley (2001). ★

Remotely Measuring Turbulent Coastal Atmospheres

W.P. Hooper,¹ G.M. Frick,¹ B.P. Michael,² and R.J. Lind³

¹Remote Sensing Division

²Command Support Division

³Naval Postgraduate School

Introduction: In April and May 2006, personnel from the Remote Sensing Division conducted joint measurements with Naval Postgraduate School (NPS) personnel in testing the capabilities of a recently developed eye-safe lidar that tracks the movement of large aerosol structures (Fig. 5). The test was conducted at Point Sur, CA, a rugged coastal region 30 km south of Monterey, CA, noted for high winds. In coastal areas where winds and large shoaling waves make in situ measurements difficult, scanning lidars represent a powerful tool for remotely measuring the winds and visualizing the airflow.

Transmitter Design: Scanning lidars have been used since the 1970s to measure winds and map aerosol structures;¹ however, eye-safety issues severely limited the use of these early systems. Powerful optical pulses are required to generate detectable backscatter signals from atmospheric aerosols. Since these pulses can damage the eye's retina, measurements could not be made near airports and in urban areas. This problem has been solved in recent years with Optical Parametric Oscillators (OPO) or Raman methane gas cells, which can convert the optical pulses to safer wavelengths (in the 1.5 μm band) that are absorbed by the eye's humor and can not reach the retina. Now the transmit power is limited not by safety issues but by the conversion process since the highly focused beam required for the conversion process can damage OPO crystals or convert methane to soot.

To increase the output power density of the eye-safe lidars, the NRL system uses deuterium instead of methane or OPO. Unlike the methane cells that require recirculating fans and are multipass, the Raman deuterium cells have no moving parts and require only a single pass to generate a backward-scattered or phase-conjugated beam. When generated by comparable lasers, a phase-conjugated pulse is found to be half the length and one third the divergence of the forward-scattered pulses from OPO crystals or methane cells. Since the photodiode detectors in the 1.5 μm band are only 200 microns in diameter, using a highly collimated transmit beam is important, allowing efficient collection and focusing of backscattered light onto the detector.

Measurements: Airflow by the Point Sur area is often dominated by the turbulent eddies generated by the Point Sur rock, which is 500 m long and 100 m high (Fig. 6). The false-color image shows a horizontal lidar measurement made at the top of the rock. Approximately once a minute, the rock produces a large eddy that travels downwind and vertically mixes aerosols

generated by surf zones — these large aerosol structures are not visible to the eye but are easily tracked by a scanning lidar².

Figure 7 shows wind observations for the first week of May when the winds changed from a 20 m/s flow from the North to a weak southerly flow and then changed back to a strong northerly flow. This oscillation is typical of airflow in the Big Sur area of the California coast. The false-color image in Fig. 7 shows another horizontal lidar scan. This scan was taken on May 5 when the winds accelerated. The conditions are very different from those shown in Fig. 6. In Fig. 7, the aerosol structures are dominated by kilometer-long roll structures that persist for about 6 hours.

Summary: The NRL scanning lidar is a powerful remote sensing tool for characterizing winds and airflow in maritime areas. During comparisons with the NPS measurements, lidar wind speeds and direction measurement errors were less than 1 m/s and 5 degrees, respectively. Since our system has been validated as eye-safe by the Navy's Laser Safety Review Board, the lidar can be used near airports and in urban areas. Field tests have already been conducted along the Chesapeake Bay and in Washington, DC. The deuterium Raman cells (designed, built, and tested at NRL) have been used for over a year and have not required any maintenance. A key future step of this research is to produce a compact, autonomous lidar system for remotely mapping wind fields from Navy ships.

[Sponsored by ONR]

References

- ¹ W.P. Hooper and E.W. Eloranta, "Lidar Measurements of the Wind in the Boundary Layer: the Method, Accuracy and Results from Joint Measurements with Radiosonde and Kytton," *J. Cli. Appl. Meteor.* **25**, 990-1001 (1986).
- ² W.P. Hooper, J.E. James, and R.J. Lind, "Lidar Observations of Truculent Vortex Shedding by an Isolated Topographic Feature," *Boundary-Layer Meteorol.* **80**, 95-108 (1996). ★

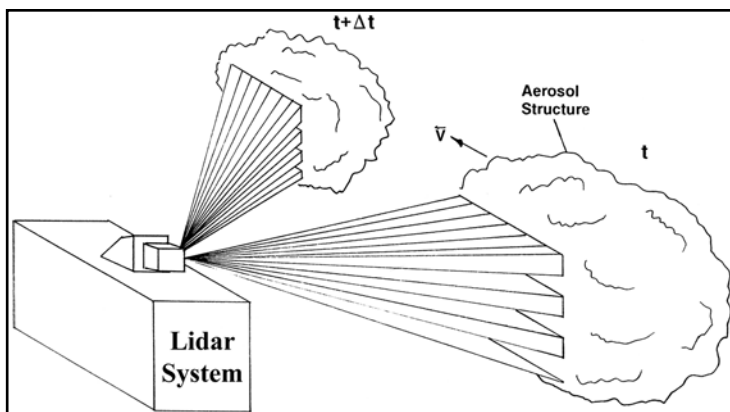


FIGURE 5
The lidar scans back and forth, mapping large aerosol structures (100 m to 1 km) and tracking their movement.

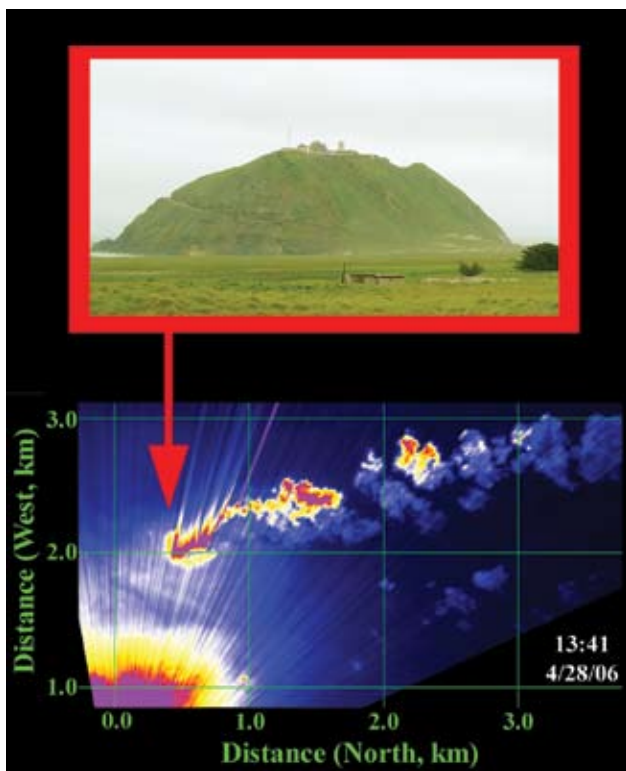
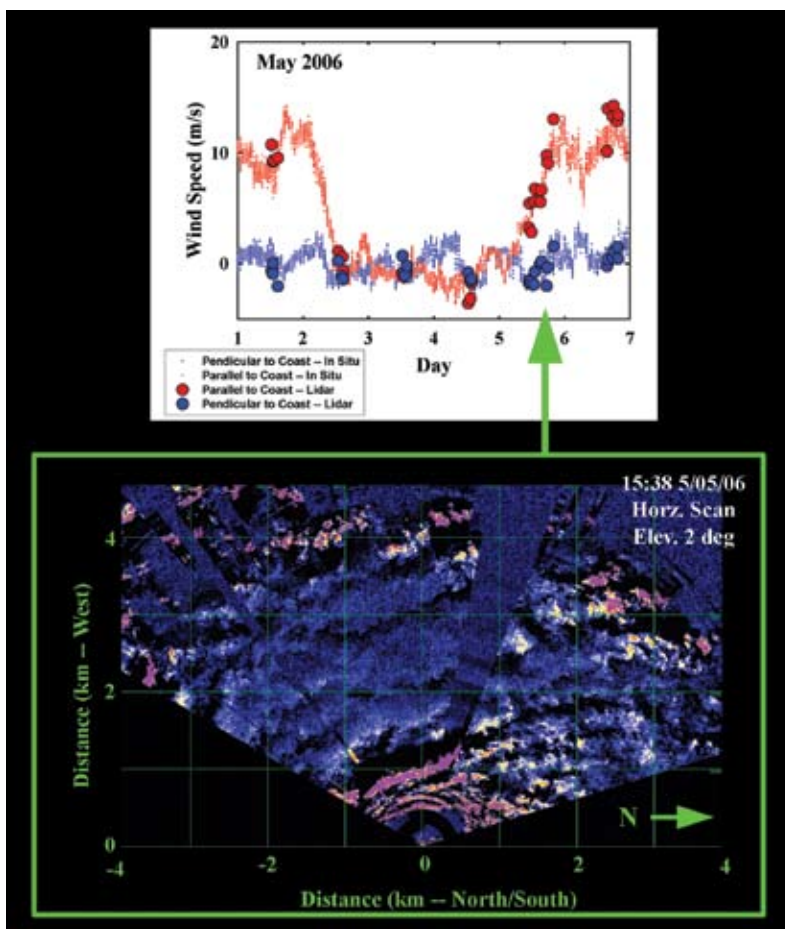


FIGURE 6
 The upper image shows the Point Sur rock, and the lower image shows a horizontal lidar scan. The color is related to the aerosol backscatter. Purple and red are the strongest returns; blue is the weakest. The rock generates eddies that move towards the North (upper right). The rock location is denoted by the red arrow.

FIGURE 7
 The upper plot shows lidar (large dots) and in situ wind measurements (small dots). The red shows the wind parallel to the coast and the blue wind perpendicular to the coast. During the first week of May, the winds decrease in speed and reverse (on May 2). Three days later, the winds reverse and increase in speed. The lower plot shows a false color image of the roll structures that are generated when the flow accelerates (the green arrow denotes the time in wind speed plot).



SIMULATION, COMPUTING, AND MODELING





217 Impact of Uncertainty on Terror Forecasting

G.S. Schmidt, J. Goffeney, and R. Willis

219 IR Photonic Bandgap Fibers for Missile Defense

I.D. Aggarwal, J.S. Sanghera, D. Gibson, F. Kung, L.E. Busse, L.B. Shaw, V.Q. Nguyen, and P.C. Pureza

221 Computational Materials Theory: Optimizing the Use of the Electromagnetic Spectrum

M.R. Pederson, M.J. Mehl, and L.L. Boyer

Impact of Uncertainty on Terror Forecasting

G.S. Schmidt,¹ J. Goffeney,² and R. Willis¹

¹Information Technology Division

²ITT Advanced Engineering & Sciences

Introduction: Intelligence analysts and military planners need accurate forecasting techniques for predicting future terror events. Terror forecasts must consider historical events, up-to-date geospatial features, terrorist behavior, and uncertainty and error in the input measurements and propagation of data. We describe our forecasting technique and investigation of the impact of uncertainty and error on predicting future terror events.

Forecasting Technique: We have developed innovative geospatial analysis and asymmetric-threat forecasting techniques for urban environments.^{1,2} The foundation of our techniques is the extraction of behavior “signatures” from associations made between information sources (for example, historical event data, sensor data, etc.) and contextual information sources (for example, geospatial and time-based demographic, economic, and political databases). The technique assumes that a terrorist’s or criminal’s choice of a certain location is influenced by a set of qualities such as geospatial features, demographic and economic factors, and recent political events.³ Focusing on geospatial information, we assume that the intended target is associated with the features located within a small distance from the event location. Furthermore, we consider the distance between key features and the event location as defining a likelihood function maxi-

mizing the values at distances common to the greatest number of events. The spatial likelihood functions are used to generate a choropleth map (a map showing differences between regions by using shading or coloring). A sample forecast for likely suicide attacks by militants in Haifa is shown in Fig. 1(a).

Inclusion of Uncertainty: Forecasts not accounting for uncertainty in the input measurements potentially mislead planners into allocating security resources to protect lower-value targets. Uncertainty and error of data play a role throughout the complete process of generating terror forecasts, ranging from data collection to generation of spatial likelihood functions to presentation of the forecasts. By working with a field expert and surveying the literature we generated a table of these factors. We preliminarily categorized the factors by: (1) *building databases* — event data collection, feature data selection, and data confidence assessment; (2) *generating forecasts* — data retrieval and transformation, uncertainty modeling, probability density function (PDF) generation, and likelihood layer aggregation; and (3) *data presentation* — data preparation, forecast visualizations generation, and user interface. We made a list of variables and values that fit into each category, some of which propagate throughout all layers of the table hierarchy. Currently, we are ranking the factors by how much they contribute to change in the forecasts.

Testing Uncertainty Impact: We investigated the impact that uncertainty has on forecasting by testing a small set of the uncertainty factors from our table. Here we highlight one experiment testing error in the



FIGURE 1

(a) Choropleth map showing threat “hotspots” color-coded by likelihood — red represents highest likelihood. (b) Inclusion of historical event position uncertainty by Monte Carlo simulation.

position of the historical event recordings. Our datasets include historical information pertaining to suicide bombings such as date, time, responsible faction, event position, and confidence. These confidence values, ranging from 1 to 5, correspond to a uniform distribution of error in the reported event position with values starting at 10 m and increasing radially by a power of 10 for each rank as assigned by analysts sorting through text descriptions of the events with information like “event X occurred in the doorway of a club while event Y occurred somewhere within a settlement.” We incorporate the event position uncertainty using a Monte Carlo simulation technique that perturbs the event location within its confidence radius. Since the distance between the event position and feature of interest varies upon each iteration of the simulation, the likelihood values for a given geo-coordinate are aggregated. We stop the Monte Carlo simulation when the coefficient of variation — a minimal number of iterations that indicates statistical significance has been achieved — is reached.¹

Starting simply, using a one-layer Geographic Information System (GIS) feature set consisting of locations of gas stations, the distance associated with the maximum likelihood of a suicide bombing event for a specific faction is about 0.5 km when uncertainty is not included. As the radius of uncertainty increases, the maximum likelihood distance increases by up to 0.4 km (see Fig. 2). This effect, though negligible on a coarse grid, is significant for neighborhood-scale forecasting where the predicted “hotspots” may shift several blocks (see Fig. 3). As the number of GIS layers increase, the uncertainty propagates and a very different surface results.

Conclusions: Our forecasting techniques excel at reducing the search area required and maximizing the placement of resources (for example, sensors, troops, and intelligence operators). Versions of our forecasting techniques are already in use by intelligence analysts and military planners within the Department

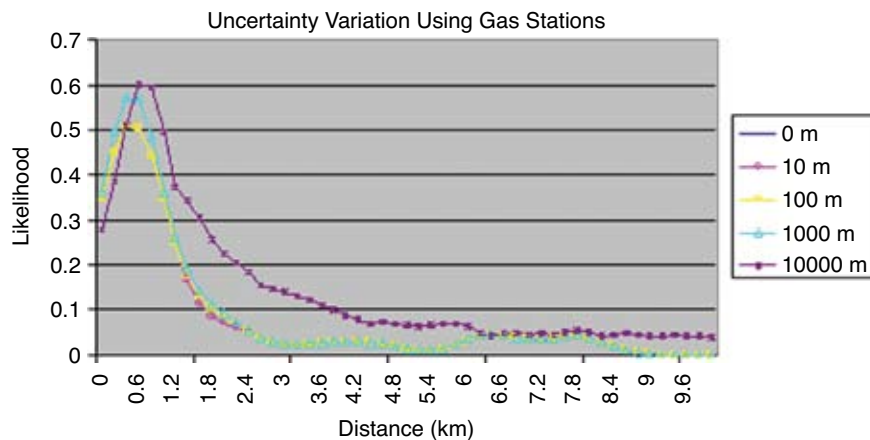


FIGURE 2 The PDFs generated for uncertainty levels of 0, 10, 100, 1000, and 10,000 m. The distance of the maximum likelihood increases and the PDFs become less defined as the uncertainty increases.

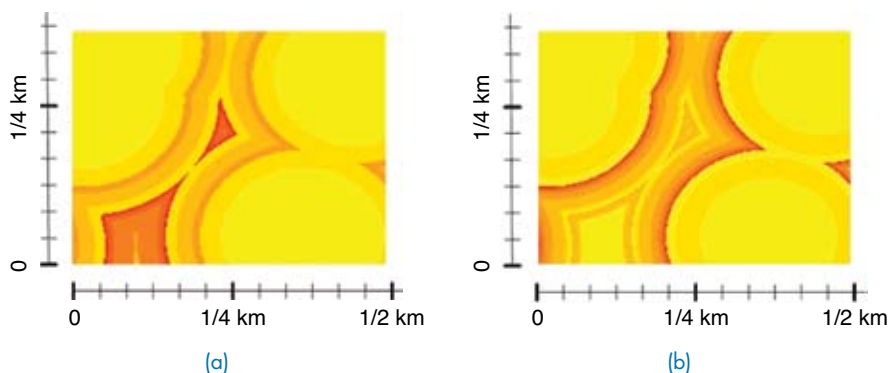


FIGURE 3 Two likelihood surfaces generated for a neighborhood in Jerusalem. (a) No uncertainty is factored in. (b) Includes variation in the event position up to 10 km. The red “hotspots” (maximum likelihoods) have moved to entirely new locations.

of Defense and the Department of Homeland Security to narrow the search space for high value individuals. Our initial investigations of the impact uncertainty has on the forecasts indicate: (1) the likelihood values shift a reasonable amount for moderate changes in data parameters (though we need to perform more parameter sensitivity tests), and (2) the range of threat “hot-spots” increases and will need to be filtered in order to comply with the goals of the forecasts — reducing the search area. We conclude showing the latter case — incorporating event position uncertainty in the Haifa region — in Fig. 1(b).

[Sponsored by OSD]

References

- ¹G. Schmidt, J. Goffeney, J. Dalton, and R. Willis, “Generating Imagery for Forecasting Terror Threats,” *SPIE Newsroom*, January 2007.
- ²J. Goffeney, G. Schmidt, J. Dalton, J. D’Archangelo, and R. Willis, “Forecast Visualizations for Terrorist Events,” *IEEE Visualization*, Nov. 2006.
- ³D. Brown, J. Dalton, and H. Hoyle, “Spatial Forecast Methods for Terrorist Events in Urban Environments,” Symposium on Intelligence and Security Informatics (ISI), 3073, 426-435, June 2004. ★

IR Photonic Bandgap Fibers for Missile Defense

I.D. Aggarwal, J.S. Sanghera, D. Gibson, F. Kung, L.E. Busse, L.B. Shaw, V.Q. Nguyen, and P.C. Pureza
Optical Sciences Division

The Application: IR-transmitting fibers fabricated at the Naval Research Laboratory (NRL) have low optical loss (~ 0.2 dB/m) and have been successfully used in aircraft missile defense system demonstrations for the 2 to 5 μm region to replace bulk optics connecting the laser to the jam head as well as being “wired” inside the jam head.¹ These conventional, solid-core fibers result in significant weight reduction. They reduce system size and complexity as well as cost of both installation and maintenance, and are capable of laser power input typical of current systems. However, advanced infrared threats require much higher laser power, which these solid-core fibers cannot tolerate.

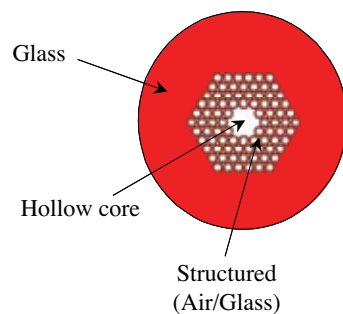


FIGURE 4

Endface view of the hollow core photonic bandgap fiber (HC-PBG) showing the microstructured region surrounding the core, as well as the protective outer layer of glass.

The Solution: A new type of fiber, called the hollow-core photonic bandgap (or HC-PBG) fiber, has been developed and demonstrated using silica glass. These fibers consist of a hollow air core, surrounded by an ordered series of holes (formed by hollow tubes) and then an outer solid glass protective clad (Fig. 4). Theoretical predictions show that greater than 99% of the light transmits through air, with the so-called “microstructured” region around the core serving as a type of Bragg grating to maintain propagation at specific ranges of wavelengths that are determined by the small holes’ spacing and diameter.

HC-PBG fibers are very attractive for the very high laser power transmission needed in missile defense systems currently under development to defeat advanced IR threats. However, even with only 1% of the light interacting with the glass, the losses for silica HC-PBG fibers are inherently too high to make them useful in the infrared. At NRL we are developing PBG fibers based on IR-transmitting materials by leveraging in-house expertise with materials purification and fabrication techniques.

Design and Fabrication: We have designed PBG fiber structures by solving Maxwell’s equations in a periodic structure as an eigenvalue problem with the electromagnetic field expanded in a basis of plane waves.² One example of a structure modeled for transmission at around 4 μm using a sulfide-based glass consists of a hole size and spacing in the micro-structured region of 3.2 and 6.4 μm , respectively, and the air fill factor in that region is 89%. By adjusting the micro-structure hole size, spacing, and fill factor, different wavelength regions for transmission can be obtained. The PBG fiber produces a uniform Gaussian modal output,² providing a low divergence output needed for systems that are increasingly requiring high brightness and spatial quality.

High purity glasses have been fabricated and made into high precision tubes using NRL’s extrusion technology. These tubes are then stretched and stacked into the appropriate geometry (Fig. 5), to make a preform that also has an outer glass surrounding the tubes to keep them fixed and to provide mechanical strength. The whole assembly is then drawn into HC-PBG

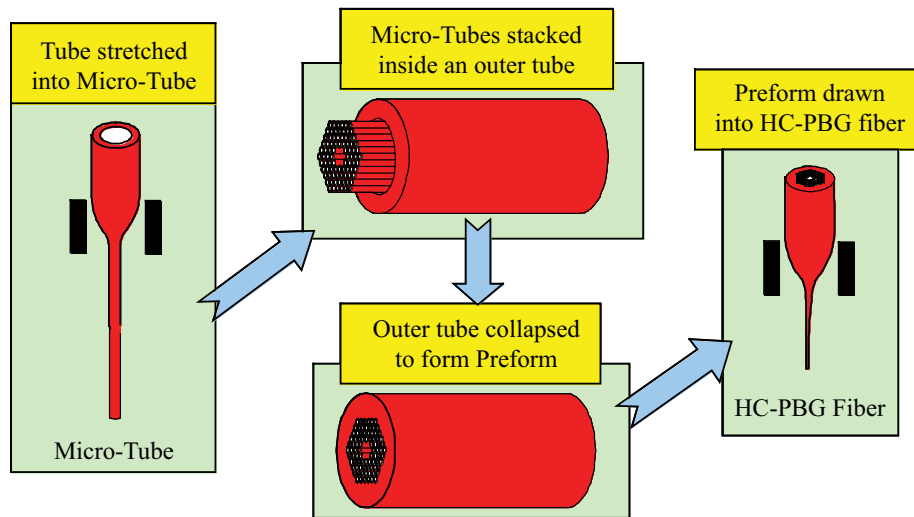


FIGURE 5 Tube stacking to make preform and drawing of HC-PBG fiber.

fiber on a draw tower with special adaptations for this purpose, and within a clean room environment. Figure 6 shows a stacked preform and preliminary fibers made from sulfide-based materials.

NRL has confirmed that HC-PBG fibers have negligible loss upon bending. This was demonstrated by no change in output from HC-PBG fiber with and without 11 half-inch bends around a mandrel. These remarkable results show the flexibility and utility of these fibers for practical systems where they may need to be routed through tight spaces.

Summary: Future missile defense systems currently under development to protect military or civilian

aircraft require higher output power due to advanced infrared threats. For the more advanced systems, we are developing infrared-transmitting HC-PBG fibers, which are capable of at least 100 times more power handling capability due to 99% of the power being transmitted through the hollow core. They possess a low divergence output, and furthermore, antireflection coatings are not needed. Fibers have been designed for transmission within the mid-IR (2 to 5 μm) region. High purity glasses have been fabricated using NRL's world class facilities, and novel extrusion technology has been developed to make microstructured preforms that have been drawn into HC-PBG fibers. The fibers exhibit high strengths comparable to their solid core

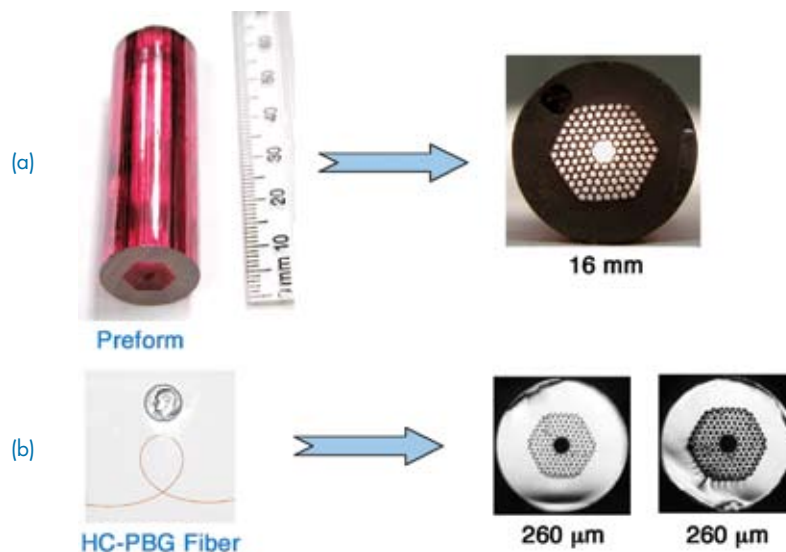


FIGURE 6 (a) Microstructure preform and (b) HC-PBG fiber made from IR transmitting sulfide glass.

counterparts. The availability of these fibers will impact next generation missile defense systems using ultra-high-power IR lasers.

[Sponsored by NRL]

References

¹L.E. Busse, J.S. Sanghera, I.D. Aggarwal, A. Carbonaro, and T.H. Evans, "Infrared-Transmitting Fibers for Advanced IRCM System Demonstrations," Proc. 39th MSS Specialty Group Meeting on Infrared Countermeasures, Volume I, Laurel, MD, 1-3 May 2001.

²L.B. Shaw, J.S. Sanghera, I.D. Aggarwal, and F.H. Kung, "As-S and As-Se Based Photonic Bandgap Fiber for IR Laser Transmission," *Opt. Express* 11 (25), 3455-3460 (2003). ★

Computational Materials Theory: Optimizing the Use of the Electromagnetic Spectrum

M.R. Pederson, M.J. Mehl, and L.L. Boyer
Materials Science and Technology Division

Introduction: The ability to computationally predict how materials respond to incident radiation is of immeasurable importance to practically every DoD and civilian technology. While applications are too numerous to list, they include spectroscopic remote sensing, infrared night vision technologies, X-ray analysis, magneto-resonance imaging, photovoltaic light harvesting, information transmission and storage, and quantum control of molecules. In principle, the ability to theoretically predict how molecules and materials respond to incident radiation has been in hand since the early days of quantum theory of materials. While more improvements are required and are on their way, today, due to long-term support of the Office of Naval Research and significant contributions from Navy researchers, scientists are able to computationally predict how materials interact with X rays, optical radiation, infrared and terahertz radiation, and extremely low frequency radiation such as that due to microwaves and static fields. Work discussed here pertains to the computational prediction of a material's ability to respond to radiation in the latter four frequency ranges.

A precise roadmap for success in this endeavor would have been difficult 40 years ago. In retrospect, we now know that it first required a very new, indeed Nobel-prize winning theorem on quantum theory (1964), which today is known as density-functional theory (DFT).¹ In essence, this ONR-supported discovery told us that the quantum aspects of nature were significantly simplified for environments, such as those found on Earth, where most molecules and materials are primarily found in their lowest-energy electronic state. While the discovery of DFT essentially

told us that computational materials science and chemistry was simpler than previously thought, unveiling the simplicity was itself a second monumentally difficult task that required approximately 30 years of dedicated analytical work before a relatively accurate DFT method, now known as the generalized-gradient approximation (GGA), was developed by Perdew and tested by coworkers.² A third major task was to computationally implement and test these fundamental insights and to convert the understanding into software that would allow a larger group of scientists to harness the predictive powers of computational materials science. Through the last four decades, ONR has further fostered the development through broad support of university researchers. In parallel, NRL has maintained a world-class effort in this area. In addition to partially supporting and collaborating on tests of the now widely used GGA,² scientists in the Center for Computational Materials Science (CCMS) have developed and applied a wide variety of computational tools for performing DFT calculations on molecules^{2,3} and bulk materials.^{2,4}

Computationally Enhanced Vibrational Sensing:

Approximately 10 years ago, fast methods for predicting the Raman, infrared, and terahertz response and spectra of molecular materials were developed in the CCMS.⁵ This capability has impacted several recent DoD-relevant efforts for which the computational understanding of the interactions between radiation and materials has arisen during the last two or three years. An early joint theory and experimental application of this method demonstrated that physisorbed organic molecules on metal surfaces could be detached by coupling an infrared source to strongly bonded surface atoms.⁶ In essence, this provides a generic approach for low-energy vaporization of small quantities of molecules that are adhered to a larger piece of inert material. From the standpoint of understanding the structure of a semiconducting neutron sensing material, the developer of these materials approached NRL-CCMS researchers to aid in characterizing the structure of the films.⁷ Similarly, the vibrational spectrum of heavy diamond-like particles, found naturally in oil deposits and used for tracking oil spills and their origins, has recently been calculated by NRL researchers.⁸ Also, work aimed at understanding the absorption spectrum and solar-induced charging of an organic photovoltaic molecule (see Figs. 7 and 8) has been performed in response to a computational challenge from the DoD High Performance Computing Modernization Office.⁹ In addition, very unique codes for predicting how magnetic nanoparticles resonantly absorb and emit low-energy electromagnetic radiation in molecular materials have been developed in the CCMS.¹⁰ The energy released, currently in the sub-THz range, may

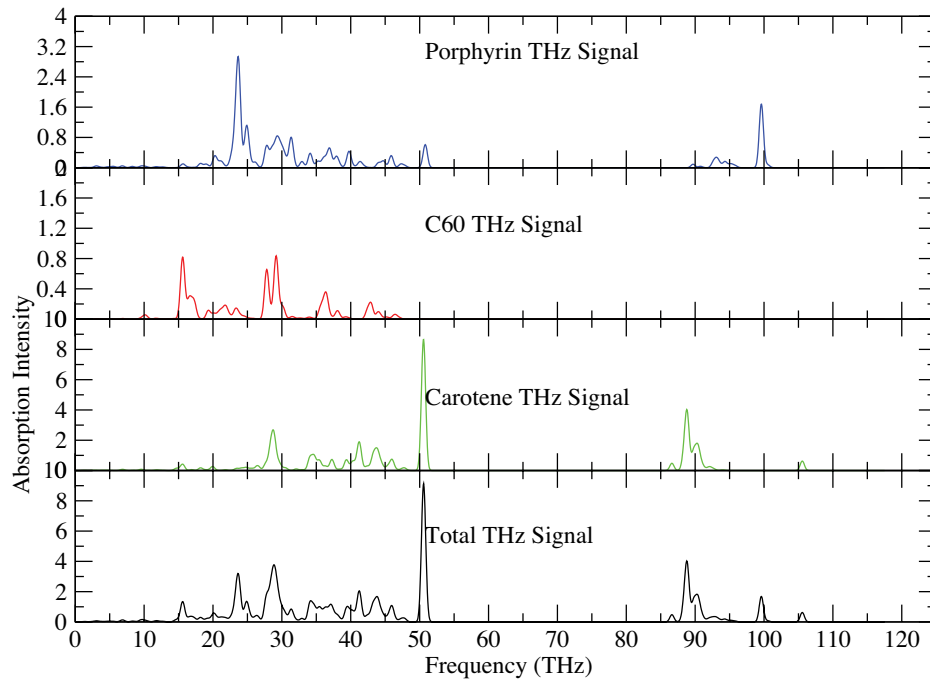


FIGURE 7
Density-functional-based prediction of charge-transfer state of a molecular photovoltaic.

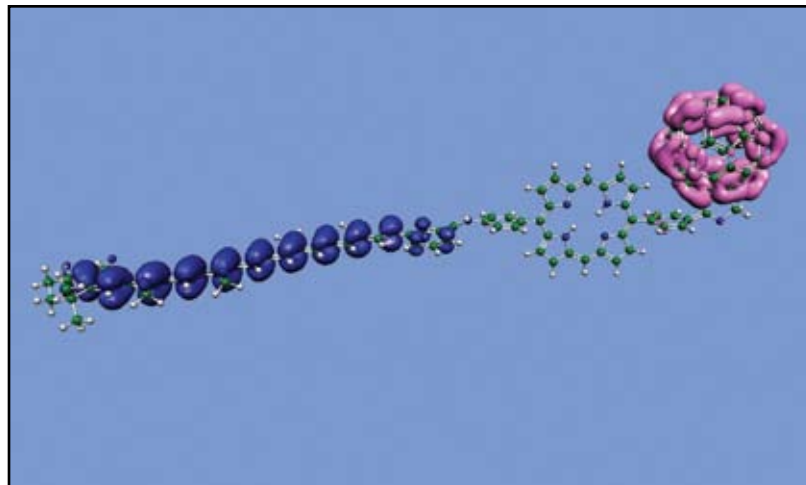


FIGURE 8
Density-functional-based determination of the THz spectra of the molecular photovoltaic depicted in Fig. 7. The weak signal in the 0 to 1 THz range underscores the fundamental scientific challenges that must be overcome to achieve sensing technologies in this energy range.

provide a key to future THz oscillators if the magnetic molecules may be further optimized computationally.

Future Challenges and Capabilities: Future fundamental developments at the intersection of computational materials science and electromagnetic sensing will further impact our capabilities in both civilian and military theaters. While NRL researchers are currently capable of determining what a material is by comparing measured and calculated vibrational and optical spectra, an important goal is to learn how to control the properties of a specific molecular material by optimizing the power distribution of an incident electromagnetic radiation source. Such a capability will allow for a variety of DoD-centric technologies, which range from lower-energy (i.e., lower-cost) synthesis of materials to sensing harmful materials. These two techniques, if combined, could possibly allow for simultaneously sensing and degrading or converting a harmful material. Conversely, for conversion of sunlight or other sources of electromagnetic radiation (such as that from lasers) into electrical energy or battery-charging applications, it is the materials properties that must be computationally controlled to optimize the efficiency of energy transfer. Solution of this fundamental problem could allow remote recharging of batteries. Work along these lines continues in the CCMS at NRL. Success along these lines will provide some of the new technologies required to respond to challenges of the near future.

Acknowledgment: This work was supported in part by the Office of Naval Research and NRL 6.1 Core funding, the DoD High Performance Computing Modernization Office, and the National Science Foundation.
[Sponsored by ONR, NRL, and NSF]

References

- ¹ P. Hohenberg and W. Kohn, "Inhomogeneous Electron Gas," *Phys. Rev.* **136**, B864 (1964); W. Kohn and L.J. Sham, "Self-Consistent Equations Including Exchange and Correlation Effects," *Phys. Rev.* **140**, A1133 (1965).
- ² J.P. Perdew, J.A. Chevary, S.H. Vosko, K.A. Jackson, M.R. Pederson, D.J. Singh, and C. Fiolhais, "Atoms, Molecules, Solids and Surfaces: Applications of the Generalized Gradient Approximation for Exchange and Correlation," *Phys. Rev. B* **46**, 6671 (1992).
- ³ M.R. Pederson, D.V. Porezag, J. Kortus, and D. Patton, "Strategies for Massively Parallel Local-orbital-based Electronic Structure Calculations," *Phys. Stat. Solidi B* **217**, 187-218 (2000).
- ⁴ M.J. Mehl, R.E. Cohen, and H. Krakauer, "Linearized Augmented Plane-wave Electronic-structure Calculations for MgO and CaO," *J. Geophys. Res. – Solid, Earth and Planets* **93**, 8009 (1988).
- ⁵ M.R. Pederson and D.V. Porezag, "Infrared Intensities and Raman-scattering Activities Within Density-functional Theory," *Phys. Rev. B* **54**, 7830 (1996).
- ⁶ M.B. Knickelbein, G.M. Koretsky, K.A. Jackson, M.R. Pederson, and Z. Hajnal, "Hydrogenated and Deuterated Iron Clusters: Infrared Spectra and Density Functional Calculations," *J. Chem. Phys.* **109**, 10692 (1998).
- ⁷ K. Park, M.R. Pederson, and L.L. Boyer, et al., "Electronic Structure and Vibrational Spectra of C₂B₁₀-based Clusters and Films," *Phys. Rev. B* **73**, 035109 (2006).
- ⁸ S.L. Richardson, T. Baruah, M.J. Mehl, and M.R. Pederson, "Theoretical Confirmation of the Experimental Raman Spectra of the Lower-order Diamondoid Molecule: Cyclohexamantane (C₂₆H₃₀)," *Chem. Phys. Lett.* **403**, 83, 2005; S.L. Richardson, T. Baruah, M.J. Mehl, and M.R. Pederson, "Cyclohexamantane (C₂₆H₃₀): First-principles DFT Study of a Novel Diamondoid Molecule," *Diamond and Related Materials* **15**, 707 (2006).
- ⁹ T. Baruah and M.R. Pederson, "Density Functional Study on a Light-harvesting Carotenoid-porphyrin-C₆₀ Molecular Triad," *J. Chem. Phys.* **125**, 164706 (2006).
- ¹⁰ A.V. Postnikov, J. Kortus, and M.R. Pederson, "Density-Functional Studies of Molecular Magnets," *Phys. Stat. Solidi B* **243**, 2533-2572 (2006). ★

SPACE RESEARCH AND SATELLITE TECHNOLOGY





227 On-Orbit Microwave Curing of Space Shuttle Repair Materials

A.W. Fliflet, M.T. Lombardi, S.H. Gold, D. Lewis III, R.W. Bruce, and A.K. Kinkead

229 The STEREO Mission: A Three-Dimensional View of the Sun and Heliosphere

J.W. Cook, J.S. Newmark, and R.A. Howard

232 The NRL Precision Orbital Transfer Vehicle

M.S. Johnson, S.R. Morgan, W.S. Vincent, K.H. Gallelli, B.P. Whalen, A. Hope, S.S. Chappie, and R.G. Skalitzky

On-Orbit Microwave Curing of Space Shuttle Repair Materials

A.W. Fliflet,¹ M.T. Lombardi,¹ S.H. Gold,¹
D. Lewis III (retired),² R.W. Bruce,³ and A.K. Kinkead⁴

¹*Plasma Physics Division*

²*Materials Science and Technology Division*

³*ICARUS Research Inc.*

⁴*LET Corporation*

Introduction: The loss on re-entry of the space shuttle *Columbia* on February 1, 2003, from launch damage to the reinforced carbon composite (RCC) wing leading edge has led NASA to require capabilities for shuttle on-orbit inspection and repair. NRL's Beam Physics Branch became involved with efforts to develop repair technologies for RCC materials through their expertise in microwave materials processing and microwave systems design and fabrication. Microwave sources are well suited for curing repair materials in the space environment because of their high electrical efficiency and ability to couple energy into repair materials volumetrically to provide rapid, localized heating. Alternative methods (heat lamp or a conductive heating blanket) were unsuitable because of inefficient surface heating with the heat lamp or difficulty in positioning the blanket in microgravity to obtain proper heating of the repair area without damaging the repair surface. The NRL team's investigation of on-orbit microwave curing of shuttle repair materials was carried out in collaboration with scientists at NASA Marshall Space Flight Center (MSFC), Huntsville, AL, and astronaut James F. Reilly II.

Technical Approach: Initial studies of applying microwave heating looked at the repair of fairly large damaged regions of the shuttle leading edge, but later work focused on the possibility of repairing small cracks and spalls, as these are the most common form of damage and are most amenable to astronaut repair on-orbit. Small cracks in the shuttle leading edge can be repaired by filling them with a material called Non-Oxide Adhesive eXperimental, or NOAX, a material developed by NASA consisting of a SiC precursor (hydridopolycarbosilane) filled primarily with SiC powder. It is designed to be applied by an astronaut using a space-adapted caulking gun and putty knife. The NOAX material couples well to 2.45-GHz microwaves; however, there is little microwave absorption by, or penetration into, the RCC material. To apply microwave heating, it was therefore necessary to use a microwave applicator capable of generating large microwave fields in the crack region. The NRL team used an approach previously developed for microwave joining.¹ This approach uses the fact that an electromagnetic

field polarized perpendicular to the crack direction can propagate into the NOAX-filled crack, which acts as a narrow dielectric-filled waveguide. The NOAX is heated by placing a simple microwave applicator, formed by tapering a standard rectangular S-band waveguide in the short dimension from 1.4 in. to 0.4 in., over the crack region. During heating, a three-stub impedance tuner placed upstream from the waveguide taper is adjusted to minimize the reflected power, thus optimizing the microwave coupling to the NOAX. Initial tests to determine the power requirements and heating protocols needed to cure the NOAX used an industrial 6 kW, 2.45 GHz magnetron. Microwave absorption by the NOAX was found to be temperature dependent, with a marked decrease occurring after pyrolyzation sets in at 800 °F, a feature that can be used as an indication of process completion. Several analog RCC samples with NOAX-filled cracks were prepared at NASA/MSFC in a vacuum glovebox, delivered to NRL by astronaut Reilly for microwave processing, and then shipped to St. Louis, MO, for successful testing in the Boeing arcjet facility. Photographs of repaired and untreated crack-containing samples are shown in Fig. 1. A typical heating protocol is shown in Fig. 2.

Prototype Development: Based on these studies, a brassboard microwave curing system (MCS) was designed and fabricated (Fig. 3). This system consists of a commercial off-the-shelf (COTS) magnetron and power supply, a tuner (for impedance matching) and the applicator. Discussions with extra-vehicular activity (EVA) tool designers at NASA Goddard Space Flight Center, MD, and Swales Aerospace, MD, made clear the necessity for compactness and ease of use by space-suited astronauts. A procedure requiring few adjustments during processing was sought. In the initial tests, the tuner was continually adjusted to minimize the reflected power. In prototype tests it was found that a single tuner setting could often be used. The overall efficiency of the magnetron and power supply was found to be about 65%, leading to thermal loads in the range of 200–400 W for output powers of 0.5–1 kW. Addressing the needs of the space environment, the magnetron convective air-cooling system was replaced by a metal heat sink. The prime power and energy storage requirements can be easily provided by a compact battery pack. Microwave leakage from the applicator was a concern, but a small skirt of wire-mesh screen placed around the applicator tip reduced this to milliwatt levels. Preliminary tests of operating in the vacuum environment were conducted in a large vacuum chamber/glove box at NASA/MSFC shortly before the end of the program. These tests confirmed the feasibility of the microwave processing approach, provided that the microwave power is restricted during

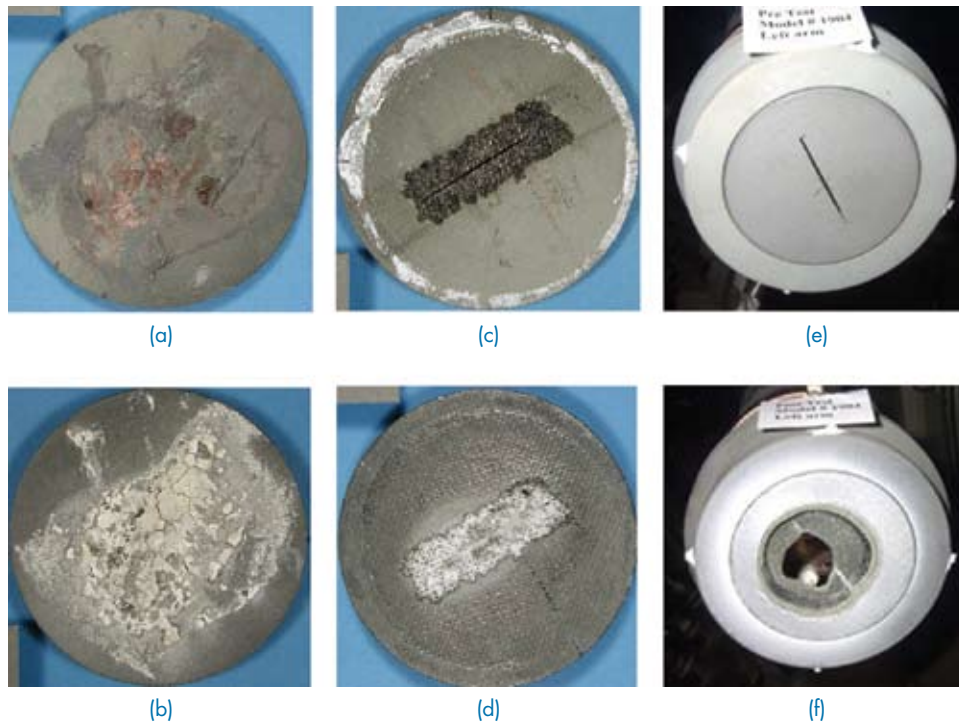


FIGURE 1
 Successful arcjet tests of microwave-cured samples (simulated crack damage in RCC analog). (a), (c) Front and back before test. A crack has been cut through the sample with SiC coating removed, on back. (b), (d) Microwave-cured NOAX crack repairs survive arcjet testing. (e) Unrepaired RCC (no NOAX), and (f) catastrophic burnthrough after arcjet testing.

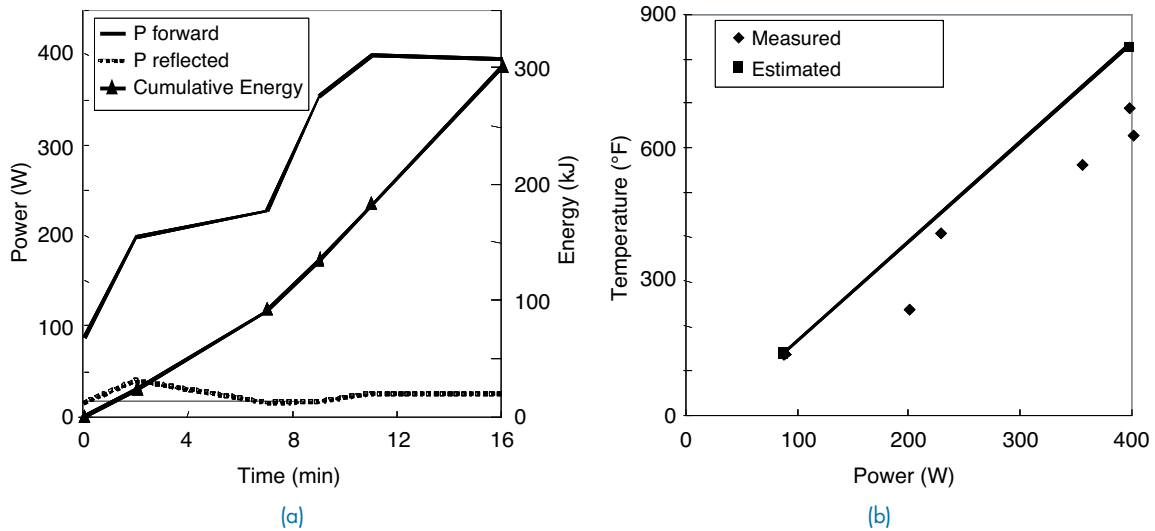


FIGURE 2
 (a) Power and energy profiles. (b) Temperature vs microwave power.

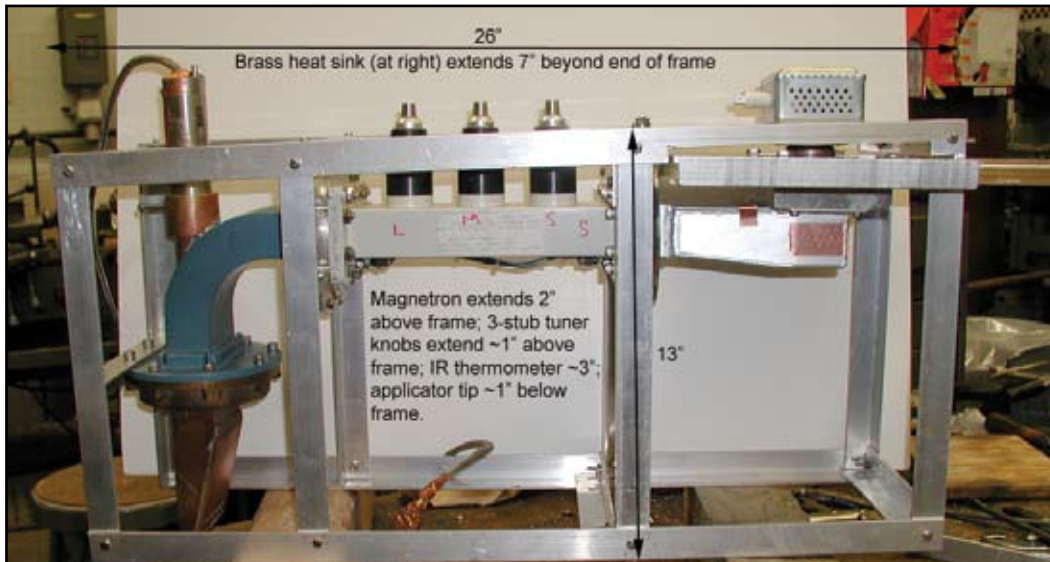


FIGURE 3
Brassboard system in aluminum frame for glove box tests.

initial heating to avoid plasma formation associated with NOAX outgassing.

This technology has demonstrated the ability to heat RCC repair materials in vacuum, and may also have land- and sea-based applications for rapid, in-situ repair of military systems such as aircraft that make use of RCC materials.

[Sponsored by NASA and ONR]

Reference

¹ S.H. Gold, D.A. Lewis, A.W. Fliflet, B. Hafizi, and J.R. Peñano, "Interference and Guiding Effects in the Heating of Ceramic Slabs and Joints with Millimeter-Wave Radiation," *J. of Materials Synthesis and Processing* **9**, 287-297 (2002). ★

The STEREO Mission: A Three-Dimensional View of the Sun and Heliosphere

J.W. Cook, J.S. Newmark, and R.A. Howard
Space Science Division

Coronal Mass Ejections: Coronal mass ejections (CMEs) are massive outflows of material from the Sun's corona, traveling into the surrounding heliosphere at speeds up to 1000–2000 kilometers per second. When directed toward the Earth, CMEs can result in damage to satellites, enhanced auroral displays, blackouts of power grids on Earth, and interference with surface radio communications. The first CME detected from space was observed by an NRL coronagraph onboard the Seventh Orbiting Solar Observatory (OSO-7) in December 1971.¹

Much of our recent knowledge of CMEs has been obtained from an NRL visible-light coronagraph (LASCO, the Large Angle Spectroscopic Coronagraph²) on the Solar and Heliospheric Observatory (SOHO) spacecraft, launched in 1995. But SOHO observes from only one viewpoint, leaving three-dimensional structure ambiguous for individual CMEs. The next step beyond SOHO is the Solar Terrestrial Relations Observatory (STEREO) mission, consisting of *two* spacecraft observing the Sun from two different viewpoints, allowing a three-dimensional view of the initiation of CMEs and their propagation outwards. In addition, STEREO will carry a new type of heliospheric coronagraph that is off-pointed from the solar disk, and can observe from the side the Sun-Earth line all the way out to Earth. The STEREO mission is meant to increase our understanding of such topics as solar structures and their properties involved in CME initiation; three-dimensional structure and kinematics of CMEs; three-dimensional structure of active regions, coronal loops, and streamers; propagation of CMEs into the corona and interplanetary medium; and the effects of CMEs through the heliosphere to the Earth.

SECCHI Instruments and Their Development:

The Sun Earth Connection Coronal and Heliospheric Investigation (SECCHI) experiment³ is one component of STEREO. SECCHI was built by an international consortium led by the Naval Research Laboratory. Major components were developed at NRL, Lockheed Martin Solar and Astrophysics Laboratory (Palo Alto, CA), Goddard Space Flight Center (Greenbelt, MD), University of Birmingham (UK), Rutherford Appleton Laboratory (UK), Max-Planck-Institut für Sonnen-

systemforschung (Germany), Centre Spatiale de Liège (CSL, Belgium), Institut d’Optique (France), and Institut d’Astrophysique Spatiale (France).

Each of the twin SECCHI instrument suites consists of five telescopes. Figure 4 illustrates how each telescope contributes to the total coverage (using existing data from SOHO observations to mimic the SECCHI observations). An extreme-ultraviolet imager (EUVI) will image the solar transition region and low corona, in four emission lines, on the disk and out to $1.7 R_{\odot}$ (solar radii). The COR1 and COR2 telescopes, visible light Sun-centered coronagraphs with nested fields of view, image the outer corona over $1.4\text{--}15 R_{\odot}$. They were split into two telescopes for better coverage of the decreasing coronal brightness over this range. The Heliospheric Imager (HI) coronagraph is off-pointed from the solar disk, and can observe from the side a distance range from $15 R_{\odot}$ out to the radius of Earth at $215 R_{\odot}$. Again, coverage is divided between two telescopes, HI-1 and HI-2. A series of linear occulters shelter HI from the glare of the Sun, while internal concentric curved baffles suppress stray light. A Guide Telescope (GT) serves as the spacecraft fine Sun sensor and provides the error signal for the EUVI fine pointing system. The SECCHI Electronics Box (SEB) was

developed by the Space Electronics Systems Development Branch at NRL. Figure 5 illustrates the SECCHI instrument suite in the laboratory.

SECCHI went through an instrument development process that included initial design, multiple project reviews, fabrication, integration to two complete packages, and laboratory testing. Characterization of the COR1, COR2, EUVI, and GT was performed at NRL, measuring stray light, spatial resolution, polarization, and photometric response. HI was calibrated at CSL, Belgium. Instrument integration and environmental testing (thermal vacuum, vibration, and electromagnetic interference and compatibility) were performed at NRL using Naval Center for Space Technology facilities prior to spacecraft integration.

Launch and Early Operations: The twin NASA STEREO spacecraft (A and B) were launched on a single Delta rocket from Cape Canaveral on October 25, 2006. Using a lunar encounter, each spacecraft was inserted into an individual final orbit, one spacecraft (B) gradually falling behind Earth in orbit and the other (A) increasingly ahead of Earth. SECCHI first light for each of the A and B telescopes was achieved during the first half of December. Figure 6 illustrates

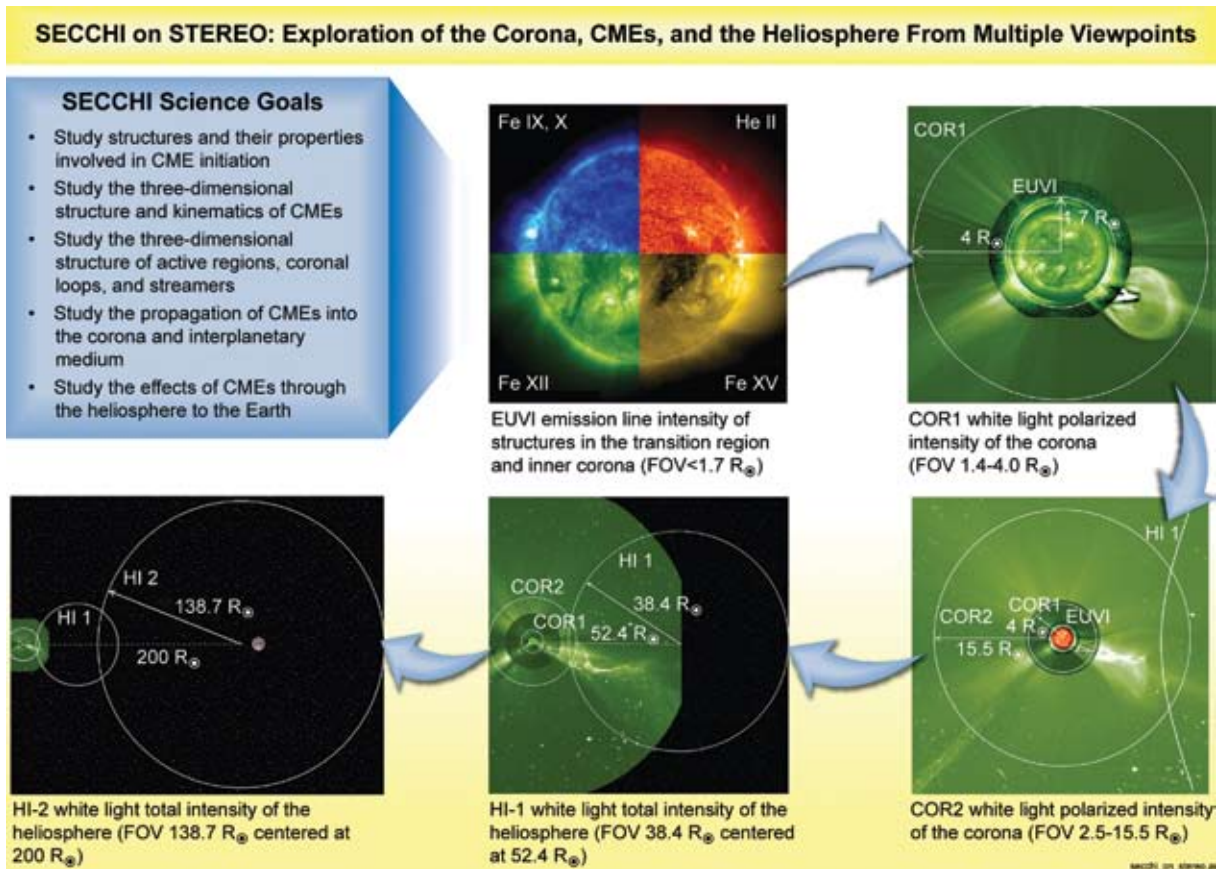


FIGURE 4
SECCHI telescopes and their fields of view.

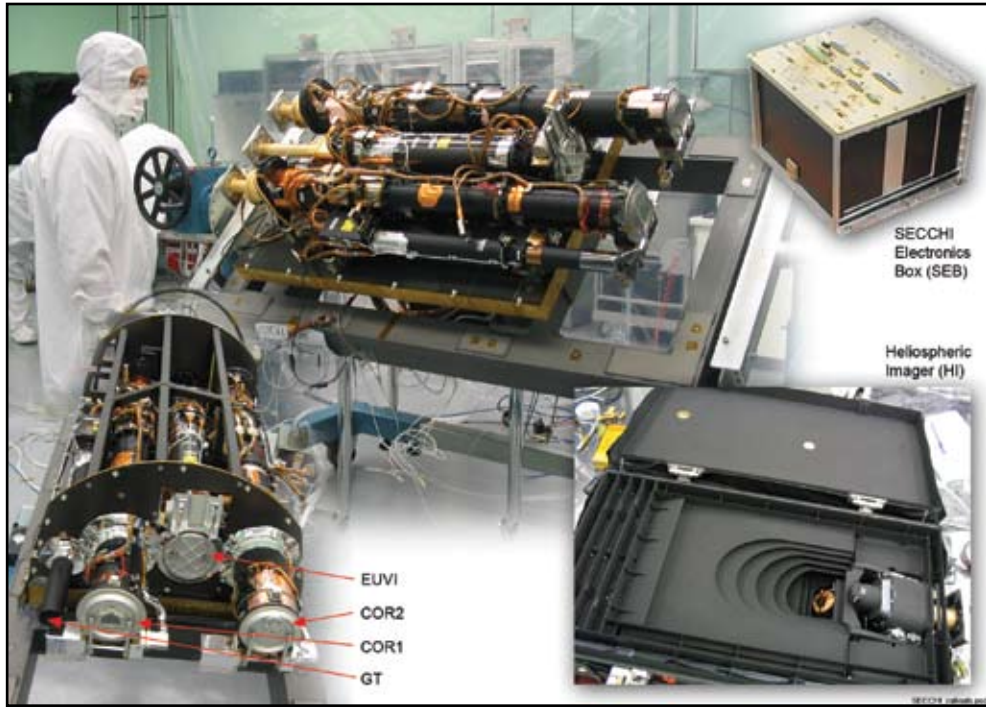


FIGURE 5
SECCHI instrument suite in the laboratory.

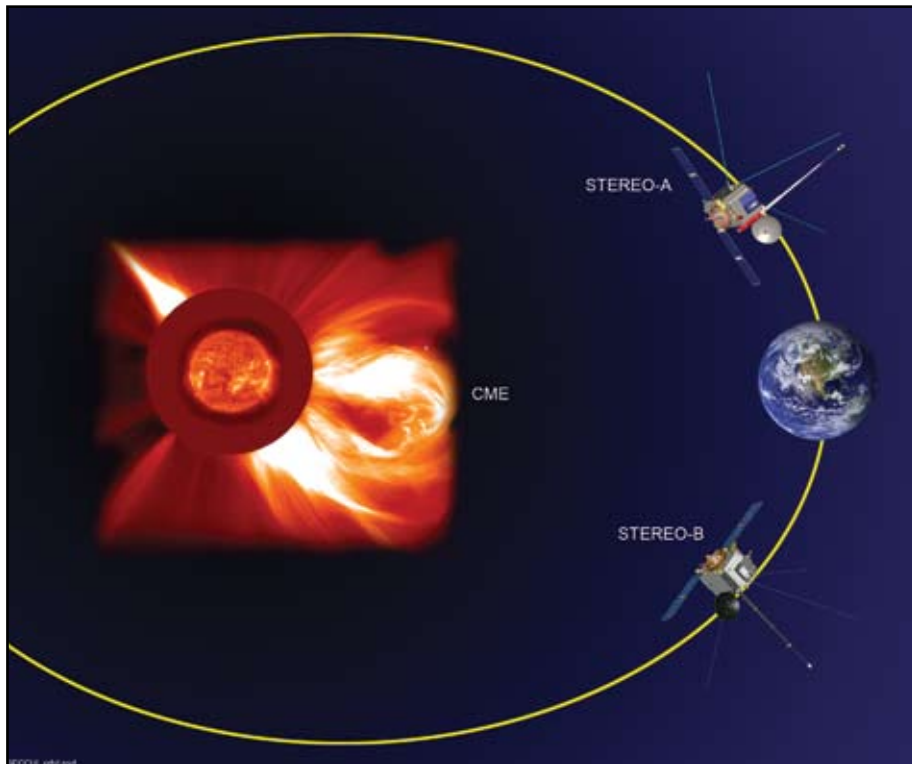


FIGURE 6
The STEREO A and B spacecraft observing an Earth-directed CME.

how the scientific observations will be undertaken, showing a simulated Earth-directed CME observed from the A and B spacecraft. The SECCHI COR2A coronagraph already observed its first CME during earliest instrument open-door operations in December 2006.

[Sponsored by NASA and ONR]

References

- ¹R. Tousey, *Space Research XIII*, 713 (1973); and see frontispiece to *Solar Physics* 24(2) (1972).
- ²G.E. Brueckner, R.A. Howard, M.J. Koomen, C.M. Korendyke, D.J. Michels, J.D. Moses, D.G. Socker, K.P. Dere, P.L. Lamy, A. Llebaria, M.V. Bout, R. Schwenn, G.M. Simnett, D.K. Bedford, and C.J. Eyles, "The Large Angle Spectroscopic Coronagraph (LASCO)," *Solar Physics* 162, 357 (1995).
- ³R.A. Howard, J.D. Moses, A. Vourlidas, J.S. Newmark, D.S. Socker, S.P. Plunkett, C.M. Korendyke, J.W. Cook, A. Hurley, J.M. Davila, W.T. Thompson, O.C. St Cyr, E. Mentzell, K. Mehalick, J.R. Lemen, J.P. Wuelser, D.W. Duncan, T.D. Tarbell, R.A. Harrison, N.R. Waltham, J. Lang, C.J. Davis, C.J. Eyles, J.P. Halain, J.M. Defise, E. Mazy, P. Rochus, R. Mercier, M.F. Ravet, F. Delmotte, V. Bothmer, D. Wang, N. Rich, S. Cooper, V. Stephens, G. Maahs, R. Baugh, and D. McMullin, "Sun Earth Connection Coronal and Heliospheric Investigation (SECCHI)," *Space Science Reviews*, in press. ★

The NRL Precision Orbital Transfer Vehicle

M.S. Johnson,¹ S.R. Morgan,¹ W.S. Vincent,¹ K.H. Gallelli,¹ B.P. Whalen,¹ A. Hope,² S.S. Chappie,¹ and R.G. Skalitzky¹

¹*Spacecraft Engineering Department*

²*Space Systems Development Department*

Introduction: The NRL Naval Center for Space Technology (NCST) successfully completed and operated a low-cost advanced propulsion spacecraft designed for the precision orbital transfer of small satellites. This Upper Stage (U/S) launched on a Boeing Delta II from Cape Canaveral Air Force Station (CCAFS), Florida, in June 2006 and completed the transfer and release of two experimental small satellites. NRL engineers operated the spacecraft from the NRL Blossom Point (BP) Mission Operations Center in southern Maryland.

Description of the Upper Stage: The Upper Stage is a propulsion module that also functions as a stand-alone spacecraft. It contains all hardware necessary for autonomous operations, including processing, software, RF communications, attitude determination/control, and power. The U/S provides the propulsion necessary to transfer the experimental small satellites from the Delta II-provided geosynchronous transfer

orbit (GTO) to the final geosynchronous orbit. The U/S development efforts began in late 2003, with the Navy providing funding to NRL as a mission partner with DARPA and the Air Force.

Spacecraft System Testing: By September 2005, the U/S flight vehicle had undergone design, analysis, integration, and initial system test activities. System tests included mission simulations, alignments, EMI/EMC, and BP/Air Force Satellite Control Network (AFSCN) ground segment compatibility tests. Prior to shipment from NRL to the launch site, final system-level environmental tests were conducted over a seven-week period. These consisted of lateral random vibration (2-axis), axial random vibration, acoustic, pyro shock, alignment verification, thermal vacuum, small satellite separation testing, and spin balance/mass properties (Figs. 7(a)-(c)). The final flight software qualification testing was performed in parallel to the vibration testing with the assistance of a high-fidelity mission simulator, allowing successful "flying" while simulating multiple mission variables. Detailed analysis and testing of the primary structure thrust cone material was conducted, along with qualification testing of the main heat shield restraint system. Modifications of the flight heat shield restraint were implemented upon completion of the qualification testing. One of the final tests prior to shipping to Florida was a fit-check with the Boeing Delta II Flight Payload Attach Fitting (PAF) (Fig. 7(d)).

Ship to the Cape, System Integration, and Fueling:

The Upper Stage and supporting mechanical and electrical ground equipment shipped via NRL truck to CCAFS on December 7, 2005. There, in the Solid Motor Assembly Building (SMAB) (Fig. 8(a)), the U/S underwent electrical, propulsion, and battery functional testing, transducer calibration, alignments, BP/AFSCN compatibility, operations rehearsals, and initial electrical interface checks with the small satellites. Due to launch vehicle delays, the U/S was powered down until the launch vehicle was ready to support. Later, the U/S was transported to the Defense Satellite Communications System (DSCS) Processing Facility (DPF). NRL propulsion engineers, working with CCAFS contractor personnel, precisely loaded the mono methyl hydrazine (MMH) and nitrogen tetroxide (NTO) hypergolic propellants into the U/S fuel tanks. Following fueling, the small satellites were installed by NRL engineers and technicians on the top deck of the U/S. The integrated stack, known as the Space Vehicle (SV), was spin balanced by NRL engineers in the DPF. Following spin balance, the SV was installed on the Delta II third stage, which had been spin balanced separately. A large modular protective canister was installed around the integrated third stage and SV. Very early one morning



FIGURE 7(a)
Lateral vibration testing in acoustic chamber.



FIGURE 7(b)
Thermal vacuum chamber testing.



FIGURE 7(c)
Sensor and thruster alignment inspections.

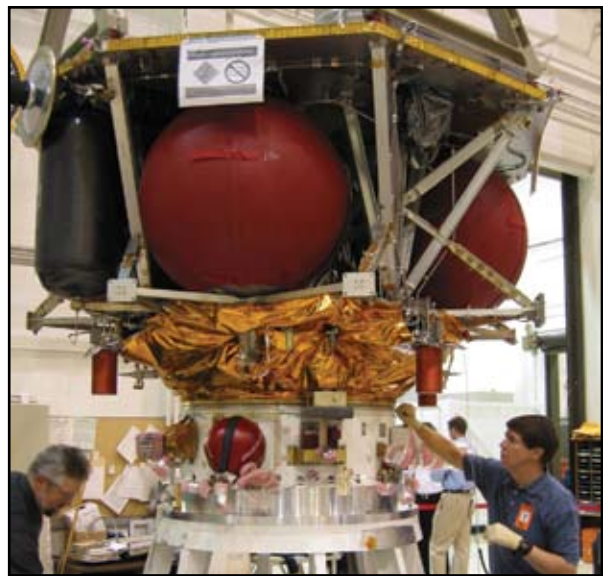


FIGURE 7(d)
Fit-check with Boeing Delta II Flight Payload Attach Fitting (PAF).



FIGURE 8(a)
Electrical testing in the SMAB high bay at CCAFS.

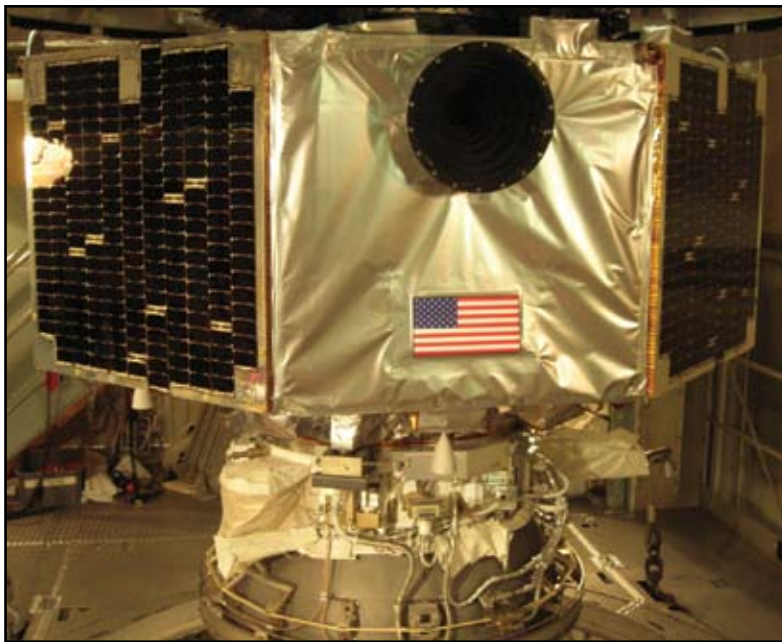


FIGURE 8(b)
The Upper Stage in its flight configuration, ready for launch.

two weeks before launch, this canister was slowly towed to Launch Complex 17A and hoisted on top of the rest of the Delta II rocket. The protective canister was removed, and final preparations of the SV were performed (Fig. 8(b)). These preparations included removing covers from sensitive surfaces, installing arming plugs, and performing pre-launch functional tests.

Launch and U/S Operations: The Upper Stage was launched into a geostationary transfer orbit on June 21, 2006, by a Boeing Delta II 7925 launch vehicle (Fig. 9). The launch was scheduled for 21:33 Z, and after two short slips into the 4-hour launch window, lifted off at 22:15 Z. The launch vehicle provided a very accurate insertion, as expected. The first contact from the U/S to the BP Mission Operations Center was made through the AFSCN Diego Garcia Remote Tracking Station (RTS).

All command and control activities for the Upper Stage were conducted from the NRL Blossom Point Tracking Facility (BPTF). NRL performed the pre-launch mission planning and the post-launch satellite orbit determination, maneuver planning/execution, and operations. Tracking data and telemetry were collected using both the AFSCN and BP assets. NRL-developed orbit determination software was used to provide accurate position and velocity data for ground antenna pointing and maneuver planning. The main mission operations successfully ended in approximately four days with the Upper Stage inserting into a near geostationary orbit and successfully separating the two small satellites. All systems and subsystems performed as planned.

Mission Integration: The NCST provided significant system support to the joint program in order to ensure mission success. NRL was responsible for ensuring that the integrated Space Vehicle (U/S and small satellites) would meet all launch requirements. Detailed integrated SV analysis was performed (or managed) by NRL engineers, including integrated structural models, thermal analysis, and nutation (fluid energy dissipation) analysis. Additionally, all launch site range activities — facilities, resources, and spacecraft fueling — were managed by NRL on behalf of the program.



FIGURE 9
Launch — June 21, 2006 (photo courtesy of USAF).

A significant NRL presence was made at CCAFS and positive long-term relationships were established.

Evaluation of Technologies: The demonstration has resulted in an innovative propulsion system capable of a range of future missions for which large amounts of delta-V are required. Key technologies demonstrated include the following: a very low mass fraction, highly integrated structure; a novel thermal shield that minimized the height of the U/S; first flight on a U.S. satellite of platinum/rhodium bi-propellant attitude control thrusters; first flight of a high-performance coated columbium delta-V thruster; commercial off-the-shelf manual valve tested to aerospace standards; lightweight Inconel-718 composite overwrap pressure vessels; very lightweight all-titanium propellant tanks with internal propellant management devices; triple-junction solar cells; lithium-ion batteries; and the first flight of a low-cost/high-performance star tracker. This experimentation and these technologies enable such missions as autonomous maneuvering, transfer of secondary payloads, and orbit plane changes.

[Sponsored by DARPA]



PROGRAMS FOR NRL EMPLOYEES

The Human Resources Office continues to support and provide traditional and alternative methods of training for employees. NRL employees are encouraged to develop their skills and enhance their job performance so they can meet the future needs of NRL and achieve their own goals for growth.

One common study procedure is for employees to work full time at the Laboratory while taking job-related scientific courses at universities and schools in the Washington, DC, area. The training ranges from a single course to full graduate and postgraduate programs. Tuition for training is paid by NRL. The formal programs offered by NRL are described here.

GRADUATE PROGRAMS

- The **Advanced Graduate Research Program** (formerly the Sabbatical Study Program, which began in 1964) enables selected professional employees to devote full time to research or pursue work in their own or a related field for one year at an institution or research facility of their choice without the loss of regular salary, leave, or fringe benefits. NRL pays all travel and moving expenses for the employee. Criteria for eligibility include professional stature consistent with the applicant's opportunities and experience, a satisfactory program of study, and acceptance by the facility selected by the applicant. The program is open to employees in Career Track NP Levels III and IV; NO Levels III, IV, and V; and NR Level IV who have completed six years of Federal Service, four of which have been at NRL.

- The **Edison Memorial Graduate Training Program** enables employees to pursue advanced studies in their fields at local universities. Participants in this program work 24 hours each workweek and pursue their studies during the other 16 hours. The criteria for eligibility include a minimum of one year of service at NRL, a bachelor's or master's degree in an appropriate field, and professional standing in keeping with the candidate's opportunities and experience.

- To be eligible for the **Select Graduate Training Program**, employees must have a college degree in an appropriate field and must have demonstrated ability and aptitude for advanced training. Students accepted into this program devote three academic semesters to

graduate study. While attending school, they receive one-half of their salary, and NRL pays for tuition and laboratory expenses.

- The **Naval Postgraduate School (NPS)**, located in Monterey, California, provides graduate programs to enhance the technical preparation of Naval officers and civilian employees who serve the Navy in the fields of science, engineering, operations analysis, and management. It awards a master of arts degree in national security affairs and a master of science degree in many technical disciplines. NRL employees desiring to pursue graduate studies at NPS may apply for a maximum of six quarters away from NRL, with thesis work accomplished at NRL. Specific programs are described in the NPS catalog. Participants will continue to receive full pay and benefits during the period of study.

- In addition to NRL and university offerings, application may be made to a number of noteworthy programs and fellowships. Examples of such opportunities are the **Capitol Hill Workshops**, the **Legislative Fellowship (LEGIS) program**, the **Federal Executive Institute (FEI)**, the **Fellowship in Congressional Operations**, and the **Executive Leadership Program for Mid-Level Employees**. These and other programs are announced from time to time, as schedules are published.

- Research conducted at NRL may be used as **thesis material for an advanced degree**. This original research is supervised by a qualified employee of NRL who is approved by the graduate school. The candidate should have completed the required course work and should have satisfied the language, residence, and other requirements of the graduate school from which the degree is sought. NRL provides space, research facilities, and supervision but leaves decisions on academic policy to the cooperating schools.

CONTINUING EDUCATION

- **Undergraduate and graduate courses** offered at local colleges and universities are subsidized by NRL for employees interested in improving their skills and keeping abreast of current developments in their fields. These courses are also available at a number of government installations in the Washington, DC, area.

- NRL offers **short courses** to all employees in a number of fields of interest including technical subjects, computer operation, and supervisory and management techniques. Laboratory employees may attend these courses at nongovernment facilities as well. Interagency courses in management, personnel, finance, supervisory development, and clerical skills are also available.

For further information on any of the above Graduate and Continuing Education programs, contact the Employee Relations and Development Branch (Code 1850) at (202) 767-6737 or via email at Training@hro.nrl.navy.mil.

- The **Scientist-to-Sea Program (STSP)** provides increased opportunities for Navy R&D laboratory/center personnel to go to sea to gain first-hand insight into operational factors affecting system design, performance, and operations on a variety of ships. NRL is a participant of this Office of Naval Research (ONR) program. For further information contact Mike McCord (Code 7120) at (202) 767-2945.

PROFESSIONAL DEVELOPMENT

NRL has several programs, professional society chapters, and informal clubs that enhance the professional growth of employees. Some of these are listed below.

- The **Counseling Referral Service (C/RS)** helps employees to achieve optimal job performance through counseling and to resolve problems such as family and work-related stress and relationship difficulties, and behavioral, emotional, and substance use problems that may adversely impact job performance. C/RS provides confidential assessments and short-term counseling, training workshops, and referrals to additional resources in the community. Contact Lois Burleigh, MSW, LGSW at (202) 767-6857.

- The **NRL Women in Science and Engineering (WISE) Network** was formed in 1997 through the merger of the NRL chapter of WISE and the Women in Science and Technology Network. Luncheon meetings and seminars are held to discuss scientific research areas, career opportunities, and career-building strategies. The group also sponsors projects to promote the professional success of the NRL S&T community and improve the NRL working environment. Membership is open to all S&T professionals. Contact Dr. Kathy Wahl at (202) 767-5419 or Ms. Jennifer Stepnowski at (202) 767-8533.

- **Sigma Xi**, The Scientific Research Society, encourages and acknowledges original investigation in pure and applied science. It is an honor society for research scientists. Individuals who have demonstrated the ability to perform original research are elected to membership in local chapters. The NRL Edison Chapter, comprising approximately 400 members, recognizes original research by presenting awards annually in pure and applied science to outstanding NRL staff members. The chapter also sponsors lectures at NRL on a wide range of scientific topics for the entire NRL community. These lectures are delivered by scientists from all over the nation and the world. The highlight of the Sigma Xi lecture series is the Edison Memorial Lecture, traditionally featuring a distinguished scientist. Contact Dr. Rhonda Stroud at (202) 404-4143.

- The **NRL Mentor Program** was established to provide an innovative approach to professional and career training and an environment for personal and professional growth. It is open to permanent NRL employees in all job series and at all sites. Mentorees are matched with successful, experienced colleagues having more technical and/or managerial experience who can provide them with the knowledge and skills needed to maximize their contribution to the success of their immediate organization, to NRL, to the Navy, and to their chosen career fields. The ultimate goal of the program is to increase job productivity, creativity, and satisfaction through better communication, understanding, and training. NRL Instruction 12400.1A provides policy and procedures for the program. Contact Ms. Dawn Brown at (202) 767-2957.

- Employees interested in developing effective self-expression, listening, thinking, and leadership potential are invited to join either of two NRL chapters of **Toastmasters International**. Members of these clubs, who possess diverse career backgrounds and talents, meet two to four times a month in an effort to learn to communicate not by rules but by practice in an atmosphere of understanding and helpful fellowship. NRL's Commanding Officer and Director of Research endorse Toastmasters as an official training medium at NRL. Contact Kathleen Parrish at (202) 404-4963 for more information.

EQUAL EMPLOYMENT OPPORTUNITY (EEO) PROGRAMS

Equal employment opportunity is a fundamental NRL policy for all employees regardless of race, color, national origin, sex, religion, age, or disability. The NRL EEO Office is a service organization whose major

functions include counseling employees in an effort to resolve employee/management conflicts, processing formal discrimination complaints, providing EEO training, and managing NRL's affirmative employment recruitment program. The NRL EEO Office is also responsible for sponsoring special-emphasis programs to promote awareness and increase sensitivity and appreciation of the issues or the history relating to females, individuals with disabilities, and minorities. Contact the NRL Deputy EEO Officer at (202) 767-5264 for additional information on any of their programs or services.

OTHER ACTIVITIES

- The award-winning **Community Outreach Program** directed by the NRL Public Affairs Office fosters programs that benefit students and other community citizens. Volunteer employees assist with and judge science fairs, give lectures, and serve as tutors, mentors, coaches, and classroom resource teachers. The program sponsors African American History Month

art and essay contests for local schools, student tours of NRL, an annual holiday party for neighborhood children in December, and a book donation program for both students and teachers. Through the Community Outreach Program, NRL has active partnerships with four District of Columbia public schools. Contact Mr. Dom Panciarelli at (202) 767-2541.

- Other programs that enhance the development of NRL employees include sports and theater groups and the **Amateur Radio Club**. The **NRL Recreation Club** encourages wide interest in sports for employees with its many facilities and programs, such as a heated indoor pool, hot tub, table tennis, basketball courts, recreation room, free weight room, new selectorized weight equipment, and volleyball courts. Sportswear and NRL and seasonal paraphernalia are available at the Recreation Club. The **Showboaters** theater group has been "in the dark" for a number of years. Visit our website at www.nrl.navy.mil/showboaters/Past_Productions.php. Contact Barbarajo Cox at (202) 404-4998 for Play Reader's meetings at NRL.

PROGRAMS FOR NON-NRL EMPLOYEES

Several programs have been established for non-NRL professionals. These programs encourage and support the participation of visiting scientists and engineers in research of interest to the Laboratory. Some of the programs may serve as stepping-stones to federal careers in science and technology. Their objective is to enhance the quality of the Laboratory's research activities through working associations and interchanges with highly capable scientists and engineers and to provide opportunities for outside scientists and engineers to work in the Navy laboratory environment. Along with enhancing the Laboratory's research, these programs acquaint participants with Navy capabilities and concerns and provide a path to full-time employment.

RECENT PH.D., FACULTY MEMBER, AND COLLEGE GRADUATE PROGRAMS

- The **National Research Council (NRC) Cooperative Research Associateship Program** selects associates who conduct research at NRL in their chosen fields in collaboration with NRL scientists and engineers. The tenure period is two years (renewable for a possible third year).

- The **NRL/ASEE Postdoctoral Fellowship Program**, administered by the American Society for Engineering Education (ASEE), aims to increase the

involvement of highly trained scientists and engineers in disciplines necessary to meet the evolving needs of naval technology. Appointments are for one year (renewable for a second and possible third year).

- The **Naval Research Enterprise Intern Program (NREIP)** is a ten-week program involving 69 NROTC colleges/universities and their affiliates. The Office of Naval Research (ONR) offers summer appointments at Navy laboratories to current sophomores, juniors, seniors, and graduate students from participating schools. Application is online at www.asee.org/nreip through the American Society for Engineering Education. Electronic applications are sent for evaluation to the point of contact at the Navy laboratory identified by the applicant. ONR will provide a stipend of \$5,500 to undergraduates and \$6,500 to graduate students.

- The American Society for Engineering Education also administers the **Navy/ASEE Summer Faculty Research and Sabbatical Leave Program** for university faculty members to work for ten weeks (or longer, for those eligible for sabbatical leave) with professional peers in participating Navy laboratories on research of mutual interest.

- The **NRL/United States Naval Academy (USNA) Cooperative Program for Scientific Interchange**

allows faculty members of the U.S. Naval Academy to participate in NRL research. This collaboration benefits the Academy by providing the opportunity for USNA faculty members to work on research of a more practical or applied nature. In turn, NRL's research program is strengthened by the available scientific and engineering expertise of the USNA faculty.

- The **National Defense Science and Engineering Graduate Fellowship Program** helps U.S. citizens obtain advanced training in disciplines of science and engineering critical to the U.S. Navy. The three-year program awards fellowships to recent outstanding graduates to support their study and research leading to doctoral degrees in specified disciplines such as electrical engineering, computer sciences, material sciences, applied physics, and ocean engineering. Award recipients are encouraged to continue their study and research in a Navy laboratory during the summer.

For further information about the above six programs, contact Ms. Lesley Renfro at (202) 404-7450.

PROFESSIONAL APPOINTMENTS

- **Faculty Member Appointments** use the special skills and abilities of faculty members for short periods to fill positions of a scientific, engineering, professional, or analytical nature at NRL.

- **Consultants and experts** are employed because they are outstanding in their fields of specialization or because they possess ability of a rare nature and could not normally be employed as regular civil servants.

- **Intergovernmental Personnel Act Appointments** temporarily assign personnel from state or local governments or educational institutions to the Federal Government (or vice versa) to improve public services rendered by all levels of government.

COLLEGE AND HIGH SCHOOL STUDENT PROGRAMS

The student programs are tailored to high school, undergraduate, and graduate students to provide employment opportunities and work experience in naval research. These programs are designed to attract applicants for student and full professional employ-

ment in fields such as engineering, physics, mathematics, and computer sciences. The student employment programs are designed to help students and educational institutions gain a better understanding of NRL's research, its challenges, and its opportunities.

Employment programs for college students include the following:

- The **Student Career Experience Program** (formerly known as the Cooperative Education Program) employs students in study-related occupations. The program is conducted in accordance with a planned schedule and a working agreement among NRL, the educational institution, and the student. Primary focus is on the pursuit of bachelor's degrees in engineering, computer science, or the physical sciences.

- The **Student Temporary Employment Program (STEP)** enables students to earn a salary while continuing their studies and offers them valuable work experience.

- The **Summer Employment Program** employs students for the summer in paraprofessional and technician positions in engineering, physical sciences, computer sciences, and mathematics.

- The **Student Volunteer Program** helps students gain valuable experience by allowing them to voluntarily perform educationally related work at NRL.

For additional information on these student programs, contact Code 1810 at (202) 767-8313.

For high school students, the **DoD Science & Engineering Apprenticeship Program (SEAP)** offers students grades 9 to 12 the opportunity to serve for eight weeks as junior research associates in a DoD laboratory. Under the direction of a mentor, students gain a better understanding of the challenges and opportunities of research through participation in scientific programs. Criteria for eligibility are based on science and mathematics courses completed and grades achieved; scientific motivation, curiosity, and capacity for sustained hard work; a desire for a technical career; teacher recommendations; and achievement test scores. The NRL Program is the lead program and the largest in DoD. For additional information, contact Dawn Brown (Code 1850) at (202) 767-2957.

GENERAL INFORMATION





- 269** Technical Output
- 270** Key Personnel
- 271** Contributions by Divisions, Laboratories, and Departments
- 274** Subject Index
- 278** Author Index
- 279** Employment Opportunities

TECHNICAL OUTPUT

The Navy continues to be a pioneer in initiating new developments and a leader in applying these advancements to military requirements. The primary method of informing the scientific and engineering community of the advances made at NRL is through the Laboratory's technical output—reports, articles in scientific journals, contributions to books, papers presented to scientific societies and topical conferences, patents, and inventions.

The figures for calendar year 2006 presented below represent the output of NRL facilities in Washington, D.C.; Bay St. Louis, Mississippi; and Monterey, California.

In addition to the output listed, NRL scientists made more than 1331 oral presentations during 2006.

Type of Contribution	Unclassified	Classified	Total
Articles in periodicals, chapters in books, and papers in published proceedings	*1047	0	1047*
NRL Formal Reports	11	3	14
NRL Memorandum Reports	71	3	74
Books	0	0	0
Patents granted			54
Statutory Invention Registrations (SIRs)			0

*This is a provisional total based on information available to the Ruth H. Hooker Research Library on February 23, 2007. Additional publications carrying a 2006 publication date are anticipated. Total includes non-refereed SPIE (International Society for Optical Engineering) and MRS (Materials Research Society) proceedings.

KEY PERSONNEL

Area Code (202) unless otherwise listed
Personnel Locator - 767-3200
DSN-297 or 754

Code	Office		Phone Number
EXECUTIVE DIRECTORATE			
1000	Commanding Officer	CAPT D.R. Gahagan, USN	767-3403
1000.1	Inspector General	CAPT W.B. Jackson, USN	767-3621
1001	Director of Research	Dr. J.A. Montgomery	767-3301
1001.1	Executive Assistant	Mr. D.J. DeYoung	767-2445
1002	Chief Staff Officer	CAPT W.B. Jackson, USN	767-3621
1004	Head, Technology Transfer	Dr. R.C. Manak	767-3083
1006	Head, Office of Program Administration and Policy Development	Mrs. L.T. McDonald	767-3091
1008	Office of Counsel	Mr. J.N. McCutcheon	767-2244
1030	Public Affairs Officer	Mr. R.L. Thompson	767-2541
1100	Director, Institute for Nanoscience	Dr. E.S. Snow	767-3261
1200	Head, Command Support Division	CAPT W.B. Jackson, USN	767-3621
1220	Head, Security	CAPT T. Lett	767-0793
1400	Head, Military Support Division	LCDR J.J. Coffey, USN	767-2273
1600	Commanding Officer, Scientific Development Squadron One	CDR H.A. Fleming, USN	301-342-3751
1800	Director, Human Resources Office	Ms. C.L. Downing	767-3421
1830	Deputy EEO Officer	Vacant	767-5264
3005	Deputy for Small Business	Ms. M.F. Thompson	767-6263
3540	Head, Safety Branch	Mr. K.J. Pawlovich	767-2232
BUSINESS OPERATIONS DIRECTORATE			
3000	Comptroller/Associate Director of Research	Mr. D.K. Therning	767-2371
3200	Head, Contracting Division	Mr. J.C. Ely	767-5227
3300	Head, Financial Management Division	Mr. D.K. Therning (Acting)	767-3405
3400	Head, Supply and Information Services Division	Ms. C. Hartman	767-3446
3500	Director, Research and Development Services Division	Mr. T.K. Hull	404-4054
SYSTEMS DIRECTORATE			
5000	Associate Director of Research	Dr. G.M. Borsuk	767-3425
5300	Superintendent, Radar Division	Dr. E.L. Mokole (Acting)	404-2700
5500	Superintendent, Information Technology Division/ NRL Chief Information Officer*	Dr. J.D. McLean	767-2903
5600	Superintendent, Optical Sciences Division	Dr. C.H. Hoffman (Acting)	767-7375
5700	Superintendent, Tactical Electronic Warfare Division	Dr. F.J. Klemm	767-6278
MATERIALS SCIENCE AND COMPONENT TECHNOLOGY DIRECTORATE			
6000	Associate Director of Research	Dr. B.B. Rath	767-3566
6030	Head, Laboratory for Structure of Matter	Dr. J. Karle	767-2665
6100	Superintendent, Chemistry Division	Dr. R.J. Colton	767-3026
6300	Superintendent, Materials Science and Technology Division	Dr. D.U. Gubser	767-2926
6400	Director, Lab. for Computational Physics and Fluid Dynamics	Dr. J.P. Boris	767-3055
6700	Superintendent, Plasma Physics Division	Dr. S.L. Ossakow	767-2723
6800	Superintendent, Electronics Science and Technology Division	Dr. B.V. Shanabrook (Acting)	767-3693
6900	Director, Center for Bio/Molecular Science and Engineering	Dr. J.M. Schnur	404-6000
OCEAN AND ATMOSPHERIC SCIENCE AND TECHNOLOGY DIRECTORATE			
7000	Associate Director of Research	Dr. E.R. Franchi (Acting)	404-8690
7100	Superintendent, Acoustics Division	Dr. E.R. Franchi	767-3482
7200	Superintendent, Remote Sensing Division	Dr. R.M. Bevilacqua	767-3391
7300	Superintendent, Oceanography Division	Dr. R.H. Preller	228-688-4670
7400	Superintendent, Marine Geosciences Division	Dr. H.C. Eppert, Jr.	228-688-4650
7500	Superintendent, Marine Meteorology Division	Dr. S.W. Chang	831-656-4721
7600	Superintendent, Space Science Division	Dr. J.P. Dahlburg	767-6343
NAVAL CENTER FOR SPACE TECHNOLOGY			
8000	Director	Mr. P.G. Wilhelm	767-6547
8100	Superintendent, Space Systems Development Department	Vacant	767-0410
8200	Superintendent, Spacecraft Engineering Department	Mr. J.P. Schaub	404-3727

*Additional Duty

CONTRIBUTIONS BY DIVISIONS, LABORATORIES, AND DEPARTMENTS

Radar Division

- 153 Numerical Analysis of Electromagnetic Bandgap Structures
S.-T. Chun and R.S. Schechter
- 155 Broadband Over Power Lines (BPL) and Its Impact on Spectrum Allocation
L.S. Cohen and A. Light

Information Technology Division

- 55 Optical Guidance for Shoreline-Following UAVs
B. Kamgar-Parsi, P. Baker, A. Kahn, and J. Kellogg
- 142 Understanding the Effect of Atmospheric Turbulence on Optical and Infrared Propagation using Hilbert Phase Analysis
C. Font, G.C. Gilbreath, M.P.J.L. Chang, and E.S. Oh
- 165 High Altitude Relay and Router
M. Rupar, J. Doffoh, and R. Mereish
- 217 Impact of Uncertainty on Terror Forecasting
G.S. Schmidt, J. Goffeney, and R. Willis

Optical Sciences Division

- 127 Fiber Optic Towed Arrays
C. Kirkendall, T. Barock, A. Tveten, and A. Dandridge
- 195 Distributed Fiber Optic Sensing for Homeland Security
C.K. Kirkendall, R. Bartolo, J. Salzano, and K. Daley
- 199 Optical Manipulation of Ultracold Atoms
F.K. Fatemi and M. Bashkansky
- 201 Real-Time Fleet Protection
L.N. Smith and J.R. Waterman
- 219 IR Photonic Bandgap Fibers for Missile Defense
I.D. Aggarwal, J.S. Sanghera, D. Gibson, F. Kung, L.E. Busse, L.B. Shaw, V.Q. Nguyen, and P.C. Pureza

Tactical Electronic Warfare Division

- 55 Optical Guidance for Shoreline-Following UAVs
B. Kamgar-Parsi, P. Baker, A. Kahn, and J. Kellogg
- 156 Near-Earth Radio Frequency Propagation
R.A. Wert and A.K. Goroch
- 159 Unmanned Sea Surface Vehicle Electronic Warfare
D. Tremper and J. Heyer

Chemistry Division

- 63 Reducing Corrosion Control Costs with Rapid-Cure Coatings
A.A. Webb, J. Verborgt, J.R. Martin, W. Groeninger, P.F. Slebodnick, K.E. Lucas, and E. Hogan
- 147 Polymeric Protection of Navy Fighter Jet Towlines
M.K. Kolel-Veetil and T.M. Keller

Materials Science and Technology Division

- 63 Reducing Corrosion Control Costs with Rapid-Cure Coatings
A.A. Webb, J. Verborgt, J.R. Martin, W. Groeninger, P.F. Slebodnick, K.E. Lucas, and E. Hogan
- 175 Initial Microstructural Evolution during Friction Stir Welding
R.W. Fonda, J.A. Wert, A.P. Reynolds, and W. Tang
- 196 Transduction of the Spin State Variable Between the Electron and Optical Polarization at Zero Magnetic Field
A.T. Hanbicki, O.M.J. van 't Erve, G. Kioseoglou, C.H. Li, and B.T. Jonker
- 221 Computational Materials Theory: Optimizing the Use of the Electromagnetic Spectrum
M.R. Pederson, M.J. Mehl, and L.L. Boyer

- 227 On-Orbit Microwave Curing of Space Shuttle Repair Materials
A.W. Fliflet, M.T. Lombardi, S.H. Gold, D. Lewis III, R.W. Bruce, and A.K. Kinkead

Laboratory for Computational Physics and Fluid Dynamics

- 177 3D Unsteady Computations of Flapping Flight in Insects and Fish
R. Ramamurti and W.C. Sandberg

Plasma Physics Division

- 125 Remote Intense Laser Acoustic Source
T.G. Jones, A. Ting, J. Peñano, P. Sprangle, and L.D. Bibee
- 227 On-Orbit Microwave Curing of Space Shuttle Repair Materials
A.W. Fliflet, M.T. Lombardi, S.H. Gold, D. Lewis III, R.W. Bruce, and A.K. Kinkead

Electronics Science and Technology Division

- 73 NRL Launches SiC Epitaxial Growth Effort for Future Power Systems
C.R. Eddy, Jr., D.K. Gaskill, K.-K. Lew, B.L. VanMil, R.L. Myers-Ward, and F.J. Kub
- 169 Efficient Linearization of Microwave Power Amplifiers
J.X. Qiu, D.K. Abe, T.M. Antonsen, Jr., B.G. Danly, B. Levush, and R.E. Myers
- 180 Highly Efficient Surface Enhanced Raman Scattering (SERS) Nanowire/Ag Composites
S.M. Prokes, O.J. Glembocki, and R.W. Rendell

Center for Bio/Molecular Science and Engineering

- 148 Single-Domain Antibodies: Rugged Recognition Elements
E.R. Goldman, J.L. Liu, J.B. Delehanty, G.P. Anderson, and A. Hayhurst

Acoustics Division

- 121 Modeling Reverberation Time Series for Shallow Water Clutter Environments
K.D. LePage
- 185 Measuring Undersea Noise from Breaking Waves
S.L. Means and M.A. Sletten

Remote Sensing Division

- 83 Vega is a Rapidly Rotating Star
T.A. Pauls and D.M. Peterson
- 107 A Multi-Sensor Aerogeophysical Study of Afghanistan
J. Brozena, V. Childers, J. Gardner, R. Liang, J. Jarvis, and J. Bowles
- 142 Understanding the Effect of Atmospheric Turbulence on Optical and Infrared Propagation using Hilbert Phase Analysis
C. Font, G.C. Gilbreath, M.P.J.L. Chang, and E.S. Oh
- 185 Measuring Undersea Noise from Breaking Waves
S.L. Means and M.A. Sletten
- 207 Pyroconvection and Climate Change
M. Fromm, S. Miller, J. Turk, and T. Lee
- 211 Remotely Measuring Turbulent Coastal Atmospheres
W.P. Hooper, G.M. Frick, B.P. Michael, and R.J. Lind

Oceanography Division

- 89 Advanced Surge and Inundation Modeling: A Case Study from Hurricane Katrina
C.A. Blain, T.C. Massey, J.D. Dykes, and P.G. Posey
- 187 Real-Time Coastal Monitoring and Prediction for Operations and Research
J.W. Book, P. Martin, M. Rixen, J. Dykes, D. Wang, S. Ladner, M. Tudor, and J. Chiggiato

Marine Geosciences Division

- 107 A Multi-Sensor Aerogeophysical Study of Afghanistan
J. Brozena, V. Childers, J. Gardner, R. Liang, J. Jarvis, and J. Bowles
- 125 Remote Intense Laser Acoustic Source
T.G. Jones, A. Ting, J. Peñano, P. Sprangle, and L.D. Bibee
- 191 A Roughness Estimation Algorithm for Sidescan
M.L. Gendron, M.C. Lohrenz, G. Layne, and J. Sample

Marine Meteorology Division

- 99 By the Light of the Sea
S.D. Miller, S.H.D. Haddock, T.F. Lee, and C.D. Elvidge
- 133 The Terrain-Induced Rotor Experiment (T-REX)
J.D. Doyle and V. Grubišić
- 137 An Advanced Framework for Battlespace Environment Data Assimilation
L. Xu, T. Rosmond, N. Baker, and J. Goerss
- 156 Near-Earth Radio Frequency Propagation
R.A. Wert and A.K. Goroch
- 207 Pyroconvection and Climate Change
M.D. Fromm, S.D. Miller, J. Turk, and T. Lee

Space Science Division

- 136 Polar Clouds from Space Shuttle Exhaust
M.H. Stevens and C.R. Englert
- 139 Understanding and Forecasting the Sun's Impact on the Battlespace Environment
J.L. Lean, J.M. Picone, J.T. Emmert, and J.P. Dahlburg

- 229 The STEREO Mission: A Three Dimensional View of the Sun and Heliosphere
J.W. Cook, J.S. Newmark, and R.A. Howard

Space Systems Development Department

- 167 Comprehensive Maritime Awareness (CMA) Joint Capabilities Technology Demonstration (JCTD)
C.T. Dwyer
- 208 Joint Demodulation of Low-Entropy Narrow-band Cochannel Signals
T. Meehan, F. Kragh, and K. Clark
- 232 The NRL Precision Orbital Transfer Vehicle
M.S. Johnson, S.R. Morgan, W.S. Vincent, K.H. Gallelli, B.P. Whalen, A. Hope, S.S. Chappie, and R.G. Skalitzky

Spacecraft Engineering Department

- 232 The NRL Precision Orbital Transfer Vehicle
M.S. Johnson, S.R. Morgan, W.S. Vincent, K.H. Gallelli, B.P. Whalen, A. Hope, S.S. Chappie, and R.G. Skalitzky

SUBJECT INDEX

- 3D Virtual and Mixed Environments Laboratory (3DVMEL), 30
- 3-MV Tandem Pelletron Accelerator Facility, 33
- 4DVAR, 137
- Acoustic Doppler current profilers (ADCPs), 43
- Acoustic Seafloor Characterization System (ASCS), 44
- Acoustic sensors, 127
- Acoustics Division, 37
- Acoustics, 125, 185
- Administrative Services Branch, 47
- Advanced Graduate Research Program, 263
- Advanced Multifunction Radio Frequency Concept (AMRFC), 27
- Advanced Silicon Carbide Epitaxial Research Laboratory (ASCERL), 35, 36
- Airborne Polarimetric Microwave Imaging Radiometer (APMIR), 42
- Airborne remote sensing, 107
- Amateur Radio Club, 265
- Antibody, 148
- Antiship cruise missiles, 201
- Antiterrorist force protection, 201
- Aqua, 44
- Arctic, 136
- Astronomy, 40
- ATDnet, 28
- Atmospheric Prediction System Development Laboratory, 44
- Atmospheric turbulence, 142
- Atomic force microscopy (AFM), 31
- Atomic resolution transmission electron microscopy (ARTEM), 33
- Audio Laboratory, 29
- Autonomous navigation, 55
- Autonomous Systems Research Lab, 51
- Bacteria, 99
- Battlespace environment, 137
- Bergen Data Center, 44, 49
- Bioluminescence, 99
- Biomaterial development, 36
- Biosensor, 148
- Bird wrasse, 177
- BoSSNET, 28
- BPL, 155
- Breaking waves, 185
- Capitol Hill Workshops, 263
- Center for Bio/Molecular Science and Engineering, 36
- Center for Computational Science (CCS), 29
- Center for Higher Learning, 49
- Centralized Atmospheric Analysis and Prediction System (CAAPS), 24
- Change detection, 191
- Channel-forming peptides, 23
- Charge-coupled device (CCD), 39
- Chemical Analysis Facilities, 32
- Chemical vapor deposition, 73
- Chemical/biological warfare defense, 36
- Chemistry Division, 31
- Chesapeake Bay Detachment (CBD), 27, 50
- Chlorofluorocarbon (CFC), 42
- Class 10 clean room, 45
- Class 100 clean room facility, 36
- Class 1000 clean room, 36
- Classification, 208
- Classified Satellite/Radar Data Processing Facility, 44
- Climate, 207
- Clutter, 121
- COAMPS, 133
- COAMPS-OS, 24
- Coastal Ocean Imaging Spectrometer (COIS), 40
- Coastal ocean modeling, 89
- Coastal ocean, 187
- Coastal prediction system, 89
- Coastal radar (CODAR), 24
- Cold atoms, 199
- College and high school student programs, 266
- Combat Development command, 50
- Communications Security (COMSEC)/Information Security (INFOSEC), 29
- Communications, 165, 208
- Community Outreach Program, 26, 265
- Compact Airborne Spectrographic Imager (CASI-1500), 39
- Compact Antenna Range, 27
- Complex terrain, 133
- Compound Semiconductor Processing Facility (CSPF), 35
- Computational Electromagnetics (CEM) Facility, 27
- Computer numerically controlled (CNC) milling machine, 36
- Conical-scanning Microwave Imager/Sounder (CMIS), 42
- Connection Machine, 40
- Continuing education, 263
- Cooperative Aircraft Identification system, 28
- Cooperative Research and Development Agreements (CRADAs), 46
- Cosmic Ray Effects on Micro Electronics (CRÈME 96), 46
- Counseling Referral Service (C/RS), 264
- Counterinsurgency pattern assessment, 22
- Coupled Ocean/Atmosphere Mesoscale Prediction System—On Scene (COAMPS-OS), 49
- Cryptographic Modernization Initiative (CMI), 22
- CT scanner, 44
- Cyber Defense Development Lab, 29
- Data assimilation, 137
- Deep-Towed Acoustics/Geophysics System (DTAGS), 43
- Defense Meteorological Satellite Program, 44
- Defense Meteorology Space Program (DMSP) Special Sensor Microwave Imager/Sounder (SSMIS) mission, 42
- Defense Research and Engineering Network (DREN), 28, 44
- Deforming fin, 177
- Density functional theory, 221
- Deuterium Raman cells, 211
- Digital acquisition buoy systems (DABS), 38
- Digital holographic imaging system, 38
- Digital Library, 48
- Digital Nautical Chart data, 44
- Digital publishing technology, 47
- Direct numerical simulations (DNS), 40
- Distributed sensing, 195
- DoD Science & Engineering Apprentice Program (SEAP), 266
- Dragon Warrior, 28
- Drosophila, 24, 177
- Eddies, 187
- Edison Memorial Graduate Training Program, 263
- Electra, 35
- Electric discharge machining (EDM), 51
- Electrical, Magnetic, and Optical Measurement Facility, 32
- Electromagnetic Gun Laboratory, 35
- Electromagnetic railgun deformation, 23
- Electron energy loss spectroscopy (EELS), 33
- Electronic Key Management System (EKMS), 29
- Electronic warfare, 159
- Electronics Research Lab, 51
- Electronics Science and Technology Division, 35
- EMI test chamber, 29
- Environmental Chemistry Laboratory, 49
- Environmental Protection Agency's Gulf of Mexico Program, 49
- Environmental quality, 36
- Epicenter, 35
- EPIGRESS reactor, 36

- Epoxy, 63
- Equal Employment Opportunity (EEO) programs, 264
- Executive Leadership Program for Mid-Level Employees, 263
- Exhibits Office, 47
- Extreme Ultraviolet Imaging Spectrometer (EIS), 25, 46
- Extreme Ultraviolet Imaging Telescope (EIT), 46
- ex-USS Shadwell (LSD-15), 32, 50
- Eye safety, 211
- FDTD, 153
- Federal Executive and Professional Association, 26
- Federal Executive Institute (FEI), 263
- Federal Technology Transfer Act, 46
- Fellowship in Congressional Operations, 263
- Fiber optics, 127, 195
- Field programmable gate array (FPGA), 29
- Finite elements, 89
- Fire I, 32
- Fire Research Facilities, 32
- Flapping foil propulsion, 23
- Flapping propulsion, 177
- Fleet Battle Experiments, 28
- Fleet Numerical Meteorology and Oceanography Center (FNMOC), 25, 42, 44, 49
- Flight Support Detachment, 26
- Focal Plane Array Evaluation Facility, 31
- Force protection/homeland defense (FP/HD), 32
- Forecasts, 217
- Forest fire, 207
- Forms and Reports Management Programs, 48
- Free-Surface Hydrodynamics Laboratory, 40
- Friction stir welding, 175
- Fronts, 187
- Gamble II, 34
- Gamma Ray Large Area Space Telescope (GLAST), 46
- General Electronics Environmental Test Facility, 28
- Geoacoustic Model Fabrication Laboratory, 39
- Geospatial Information Data Base (GIDB), 44
- Global Assimilation of Ionospheric Measurement (GAIM), 46
- Global Information Grid Evaluation Facility (GIG-EF), 28
- Global war on terrorism, 201
- GOES-E, 44
- GOES-W, 44
- Graduate programs, 263
- Graphics support, 47
- Heat shield, 232
- Heliosphere, 229
- Helium Resonance Scatter in the Corona and Heliosphere (HERSCHEL) experiment, 45
- High altitude, 165
- High Energy Laser Laboratory, 35
- High Frequency Active Auroral Research Program (HAARP), 30
- High performance organic fiber, 147
- High voltage, 73
- Hilbert phase analysis, 142
- Homeland security, 195
- Human Resources Office, 263
- Hurricane Ivan, 24
- Hurricane Katrina, 89
- Hydrodynamics, 40
- Hydroxyl, 136
- Image and signal processing, 191
- Immersive Simulation Laboratory (ISL), 29
- Immunoassay, 148
- Improvised explosive devices (IEDs), 23
- In Situ Sediment Acoustic Measurement System (ISSAMS), 44
- Inertial confinement fusion (ICF), 34
- Information Technology Division (ITD), 28
- Infrared fibers, 219
- Infrared search and track, 201
- Infrared spectroscopy, 221
- Infrared Test Chamber, 31
- Insect, 177
- Institute for Nanoscience, 27
- Integrated Communications Technology (ICT) Test Lab, 28
- Intense laser, 125
- Intent/Deception (ID) Laboratory, 30
- Inundation, 89
- Inverse synthetic aperture radar (ISAR), 27
- IR Missile-Seeker Evaluation Facility, 31
- JEOL 2010F transmission electron microscope, 33
- Joint detection, 208
- Joint Experimentation, 28
- Joint Forces Command Modeling & Simulation, 28
- Joint Tactical Radio System, 28
- Joint Typhoon Warning Center, 44
- JTF WARNET, 28
- Key Management Infrastructure (KMI), 29
- Laboratory for Advanced Materials Synthesis (LAMS), 35
- Laboratory for Computational Physics and Fluid Dynamics (LCP&FD), 34
- Laboratory for Structure of Matter, 31
- LabVIEW-based data acquisition system, 38
- Langmuir film balance, 40
- Large Angle Spectrometric Coronagraph (LASCO), 45
- Large Area Plasma Processing System (LAPPS), 34
- Large-Optic, High-Precision Tracker system, 31
- Laser acoustic source, 125
- Legislative Fellowship (LEGIS) program, 263
- Leo scanning electron microscope, 34
- Lidar system, 42, 211
- Linearization, 169
- Line-of-sight, 165
- LINUX cluster, 45
- Liquid chromatograph–mass spectrometer (LC-MS), 36
- Long Wavelength Array (LWA), 40
- Low mass fraction structures, 232
- Low-entropy, 208
- Magneto-electronics Fabrication Facility, 32
- Major Shared Resource Center (MSRC), 49
- Marine biology, 99
- Marine Corrosion Test Facility, 32, 50
- Marine Geosciences Division, 43
- Marine Meteorology Center, 51
- Marine Meteorology Division, 44, 49
- Maritime Hyperspectral Imaging (HSI), 39
- Maritime threat anomaly, 167
- Mars Advanced Technology Airplane for Deployment, Operations, and Recovery (MATADOR), 23
- Mass Spectrometer and Incoherent Scatter Radar (MSIS), 46
- Master Environmental Library (MEL), 44, 49
- Materials Processing Facility, 33
- Materials Science and Technology Division, 32
- Materials Synthesis/Property Measurement Facility, 32
- Mechanical Characterization Facility, 33
- Mercury, 34
- Mesoscale atmospheric modeling, 133
- Microbial ecology, 99
- Micro-Nano Structure Characterization Facility, 33
- Microsatellite Technology Experiment (MiTeX), 25
- Microwave curing, 227
- Microwave Microscope (MWM), 28
- Microwave power amplifiers, 169
- Midway Research Center (MRC), 50
- Milky Seas Bioluminescence, 25
- Millimeter-Wave Structure Synthesis Facility (MWSSF), 35, 51
- Mine warfare, 191
- Missile Defense Agency, 50
- Missile defense, 219
- Mobile and Dynamic Network Laboratory, 28
- Mobile Atmospheric Aerosol and Radiation Characterization Observatory (MAARCO), 45
- MODIS, 43
- Modulating retroreflector (MRR), 22
- Molecular beam epitaxy (MBE), 35
- Monitoring, 187
- Monterey Bay Crescent Ocean Research Consortium, 50
- Motion Imagery Laboratory (MIL), 29
- Mountain waves, 133
- Moving Map Composer Facility, 44
- Multiresident AFS (MRAFS) system, 34
- Multiuser detection, 208
- Nanometer Measurement/Manipulation Facility, 32
- Nanowires, 180
- National Coastal Data Development Center, 49
- National Data Buoy Center, 49

- National Defense Science and Engineering Graduate Fellowship Program, 266
- National Polar-orbiting Operational Environmental Satellite system (NPOESS), 42
- National Radio Astronomy Observatory's (NRAO) Very Large Array (VLA), 40
- National Research Council (NRC) Cooperative Research Associateship Program, 265
- National Weather Service Forecast Office (NWSFO), 49
- NATO Undersea Research Center (NURC), 43
- Naval Center for Space Technology (NCST), 46
- Naval Cryptographic Technology Laboratory, 29
- Naval Key Management Laboratory, 29
- Naval Meteorology and Oceanography Command, 49
- Naval Oceanographic Office, 49
- Naval Postgraduate School (NPS), 49, 263
- Naval Research Enterprise Intern Program (NREIP), 265
- NAVDAS-AR, 137
- Navy Cyber Defense Operations Command (NCDOC), 29
- Navy fighter jet, 147
- Navy Integrated Tactical Environmental System (NITES), 49
- Navy Operational Global Atmospheric Prediction System—Advanced Level Physics High Altitude (NOGAPS-ALPHA), 46
- Navy Prototype Optical Interferometer (NPOI), 40
- Navy Small Craft Instruction and Training Center, 49
- Navy Technology Center for Safety and Survivability, 50
- Navy/ASEE Summer Faculty Research and Sabbatical Leave Program, 265
- Near Earth propagation, 156
- Nearfield scanning optical microscope (NSOM), 37
- Nike 3-kJ KrF laser facility, 34
- NOAX, 227
- Noise, 185
- Nonlinear distortion, 169
- NOWCAST, 45
- NP-3D EW flying laboratory, 31
- NP-3D Orion aircraft, 50
- NRL Federal Credit Union (NRLFCU), 26
- NRL Mentor Program, 264
- NRL/ASEE Postdoctoral Fellowship Program, 265
- NRL/United States Naval Academy (USNA) Cooperative Program for Scientific Interchange, 265
- NRL/USCG Vessel Tracking Project (VTP), 25
- Numerical weather prediction (NWP), 44
- Ocean Dynamics and Prediction Computation Network Facility, 42
- Ocean surface velocities, 24
- Oceanography Division, 42
- Offboard countermeasure, 159
- Office of Technology Transfer, 46
- Online Bibliography service, 48
- On-orbit repair, 227
- Operation Linescan System (OLS), 25
- Opteron, 29
- Optical Calibration Facility, 39
- Optical guidance, 55
- Optical interferometry, 83
- Optical Sciences Division, 30
- Optical trapping, 199
- Optics, 125
- Orbit determination, 232
- ORION, 22
- Oxidation, 147
- P-3 aircraft, 27
- Patent licensing agreements (PLAs), 47
- PCSAs, 147
- PEIP Phase II (PEIP-II), 22
- Pentacene and silole derivatives, 23
- Pharos III, 34
- Phillips CM30 transmission electron microscope, 34
- Photographic services, 47
- Photonic bandgap, 153, 219
- Plasma Physics Division, 34
- Plural component, 63
- POAM II, 42
- POAM III, 42
- Polar mesospheric clouds, 136
- Polar Ozone and Aerosol Measurement (POAM), 42
- Polymeric protection, 147
- Polyurethane, 63
- Portable Hyperspectral Imager for Low-Light Spectroscopy (PHILLS) system, 39
- Power Device Characterization Facility, 35, 36
- Power electronics, 73
- Prediction, 187
- Predistortion linearization, 169
- Professional appointments, 266
- Profiling Optics Package, 40
- Programmable Embeddable Information Security (INFOSEC) Product (PEIP), 22
- Publication services, 47
- Pulsed laser deposition (PLD), 33
- PyroCb, 207
- QAM, 169
- QuadGard Phase V, 23
- Quikscat, 44
- Quorum sensing, 99
- Radar Division, 27
- Radar Imaging Facility, 27
- Radar Signature Calculation Facility, 27
- Radar Testbed Facility, 27
- Radar, 185
- Radio frequency, 156
- Radio, 165
- Raman, 180
- Rampant Lion, 50
- Rapid cure, 63
- RC-12 Beech King Air research aircraft, 50
- RCC, 227
- Real-time, 187
- Records management services, 48
- Recreation Club, 26, 265
- Recrystallization, 175
- Reinforced carbon composite (RCC), 24
- Remote Sensing Division, 39
- Reverse transcriptase–polymerase chain reaction (RT-PCR) process, 24
- Riverine, 55
- Robotics Laboratory, 29
- Rotors, 133
- Ruth H. Hooker Research Library, 48
- Salt Water Tank Facility, 38
- Satellite Data Processing Laboratory, 44
- Satellite remote sensing, 99
- Satellite/Radar Processing Facility, 49
- Scanfish, 43
- Scanning transmission electron microscopy (STEM), 33
- Scanning tunneling microscopy (STM), 31
- Scientific Development Squadron One (VXS-1), 50
- Scientist-to-Sea Program (STSP), 264
- SEAWifs, 44
- SECCHI Payload Operations Center (POC), 46
- Security information exchange, 167
- Sediment Core Laboratory, 44
- Sediment Physical and Geotechnical Properties Laboratory, 44
- Seismic sensors, 195
- Select Graduate Training Program, 263
- Sensors, 221
- SEPTR instrument, 43
- SERS, 180
- SGI Origin 2000, 44
- Ship protection, 159
- Ship-motion simulator (SMS), 50
- Shoreline following, 55
- Showboaters, 265
- Sigma Xi, 26, 264
- Signal processing, 208
- Silicon Carbide Processing Facility (SCPF), 35
- Silicon carbide, 73
- Silicon Graphics 4700 blade-based system, 29
- Silicon Graphics Altix 3700 Supercomputer, 29
- Silicon Graphics Prism Supercomputer, 29
- Single crystal, 175
- SIPRNET, 45
- Situational awareness, 159
- Slocum Gliders, 43
- Solar and Heliospheric Observatory (SOHO) spacecraft, 45
- Solar Coronagraph Optical Test Chamber (SCOTCH), 45
- Solar Terrestrial Relations Observatory (STEREO), 45
- Solar-B extreme ultraviolet imaging spectrometer, 25
- Sonar, 121
- Sound speed profiles, 187
- Space Physics Simulation Chamber (SPSC), 51
- Space research, 229

- Space Science Division, 45, 51
- Space Shuttle, 136, 227
- Space Solar Cell Characterization Facility (SSCCF), 35
- Space Systems Technology Lab, 51
- Spacecraft operations, 232
- Spacecraft testing, 232
- Spatial Heterodyne Imager for Mesospheric Radicals (SHIMMER), 46
- Special Boat Team-Twenty-two, 49
- Spectrum allocation, 155
- Spin injection, 196
- Spintronics, 196
- SPOT 3 satellite, 42
- Stellar surfaces, 83
- Stennis Space Center (NRL-SSC), 49
- Storm surge, 89
- Strength member, 147
- Student Career Experience Program, 26, 266
- Student Temporary Employment Program (STEP), 266
- Student Volunteer Program, 266
- Summer Employment Program, 266
- Sun Earth Connection Coronal and Heliospheric Investigation (SECCHI) experiment, 45
- Sun, 229
- Sun's impact on battlespace environment, 139
- Supercomputing Resource Center, 49
- Superconducting quantum interference device (SQUID), 32
- Surface enhanced Raman scattering (SERS), 24
- Synchrotron Radiation Facility, 32
- Table-Top Terawatt (T³) laser, 34
- Tactical Electronic Warfare (TEW) Division, 31
- Technical Information Services (TIS) Branch, 47
- Tera, 44
- Terror events, 217
- Tether Physics and Survivability Experiment (TiPS), 46
- Texture, 175
- The Corporate Facilities Investment Plan (CFIP), 51
- Thin-Film Materials Synthesis and Processing Facility, 33
- Thrusters, 232
- Thunderstorm, 207
- Ti:Sapphire Femtosecond Laser (TFL), 34
- Toastmasters International, 26, 264
- Topographic Rossby waves, 24
- TORPEDO Ultra, 48
- Towed arrays, 127
- Towed decoy, 147
- Towline, 147
- Transmission electron microscopy (TEM), 33
- Transmission Technology Branch, 30
- T-REX, 133
- TRMM, 44
- TWTs, 169
- U.S. Geological Survey, 49
- UAV, 55
- Ultrafast Laser Facility (ULF), 35
- Ultralow-loss Infrared (IR) Fiber-Optic Waveguide Facility, 31
- Ultraviolet photoelectron spectroscopy (UPS), 31
- Uncertainty, 217
- United Arab Emirates United Aerosol Experiment (UAE²), 45
- Unmanned vehicles, 159
- Unsteady flow, 177
- Unstructured mesh, 177
- Upper Stage spacecraft, 25, 232
- Vacuum Electronics Fabrication Facility (VEFF), 35
- Vacuum Ultraviolet Space Instrument Test Facility, 45
- Vertical Microstructure Profiler (VMP), 43
- Video services, 47
- Wafer Bonding Facility (WBF), 35
- Water vapor, 136
- Waves, 187
- W-band Advanced Radar for Low Observable Control (WARLOC), 27
- WindSat, 42
- Women in Science and Engineering (WISE) Network, 26, 264
- X-ray photoelectron spectroscopy (XPS), 31
- Z-contrast imaging, 33

AUTHOR INDEX

- Abe, D.K., 169
 Aggarwal, I.D., 219
 Anderson, G.P., 148
 Antonsen, Jr., T.M., 169
 Baker, N., 137
 Baker, P., 55
 Barock, T., 127
 Bartolo, R., 195
 Bashkansky, M., 199
 Bibee, L.D., 125
 Blain, C.A., 89
 Book, J.W., 187
 Bowles, J., 107
 Boyer, L.L., 221
 Brozena, J., 107
 Bruce, R.W., 227
 Busse, L.E., 219
 Chang, M.P.J.L., 142
 Chappie, S.S., 232
 Chiggiato, J., 187
 Childers, V., 107
 Chun, S.-T., 153
 Clark, K., 208
 Cohen, L.S., 155
 Cook, J.W., 229
 Dahlburg, J.P., 139
 Daley, K., 195
 Dandridge, A., 127
 Danly, B.G., 169
 Delehanty, J.B., 148
 Doffoh, J., 165
 Doyle, J.D., 133
 Dwyer, C.T., 167
 Dykes, J., 187
 Dykes, J.D., 89
 Eddy, Jr., C.R., 73
 Elvidge, C.D., 99
 Emmert, J.T., 139
 Englert, C.R., 136
 Fatemi, F.K., 199
 Fliflet, A.W., 227
 Fonda, R.W., 175
 Font, C., 142
 Frick, G.M., 211
 Fromm, M., 207
 Gallelli, K.H., 232
 Gardner, J., 107
 Gaskill, D.K., 73
 Gendron, M.L., 191
 Gibson, D., 219
 Gilbreath, G.C., 142
 Glembocki, O.J., 180
 Goerss, J., 137
 Goffeney, J., 217
 Gold, S.H., 227
 Goldman, E.R., 148
 Goroch, A.K., 156
 Groeninger, W., 63
 Grubišić, V., 133
 Haddock, S.H.D., 99
 Hanbicki, A.T., 196
 Hayhurst, A., 148
 Heyer, J., 159
 Hogan, E., 63
 Hooper, W.P., 211
 Hope, A., 232
 Howard, R.A., 229
 Jarvis, J., 107
 Johnson, M.S., 232
 Jones, T.G., 125
 Jonker, B.T., 196
 Kahn, A., 55
 Kamgar-Parsi, B., 55
 Keller, T.M., 147
 Kellogg, J., 55
 Kinkead, A.K., 227
 Kioseoglou, G., 196
 Kirkendall, C.K., 127, 195
 Kolel-Veetil, M.K., 147
 Kragh, F., 208
 Kub, F.J., 73
 Kung, F., 219
 Ladner, S., 187
 Layne, G., 191
 Lean, J.L., 139
 Lee, T.F., 99, 207
 LePage, K.D., 121
 Levush, B., 169
 Lew, K.-K., 73
 Lewis III, D., 227
 Li, C.H., 196
 Liang, R., 107
 Light, A., 155
 Lind, R.J., 211
 Liu, J.L., 148
 Lohrenz, M.C., 191
 Lombardi, M.T., 227
 Lucas, K.E., 63
 Martin, J.R., 63
 Martin, P., 187
 Massey, T.C., 89
 Means, S.L., 185
 Meehan, T., 208
 Mehl, M.J., 221
 Mereish, R., 165
 Michael, B.P., 211
 Miller, S.D., 99, 207
 Morgan, S.R., 232
 Myers, R.E., 169
 Myers-Ward, R.L., 73
 Newmark, J.S., 229
 Nguyen, V.Q., 219
 Oh, E.S., 142
 Pauls, T.A., 83
 Pederson, M.R., 221
 Peñano, J., 125
 Peterson, D.M., 83
 Picone, J.M., 139
 Posey, P.G., 89
 Prokes, S.M., 180
 Pureza, P.C., 219
 Qiu, J.X., 169
 Ramamurti, R., 177
 Rendell, R.W., 180
 Reynolds, A.P., 175
 Rixen, M., 187
 Rosmond, T., 137
 Rupar, M., 165
 Salzano, J., 195
 Sample, J., 191
 Sandberg, W.C., 177
 Sanghera, J.S., 219
 Schechter, R.S., 153
 Schmidt, G.S., 217
 Shaw, L.B., 219
 Skalitzky, R.G., 232
 Slebodnick, P.F., 63
 Sletten, M.A., 185
 Smith, L.N., 201
 Sprangle, P., 125
 Stevens, M.H., 136
 Tang, W., 175
 Ting, A., 125
 Tremper, D., 159
 Tudor, M., 187
 Turk, J., 207
 Tveten, A., 127
 van 't Erve, O.M.J., 196
 VanMil, B.L., 73
 Verborgt, J., 63
 Vincent, W.S., 232
 Wang, D., 187
 Waterman, J.R., 201
 Webb, A.A., 63
 Wert, J.A., 175
 Wert, R.A., 156
 Whalen, B.P., 232
 Willis, R., 217
 Xu, L., 137

EMPLOYMENT OPPORTUNITIES

NRL

NRL offers a wide variety of challenging positions that involve the full range of work, from basic and applied research to equipment development. The nature of the research and development conducted at NRL requires professionals with experience. Typically there is a continuing need for electronics, mechanical, aerospace, and materials engineers, metallurgists, computer scientists, and oceanographers with bachelor's and/or advanced degrees and physical and computer scientists with Ph.D. degrees.



Chemists. Chemists are recruited to work in the areas of combustion, polymer science, bioengineering and molecular engineering, surface science, materials, synthesis, nanostructures, corrosion, fiber optics, electro-optics, microelectronics, electron-device technology, and laser physics.

Physicists. Physics graduates may concentrate on such fields as materials, solid-state physics, fiber optics, electro-optics, microelectronics, vacuum science, plasma physics, fluid mechanics, signal processing, ocean acoustics, information processing, artificial intelligence, electron-device technology, radio-wave propagation, laser physics, ultraviolet/X-ray/gamma-ray technology, electronic warfare, electromagnetic interaction, communications systems, radio frequency/microwave/millimeter-wave/infrared technology, computational physics, radio and high-energy astronomy, solar physics, and space physics.

Biologists. Biologists conduct research in areas that include bio-sensor development, tissue engineering, molecular biology, genetic engineering, proteomics, and environmental monitoring.

Oceanographers, Meteorologists, and Marine Geophysicists. These employees work in the areas of ocean and atmospheric dynamics, air-sea interaction, upper-ocean dynamics, oceanographic bio-optical modeling, oceanic and atmospheric numerical modeling and prediction, data assimilation and data fusion, retrieval and application of remote sensing data, benthic processes, aerogeophysics, marine sedimentary processes, advanced mapping techniques, atmospheric physics, and remote sensing. Oceanographers and marine geophysicists are located in Washington, DC, and at the Stennis Space Center, Bay St. Louis, Mississippi. Meteorologists are located in Washington, DC, and Monterey, California.

for
**Highly Innovative, Motivated,
and Creative Professionals**

Electronics Engineers and Computer Scientists. These employees may work in the areas of communications systems, electromagnetic scattering, electronics instrumentation, electronic warfare systems, radio frequency/microwave/millimeter-wave/infrared technology, radar systems, laser physics technology, radio-wave propagation, electron device technology, spacecraft design, artificial intelligence, information processing, signal processing, plasma physics, vacuum science, microelectronics, electro-optics, fiber optics, solid state, software engineering, computer design/architecture, ocean acoustics, stress analysis, and expert systems.



Mechanical and Aerospace Engineers. These employees may work in areas of spacecraft design, remote sensing, propulsion, experimental and computational fluid mechanics, experimental structural mechanics, solid mechanics, elastic/plastic fracture mechanics, materials, finite-element methods, nondestructive evaluation, characterization of fracture resistance of structural alloys, combustion, CAD/CAM, and multi-functional material response.

Materials Scientists/Engineers. These employees are recruited to work on materials, microstructure characterization, electronic ceramics, solid-state physics, fiber optics, electro-optics, microelectronics, fracture mechanics, vacuum science, laser physics and joining technology, and radio frequency/microwave/millimeter wave/infrared technology.



For more information on current vacancy listings,
visit <http://hroffice.nrl.navy.mil/>

NAVAL RESEARCH LABORATORY

4555 Overlook Ave., SW • Washington, DC 20375-5320

LOCATION OF NRL IN THE CAPITAL AREA

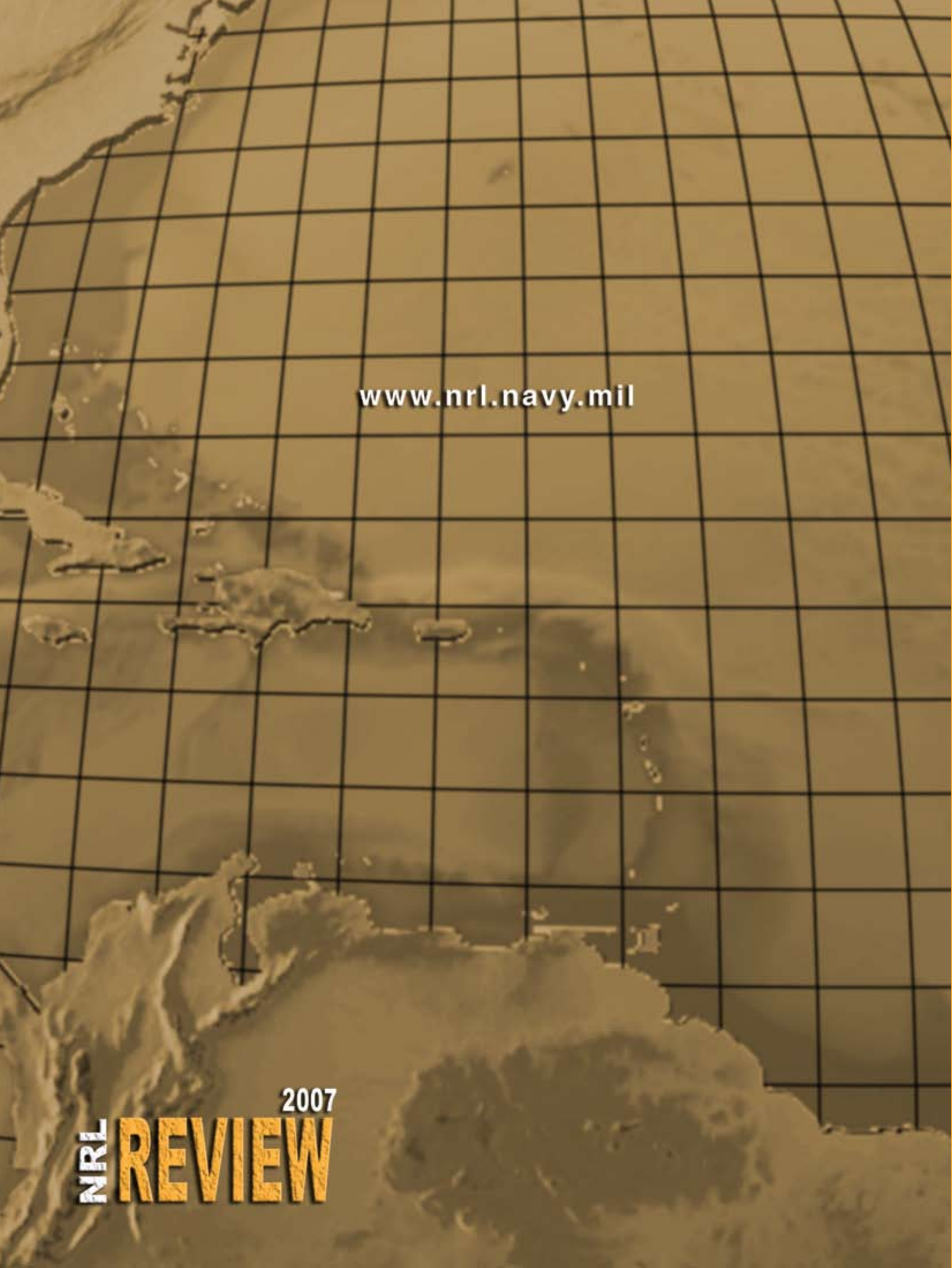


Quick Reference Telephone Numbers

	NRL Washington	NRL- SSC	NRL- Monterey	NRL CBD	NRL VXS-1 Patuxent River
Hotline	(202) 767-6543	(202) 767-6543	(202) 767-6543	(202) 767-6543	(202) 767-6543
Personnel Locator	(202) 767-3200	(228) 688-3390	(831) 656-4763	(410) 257-4000	(301) 342-3751
DSN	297- or 754-	828	878	—	342
Direct-in-Dialing	767- or 404-	688	656	257	342
Public Affairs	(202) 767-2541	(228) 688-5328	(202) 767-2541	—	(202) 767-2541

Additional telephone numbers are listed on page 270.

Approved for public release; distribution is unlimited.



www.nrl.navy.mil

2007
NRL REVIEW